



# Infectious Disease Transmission in Airliner Cabins

\*Qingyan “Yan” Chen, Ph.D.; James J. McDevitt, Ph.D., CIH; Jitendra K. Gupta, Ph.D.; Byron W. Jones, P.E., Ph.D.; Sagnik Mazumdar, Ph.D.; Stephane B. Poussou, Ph.D.; and John D. Spengler, Ph.D.

National Air Transportation Center of Excellence for  
Research in the Intermodal Transport Environment (RITE)  
Airliner Cabin Environment Research Program  
Harvard School of Public Health; Kansas State University; and Purdue  
University

February 22, 2012

Report No. RITE-ACER-CoE-2012-01

\*Authors' names appear alphabetically.

## **NOTICE**

---

This document is disseminated under the sponsorship of the U.S. Department of Transportation in the interest of information exchange. The United States Government assumes no liability for the contents thereof.

---

This work was funded by the U.S Federal Aviation Administration Office of Aerospace Medicine under Cooperative Agreements 07-C-RITE and 10-C-RITE.

---

This publication is available in full-text from the publications Web site of the National Air Transportation Center of Excellence for Research in the Intermodal Transport Environment (RITE) at:  
*[www.acer-coe.org](http://www.acer-coe.org)*

**Technical Report Documentation Page**

1. Report No. <b>RITE-ACER-CoE-2012-01</b>		2. Government Accession No.		3. Recipient's Catalog No.	
4. Title and Subtitle <b>Infectious Disease Transmission in Airliner Cabins</b>				5. Report Date <b>February 22, 2012</b>	
				6. Performing Organization Code	
7. Author(s) <b>Qingyan "Yan" Chen, James J. McDevitt, Jitendra K. Gupta, Byron W. Jones, Sagnik Mazumdar, Stephane B. Poussou, and John D. Spengler</b>				8. Performing Organization Report No.	
9. Performing Organization Name and Address <b>Harvard School of Public Health   Boston, Massachusetts Kansas State University   Manhattan, Kansas Purdue University   West Lafayette, Indiana</b>				10. Work Unit No. (TRAIS)	
				11. Contract or Grant No. <b>07-C-RITE and 10-C-RITE</b>	
12. Sponsoring Agency name and Address <b>Office of Aerospace Medicine  Federal Aviation Administration 800 Independence Ave., S.W. Washington, DC 20591</b>				13. Type of Report and Period Covered <b>Technical Report 2/1/2009 to 12/31/2011</b>	
				14. Sponsoring Agency Code	
15. Supplemental Notes <b>Work was accomplished under Public law 108-76.</b>					
16. Abstract <p>Airborne disease transmission has always been a topic of wide interest in various fields for decades. This report shows the study of the entire disease transmission route in an airliner cabin from the infectious agents generated by an index patient to the fellow passengers and crew members. The investigation developed exhalation/inhalation models for coughing, breathing and talking with human subjects. The transport of these expiratory droplets in an aircraft was investigated using the CFD methods. It was found that the bulk airflow pattern in the cabin played the most important role on the droplet transport. The deterministic and probabilistic approaches (Wells Riley equation) can be used to quantify the risk of infection based on the inhaled infectious dose. By assuming an index passenger with influenza the deterministic approach can calculate the amount of influenza virus ribonucleic acid (RNA) particle inhaled by each passenger and the probabilistic approach can determine the risk of infection for each passenger. Further experimental and CFD investigations revealed that in-flight movement of passengers and crew members had a significant impact on infectious disease transmission inside airliner cabins. The investigation showed that the movement of a passenger/crew member could be the reason behind the transmission of SARS viruses to passengers seated as far as seven rows from the infected passenger during the SARS outbreak in 2003. An important route for disease transmission is by deposition of droplets or particles on surfaces followed by contact with the surfaces. Experimental methods to measure particle deposition in a full-scale cabin mockup were developed. This investigation has also developed a better understanding of surface contamination in the air cabin through laboratory investigation and a pilot field study. The laboratory investigation focused on evaluating survival of influenza virus on surfaces and developing a field, microbial, surface sampling protocol for use in the air cabin environment. The results of our investigation show that influenza survival on stainless steel surfaces are impacted by relative humidity.</p>					
17. Key Words <b>Virus, influenza, SARS, models, experiment, risk, airflow, relative humidity, particles, deposition, movement, in-flight</b>			18. Distribution Statement		
19. Security Classif. (of this report) <b>Unclassified</b>		20. Security Classif. (of this page) <b>Unclassified</b>		21. No. of Pages <b>172</b>	22. Price

## EXECUTIVE SUMMARY

Airborne disease transmission has always been a topic of wide interest in various fields for decades. The transmission of bacterial and viral pathogens from inanimate surfaces to susceptible persons is a concern with regard to infectious disease transmission. For infection to occur, the pathogenic organisms must be present and survive on the environmental surface until such a time that the pathogen is transferred to a susceptible host at the appropriate route of entry. The air cabin is a unique environment for disease transmission. The air cabin has a high occupation density with a high passenger through-put. While seated for hours at a time, “sick” individuals have ample opportunity to contaminate their surrounding area. Once surfaces in the air cabin become contaminated, susceptible persons in the immediate area may come into contact with the contaminated surfaces.

The transmission of airborne disease starts when the infectious agents such as the influenza virus or Mycobacterium tuberculosis are exhaled from an infected person. The infectious agents are then dispersed and finally inhaled by a susceptible person. The transmission of infectious diseases in indoor environments, especially in aircraft cabins may represent great risk as they have high occupant density and need to be investigated. With the recent advancements, Computational Fluid Dynamics (CFD) has become a powerful tool for predicting the transmission of airborne diseases in indoor environments. The CFD simulations need precise thermo-fluid boundary conditions for the exhalation/inhalation during various respiratory events and reliable flow models to accurately predict the transport of the infectious agents.

The present study first developed exhalation/inhalation models for coughing, breathing and talking. The study conducted measurements on the exhaled/inhaled flow rate, flow direction and area of mouth/nose opening with human subjects. The flow rate variation over time can be defined as a combination of gamma functions for a cough; sinusoidal function for breathing, and a constant for talking process. The variables required to define these flow rate functions can be obtained from the physiological details of a person. The direction of the exhalation jet and the area of mouth/nose opening did not vary significantly during these processes. Though variation among people existed but had no correlation with the physiological details of a person. Thus a mean value for these parameters can be used as boundary condition. In summary, a set of mathematical equations were developed to provide the flow boundary conditions to the CFD simulations for the coughing, breathing and talking processes. The equations account for the variation in the flow boundary conditions with time and people.

The droplets exhaled by an infectious person are the carriers of infectious agents. The transport of these expiratory droplets in an aircraft was investigated using the CFD methods. The developed exhalation/inhalation boundary conditions were used. A seven-row, twin-aisle, fully-occupied cabin with index passenger seated at the center was investigated. The droplets exhaled were from a single cough, a single breath and a 15-s talk of the index passenger. The droplets were tracked by using Lagrangian method and their evaporation was modeled. It was found that the bulk airflow pattern in the cabin played the most important role on the droplet transport. The droplets were contained in the row before, at, and after the index patient within 30 s and dispersed uniformly to all the seven rows in 4 minutes. For the cough case, the total airborne droplet fraction

reduced to 48%, 32%, 20%, and 12% after 1, 2, 3 and 4 minutes respectively. Similar observations were made for the breathing and talking cases.

The study further developed methods to predict the spatial and temporal distribution of expiratory droplets for any flight duration based on the 4 minutes of CFD simulations. The CFD simulations indicated that the local droplet concentrations were higher in the zone, where the expiratory droplets first reached. The droplets concentration then reduced due to the constant dispersion and removal of the droplets from the outlets. The variation in the droplet concentration in the vicinity of the passengers with time indicated that the droplets got well mixed in the cabin in 3 minutes, thus perfectly mixed conditions can be assumed beyond 3 minutes. The droplets from multiple exhalations from the index passenger were found to follow similar tracks. This indicates that the airflow in most of the cabin was steady. It is proposed that the concentration of the droplets in a zone can be obtained by adding the concentrations in the zone from all the exhalations taken place until that time provided with a time shift. Finally, the amount of droplets inhaled by the susceptible passengers was calculated for 4 hours of flight duration under three scenarios.

The study used the deterministic and probabilistic approaches (Wells Riley equation) to quantify the risk of infection based on the inhaled infectious dose. The inhaled dose was calculated using the amount of inhaled droplets and the infectious dose contained in a droplet. A case with index passenger suffering with influenza was analyzed. For the deterministic approach, the amount of influenza virus ribonucleic acid (RNA) particle inhaled by each passenger was calculated. For the probabilistic approach, the risk of infection for each passenger was evaluated based on the amount of inhaled quanta. The effectiveness of masks in reducing the risk of infection was also explored.

Further experimental and CFD investigations revealed that in-flight movement of passengers and crew members can change the airflow and contaminant transmission inside airliner cabins. Experiments were performed using a one-tenth scale, water-based empty cabin model to facilitate measurements and to generate high quality experimental data using Particle Image Velocimetry (PIV) and Planar Laser-Induced Fluorescence (PLIF). The results indicate that seats and passengers tend to obstruct the lateral transmission of contaminants and restrict the spread to the aisle of the cabin if a contaminant is released from a moving body. Investigations showed that movement could be the reason behind the transmission of SARS contaminants to passengers seated as far as seven rows from the infected passenger during the SARS outbreak in 2003.

An important route for disease transmission is by deposition of droplets or particles on surfaces followed by contact with the surfaces. There are few experimental measurements that can be used to aid in developing accurate CFD models. To fill this need, experimental methods to measure particle deposition in a full-scale cabin mockup were developed. These methods use microphotographs to count particles on surfaces following controlled particle releases in the cabin. These measurements are ongoing. When completed, the resulting data set will be combined with the corresponding data set for airborne concentrations already collected to relate deposition rates to airborne concentrations.

This investigation has also developed a better understanding of surface contamination in the air cabin through laboratory investigation and a pilot field study. The laboratory investigation focused on evaluating survival of influenza virus on surfaces

and developing a field, microbial, surface sampling protocol for use in the air cabin environment. While the pilot field study focused on developing a rational method for evaluating microbial contamination on air cabin surfaces. The results of our investigation show that influenza survival on stainless steel surfaces are impacted by relative humidity. There was a trend of increasing influenza inactivation with increasing relative humidity. The inactivation rates for influenza virus were statistically higher at 75% compared to 25 and 50% RH. The low RH in the air cabin may be conducive to influenza survival and increase infection risk. Recovery of bacteria from surfaces varied and was inconsistent among a variety of swab types. The sampling kit used in the pilot field study recovered a wide variety of bacteria, but only a single type of virus. The strategy of sampling aircraft at the end of the flight day, and prior to cleaning, provided an efficient means of evaluating microbial surface contamination on a variety of aircraft.

## TABLE OF CONTENTS

EXECUTIVE SUMMARY .....	1
<b>Part 1: Respiratory Exhalation/Inhalation Models and Assessment of Airborne Infection Risk in Commercial Aircraft Cabins</b> .....	<b>8</b>
<b>1. INTRODUCTION</b> .....	<b>9</b>
1.1 EXHALATION AND INHALATION MODELS FOR RESPIRATORY EVENTS .....	11
1.2 PREDICTION OF INFECTION SPREAD IN AN AIRCRAFT CABIN .....	11
<b>2. THE STATE OF THE ART</b> .....	<b>13</b>
2.1 EXHALATION AND INHALATION DURING RESPIRATORY EVENTS .....	13
2.1.1 <i>Coughing</i> .....	13
2.1.2 <i>Breathing</i> .....	15
2.1.3 <i>Talking</i> .....	15
2.2 PREDICTION OF TRANSPORT OF EXPIRATORY DROPLETS IN AN AIRCRAFT CABIN .....	15
2.2.1 <i>Considerations for CFD Modeling</i> .....	15
2.2.2 <i>Prediction of Expiratory Droplet Transport in an Aircraft Cabin</i> .....	16
2.3 EVALUATION OF RISK OF INFECTION IN AN AIRCRAFT CABIN.....	17
2.4 CONTROLLING THE RISK OF INFECTION .....	18
2.4.1 <i>Effectiveness of Masks against the Infectious Agents</i> .....	18
2.5 SUMMARY .....	21
<b>3. FLOW CHARACTERIZATION OF A COUGH</b> .....	<b>23</b>
3.1 MEASUREMENT METHODS .....	23
3.2 RESULTS.....	24
3.2.1 <i>Flow Rate of a Cough</i> .....	24
3.2.2 <i>Flow Direction of a Cough</i> .....	30
3.2.3 <i>Mouth Opening Area</i> .....	32
3.3 DISCUSSION .....	34
3.4 CONCLUSIONS .....	34
<b>4. FLOW CHARACTERIZATION OF BREATHING AND TALKING</b> .....	<b>36</b>
4.1 MEASUREMENT METHODS .....	36
4.2 RESULTS.....	37
4.2.1 <i>Breathing</i> .....	37
4.2.2 <i>Talking</i> .....	43
4.3 DISCUSSION .....	46
4.4 CONCLUSIONS .....	48
<b>5. TRANSPORT OF EXPIRATORY DROPLETS IN AN AIRCRAFT CABIN</b> .....	<b>49</b>
5.1 RESEARCH METHOD .....	49
5.1.1 <i>Domain of Study</i> .....	49

5.1.2	<i>Numerical Schemes</i> .....	50
5.1.3	<i>Case Setup</i> .....	53
5.1.4	<i>Grid Independence and Cabin Section End Conditions</i> .....	58
5.2	RESULTS.....	63
5.2.1	<i>Steady-State Airflow in the Cabin</i> .....	63
5.2.2	<i>Evaporation of Droplets in the Cabin</i> .....	65
5.2.3	<i>Transport of Droplets Exhaled from the Coughing</i> .....	66
5.2.4	<i>Transport of Droplets Exhaled from the Breathing</i> .....	69
5.2.5	<i>Transport of Droplets Exhaled from the Talking</i> .....	71
5.3	DISCUSSION .....	73
5.4	CONCLUSIONS .....	74
<b>6.</b>	<b>INHALATION OF DROPLETS IN AN AIRCRAFT CABIN</b> .....	<b>75</b>
6.1	RESEARCH METHODS.....	75
6.1.1	<i>Extension of Droplet Concentration for Real Flight Durations</i> .....	75
6.1.2	<i>Droplets Inhaled by the Passengers due to Multiple Exhalations from the Index Passenger</i> .	79
6.1.3	<i>Case Setup</i> .....	82
6.2	RESULTS .....	83
6.3	DISCUSSION .....	84
6.4	CONCLUSIONS .....	85
<b>7.</b>	<b>EVALUATION OF AIRBORNE RISK OF INFECTION IN AN AIRCRAFT CABIN</b> .....	<b>86</b>
7.1	RISK ASSESSMENT MODELS.....	86
7.2	CASE DESCRIPTION .....	87
7.3	AMOUNT AND VIABILITY OF DOSE .....	88
7.3.1	<i>Deterministic Models</i> .....	88
7.3.2	<i>Probabilistic Model: Wells Riley Equation</i> .....	88
7.4	RESULTS.....	89
7.4.1	<i>Risk of Infection from Influenza using the Deterministic and Probabilistic Models</i> .....	89
7.4.2	<i>Effect of N-95 Mask</i> .....	91
7.5	DISCUSSION .....	93
7.6	CONCLUSION.....	93
<b>8.</b>	<b>INFLUENCE OF MOVING BODY THROUGH EXPERIMENTAL AND CFD INVESTIGATIONS IN A SMALL-SCALE CABIN</b> .....	<b>94</b>
8.1	RESEARCH METHODOLOGIES.....	94
8.2	EXPERIMENTAL METHOD.....	95
8.2.1	<i>Experimental Setup</i> .....	95
8.2.2	<i>Experimental Techniques</i> .....	97
8.3	CFD MODELING .....	99
8.4	RESULTS AND DISCUSSION .....	100
8.4.1	<i>Cross-sectional Flow</i> .....	100
8.4.2	<i>Longitudinal Flow</i> .....	108
8.4.3	<i>Contaminant Transport</i> .....	110
8.5	CONTAMINANT TRANSMISSION DUE TO MOVEMENT IN THE SARS INFECTED CABIN.....	113
8.6	CONCLUSIONS .....	118

<b>9.</b>	<b>CONCLUSIONS AND FUTURE WORK</b> .....	<b>119</b>
9.1	CONCLUSIONS .....	119
9.2	RECOMMENDATION FOR FUTURE STUDIES .....	122
<b>10.</b>	<b>REFERENCES</b> .....	<b>124</b>
<b>Part 2: Measurement of Particle Deposition Behavior in an Aircraft Cabin</b>		<b>135</b>
<b>11.</b>	<b>INTRODUCTION</b> .....	<b>136</b>
<b>12.</b>	<b>EXPERIMENTAL METHODS</b> .....	<b>137</b>
<b>13.</b>	<b>RESULTS</b> .....	<b>141</b>
<b>14.</b>	<b>CONCLUSIONS AND NEXT STEPS</b> .....	<b>144</b>
<b>15.</b>	<b>REFERENCES</b> .....	<b>145</b>
<b>Part 3: Role of Relative Humidity in the Inactivation of Influenza Viruses on Steel Surfaces and Microbial Surface Sampling in the Air Cabin</b>		<b>146</b>
<b>16.</b>	<b>INTRODUCTION</b> .....	<b>147</b>
<b>17.</b>	<b>BACKGROUND</b> .....	<b>149</b>
17.1	RELATIVE HUMIDITY AND INFLUENZA SURFACE SURVIVAL .....	149
17.2	SURFACE SAMPLING PROTOCOL DEVELOPMENT .....	149
17.3	FIELD STUDY .....	150
<b>18.</b>	<b>METHODS</b> .....	<b>152</b>
18.1	TEST ORGANISMS .....	152
18.1.1	<i>Influenza Virus</i> .....	152
18.1.2	<i>Bacteria</i> .....	152
18.2	RELATIVE HUMIDITY AND INFLUENZA SURFACE SURVIVAL .....	153
18.2.1	<i>RH Control Chamber</i> .....	153
18.2.2	<i>RH Survival Tests</i> .....	153
18.2.3	<i>Data Analysis</i> .....	154
18.3	SURFACE SAMPLING PROTOCOL DEVELOPMENT .....	154
18.3.1	<i>Swab Selection</i> .....	154
18.3.2	<i>Swab Surface Testing</i> .....	155
18.3.3	<i>Surface Testing Data Analysis</i> .....	156
18.4	FIELD STUDY .....	156
18.4.1	<i>Field Study Sampling Plan</i> .....	156
18.4.2	<i>Field Study Sample Processing</i> .....	157
<b>19.</b>	<b>RESULTS</b> .....	<b>158</b>
19.1	RELATIVE HUMIDITY AND INFLUENZA SURFACE SURVIVAL .....	158
19.2	SURFACE SAMPLING PROTOCOL DEVELOPMENT .....	159
19.3	FIELD STUDY .....	161
<b>20.</b>	<b>DISCUSSION</b> .....	<b>166</b>
20.1	RELATIVE HUMIDITY AND INFLUENZA SURFACE SURVIVAL .....	166

20.2	SURFACE SAMPLING PROTOCOL DEVELOPMENT AND FIELD STUDY.....	167
21.	<b>CONCLUSIONS.....</b>	<b>170</b>
22.	<b>REFERENCES.....</b>	<b>171</b>

## **Part 1:**

# **Respiratory Exhalation/Inhalation Models and Assessment of Airborne Infection Risk in Commercial Aircraft Cabins**

Prepared by  
Jitendra K. Gupta, Ph.D., Sagnik Mazumdar, Ph.D., Stephane B. Poussou, Ph.D., and  
Qingyan “Yan” Chen, Ph.D.  
School of Mechanical Engineering  
Purdue University  
West Lafayette, Indiana

February 10, 2012

## 1. INTRODUCTION

Airborne infection has always been a major source of morbidity and mortality worldwide (Corbett et al., 2003). There are common airborne infectious diseases such as cold and influenza, and severe ones as Severe Acute Respiratory Syndrome (SARS), tuberculosis (TB) and avian flu. Dye et al. (1999) evaluated the global burden of TB. About 22 countries were found to have TB infections with a total of 1.87 million deaths. Influenza epidemics were found to cause about 47,200 deaths each year in the United States with similar figures in Europe (Viboud et al., 2004). The Spanish flu of 1918-19 (H1N1) was by far the most lethal flu pandemic of the 20<sup>th</sup> century. According to the World Health Organization (WHO) estimates, it infected about one-quarter of the global population and took more than 40 million lives (WHO, 2002). Not only avian flu could be deadly; there were 8098 people infected by SARS and 774 of them died according to statistics from the World Health Organization (WHO, 2004). In a recent swine flu epidemic (2009) about 0.6 million people (laboratory confirmed) got infected (WHO, 2009). The list of such social and economic disruption caused by these and many more airborne diseases is endless. Thus it is important to understand, predict and control the transmission of airborne diseases to trim down the deaths.

Airborne disease transmission starts from infectious agents exhaled from an infected person (Cole and Cook, 1998). Then the infectious agents disperse in the air and are finally inhaled by a susceptible person. The infectious agents can spread at indoor and outdoor spaces. At the outdoors the infectious droplets can rapidly disperse and quickly render to a nonviable stage because of sky/sun light (Edwards and Dragsted, 1952). On the other hand, the indoor spaces are confined with low air exchange rate as compared to outdoors and thus may have major risk for infection transmission (Houk et al., 1998 WHO 1998; WHO 1999 and Mangili and Gendreau, 2005). Moreover, people spend 90% of their time indoors (Klepeis et al., 2003 and Aliaga and Winqvist, 2003). Thus it is important to investigate the transmission of infectious diseases in indoor environments such as office spaces (Kenyon et al., 2000), hospitals (WHO, 1999), and aircraft cabins (WHO, 1998).

The airborne disease transmission during air travel has been given high importance (WHO, 1998). This is because aircraft cabins have high occupancy rate and long exposure time, people sit in quite proximity of each other, and cannot leave the cabin, and thus would very likely be infected by airborne infectious agents if there is a pandemic. Some of the TB outbreaks were believed to be caused by in-flight infection transmission (Kenyon et al., 1996). The SARS infected passengers in the flight from Hong Kong to Beijing (Olsen et al., 2003) were believed to get infected due to the in-flight transmission. Mangili and Gendreau (2005) reviewed the risks of airborne infection spread among the passengers inside the aircraft cabin from various respiratory outbreaks and suggested that in-flight infection disease transmission is of greatest risk. Moreover, now it has become more of a public issue as more than two billion people are traveling each year (Gendreau and DeJohn, 2002) in commercial flights. Thus the current study is focused on investigating airborne disease transmission in aircraft cabins.

The airborne disease transmission can be predicted by computer simulations or experimental methods. The experimental methods are expensive, time consuming and less flexible to changes, though they can provide realistic information (Zhang, 2007a;

Zhang, 2007; Sze To et al. 2009 and Yan et al., 2009). It may not be feasible to conduct experiments on a real aircraft cabin with passengers and crew members as the cost involved could be extremely high. Zhan (2007) estimated that the experimental studies for a few rows can easily go up to a million dollar and may not represent real cabin conditions. The aircraft cabins are long and thus it may really take long time to conduct measurements. The computational methods on the other hand are inexpensive, fast and more flexible to changes in comparison with the experiments. The main computational methods include multizone models (Axley, 2007), zonal models (Megri and Haghghat, 2007), fast fluid dynamics (FFD) (Zuo and Chen, 2009) and computational fluid dynamics (CFD) (Norton and Sun, 2006). The aircraft cabin is a complex geometry and the airflow and contaminant transport is three-dimensional (Zhang et al., 2009). The multizone models assume uniform air temperature, and chemical-species concentration in a zone, which is not a valid assumption for large spaces like aircraft cabins. The zonal based models are fast but can give approximate results as it considers macroscopic flow between the zones. Thus it may not provide intricate details required for the prediction of infection transmission. The FFD based models are faster than the CFD models but are not as accurate as the CFD models especially when the flow is turbulent (Zuo and Chen, 2009). On the other hand, the CFD based models are relatively time consuming but can provide accurate information. The CFD models can effectively predict airborne contaminant transport in commercial aircraft cabins (Lin et al., 2005a and 2005b; Wan et al., 2009; Yan et al., 2009 and Zhang, 2007) and the associated non-uniformities. Moreover, CFD predictions of contaminant transport matched reasonably well with the experimental data (Zhang, 2007; Wan et al., 2009 and Yan et al., 2009). Thus for the current investigations, the CFD simulations are used for predicting the airborne disease transmission.

Accurate prediction of the transmission by these CFD simulations requires, precise information on boundary conditions (Zhang, 2007) such as, sources and sinks of infectious agents and appropriate flow models such as, turbulence and dispersion model (Zhang, 2007). The exhaled air of an infected human is the source of infectious agents. These agents enter the body of the victim through inhalation, deposit on a surface, or are extracted through a ventilation exhaust, which are called sinks. There are a number of turbulence models (Zhang, 2007) and dispersion models (Zhang and Chen, 2007c) that are used to study the indoor environment airflow. The selection of the model depends on the application, available computational resources and time. To our knowledge there is no comprehensive literature on the exhalation and inhalation characterization from various respiratory events. Also the available literature on the prediction of in-flight disease transmission though gives quite an insight on the airflow and dispersion but has its pros and cons. These are discussed in details in the state of the art chapter. Thus it is required to develop models for exhalations/inhalations from various respiratory events and further investigate the in-flight disease transmission.

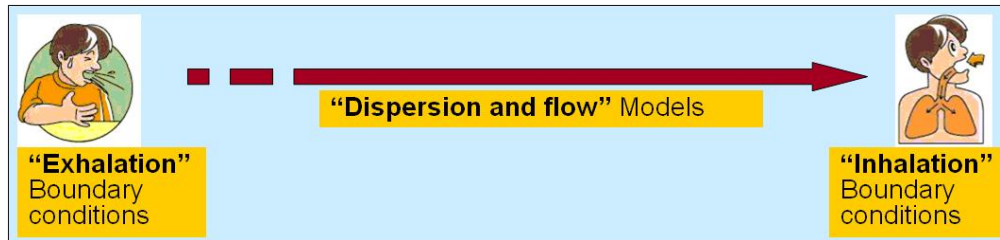


Figure 1.1 CFD simulation layout for the prediction of airborne disease transmission.

## 1.1 Exhalation and Inhalation Models for Respiratory Events

The present study first developed models for the exhalations and inhalations, which can be used as thermo-fluid boundary conditions in CFD simulations. The thermo-fluid boundary conditions include the flow rate, direction, area of mouth/nose opening, duration of the event, temperature, and droplet size distribution. These parameters are transient and can have considerable variation among people. But most of the CFD simulations (Zhu et al., 2006a, 2006b and Zhao et al., 2005) for infectious agent dispersion predictions have treated these boundary conditions as arbitrary periodic profile with assumed direction, temperature, and a ballpark number for the area of the mouth or nose opening. This assumption could be due to scarcity of reliable exhalation/inhalation models. Thus it is required to develop models, which can provide accurate information on these boundary conditions.

The main exhalation/inhalation modes include coughing, sneezing, talking, and breathing. All these exhalation modes can introduce significant amount of infectious agents. The coughing and sneezing have a higher exhalation velocity and droplet concentration but a lower event frequency, while the breathing and talking have a lower velocity and droplet concentration but a higher event frequency. This investigation is focused on the coughing, breathing and talking processes. The study conducted measurements on the exhaled/inhaled flow rate, flow direction and area of mouth/nose opening with human subjects, and developed a set of equations to provide the thermo-fluid boundary conditions for coughing, breathing and talking processes.

## 1.2 Prediction of Infection Spread in an Aircraft Cabin

The transport of droplets exhaled from the coughing, breathing and talking of an index passenger was investigated in a seven row section of a twin aisle cabin using CFD methods. The developed exhalation/inhalation models along with the appropriate information of the expiratory droplets distribution were fed in the CFD simulations. The index passenger could release the infectious agents/droplets through multiple exhalations for several hours during the air travel. Performing CFD studies for all such possible combinations of exhalations for realistic flight durations is impractical. Therefore a method was developed to extend the information on the droplet obtained from the single cough, single breath and 15s talking CFD simulations of 4 minutes to multiple exhalation scenarios over realistic flight durations. Using the spatial and temporal distribution of expiratory droplets the amount of droplets inhaled by the passengers was calculated. The amount of infectious dose inhaled by the passengers and the corresponding risk to the

passengers was then calculated. Based on the comprehensive literature review the reduction in the risk obtained by using the N-95 mask was also calculated.

## 2. THE STATE OF THE ART

This chapter first shows the available studies on the flow characterization of exhalation and inhalation during coughing, breathing, and talking. The available literature on the requirements for the CFD modeling for predicting the transport of expiratory droplets is then presented. The literature on the transport of expiratory contaminants and risk prediction in an aircraft cabin is then explored. Finally, a comprehensive review on protection provided by the masks is presented.

### 2.1 Exhalation and Inhalation during Respiratory Events

This section discusses the available literature on the exhalation and inhalation flow rate, flow direction and area of opening of the mouth/nose during coughing, breathing and talking processes.

#### 2.1.1 Coughing

Figure 1 shows the typical flow generated from a cough over time. Information about cough flow rate is available from the literature (Leiner et al., 1966; Mahajan et al., 1994 and Singh et al., 1995), such as Cough Peak Flow Rate (CPFR), Cough Expired Volume (CEV) that is the area under the curve, and Peak Velocity Time (PVT). The information is of great medical interests (Lamb et al., 1993), but cannot be used as boundary conditions in the CFD simulations. However, the information provides good insight of the flow behavior. Leiner et al. (1966) correlated CPFR with the height and age of human subjects through a regression analysis. Mahajan et al. (1995) further developed relations between CPFR, CEV and PVT.

Later, Singh et al. (1995) corrected the relationship between CPFR and PVT for different genders and found the difference caused by the larynx size in male and female. The total cough expired volume measured by Zhu et. al (2006b) had a variation of 0.8-2.2 liter with an average of 1.4 liter. This was low compared to the studies by Mahajan et al. (1994), who observed a variation of up to 5 L with an average of about 3 L. Though these studies gave some information on cough but did not quantify the dynamics of the cough profile.

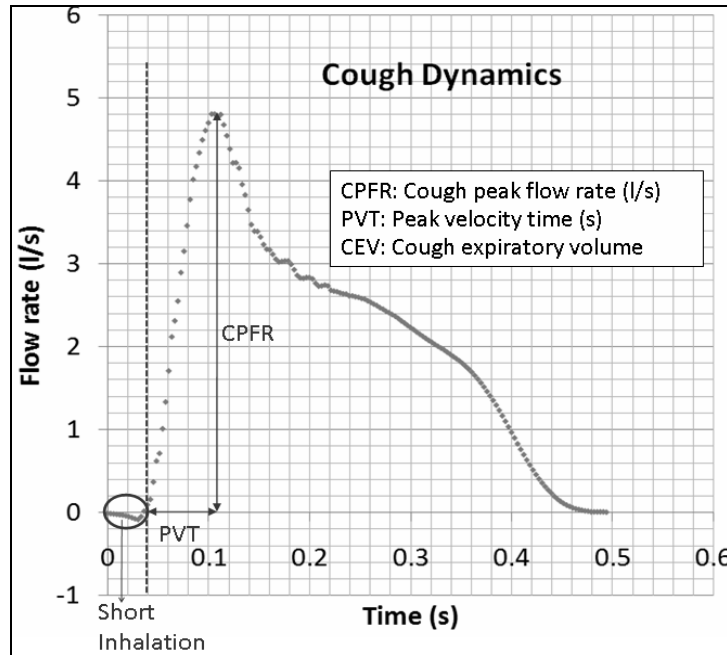


Figure 2.1 Cough flow rate variation with time.

There were a number of studies visualizing the coughing process that could be used to create boundary conditions for CFD simulations. Jennison (1942) visualized cough through high speed photography using strobe (Edgerton and Barstow 1959). Their main emphasis was on droplet size distribution but he also revealed qualitatively the droplet dispersion to 2-3 feet from mouth. Settles et al. (1995) captured the thermal plume coming out of a cough through Schlieren imaging. But none of these studies could characterize the transient process or direction of the jet. Particle Image Velocimetry (PIV) (Afshari et al., 2002; Badeau et al., 2002; VanSciver; Zhu et al., 2006b and Chao et al., 2009) measurements were also performed to capture the flow field. Mahajan et al. (1995) pointed out that the PVT was in the order of a few milliseconds. Hence to capture the cough jet variation and its direction, it becomes essential to have a high frequency of measurements. PIV measurements by Afshari et al. (2002) and Badeau et al. (2002) were done at an interval of 67 ms. The interval was too large to capture the flow features. Chao et al. (2009) investigated the maximum and average velocities but the velocity variation with time was not studied. The PIV studies by VanSciver et al. gave detailed flow information but with an even larger interval of 267 ms. The efforts by Zhu et al. (2006b) were also with a large interval of 70 ms. Therefore, none of these studies could be used to characterize the direction of a cough jet for the CFD simulations. The measurements of the flow rate and direction must be performed with a frequency of 100 Hz or higher.

The area of mouth opening is required to obtain the velocity from the flow rate. The PIV studies by Zhu et al. (2006b) indicated the peak cough velocity varied from 6 to 22 m/s with an average of 11.2 m/s. To our best knowledge, little experimental studies were available on the area of mouth opening during a cough. Most researchers have assumed (Zhu et al., 2006a, 2006b and Zhao et al., 2005) the area to be a few square centimeters. Thus the available literature provides good understanding of the flow behavior of the coughing but not the information that can be used as boundary condition for CFD simulations.

### 2.1.2 Breathing

Some information on breathing airflow is available in the literature, such as Respiration Frequency (RF), Minute Volume (MV), and Tidal Volume (TV). The RF is defined as the number of breaths in a minute; MV the volume expired in a minute; and TV the volume expired in a single breath. These parameters are of medical interest and had been studied thoroughly (Handbook of Physiology, 1986 and Altman et al., 2004). The RF, MV, and TV vary with age, height, weight, body surface area, sex, posture and physical load (Handbook of Physiology, 1986 and Altman and Dittmer, 1971). Flow-volume studies by Araujo et al., (2004) were on evaluating the effect of physical load but not on quantifying the flow rate variation over time. All these studies provide a good insight but not the information as boundary conditions for CFD simulations.

### 2.1.3 Talking

Most of the past efforts on characterizing a talking process were focused on establishing droplet size distribution (Duguid, 1946; Jennison, 1942 and Wells et al., 1939). Duguid (1946) revealed that the velocities of speech can go up to 16 m/s. Jennison (1942) found that consonants, like 'F', when pronounced loudly can generate high flow. Wells et al., (1939) used the Tyndall effect to visualize the pronunciation of the letters 'P' and 'T'. But none of the studies quantified the flow rate transience. The information is incomplete for CFD simulations because the flow rate and direction of talking jets and opening area of mouth/nose are not available. Thus it is required to study the exhalation and inhalation during the coughing, talking and breathing processes and develop models that can provide the flow rate, flow direction of the jet and the area of mouth/nose opening during the processes.

## 2.2 Prediction of Transport of Expiratory Droplets in an Aircraft Cabin

This section explores the factors to be considered for modeling the expiratory droplet transport in an aircraft cabin. The contaminant transport in an aircraft cabin and the associated risk studies are then presented.

### 2.2.1 Considerations for CFD Modeling

Selection of appropriate control volume and geometrical details: The aircraft cabin with seats, passengers, airflow inlets and outlets, is a complex and big geometry. The airflow and the contaminant transport in the cabin are three-dimensional and non-uniform (Singh et al., 2002 and Zhang et al., 2009). Thus it is essential to account for the geometrical details of the whole cabin configuration including the passengers (Singh et al., 2002). Another important thing is to decide on the domain of study, i.e. how many rows? Zhang et al. (2009) suggested that only a few rows may not represent real cabin conditions. The SARS infection in the flight from Hong Kong to Beijing spread in 7 rows (Olsen et al., 2003).

Information on the boundary conditions for the control surfaces: The boundaries (control surfaces) in the aircraft cabin are the walls of the cabin, airflow inlets and outlets of the cabin, seat walls, passenger body, nose and mouth opening of the passengers. Numerical simulations are very sensitive to these boundary conditions (Zhang, 2007).

Appropriate flow models: The selection of equations to be solved, such as, turbulence model and the particle transport model (Zhang, 2007) is very crucial for accurate prediction of transport of infectious agents. Moreover, the expiratory droplets are volatile and can quickly evaporate (Morawska, 2007). Thus it is important to model the evaporation of the expiratory droplets.

The selection of turbulence model is another crucial step in particle transport and deposition pattern. Zhang (2007) evaluated the performance of various turbulence models for indoor environments. He compared the performance of indoor zero-equation model (Chen and Xu, 1998), the RNG  $k-\epsilon$  model (Yakhot and Orszag, 1986), a low Reynolds number  $k-\epsilon$  model (LRN-LS) (Launder and Spalding, 1974), the SST  $k-\omega$  model (SST) (Menter, 1994), a modified  $v2f$  model ( $v2f-dav$ ) (Davidson et al., 2003), Reynolds stress model (RSM-IP) (Gibson and Launder, 1978), the large eddy simulation (LES) (LES-Dyn) (Germano et al., 1991 and Lilly 1992), and the detached eddy simulation (DES-SA) (Shur et al., 1999) under natural convection, forced convection, mixed convection, and strong buoyant flows. Airflow in aircraft cabins is mixed convection in nature. Zhang, (2007) recommended  $v2f-dav$  and RNG  $k-\epsilon$  models for mixed convection scenario in terms of efficiency, accuracy and robustness.

The transport of particle in CFD is usually predicted either through Eulerian or Lagrangian method. The selection of particle transport method depends on the problem and the associated objectives. Eulerian methods are used to predict the particle concentration distribution (Murakami et al., 1992; Mazumdar et al., 2008 and Yan et al., 2009) while the Lagrangian methods are used to predict the particle dispersion pattern (Loomans and Lemaire, 2002; Zhang et al., 2006 and Wan et al., 2009). Zhang and Chen, 2007c compared the two methods and recommended Lagrangian method for transient prediction of particle transport. He found out that Eulerian methods requires small time steps and higher number of iteration per time step to converge, thus is time consuming. Moreover, Lagrangian method can predict detailed particle distribution.

In summary, for accurately and efficiently modeling the transport of expiratory droplets in an aircraft cabin, it is essential to consider the geometrical details along with the passengers and seats, appropriate domain (7 rows or may be full cabin), precise boundary condition on the surfaces (including exhalation/inhalation) and appropriate turbulence (RNG  $k-\epsilon$ ), dispersion models (Lagrangian), and evaporation models.

### 2.2.2 Prediction of Expiratory Droplet Transport in an Aircraft Cabin

There are a number of studies on in-flight contaminant transport (Aboosaidi et al., 1991; Lin et al., 2005a; Lin et al., 2005b; Zhang et al., 2009; Yan et al., 2009 and Wan et al., 2009)

Aboosaidi et al. (1991) considered an empty cabin but Singh et al. (2002) pointed out that the airflow inside the cabin can change significantly if heating load of the passengers is considered. Investigations by Lin et al. (2005a) and Lin et al. (2005b) provided great insight for the airflow in the aircraft cabin. But the domain consisted of just 2 rows,

which may not be sufficient (Olsen et al., 2003; Mazumdar et al., 2008 and Zhang and Chen, 2009).

Zhang et al. (2009) studied contaminant transport in a twin aisle aircraft cabin for 4 rows. They pointed out that the bulk airflow governs the track of contaminants. But again only a few rows were considered, which may not represent real cabin conditions.

Yan et al. (2009) studied the contaminant transport in a 5-row, twin-aisle cabin with passengers. They have used tracer gas to investigate the transmission and used standard k- $\epsilon$  model. The study provided meaningful results but again may lack accuracy as unsteady particle tracking (Zhang, 2007) and RNG k- $\epsilon$  model (Zhang, 2007 and Wan et al., 2009) were not used, which are best suited for the aircraft cabin environment simulation.

Recently, Wan et al. (2009) have studied the transport and deposition of polydispersed droplets in a 3-row-two-aisle cabin configuration using Lagrangian method. The passengers were treated as cylinders with heat source. The passenger seated at the last row at the center was used as an infection source and was provided exhalation velocity of 10.6 m/s over a 1 s of time period with an opening of 0.38 cm<sup>2</sup> for the last passenger seating at the center. They have evaluated the infection risk due to inhalation and from direct contact with the surfaces. They pointed out that the fate of the particle depends upon its size. The study provides a good insight but only three rows are considered with passengers as cylinders and the source boundary conditions are not reliable, i.e. cough lasts for a fraction of a second and the mouth opening is about 4 cm<sup>2</sup>.

It is thus required to further investigate the transport of contaminants (expiratory droplets) by considering more number of rows and realistic passenger geometry and precise boundary conditions for the exhalation and inhalation using the CFD methods. Moreover, as these detailed CFD simulations could be time consuming (Gupta et al., 2010b), it is not practical and feasible to perform the CFD simulations for realistic flight times for a multiple exhalation scenario from the index passenger. Therefore, it is required to develop methods to predict the spatial and temporal distribution of expiratory droplets and thus, the amount of inhaled droplets by the passengers for realistic flight durations.

### 2.3 Evaluation of Risk of Infection in an Aircraft Cabin

The droplets inhaled by the passengers do not necessarily reflect active infectious agents and therefore the risk of infection. It is thus required to develop methods to quantify the risk of infection in an aircraft cabin.

The airflow in the aircraft cabins is not uniform (Yan et al., 2009). The pulse release of infectious agents by the index passenger through coughing, breathing or talking makes the infectious agent transport transient. Therefore, there will be a spatial and temporal variation in the risk of infection to the passengers based on the amount of inhaled infectious agent.

Walkinshaw, 2010 predicted the risk of infection from influenza in an aircraft cabin. He quantified the amount of influenza virus ribonucleic (RNA) particles inhaled by the passengers assuming perfectly mixed environment under transient conditions. Ko et al., 2004 and Jones et al., 2009 used the multizone models to quantify the risk based on the dose response model under steady and unsteady scenarios respectively. Wan et al.,

2009 performed detailed steady-state CFD simulations and quantified the risk of infection from influenza in an aircraft cabin. Risk from inhalation and surface contact was quantified using the dose-response model.

These studies account for either the spatial or the temporal variation of risk of infection in an aircraft cabin but not for both the variations except the transient zonal models (Jones et al., 2009). Thus it is required to develop risk models based on the spatial and temporal distribution of amount of inhaled infectious agents.

## 2.4 Controlling the Risk of Infection

After predicting the risk of infection, it is required to explore ways to mitigate the risk. The risk of infection from the infectious agents can be brought down by reducing the level of infectious agents in the inhaled air of the occupants. It can be done by either cleaning/decontaminating the bulk air or reducing the level of infectious agents locally in the breathing zone of the occupants.

The bulk air can be cleaned by increasing the ventilation rate. This will increase the rate of removal and will dilute the infectious agents. But increasing the ventilation rate increases the energy consumption. The other way could be by sterilizing the bulk air using the ultra violet (UV) rays with wavelength ranging from 254 to 260 nm (Weiss et al., 2007). McLean, (1961) found that the incidence of influenza reduced to 2% from 19% by installing the UV light in a hospital. The UV rays are constrained well above the head level and the UV rays sterilize the air in this zone. The convection currents generated by the buoyancy and mechanical ventilation mixes the air and that is how all the air gets sterilized. The germicidal effects of UV rays are good for humidity levels below 70% (Laurell and Ronge, 1955) and thus can be used for indoor environment such as office spaces and hospitals. The other light disinfection techniques include photocatalysis (Zhao and Yang, 2003) and X-rays (Raber and McGuire, 2002). But these techniques cannot be used in aircraft cabins as the cabins do not have enough height. The chemicals, such as the vaporized hydrogen peroxides can also be used to disinfect the bulk air (Block, 1991) but is good for unoccupied cabins.

The other way of reducing the risk of infection is to reduce the level of infectious agents locally in the inhaled air of the occupants. This can be done by filtering the air available for inhalation, using the protection device, such as masks (Weiss et al., 2007) or by supplying clean air to the breathing zone using personalized ventilation (Melikov, 2004 and Cermak et al., 2006). Both of these techniques can be used for occupied aircraft cabins.

The current study presents a brief summary of existing literature on protection provided by the surgical and respirator masks against the infectious agents. The effect of personalized ventilation used in aircraft cabins, commonly known as gasper on the inhalation of infectious agents will be investigated in future.

### 2.4.1 Effectiveness of Masks against the Infectious Agents

Masks are equipped with filters that purify the air passing them. It can be used to filter the air exhaled by an infected wearer (surgical masks) or to filter the air inhaled by

the wearer (respirator mask). In both the cases, the role of masks is to bring down the level of contaminants in the inhaled air of the occupants.

The current study reviewed the investigations on the performance of surgical and respirator masks, when used to filter the air inhaled by the wearer. The performance or effectiveness of a mask is defined by the amount of contaminants present in the inhaled air relative to the amount of contaminants in the surrounding air. The air inhaled by the wearer can come through the filter (gets purified) and face seal (leakages, not purified). Thus the level of protection provided by a mask depends on the filtration performance and the amount of leakages from the face seal. The filtration performance of a mask can vary with the particle size, particle type, and the flow velocities.

National Institute of Occupational Safety and Health (NIOSH) has standard test protocols for testing the filtration performance of respirator masks and certifying them. Respirator masks are rated as N, R, or P for protection against oils. N stands for not resistant to oil, R if somewhat resistant to oil and P for strongly resistant to oil. They also have a filtration rating, tested for most penetrating particle size. The ratings are 95, 99 or 100 and indicate that the mask filtered out 95%, 99% or 99.97% of airborne particles with most penetrating size. The N-95 is the most popular and widely available mask.

For the surgical masks, the FDA recommends (FDA, 2004) the particulate filtration efficiency (PFE) and bacterial filtration efficiency (BFE) tests (Oberg and Brosseau, 2008). Oberg and Brosseau, (2008) found that particle penetration through the surgical masks when tested using the NIOSH or Occupational Safety and Health Administration (OSHA) protocol is much higher than the PFE and BFE tests. Grinshpun et al., (2009), Lee et al., (2008) and Oberg and Brosseau, (2008) tested the surgical masks and found that the total penetration through the mask ranges from 10-50% and is way higher than the commonly used respirator mask (N-95). Therefore the current survey is focused on the studies on evaluating the performance of N-95 masks.

NIOSH certifies the N-95 masks by testing them against NaCl particles with mass median diameter of 300 nm (most penetrating particle size) at a constant flow rate of 85 l/min (Code of Federal Regulation Title 42, 1994). They use scanning and differential based particle sizer. As these tests are performed under specific conditions, the scientific community in the area raised following concerns

1. Particle Size and type: Do NaCl particles of size of 300 nm have the most penetration among the wide range infectious agents and droplets exhaled by an infectious occupant?
2. Flow conditions: Does a constant flow rate of 85 l/min represent the realistic inhalation transience?
3. Instrumentation: Is the instrumentation used accurate enough to capture all the particle sizes?
4. Human subjects versus manikins or Portacount: What will be the filtration capacity if human subjects are used?
5. Leakages: How much is the leakage from the face seal?

To investigate these concerns a comprehensive review was performed.

Particle Size and type: The size of infectious viruses and bacteria range from 0.08 to 0.14  $\mu\text{m}$  (Ksiazek et al., 2003 and Mandell et al., 1995) and 0.6 to 1.5  $\mu\text{m}$  (Nevalainen et al., 1993) respectively. The size of droplets carrying these agents can vary with the

exhalation process. The droplets exhaled during coughing, breathing, and talking range from 0.62 to 15.9  $\mu\text{m}$  (Yang et al., 2007), 0.3 to 5  $\mu\text{m}$  (Fabian et al., 2008), and 1 to 100  $\mu\text{m}$  (Duguid, 1946) respectively. The particle size associated with infectious agents or the droplets thus range from 0.08 to 100  $\mu\text{m}$ . It is required to investigate if the NaCl particles of size 0.3  $\mu\text{m}$  have the most penetration for this range. Balazy et al., (2006) evaluated the performance of N-95 masks against the MS2 virus (similar to pathogens) of size 10 to 80 nm. The filter penetration was found to be less than 7%. Brosseau et al., (1997) tested 16 respirator masks against the 0.55  $\mu\text{m}$  latex sphere and Mycobacterium Abscessus and found that the median penetration of the particle was 2, 0.4 and 0.02% for dust mist, dust fume mist and high efficiency particulate air filter. Qian et al., (1998) tested three N95 masks from different manufacturers against NaCl particles of size 0.1 to 1  $\mu\text{m}$  and bacteria of shape and size similar to Mycobacterium Tuberculosis (B. Subtilis and B. Megatherium, size 1-2  $\mu\text{m}$ ). They found that the penetration through the N95 masks was well below 5% against all the particles. Willeke and Qian, (1998) also had similar conclusions. Coffey et al., (1999) tested 21 models of N95 masks against ambient particles and indicated that the penetration from the masks can go as high as 16% under fit testing. Balazy et al., (2005) found that the penetration through the N95 masks for the NaCl particles ranging from 0.01 to 0.6  $\mu\text{m}$  was less than 7%. They found that most of the penetration takes place at around 0.04 to 0.05  $\mu\text{m}$  size. Rengasamy et al., (2008) tested five models of N95 masks against silver and NaCl particle of size 0.004 to 0.03  $\mu\text{m}$  and 0.02 to 0.4  $\mu\text{m}$  respectively and found that they provide expected level of protection. Lee et al., (2008) found that the penetration of particles of size 0.04 to 1.3  $\mu\text{m}$  for the four models of N95 masks tested could be more than 10% in some cases. But this also includes the leakages that might be taking place through the face seal. Eshbaugh et al., (2009) tested the N95 masks particles of size 0.02 to 2.9  $\mu\text{m}$  and found that the mask provided expected level of protection under constant flow rate of 85 l/min. The studies covered the range of particle from 4 nm to 3  $\mu\text{m}$ . The most penetrating size was found to lie in the range of 20 to 60 nm. It was found that the penetration from the filter for most of the masks was below 5% but can go up to 10% even under tight fit testing. It is hard to comment if the particle type had any influence but the penetration for all the biological and non-biological particle remained below 10%.

**Flow conditions:** The penetration through the masks increases with increase in flow rate (Eshbaugh et al., 2009; Balazy et al., 2005 and Brosseau et al., 1997). The normal breathing minute volume and peak flow rate range from 4 to 16 liter and 10 to 50 l/min respectively (Gupta et al., 2009), which is lower than the flow rate of 85 l/min at which NIOSH certifies the masks. Therefore for normal breathing, penetration would be less than the penetration predicted by the NIOSH test for the particle size. But during heavy breathing the peak velocities may be high. Eshbaugh et al., (2009) found that under cyclic breathing and constant flow conditions the penetration through most of the N95 masks was below 10% even for flow as high as 360 l/min. Balazy et al., (1995) and Brosseau et al., (1997) tested N95 masks at lower flow rate and found that the penetration was well below 5%. In summary, under the normal breathing conditions the penetration was well below 5%.

**Instrumentation:** Researchers have used different instrumentation for measuring the particle concentrations to evaluate the filtration performance of the masks. Appropriate care must be taken to understand the filtration performance values as these

instruments could measure a limited range of particle size. Eninger et al., (2008) pointed out that the TSI portacount (instrument deployed by NIOSH) can capture diameters of size 100 nm or more. In order to measure the nano size particles, Anderson seven stage sampler (Brosseau et al., 1997) or the differential mobility analyzer and condensation particle counter (Balazy et al., 2006) can be used. Therefore, the penetration predicted by NIOSH does not include the penetration of particle below 100nm.

Human Subjects versus manikin: The masks are usually tested either by putting them on human subjects (Coffey et al., 1999 and Grinshpun et al., 2009), manikins (Balazy et al., 2005 and Cho et al., 2009), or doing a fit testing where it is tightly fitted (Coffey et al., 1999 and Rengasamy et al., 2008) and the particle concentration on both the sides of the filter is measured. The fit test can account for the filtration penetration but not the leakages. Masks tested on manikin under realistic breathing profile may account for total penetration but may not reflect the realistic fitting with the face (Eninger et al., 2008). Therefore the masks tested on human subjects can only provide a realistic estimation on total penetration (Eninger et al., 2008).

Leakages: The ambient contaminant can enter through the masks from the gaps between the face and the masks (Coffey et al., 1999) in addition to through the filter. Therefore the total penetration could be higher than the penetration from the filter material. Coffey et al., (1999) have performed tests on human subjects and found out that the average penetration without fit testing was 33%, while with fit testing it was 4%. This clearly indicates that the face seal leakages could be way higher than the filter penetration. Recent study by Grinsphun et al., (2009) on human subjects found that the face seal leakages from the N-95 respirators ranged from 2 to 7%, while the penetration from the filter was less than 1% for particle size range 0.04 to 1  $\mu\text{m}$ . Cho et al., (2008) performed similar studies using manikins for particle size range 0.85 to 4  $\mu\text{m}$  under cyclic breathing. He found that the penetration from the face seal could be 2 to 8 times the filter penetration. Though the penetration was less than 1.2%, which could be due to the higher particle sizes and manikins. In addition to face seal, there could be leakages from the exhalation valve seal provided in some of the N95 masks. Lee et al., (2008) conducted the total penetration tests on human subjects using the OSHA protocol and found that the masks with and without the valve have the same performances. They also found that the total penetration can be higher than 10% for particle size range of 0.04 to 1.3  $\mu\text{m}$ .

In a nutshell, the total penetration through the mask for the particle size of ranging from 0.04 to 4  $\mu\text{m}$  was 10% for most of the N-95 masks under normal breathing conditions. Though some of the measurements have indicated average total penetration of 33%, which could be due to very poor fitting of the masks. Thus for the further analysis, we considered the penetration from the masks including the face seal leakages to be 10%.

## 2.5 Summary

There is no comprehensive analysis on exhalation and inhalation during coughing, breathing, and talking that can provide boundary conditions for the CFD simulations. The CFD simulations are highly sensitive to the boundary conditions and need information on thermo-fluidic boundary conditions for these exhalations/inhalations to accurately predict the infectious agent transport. It is thus required to characterize the flow dynamics of

these exhalations/inhalations. Therefore our investigations were first focused on developing exhalation/inhalation models to provide flow boundary conditions for coughing, breathing and talking by conducting experiments with human subjects.

There are a number of studies on transport of contaminants in aircraft cabins. These studies provided good insight on the airflow and contaminant transport but have their pros and cons. In most of the studies only a few rows (3-5 rows) wide domain is investigated. But Mazumdar and Chen (2008) and Olsen et al. (2003) have pointed out that the infection can spread up to 7-13 rows. Some of the investigations were performed on an empty cabin but Singh et al. (2002) pointed out that the occupancy and associated thermal load need to be considered to accurately predict the contaminant transport. Most of these studies have assumed the exhalation and inhalation boundary conditions for various respiratory events. In some of the investigations, Eulerian method was used to predict the infection transmission but Lagrangian method can provide better results under transient conditions (Zhang and Chen, 2007c). Thus, this study further investigated the expiratory droplet transport in an aircraft cabin with passengers using the exhalation/inhalation boundary condition developed in the first phase and appropriate turbulence, dispersion and evaporation models.

As the infectious (index) passenger can release the contaminants through a number of exhalations during his air travel, it is required to develop methods to predict the spatial and temporal distribution of expiratory droplets and the amount of such droplets inhaled by the passengers for realistic flight times. It is also required to evaluate the spatial and temporal distribution of risk of infection in an aircraft cabin. We extended the information obtained from the four minutes of CFD simulations of expiratory droplet transport from a single exhalation to realistic flight duration and quantified the risk of infection.

Studies on evaluating the performance of masks have indicated that the total penetration from the masks for the virus, bacteria and droplet size range was 10%. This could be helpful in reducing the risk of infection. Therefore the risk of infection for a scenario with passengers wearing masks should be evaluated. We quantified the reduction in risk if masks are used by the passengers.

### 3. FLOW CHARACTERIZATION OF A COUGH

Coughing is defined as a violent release of air from the lungs following the opening of the glottis. It is a pulse process and lasts for just a fraction of second. But it has a much higher velocity and droplet concentration, which makes it the prime source for introducing infectious agents.

In this chapter, first the experimental methods to measure the flow rate, flow direction and area of opening of mouth of a cough are discussed. The results obtained on these measured parameters are then discussed. A set of simple equations is developed that can be used to generate boundary conditions for the flow rate, direction, and area of mouth opening for a cough. As has been mentioned earlier, the boundary conditions should also include the exhaled air temperature and droplet distribution; hence appropriate models from literature are identified for them.

#### 3.1 Measurement Methods

The present study measured flow rates, flow directions and mouth opening areas of coughs. A Spirometer based on Fleish type pneumotachograph (Sancho et al., 2004 and Bongers and O'Driscoll, 2006) was used to measure the cough flow rates generated over time with a frequency of 330 Hz. The Spirometer is consisted of numerous capillary tubes in parallel and gives the flow proportional to the pressure drop. It is based on Poiseuille's Law, which states that, under capillary conditions, in a straight rigid tube, flow is proportional to pressure loss per unit length. The flow directions were visualized through moderate-speed photography (120Hz) with 1 Mega Pixel resolution. Cigarette smoke was used as seeding fluid. The cigarette smoke particle size is about 0.2  $\mu\text{m}$  (Klepeis and Nazaroff, 2002) in diameter and the measured temperature of the cigarette smoke was close to exhaled air temperature. Thus the exhaled smoke jet should closely follow the cough air jet profile. The mouth opening areas were measured through the moderate speed photography (120Hz). All the measurements were conducted with vertical head posture as shown in Fig. 3.1. The head posture may affect the flow rate and flow direction in particular. But as the velocities during a cough are high, gravity effects may be negligible and the direction with respect to mouth may not change significantly.

All the measurements were performed over 12 female and 13 male subjects to obtain realistic flow features with an approval from the Institutional Review Board for human subject experimentation. Normal healthy subjects were recruited for the study. The subjects were first given an overview of the research and were told about the risk involved in the measurements. Every subject signed a consent form before proceeding for the measurements.

The flow rate measurements were done by placing a mask on subject's face. The mask had ports for mouth and nose and the ports were connected to a filter then further to the Spirometer as shown in Fig 3.1.



*Figure 3.1 Subject with a mask holding the Spirometer during test.*

Two types of flow measurements, single cough and sequential cough, were conducted. The single cough coughed just once while sequential cough coughed twice. Each test was repeated three times for every subject.

The flow visualization study was performed on smoker subjects. A light source was placed beneath a subject face to throw light upwards. The light source along with a dark background helped the flow visualization. The subjects were asked to exhale smoke out through coughing. The measurements of mouth opening area were performed over 8 male and 8 female subjects. The subjects were asked to cough and the front views close to their lips were captured for the whole event.

## 3.2 Results

This section presents the experimental results on cough flow dynamics obtained from this investigation.

### 3.2.1 Flow Rate of a Cough

The flow rate characterization of a cough is to develop a simple mathematical model describing the boundary conditions for CFD simulations.

#### Single Cough

Fig. 3.2 shows the flow rate generated from a typical cough over time from a subject. The results indicate that the cough began with a very short inhalation (<1% of the total exhaled air volume), a very high acceleration afterwards in exhalation and subsequently a decay. The inhalation volume was very small and may be neglected.

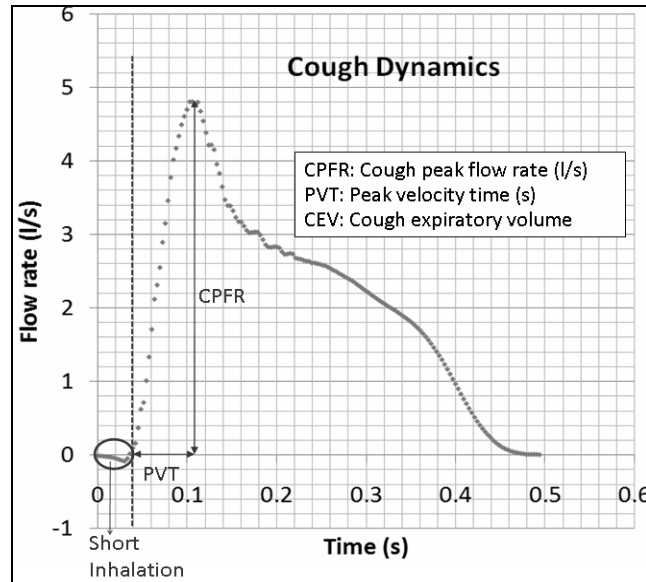


Figure 3.2 Cough flow rate variation with time.

Figure 3.3 illustrates the transient flow of a cough for all the subjects studied. A large variation existed among the subjects. For example, the difference between the maximum and minimum values of CPFR, CEV and PVT for the male subjects is about 200%, 300% and 100% respectively. Table 3.1 summarizes the variation range of the CPFR, PVT and CEV for the subjects. Thus, neither the cough flow characteristics from a subject can be used to represent the whole population, nor a standard cough exists.

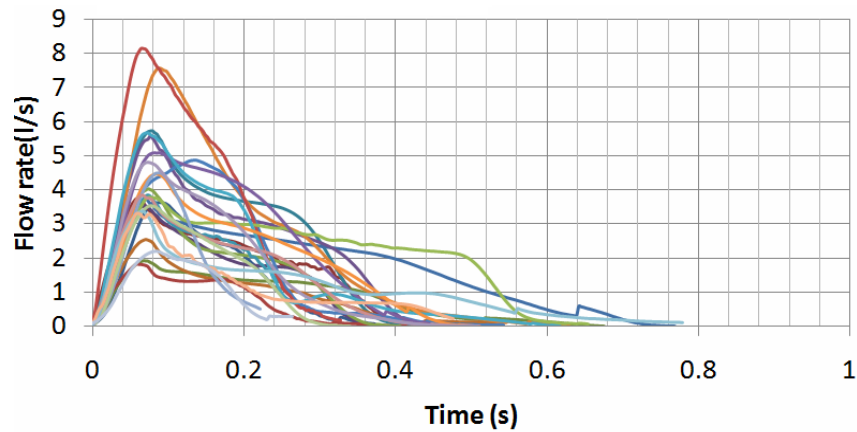


Figure 3.3 Cough flow rates for the 25 subjects.

Table 3.1 Variation observed in cough flow characteristics.

	Male	Female
CPFR	3 - 8.5 l/s	1.6 - 6 l/s
CEV	400-1600 ml	250-1250ml
PVT	57 - 96 ms	57 - 110 ms

To describe the flow characteristics, this study used non-dimensional parameters. The dimensionless flow rate is defined as:

$$\overline{M} = \frac{\text{Flowrate}}{\text{CPFR}}. \quad (3.1)$$

The dimensionless time is defined as:

$$\tau = \frac{\text{Time}}{\text{PVT}}. \quad (3.2)$$

Figure 3.4 is exactly the same as Fig. 3.3 but in non-dimensional form. With the re-arrangement, one can see that when  $\tau < 1.2$  all the curves are coincident. After that time the variation existed but the trend looks similar. Moreover, it can be seen that the dimensionless flow rate variation with time closely follows a gamma probability function till about 1.2 dimensionless time. Also, it was found that by superimposing another gamma probability distribution function, the inflation zone including the cough flow rate decay can be captured.

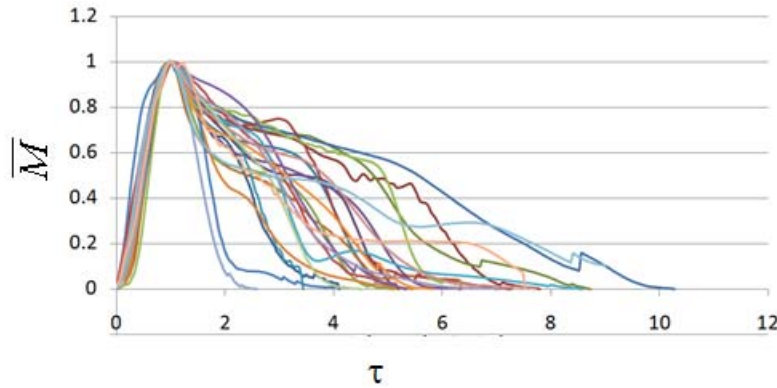


Figure 3.4 Dimensionless cough flow rates from the 25 subjects.

Equations (3.3) and (3.4) show these functions. The dimensionless flow rate for dimensionless time less than 1.2 is given by:

$$\overline{M} = \frac{a_1 \tau^{b_1-1} \exp(-\tau/c_1)}{\Gamma(b_1) c_1^{b_1}} \quad \text{for } \tau < 1.2. \quad (3.3)$$

The dimensionless flow rate for dimensionless time greater than 1.2 is given by:

$$\overline{M} = \frac{a_1 \tau^{b_1-1} \exp(-\tau/c_1)}{\Gamma(b_1) c_1^{b_1}} + \frac{a_2 (\tau - 1.2)^{b_2-1} \exp(-(\tau - 1.2)/c_2)}{\Gamma(b_2) c_2^{b_2}} \quad \text{for } \tau > 1.2. \quad (3.4)$$

Eq. (3.3) for  $\tau < 1.2$  that contains only CPFR and Eq. (3.4) for  $\tau \geq 1.2$  that contains CPFR, PVT and CEV. Finally, a non linear least square curve fitting analysis was performed in MATLAB to obtain the optimum values of the variables required to define the gamma probability distribution function for each cough and are given by:

$$\begin{aligned}
 a_1 &= 1.680, \\
 b_1 &= 3.338, \\
 c_1 &= 0.428, \\
 a_2 &= \frac{CEV}{PVT \times CPFR} - a_1, \\
 b_2 &= \frac{-2.158 \times CEV}{PVT \times CPFR} + 10.457, \\
 c_2 &= \frac{1.8}{b_2 - 1}.
 \end{aligned}
 \tag{3.5}$$

Fig. 3.5 compares the measured flow rate with the fitted one obtained from equations (3.3) and (3.4) for a subject. Such a good agreement was found for all the subjects.

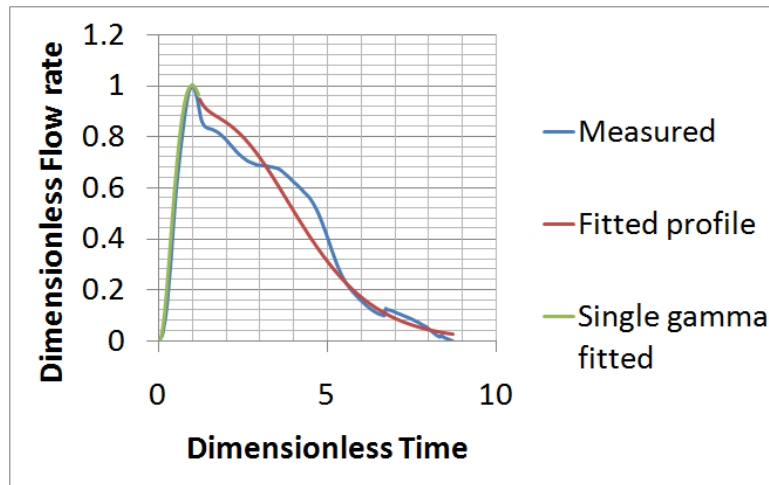


Figure 3.5 Comparison of the flow rate calculated by Eqs. (3.3) and (3.4) for a single cough from a subject with the measured data.

Please note that the CPFR, PVT and CEV are unknown for a new subject. In order to apply the two equations to a new subject, it is essential to link these variables to the subject's characters, such as height, weight, and gender. Our regression analysis by the solid lines shown in Fig. 3.6 indicates that these medical parameters were inter-related. Figs. 3.6(a) and 3.6(b) show the variation of the CEV with the CPFR for the male and female subjects, respectively. The figures show a positive correlation between all the parameter ( $r > 0.5$ ,  $p < 0.005$  for all). Since the CEV increases with the CPFR, this implies that the higher the peak flow rate the higher would be the total volume exhaled. The CPFR for the female subjects were lower than that for the male subjects. Mahajan et al.

(1994) proposed using a single equation to correlate the CEV with the CPFR for both genders. As shown in Fig. 3.6, their regression lines deviate significantly from our data. Our two regression lines that distinguish the genders fit the best to the data.

Similarly, Figs. 3.7(a) and 3.7(b) show the variation of the PVT with the CPFR for the male and female subjects, respectively. The results again indicate that the PVT increased with the CPFR. The PVT for the female subjects was higher than that for the male subjects. This could be attributed to the difference in their larynx sizes as indicated by Singh et al. (1995). The slope of the PVT versus the CPFR variation is similar to that obtained by him, but the intercept is higher by about 50 ms in our measurements. Our measurements were performed at 330 Hz and can capture the initial period, which could have got missed out in previous studies.

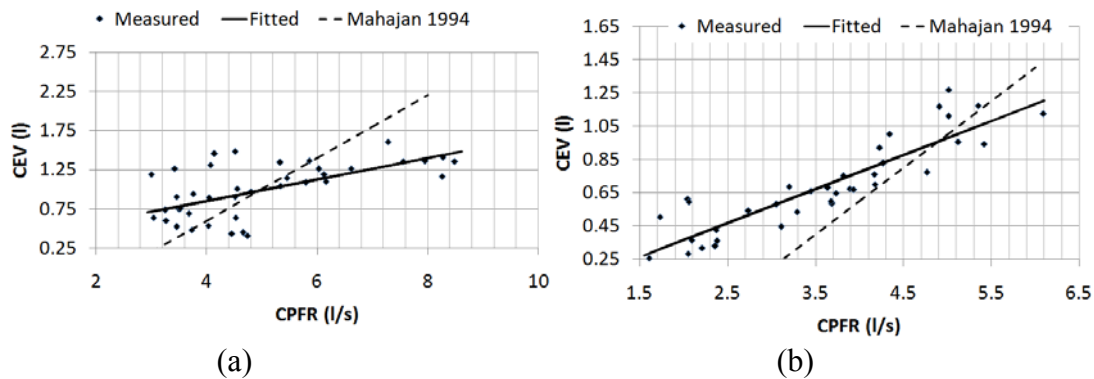


Figure 3.6 The relationship between CEV and CPFR for (a) male and (b) female subjects.

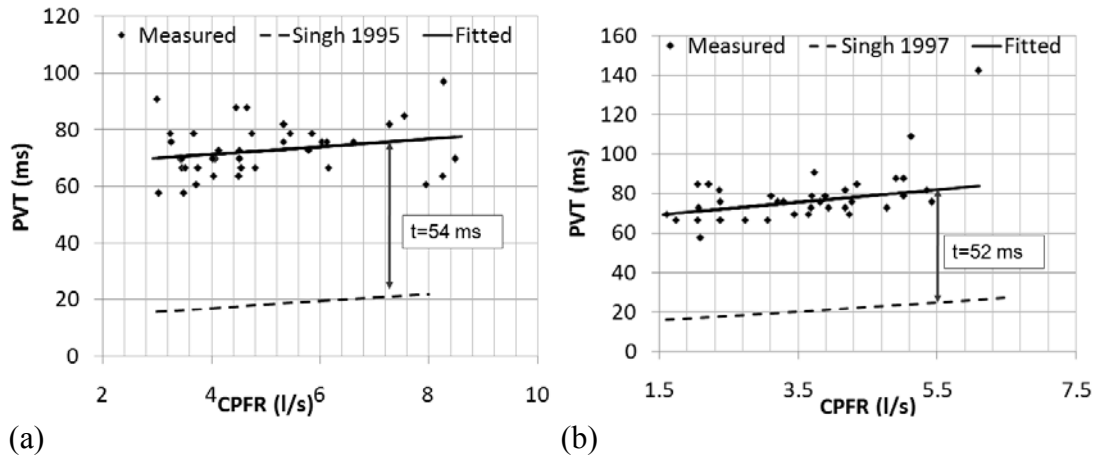


Figure 3.7 The relationship between PVT and CPFR for (a) male and (b) female subjects.

The cough expired volume (CEV) for male subjects can be written as:

$$CEV(l) = 0.138CPFR(l/s) + 0.2983. \quad (3.6)$$

The cough expired volume (CEV) for female subjects can be written as:

$$CEV(l) = 0.204CPFR(l/s) - 0.043. \quad (3.7)$$

The peak velocity time (PVT) for male subjects can be written as:

$$PVT(ms) = 1.360CPFR(l/s) + 65.860. \quad (3.8)$$

The peak velocity time (PVT) for female subjects can be written as:

$$PVT(ms) = 3.152CPFR(l/s) + 64.631. \quad (3.9)$$

With the two sets of equations and the CPFR, one can determine the cough flow rate over time by Eqs. (3.3) and (3.4). By using our data and multiple regression analyses, this study found that the CPFR depends mainly on subject height. For the male subjects, the subject weight has some impact on the CPFR as well. The regression analyses lead to the following two equations for calculating the CPFR from the height and weight of a subject. For male population the regression equation is given by:

$$CPFR(l/s) = -8.8980 + 6.3952h(m) + .0346w(kg). \quad (3.10)$$

For female population the regression equation can be written as:

$$CPFR(l/s) = -3.9702 + 4.6265h(m). \quad (3.11)$$

The two equations can calculate the CPFR with an error no greater than 20% by comparing it with the data in our database. The equations indicate that the CPFR increases with the height and weight of the subject.

Thus, from the physiological information such as the height, weight, and gender, the CPFR can be calculated using equations (3.10) and (3.11). The CEV and PVT can be calculated from the CPFR using equations (3.6) to (3.9). With the CPFR, CEV and PVT, the dimensionless flow rate can be obtained from equations (3.3) and (3.4). Equations (3.1) and (3.2) can be utilized to convert the dimensionless flow rate into the dimensional one. Hence, the flow rate over time for a single cough can be obtained from the physiological information.

### Sequential Cough

A sequential cough is defined one cough followed immediately by the other. Fig. 3.8 shows the flow generated for a sequential cough from a subject. The flow behavior for the two coughs in the sequential cough was similar to that of a single cough and can also be described by equations (3) and (4). The first cough closely followed the features of a single cough while the second one was a scaled down of the first one. Tables 3.2 and 3.3 compare the sequential coughs with the single coughs from the male and female subjects, respectively. The PVT for the two coughs in the sequential coughs was approximately the same as that of the single coughs while the CPFR and CEV for the second cough were approximately 0.5-0.6 times of the single coughs.

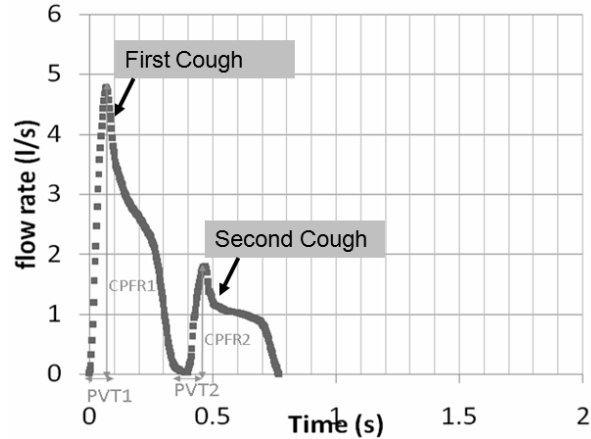


Figure 3.8 Flow rate over time for a sequential cough from a subject.

Table 3.2 Relationship between sequential and single coughs for male.

	correlation with Single cough								
	CPFR			PVT			CEV		
	r	P	correlation	r	P	correlation	r	P	correlation
First cough	0.77	<.001	1.008*CPFR	0.58	<.001	1.105*PVT	0.6	<.001	0.8184*CEV
Second Cough	0.53	<.001	0.602*CPFR	0.33	<.001	0.9568*PVT	0.45	<.001	0.602*CEV

Table 3.3 Relationship between sequential and single coughs for female.

	correlation with Single cough								
	CPFR			PVT			CEV		
	r	P	correlation	r	P	correlation	r	P	correlation
First cough	0.8	<.001	1.038*CPFR	0.7	<.001	1.107*PVT	0.63	<.001	0.8613*CEV
Second Cough	0.7	<.001	0.6335*CPFR	0.51	<.001	0.8697*PVT	0.55	<.001	0.5294*CEV

Thus, the CPFR, PVT and CEV for the first cough can be obtained from equations (3.6) to (3.11), while those for the second cough should be corrected with Tables 3.2 and 3.3. The flow rate can then be obtained by equations (3.3) and (3.4) for the two coughs.

### 3.2.2 Flow Direction of a Cough

The flow direction of a cough was obtained from flow visualization. Figure 3.9 shows the sequence of images taken at 120 Hz for a typical cough process from  $t=0$  to  $36/120$  seconds. The first three images were for  $t=0$  to  $3/120$  seconds, when the mouth was closed. Then the images were from  $t=9/120$  to  $36/120$  seconds at an interval of  $1/120$  seconds. At  $t=9/120$  seconds, the mouth completely opened up but the smoke came out after  $t=11/120$  seconds.

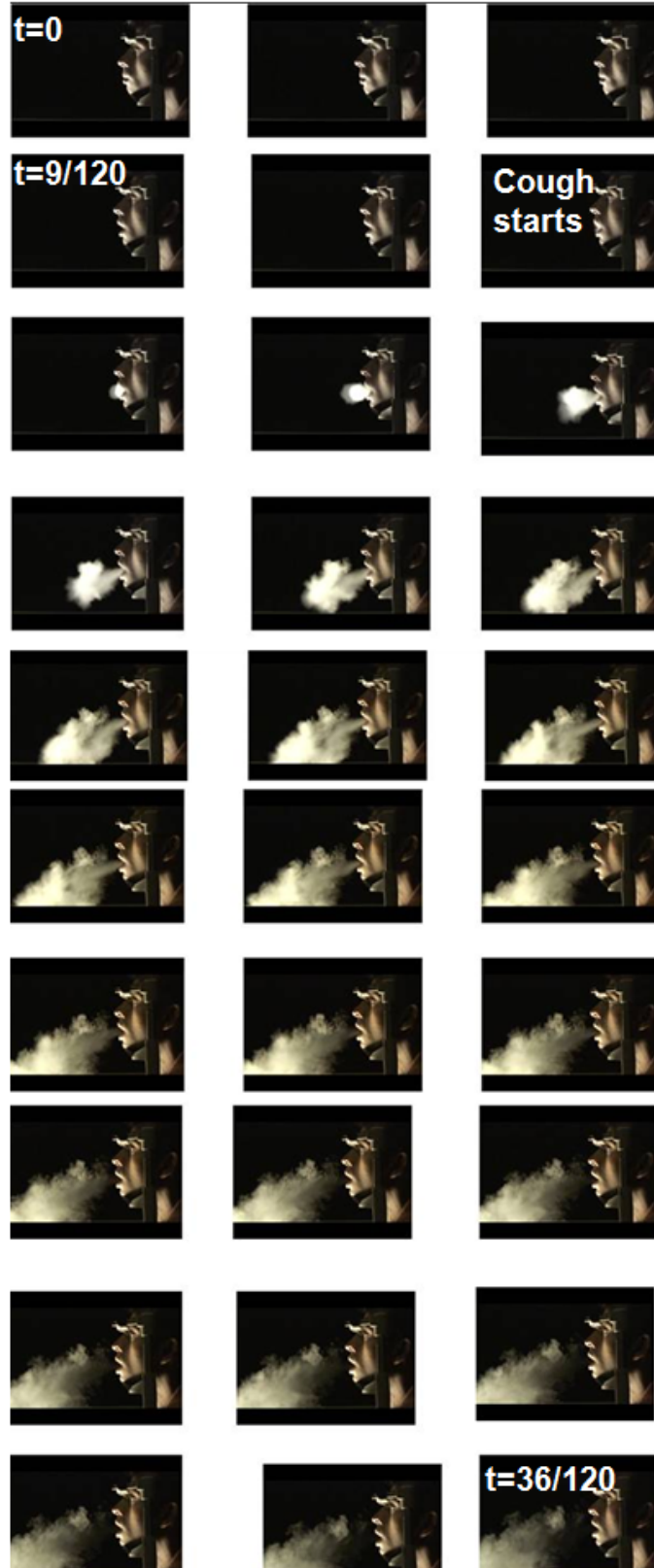


Figure 3.9 The side view of a cough process recorded with a frequency of 120 Hz.

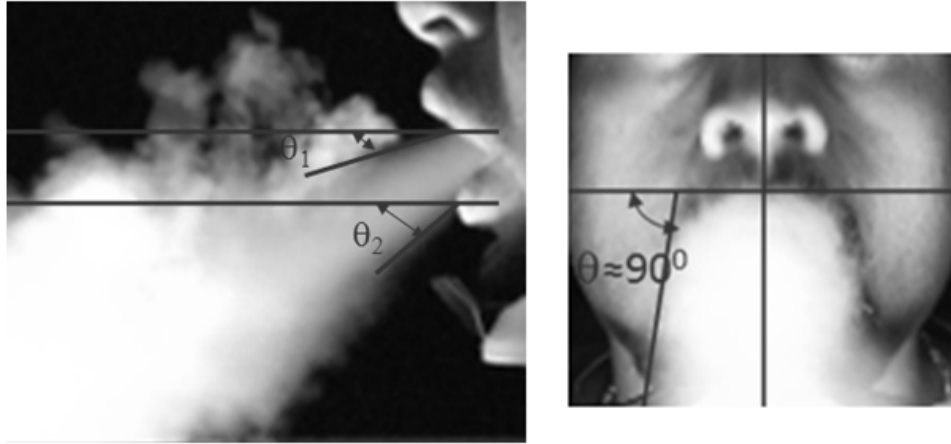


Figure 3.10 The cough jet direction from the side and front views.

The downward jet can be defined with two angles,  $\theta_1$  and  $\theta_2$ , as shown in Fig. 3.10. The jet has negligible spread in this view. Fig. 3.11 shows little variation in the cough angles for all the subjects. The 95% confidence bounds for the mean angles can be determined by:

$$\theta_1 = 15^\circ \pm 5^\circ, \quad (3.12)$$

and

$$\theta_2 = 40^\circ \pm 4^\circ. \quad (3.13)$$

The two mean angles can be used as boundary conditions for CFD modeling.

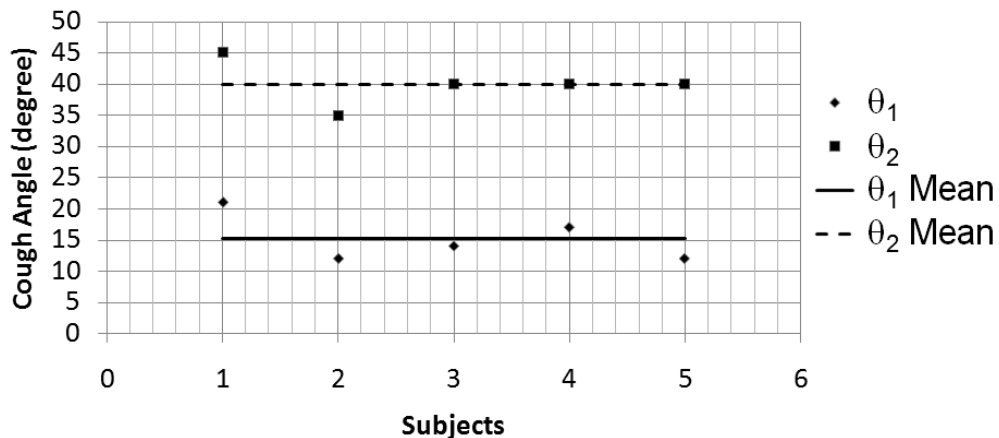


Figure 3.11 Variation in the two Cough angles among all the subjects.

### 3.2.3 Mouth Opening Area

The mouth opening area is defined as the area between the lips during a cough. Figure 3.9 shows the sequence of images during a cough. Initially the mouth was closed

and then opened up fully at  $t=9/120$  seconds. The mouth remained opened for the rest of the cough process. This can be further confirmed from the images of the front view for all the subjects. Fig. 3.12 shows the mouth opening area over time for a subject. It can be seen that the mouth opening area was almost constant when there was flow from the mouth.

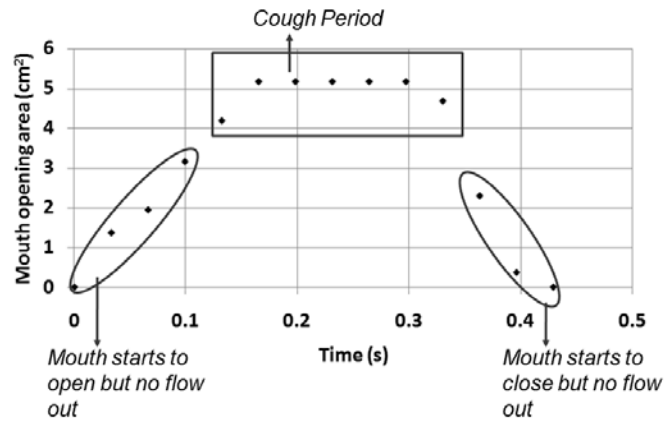


Figure 3.12 Change of mouth opening area during a cough.

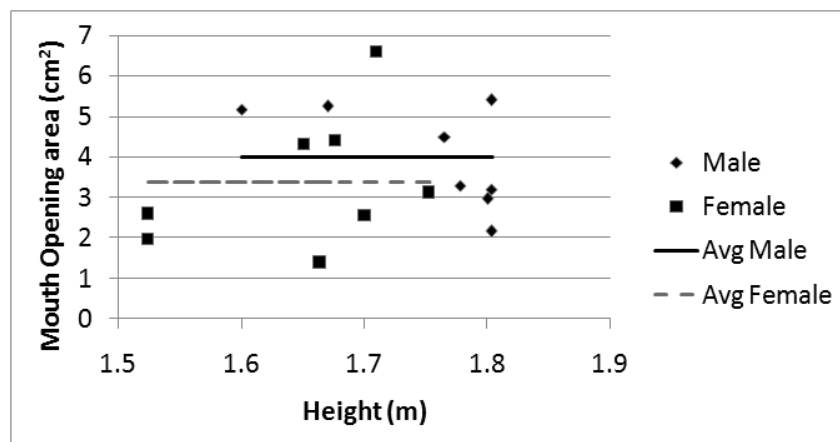


Figure 3.13 Variation in mouth opening area during a cough with the heights of all the subjects.

Fig. 3.13 shows the variation in mouth opening area during a cough with the heights of all the subjects. But the figure does not indicate any clear trend. Hence this study proposed to use an average value. The mean mouth opening area for the female subjects was smaller than that of the male subjects. The mouth opening area for the male subject is given by:

$$\text{Mouth Opening Area} = 4.00 \pm 0.95 \text{ cm}^2. \quad (3.14)$$

For female subjects it is given by:

$$\text{Mouth Opening Area} = 3.37 \pm 1.40 \text{ cm}^2. \quad (3.15)$$

### 3.3 Discussion

This investigation has developed a set of simple equations that can be used to generate boundary conditions (or a source model) for predicting infectious virus transport by CFD due to coughing. Our effort focused on the flow rate, flow direction, and air velocity that can be determined from flow rate and mouth opening area. The inputs required are height, weight, and gender of a person.

The boundary conditions required by CFD simulations should also include the temperature of the exhaled air and the droplet distribution. The study by Hoppe (1981) can be utilized to obtain the exhaled air temperature under various ambient temperature and humidity. He found that ambient temperature is the most influential parameter. There are a few studies on cough droplet size measurements (Duguid, 1946; Fairchild and Stampfer, 1987; Papineni and Rosenthal, 1997; Fennelly et al., 2004; Yang et al., 2007; Hersen et al., 2008; Chao et al., 2009 and Morawska et al., 2009). The measurements were done over healthy subjects (Duguid, 1946; Fairchild and Stampfer, 1987; Papineni and Rosenthal, 1997; Yang et al., 2007; Hersen et al., 2008; Chao et al., 2009 and Morawska et al., 2009) and the subjects infected by TB (Fennelly et al., 2004) and with cough and cold (Hersen et al., 2008). The latest measurements (Yang et al., 2007; Hersen et al., 2008) indicated that the droplet concentration was of the order of  $10^6$  and the size varied from 0.1 to 10  $\mu\text{m}$ . The study by Yang et al. (2007) indicated a linear trend with mean cough flow rate. Hence by knowing the mean cough flow rate from our model, the droplet concentration can be obtained.

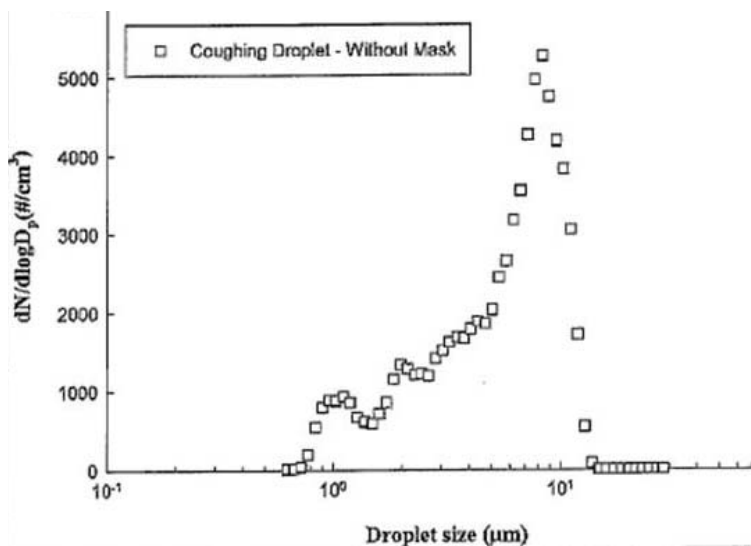


Figure 3.14 Droplet distribution for a cough (Yang et al., 2007).

### 3.4 Conclusions

In this section our efforts were focused on characterizing the flow behavior of cough. The flow rate, flow direction and mouth opening area were measured for 25 human subjects, which could be used as boundary conditions in CFD simulations.

The flow rate can be defined as a combination of gamma probability distribution functions. The variables in the functions can be represented by medical parameter i.e. CPFR, PVT and CEV. These medical parameters are related to the height, weight, and gender of a person.

A sequential cough was found to be the combination of two single coughs. The first one behaved approximately the same as that of a single cough, while the second one was a scaled down version of the first one.

The cough flow direction was visualized through the moderate speed photography using smoke. The flow direction did not vary very much among the subjects and can be determined by two angles.

The mouth opening area was constant during a cough. The mouth opening area varied among the subjects but without a clear correlation with the subject height. Hence this study proposed to use a mean mouth opening area during a cough.

#### 4. FLOW CHARACTERIZATION OF BREATHING AND TALKING

Breathing is defined as the regular intake of oxygen and outflow of carbon dioxide through the mouth or nose. As compared to coughing, which is pulse exhalation, breathing is periodic in nature. The process of talking on the other hand is highly nonspecific and can change significantly from person to person and per the matter of conversation. As conversations can be for minutes or hours, thus talking can be treated as a continuous process averaged over the time of the conversation. The flow rates in breathing and talking are lower when compared to coughing. But as they can have higher event frequency, its contribution in introducing the contaminants could be significant.

In this chapter, first, the experimental methods to measure the flow rate, flow direction and the area of opening of mouth/nose during normal breathing and talking are discussed. The results obtained from the experiments are then analyzed. A set of simple equations was developed to generate boundary conditions for the flow rate, direction, and the area of mouth/nose opening during breathing and talking. Similar to the study of the cough, the appropriate temperature and droplet models for breathing and talking are identified from the literature to generate boundary conditions for them.

##### 4.1 Measurement Methods

The present study measured flow rates, jet direction, and the area of opening of the mouth/nose for breathing and talking. The instrumentation, population, and research protocol were similar to cough measurements as has been explained in section 3. But the exercises that have been performed were different. The most common postures are sitting and standing; and the common routes of breathing are through the mouth and the nose. Thus the measurements were conducted with these variations, with a total of four sets of measurements, as described in Table 4.1.

*Table 4.1 Design of experiments for breathing.*

Organ	Posture
Mouth	Sitting
Nose	Standing

The flow rate measurements for talking consisted of three exercises. The first set was based on articulating letters from the alphabet. An alphabet set consists of 6 letters: F, E, C, O, S and T. F, S, and T were found to have the maximum exhalation flow rates, while E, C, and O are the most frequently used letters. Peak velocities of these measurements were analyzed. The second set of measurements was based on enunciating the numbers from one to ten. This was done to correlate the number of droplets with flow rates as the measurements on droplet sizes were done for this kind of exercise (Papineni and Rosenthal, 1997). The third set was based on the pronunciation of a reading rainbow passage (Fairbanks, 1940). This passage contains a mixture of oral and nasal consonants in the approximate proportion found in everyday speech (Seaver et al., 1991) and, hence,

provides a reflection of the possible combination of flow rates that can be found in a conversation. The airflow rates from both the subject's mouth and nose were recorded during this exercise.

## 4.2 Results

### 4.2.1 Breathing

In this section experimental results on normal breathing under various postures with mouth and nose are investigated. The normal breathing flow rate can be best represented by a sine wave for all the subjects, and for all the breathings shown in table 4.1, although the time of inhalation was shorter than that of exhalation. Fig. 4.1 shows the typical flow rate variation over time.

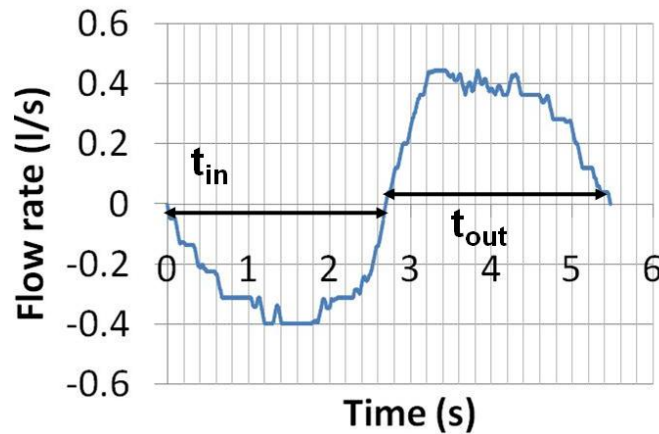


Figure 4.1 Flow generated over time for a subject for normal breathing.

The functional form of the flow rate during breathing can be expressed as:

$$\text{Flow Rate for Breathing} = a \sin(\beta t) \quad (4.1)$$

where,  $\beta$  and  $a$  can be calculated from Equations (4.2) – (4.4). As inhalation and exhalation time periods are different, subscript  $x$  can be replaced by “in” for inhalation and “out” for exhalation. The amplitude of the sine wave is given by:

$$a_x = \frac{\beta_x TV}{2}. \quad (4.2)$$

The tidal volume ( $TV$ ) is defined as:

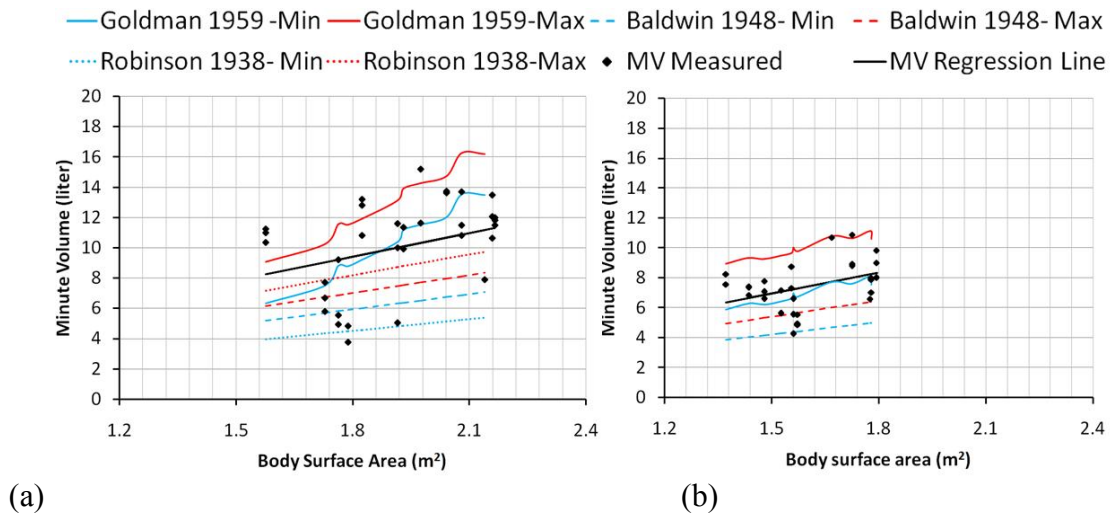
$$TV = \frac{MV (RF_{in} + RF_{out})}{2RF_{in}RF_{out}}. \quad (4.3)$$

The  $\beta$  is defined as:

$$\beta_x = \frac{\pi RF_x}{30}. \quad (4.4)$$

The MV and RF can vary with the subject, organ of breathing or human posture, and so will “a” and “β”. We conducted statistical tests to investigate the influence of organ of breathing and human posture on MV and RF. The RF and thus MV can change with the organ of breathing due to the differences in the routes of respiration (Douglas et al., 1983), but the hypothesis testing through the paired t tests indicated no significant differences in the current data. Human posture affects the activity of the abdominal muscle and thus may influence the breathing (Kera and Maruyama, 2005). The paired t test indicated no significant differences in the MV and RF due to the change in the posture. This is in agreement with studies by Kera and Maruyama, (2005). Therefore further analysis was performed on the nose breathing in sitting posture.

Our study indicated that the minute volume was proportional to the body surface area, which is in agreement with the literature (Goldman and Becklake, 1959; Baldwin et al., 1948, and Robinson, 1938). The body surface area can be obtained from the height and weight of a person (Gehan et al., 1970). Figs. 4.2(a) and (b) show the variation of minute volume with the body surface area of the male and female subjects, respectively. All the values lie between the confidence intervals from several previous studies. One of the main reasons for the wide spread could be the wide variation in ethnicity of the subjects in the current study. It was found that the minute volume for the female subjects was lower than that for the male subjects.



(a) (b)  
Figure 4.2 Variation of minute volume with the body surface area of (a) the male subjects and (b) the female subjects.

The relationship between the minute volume and the body surface area was obtained by a linear regression analysis. The correlation coefficient for both groups of the subjects was found to be more than 0.4 for a p less than 0.05. The relationship for the male and female subjects can be described by Equations (4.5) and (4.6) respectively.

For male population, minute volume ( $MV$ ) can be written as:

$$MV_{male}(\text{liter}) = 5.225 \times BSA(m^2). \quad (4.5)$$

For female population, minute volume ( $MV$ ) can be written as:

$$MV_{female}(\text{liter}) = 4.634 \times BSA(m^2). \quad (4.6)$$

The confidence interval for the slope for the male and female subjects was from 4.838 to 5.868 liter/m<sup>2</sup> and 4.421 to 5.16 liter/m<sup>2</sup>, respectively.

Figures 4.3(a) and (b) show the variation in respiratory frequency for the male and female subjects, respectively. The exhalation time was longer than the inhalation for both the genders. The multiple regression analysis showed that the respiratory frequency was mainly dependent on the height. With an increased height that may be associated with an increased lung capacity, the frequency would be decreased for the same minute volume. For the male subjects, a slight dependency on weight was also found. An increase in weight increased the frequency and, hence, reduced the time period of each breath. Therefore, a heavier person typically has a shorter breath. Equations (4.7) – (4.10) give the relationship between the respiration frequency and the physiological parameters for the male and female subjects.

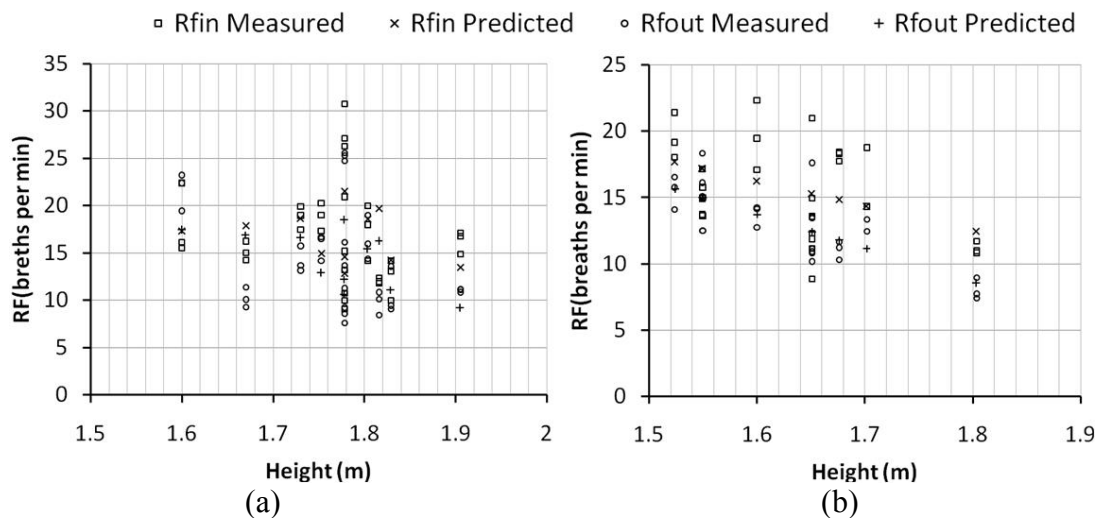


Figure 4.3 Variation of respiratory frequency for (a) the male subjects and (b) the female subjects.

### For Male

The obtained regression equation for respiratory frequency for inhalation is given by:

$$RF_{in} = 55.55 - 32.86 H(m) + 0.2602 W(kg). \quad (4.7)$$

The regression equation for respiratory frequency for exhalation is given by:

$$RF_{out} = 77.03 - 45.42H(m) + 0.2373W(kg). \quad (4.8)$$

#### For Female

Similarly for the female population, the equation for respiratory frequency for inhalation is given by:

$$RF_{in} = 46.43 - 18.85H(m). \quad (4.9)$$

The equation for respiratory frequency for exhalation can be written as:

$$RF_{out} = 54.47 - 25.48H(m) \quad (4.10)$$

where,  $RF$  is respiration frequency,  $H$  body height, and  $W$  body weight.

Thus, with physiological parameters of a person, the minute volume and respiratory frequencies can be obtained using equations (4.5) – (4.10). The amplitude and frequency of the breathing sine wave can then be calculated from the  $MV$ ,  $RF_{in}$ , and  $RF_{out}$  through equations (4.2) – (4.4). Finally the flow rate over time can be obtained with the “ $a$ ” and “ $\beta$ ” values via equation (4.1).

The nose breathing direction was investigated by visualizing the jets from the front and side views. The jets can be better defined with two angles from each view. Fig. 4.4 shows these views and the angles for one of the jets. The  $\theta_m$  and  $\phi_m$  are the mean side and front angle, while the  $\theta_s$  and  $\phi_s$  are the front and side spreading angle, respectively.



Figure 4.4 Angles needed to define the direction of a nose breathing jet.

The mean side and front angles did not vary much among the subjects as shown in Fig. 4.5. Hence, an average angle calculated from these mean angles could be used for the nose breathing direction. Equations (4.11) and (4.12) give a 95% confidence bound for the side and front mean angles. The mean side angle is given by:

$$\theta_m = 60^\circ \pm 6^\circ. \quad (4.11)$$

The mean front angle is given by:

$$\phi_m = 69^\circ \pm 8^\circ. \quad (4.12)$$

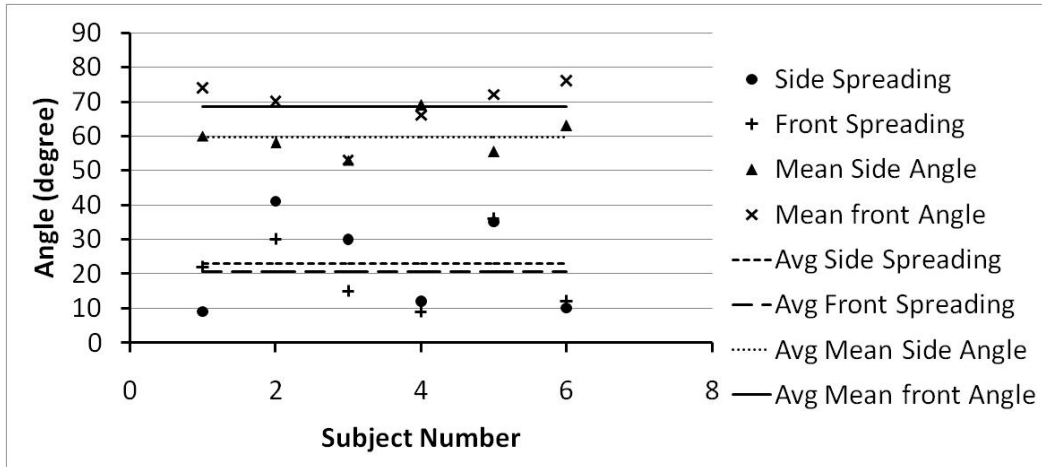


Figure 4.5 The mean angles for nose breathing.

Similar variation was observed for the spreading angle though there was variation among the subjects as shown in Fig. 4.5. Thus, averaged mean and spreading angles with 95% confidence bounds are proposed and are given by equations (4.13) and (4.14) respectively. The side spreading angle is given by:

$$\theta_s = 23^\circ \pm 14^\circ. \quad (4.13)$$

The front spreading angle is given by:

$$\phi_s = 21^\circ \pm 10^\circ. \quad (4.14)$$

Figure 4.6 shows a mouth breathing jet. The mouth breathing jet was discharged approximately in the horizontal direction with a spreading angle of  $30^\circ$ . Table 4.2 shows variations of the mouth breathing angles among the subjects.

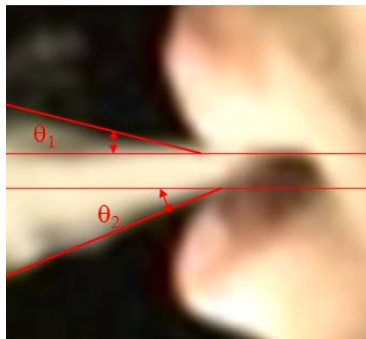


Figure 4.6 Visualization of a mouth breathing jet.

The mouth breathing jet was observed to have a negligible spread from the front and, hence, the side angle is deemed sufficient to define the direction of the jet. The side spread can be described by a single value:

$$\theta_s = 30^\circ. \quad (4.15)$$

Table 4.2 Variation in jet angle from mouth breathing among different subjects.

Subjects	$\theta_1$	$\theta_2$	Spreading angle $\theta_s (= \theta_1 + \theta_2)$
A	11	23	34
B	13	20	33
C	11	16	27
D	10	17	27

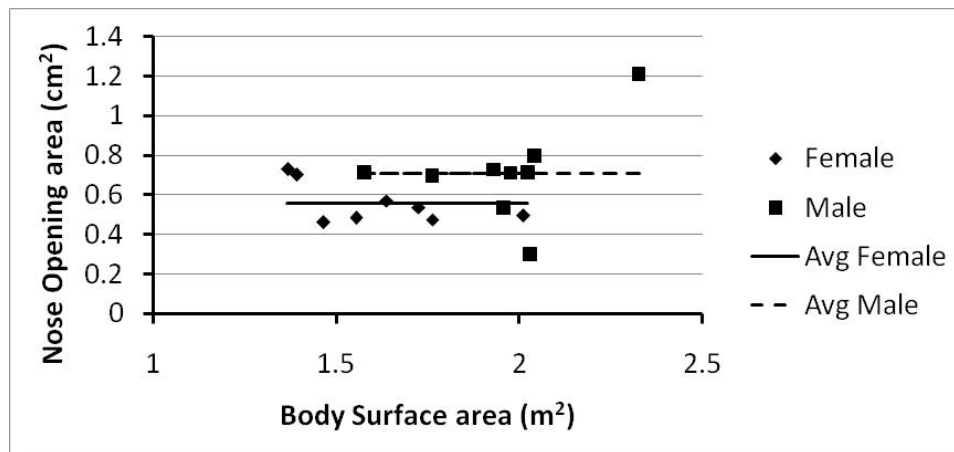
This investigation found that the nose opening area did not change during normal breathing for a subject but variation existed among some of the subjects as shown in Figure 4.7. The mean nose opening area for the female subjects was smaller than that of the male subjects. Equations (4.16) and (4.17) give the mean nose opening area with 95% confidence bounds for the male and female subjects respectively.

The mean nose opening area for male subjects is given by:

$$\text{Mean Nose Opening Area} = 0.71 \pm 0.23 \text{ cm}^2. \quad (4.16)$$

The mean nose opening area for female subjects is given by:

$$\text{Mean Nose Opening Area} = 0.56 \pm 0.10 \text{ cm}^2. \quad (4.17)$$



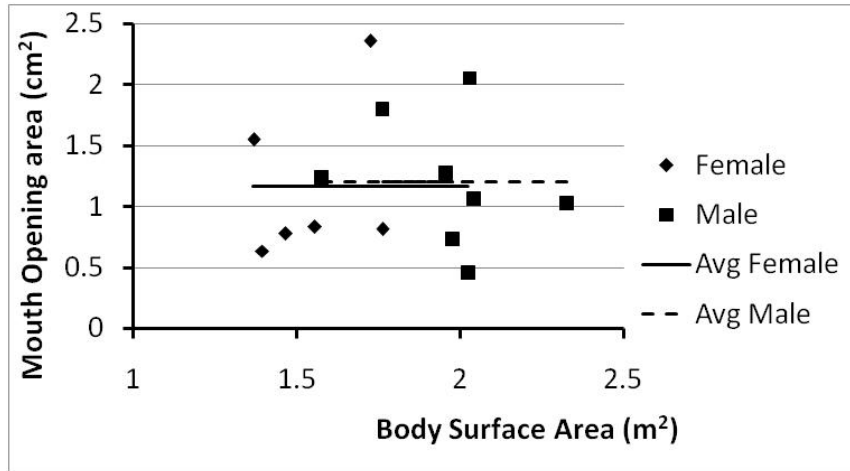


Figure 4.8 Correlation of mouth opening area during breathing with body surface area.

The mouth opening area for male subjects can be written as:

$$\text{Mouth Opening Area} = 1.20 \pm 0.52 \text{ cm}^2. \quad (4.18)$$

The mouth opening area for the female subjects can be written as:

$$\text{Mouth Opening Area} = 1.16 \pm 0.67 \text{ cm}^2. \quad (4.19)$$

#### 4.2.2 Talking

This section first discusses the flow rate, jet direction and mouth opening area measured or observed during talking. As mentioned in the research design, the talking study consisted of three parts: counting from one to ten, pronouncing six letters, and reading a passage.

Figure 4.9 shows the flow rate over time for all the three exercises. The peak flow rates of counting three times consecutively numbers two, three, eight, and ten were higher than others. The same was observed for alphabets F, S, and T than the other alphabets. The flow rate over time for the passage was found to be irregular. The breathing during talking was not normal; most of the outflow (i.e. exhalation) took place from the mouth, while inhalation through the nose. Table 4.3 shows the volume of exhalation and inhalation from the nose and mouth of a subject. The air volume imbalance was probably due to the leakages from the mask used to collect the flow. As it would be difficult to accurately describe the irregular flow, a time averaged flow rate was obtained from this study. As most of the exhalation took place through mouth, this average flow rate can be used as boundary conditions for the mouth for modeling the exhalation of talking. Similarly, as most of the inhalation took place from the nose, the average flow rate can be used as a boundary condition at the nose for modeling inhalation of talking.

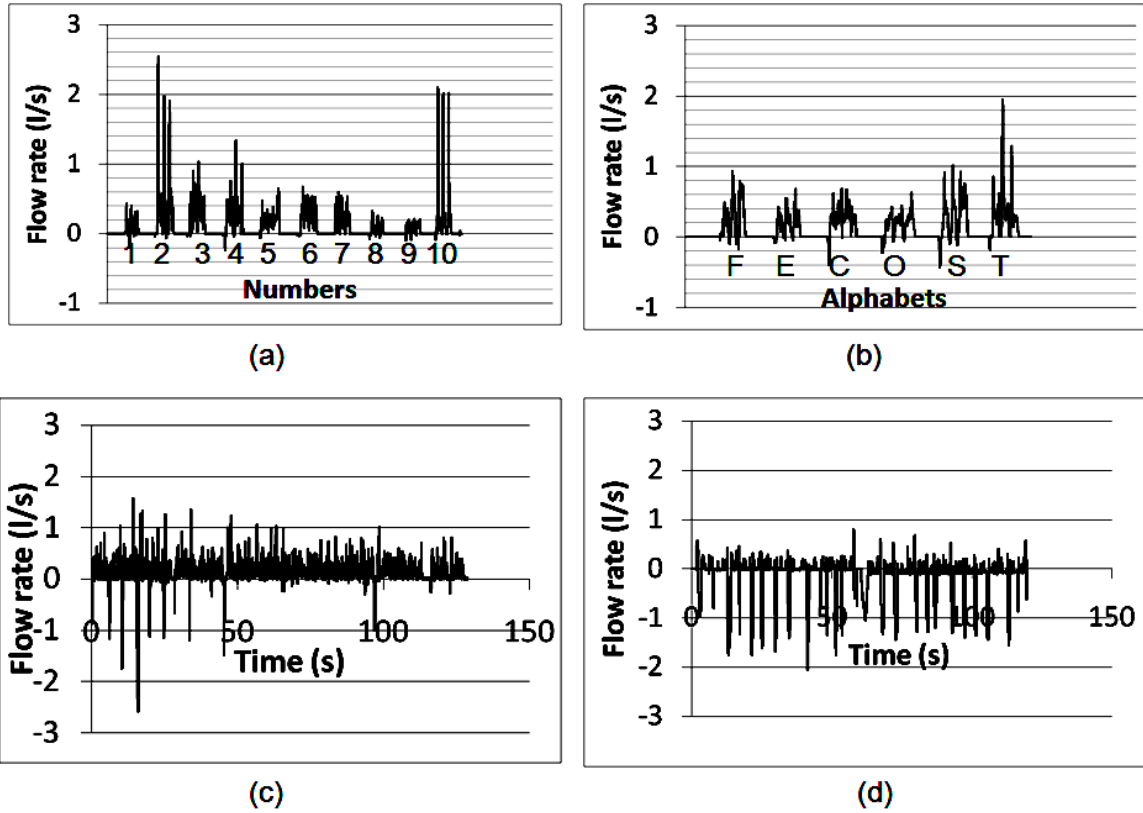


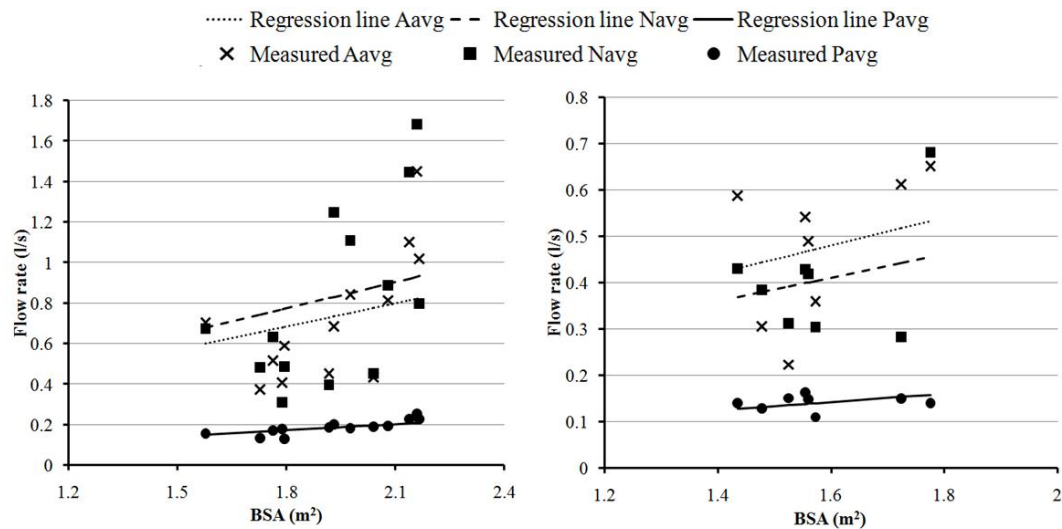
Figure 4.9 Flow rate measured for a subject: (a) from the mouth by counting the numbers three times consecutively, (b) from the mouth by pronouncing the alphabets three times consecutively, (c) from the mouth for reading the passage, and (d) from the nose for reading the passage.

Table 4.3 Air volume inhaled and exhaled from the nose and mouth of a subject during the passage reading.

	Mouth	Nose	Total
Volume inhaled (L)	4.02	23.92	27.94
Volume exhaled (L)	21.96	3.89	25.85
Imbalance (%)	7.5		

Figures 4.10 (a) and (b) show the measured airflow rate for pronouncing the alphabets ( $A_{avg}$ ), counting the numbers ( $N_{avg}$ ) and reading the passage ( $P_{avg}$ ) for the male and female subjects respectively. It was found that the  $A_{avg}$ ,  $N_{avg}$  and  $P_{avg}$  for both genders increase with the body surface area (BSA). This behavior is quite similar to breathing. In breathing, the minute volume (volume exhaled in a minute) increases linearly with BSA (Goldman and Becklake, 1959). Thus a linear regression analysis was performed on the talking flow rate data to obtain a relationship similar to breathing (equation 4.5 or 4.6). Equation (4.20) shows the relationship for various talking flow rates. Table 4.4 shows the value of the slope ( $m$ ) for various exercises for the male and female populations. The relationship for the average flow rate from talking can be written as:

$$Avg. Flow rate(l / s) = m \times BSA(m^2). \tag{4.20}$$



(a) (b)  
 Figure 4.10 Measured airflow rate for counting the numbers ( $N_{avg}$ ), pronouncing the alphabets ( $A_{avg}$ ) and reading the passage ( $P_{avg}$ ) vs. body surface area (BSA) for (a) the male subjects and (b) the female subjects.

Table 4.4 Value of slope ( $m$ ) as defined in equation 20 obtained from the regression analysis.

	$A_{avg}$	$N_{avg}$	$P_{avg}$
Male	$0.3808 \pm 0.0864$	$0.4306 \pm 0.1200$	$0.0965 \pm 0.0072$
Female	$0.3000 \pm 0.0746$	$0.2566 \pm 0.0624$	$0.0888 \pm 0.0095$

The talking process was visualized to determine jet directions. As no single event can define a talking process, its direction should be determined by equation (4.15) for mouth breathing jet. The mouth opening during talking is the area between the lips when certain words/letters are said. As the lip movement is continuous during talking, the mouth opening varies over time. Fig. 4.11 shows the change in the mouth opening area over time for a subject when he/she counted numbers from one to ten. Initially the mouth opening area increased and then stayed almost unchanged and finally reduced to zero. The variation in the mouth opening area while reading the rainbow passage would be the sequence of the variations in mouth opening areas when the words in the passage are said. Thus the average of these mouth opening areas can be used to model the talking process. The variation in the mouth opening area when numbers from one to ten are said could be a representative of mouth opening area for various words in the rainbow passage. Hence, this study recommends using a time averaged area, averaged over all the numbers for modeling the talking process with passage flow rates.

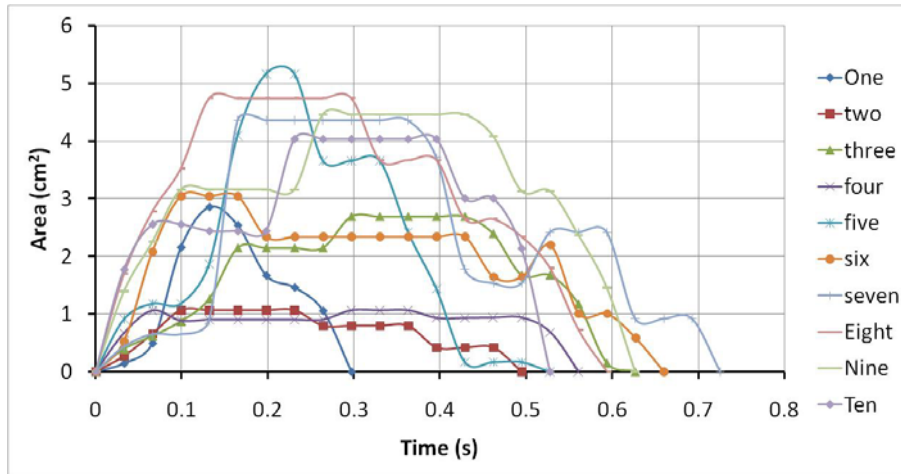


Figure 4.11 Mouth opening area variation with time when a subject counted numbers from one to ten.

Figure 4.12 shows the variation in this average area of mouth opening with the height for all the subjects. No clear trend with height or any other physiological parameter was observed. Thus, an average area of mouth opening is proposed for both of the genders and is given by equation (4.21). The area of mouth opening during talking for male and female subjects can be written as:

$$\text{Area of mouth Opening for talking for male and female} = 1.8 \pm 0.03 \text{ cm}^2. \quad (4.21)$$

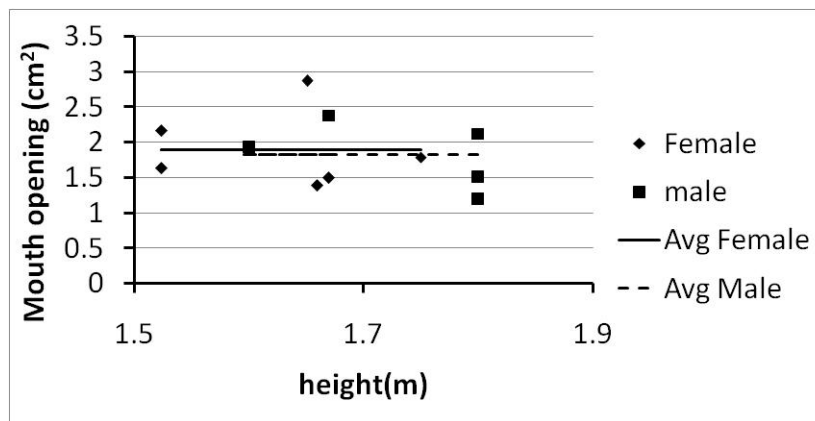


Figure 4.12 Variation in average mouth opening with height for talking.

### 4.3 Discussion

In a manner similar to the study of coughing, this investigation has developed a set of simple equations that can be used to generate boundary conditions (or a source model) for breathing and talking. Our efforts have focused on the flow rate, flow direction, and air velocity which can be most accurately determined from the flow rate

and mouth opening area. The inputs required are the height, weight, and gender of a person.

As was mentioned earlier, the boundary conditions required by CFD simulations should also include the temperature of the exhaled air and the droplet distribution. By working with methods similar to the cough studies by Hoppe, (1981), one can obtain the exhaled air temperature for breathing and talking. There are a few studies on breathing droplet size measurements (Fairchild and Stampfer, 1987; Papineni and Rosenthal, 1997; Edwards et al., 2004 and Fabian et al., 2008). The measurements were done over healthy subjects (Fairchild and Stampfer, 1987; Papineni and Rosenthal, 1997 and Edwards et al., 2004) and the subjects infected by influenza (Fabian et al., 2008). Most of the measurements were performed on mouth breathing. The measurements (Fairchild and Stampfer, 1987; Edwards et al., 2004 and Fabian et al., 2008) indicated that the droplet concentration was of the order of  $10^3$  and the size varied from 0.3 to 5  $\mu\text{m}$ . Fig. 4.13 shows the distribution.

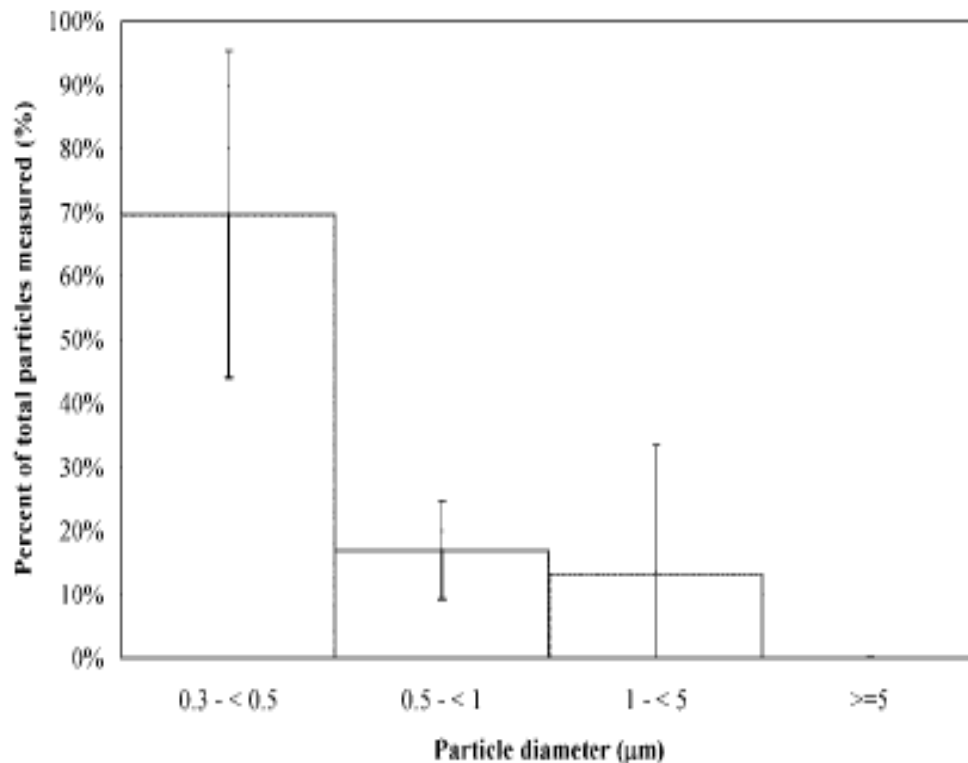


Figure 4.13 Droplet size distribution for breathing (Fabian, 2008).

There have been only a few studies conducted on talking droplet size measurements (Duguid, 1946 and Fairchild and Stampfer, 1987). The measurements were conducted on healthy subjects. The measurements indicated that the droplet concentration was of the order of 250 and that the size varied from 5 to 75  $\mu\text{m}$ . Table 4.5 shows the distribution.

Table 4.5 Droplet distribution for talking (Duguid, 1946).

Droplet Diameter (mm)	No of droplets Counting loudly 1-100
1-2	1
2-4	13
4-8	52
8-16	78
16-24	40
24-32	24
32-40	12
40-50	6
50-75	7
75-100	5
100-125	4
125-150	3
150-200	2
200-500	1
500-1000	3

#### 4.4 Conclusions

This study was focused on characterizing the flow dynamics of breathing of human beings. The flow rate, flow direction, and mouth/nose opening area were measured during normal breathing and talking for 25 healthy human subjects, which could be used as boundary conditions for CFD simulations.

The breathing flow rate variation with time was sinusoidal. The amplitude and frequency of the sine function were related to body height, weight, and gender. No significant difference in the breathing flow rate was observed due to either a change of breathing organ or posture. The flow direction of the exhaled jet during breathing can be characterized by two front angles and two side angles for nose breathing and one side-angle for mouth breathing. The breathing flow directions did not change much among the subjects tested. The mouth and nose opening areas were constant during breathing.

The talking flow rate was found to be irregular in nature and, hence, is defined as an average flow rate over time. The flow rate was related to body surface area which can be obtained from the height and weight of a person. As no single event can define talking direction, it is proposed to use the directions of normal mouth breathing. The mouth opening area during talking was found to vary with time and words. A time averaged area, averaged over numbers, is therefore proposed for talking. The mouth opening area varied among subjects, but no clear trend was observed; thus, a mean value is proposed for the mouth opening area during talking.

## 5. TRANSPORT OF EXPIRATORY DROPLETS IN AN AIRCRAFT CABIN

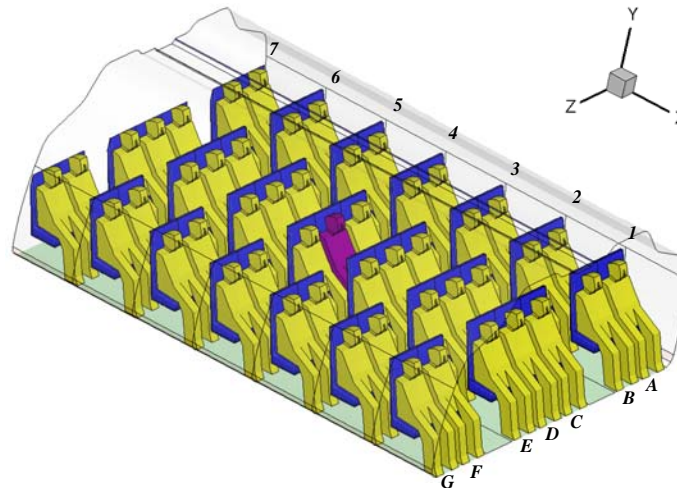
The airborne infectious agents are typically carried by the droplets exhaled by a patient with infectious disease such as influenza or tuberculosis. The droplets disperse in the air and then inhaled by a susceptible person. It is essential to study the transport of these expiratory droplets in the cabin air to understand how a passenger could become infected. The previous chapters discussed the flow models developed for the exhalations such as, coughing, breathing and talking. This chapter is focused of the prediction of transport of droplets exhaled from the coughing, breathing and talking of an index passenger in an aircraft cabin. The CFD methods were adopted and the developed exhalation/inhalation boundary conditions were used to study the transport. The research methods are first presented and finally the results obtained are analyzed.

### 5.1 Research Method

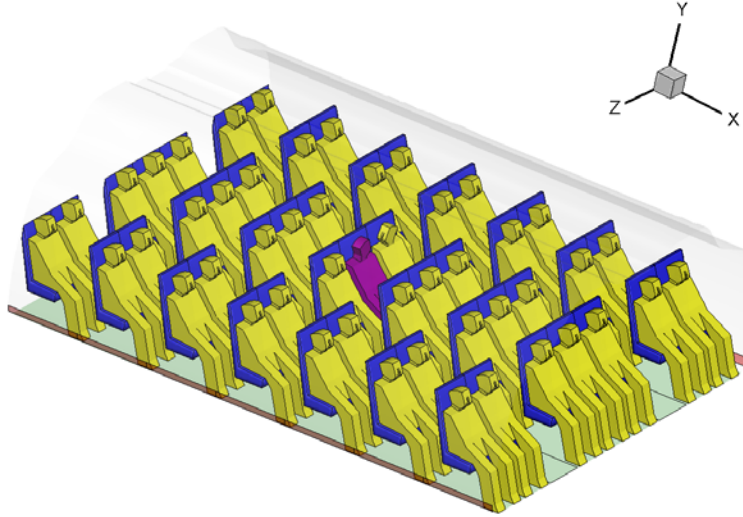
The domain under study is first described. The numerical schemes and boundary conditions used in the simulations are then presented.

#### 5.1.1 Domain of Study

This investigation studied droplet transport due to coughing, breathing, and talking in a seven-row, twin-aisle, fully-occupied cabin as shown in Fig. 5.1. The index patient sat in the middle as marked by purple color. The passenger seats were with an inclination of  $15^\circ$  to the back from the vertical, as passengers generally prefer to sit in this position for a long flight. For talking passengers were modeled facing each other. A mouth opening of  $4 \text{ cm}^2$  and a nose opening of  $0.71 \text{ cm}^2$  (for each nostril) was used for each passenger as measured by our studies (Gupta et al., 2009 and 2010a).



(a)



(b)

Figure 5.1 Section of a seven-row, twin-aisle, fully occupied cabin used for (a) Coughing and breathing case (b) Talking case.

### 5.1.2 Numerical Schemes

The cabin was studied for airflow, temperature distribution, humidity distribution and expiratory droplet transport. A commercial CFD solver FLUENT was used to solve the appropriate equations for the problem. The airflow in the cabin is three dimensional, incompressible, and turbulent; and is mixed convection in nature. The effect of change in density due to change in temperature was taken into account, the rest of the physical properties were assumed to be constant. Mean values for these properties were used at the mean temperature.

The airflow and temperature was obtained by solving the mass balance equation, Navier Stokes equations for momentum balance, and the energy conservation equation. Equation (5.1) shows the general form of the conservation equations and is given by:

$$\rho \frac{\partial \bar{\phi}}{\partial t} + \rho u_j \frac{\partial \bar{\phi}}{\partial x_j} - \frac{\partial}{\partial x_j} \left( \Gamma_{\phi, effective} \frac{\partial \bar{\phi}}{\partial x_j} \right) = S_{\phi}. \quad (5.1)$$

Table 5.1 shows the values of parameters for the equations. The effect of temperature on density was accounted by using the ideal gas equation for density calculations (incompressible ideal gas assumptions). As a mixture of water vapor and air was modeled, an effective density was used for the simulations. For turbulence the renormalization group (RNG) k-ε model was used (Yakhot et al., 1986). The model is similar to standard k-ε model but has different constants and a few additional terms and function in the transport equation of k and ε. The additional functions and terms improves the predictions for highly swirl flows, rapidly strained flows and has analytical formula for effective viscosity, which accounts for the low Reynolds number effects. Equation (5.1) also shows the general form of the turbulent transport equation for k and ε while the

table 5.1 provides the specific values for it. A standard wall function approach was adopted.

Table 5.1 Values of parameters and constants for the transport equations.

Equation	$\phi$	$\Gamma_{\phi, effective}$	$S_{\phi}$	Constants
Continuity	1	0	-	-
momentum	$u_i, u_j$ and $u_k$ (velocity Components)	$\mu_{eff}$	$-dp/dx_j$	-
Energy	T (Temperature)	$(k/C_p)_{eff}$	Heat Sources	-
Species	Water vapor concentration	$\rho D + \mu_t / Sc_t$ (D is the Molecular Diffusivity)	Mass sources	$m_t$ is turbulent viscosity and $Sc_t$ is turbulent Schmidt Number
Turbulent Kinetic Energy (k)	k	$\mu + \mu_t / \sigma_{k,t}$	$G_k - \rho \varepsilon + G_B$	$\mu_t = C_{\mu} \rho \frac{k^2}{\varepsilon};$ $G_k = \mu_t S^2;$ $S \equiv \sqrt{2 S_{ij} S_{ij}};$ $G_B = \beta g_i (\mu_t / \sigma_{T,t}) \frac{\partial \bar{T}}{\partial x_i}$
Turbulent Dissipation ( $\varepsilon$ )	$\varepsilon$	$\mu + \mu_t / \sigma_{\varepsilon,t}$	$C_{\varepsilon 1} G_k \varepsilon / k - C_{\varepsilon 2} \rho \varepsilon^2 / k$	$C_{\varepsilon 1}^* = 1.44; C_{\varepsilon 1}^* = 1.92;$ $C_{\mu} = 0.09; \sigma_{T,t} = 0.9;$ $\sigma_{k,t} = 1.0; \sigma_{\varepsilon,t} = 1.3;$ $\sigma_{C,t} = 1.0$

The discrete phase (expiratory droplets) was tracked using Lagrangian scheme, while the continuous phase (air) is solved using Eulerian scheme. The discrete phase is solved from the calculations of the continuous field. A force balance is applied to calculate the trajectory of the discrete phase as given by:

$$\frac{du_d}{dt} = F_D(u - u_d) + \frac{g_i(\rho_d - \rho)}{\rho_d} + F_i \quad (5.2)$$

where i represents the direction of force.

The first term on the right hand side is the drag force term, and  $F_i$  represents the additional forces in the  $i^{\text{th}}$  direction. In the current problem the drag force and the gravity are the important forces and need to be considered. The drag force can be written as:

$$F_D = \frac{18\mu C_D Re}{\rho_d d_d^2 24}. \quad (5.3)$$

The Reynolds number can be written as:

$$Re = \frac{\rho_d |u - u_d| d_d}{\mu}. \quad (5.4)$$

The expiratory droplets consisted on liquid and solid matter. The liquid matter was assumed to be volatile and is 90% of the total volume of the expiratory droplets (Potter et al., 1963). The evaporation of the expiratory droplets was also modeled through analytical equations. The droplets will evaporate if the droplet temperature ( $T_d$ ) is higher than the vaporization temperature of the volatile liquid ( $T_{vap}$ ) and if it has volatile matter (mass) in it. The droplet will continue to evaporate until it reduces down to its non volatile content or it completely evaporates. In the present case as we have 10% non volatile matter, it will evaporate till that point if its temperature is higher than dew point temperature ( $T_{dp}$ ). The rate of evaporation is given by:

$$N_i = k_c (C_{i,s} - C_{i,\infty}) \quad (5.5)$$

where,  $N_i$  is the molar flux of vapor ( $\text{kgmolm}^{-2}\text{s}^{-1}$ ),  $k_c$  is the mass transfer coefficient (m/s),  $C_{i,s}$  is the vapor concentration at the droplet surface ( $\text{kgmolm}^{-3}$ ),  $C_{i,\infty}$  is the vapor concentration in the bulk gas ( $\text{kgmolm}^{-3}$ ).

The concentration of vapor at the surface of the droplet is evaluated by assuming the pressure to be the saturation pressure at the droplet temperature and is given by:

$$C_{i,s} = \frac{p_{sat}(T_d)}{RT_d} \quad (5.6)$$

where, the relationship between saturation pressure and droplet temperature can be obtained from Flatau et al. (1992).

The concentration of the vapor in the bulk gas is obtained by using the vapor bulk mole fraction ( $X_i$ ) and the bulk mixture properties (p, T) and is given by:

$$C_{i,\infty} = X_i \frac{P}{RT}. \quad (5.7)$$

The mass transfer coefficient can be obtained from

$$k_c = Sh_{AB} \frac{D_{i,m}}{d_d} \quad (5.8)$$

where  $Sh_{AB}$  is the Sherwood number for the binary mixture (water and air in our case) and  $D_{i,m}$  is the diffusion coefficient of the vapor in the bulk ( $\text{m}^2/\text{s}$ ).

Sherwood number can be obtained from following relationship (Ranz and Marshall, 1952):

$$Sh_{AB} = 2.0 + 0.6 Re_d^{1/2} Sc^{1/3}. \quad (5.9)$$

Sc is the Schmidt number given by:

$$Sc = \frac{\mu}{\rho D_{i,m}}. \quad (5.10)$$

The mass of the droplet is then reduced according to the following relationship:

$$m_d(t + \Delta t) = m_d(t) - N_i M_{w,i} \Delta t \quad (5.11)$$

where  $M_{w,i}$  is the molecular weight of the evaporating species.

Heat transfer in the droplet is calculated through the energy conservation i.e Energy stored = Energy obtained from convection + latent heat transfer; and can be written as:

$$m_d C_p \frac{dT_d}{dt} = h A_d (T_\infty - T_d) + \frac{dm_d}{dt} h_{fg} \quad (5.12)$$

where,  $C_p$  is the droplet heat capacity ( $\text{Jkg}^{-1}\text{K}^{-1}$ ),  $h$  is the convective heat transfer coefficient ( $\text{Wm}^{-2}\text{K}^{-1}$ ),  $T_\infty$  is the bulk mixer temperature, and  $h_{fg}$  is the latent heat of vaporization ( $\text{Jkg}^{-1}$ ).

The second order upwind discretization schemes were used for all the variables except pressure. Pressure discretization was based on PRESTO scheme (FLUENT, 2005). The momentum and pressure equations were coupled through SIMPLE algorithm (Patankar, 1980). For the transient transport of droplets a time step size of 0.05s was used. For coughing period a time step of 0.001s was compared with 0.05s and no significant differences in the cough jet behavior were observed, therefore a time step of 0.05s can also be used for the exhalation period.

### 5.1.3 Case Setup

The droplet transport simulations used the steady-state airflow pattern in the cabin as the initial condition. The airflow was created by the air supplied from and exhausted by the environmental control systems and the thermal boundary conditions on the cabin surfaces and passengers. Figure 5.2 and Table 5.2 show the boundary schematic and conditions. The air exchange rate for the supply inlet conditions was 33.7 ACH.

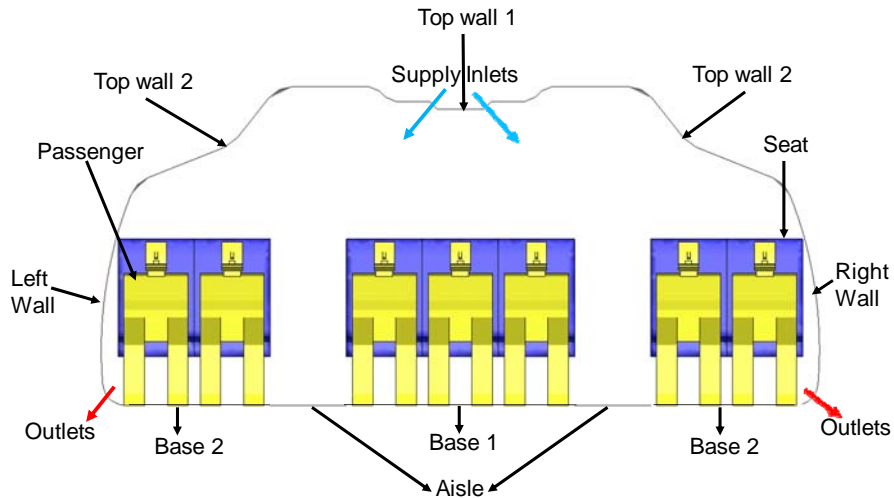


Figure 5.2 Boundary surfaces in the cabin.

The boundary conditions and the exhalation jet direction for coughing, breathing and talking processes of the passengers were specified according to our previous study (Gupta et al., 2009 and 2010a). The flow boundary conditions at the nose and mouth of the index passenger were different depending on whether he/she was coughing, breathing or talking. For rest of the passengers, the mouth was assumed to be closed all the time except for the talking case where the talking boundary conditions were implemented for the passengers in conversation. In real situations all the passengers, including the index passenger will breathe. The passengers can breathe differently, thus an asynchronous (random) breathing pattern was assigned for each passenger to simulate one such case. The random breathing pattern was assigned to these passengers such that every passenger had a random breathing minute volume, breathing frequency and start of the breathing cycle. Figure 5.3 shows the representative breathing pattern assigned to the passengers in a row.

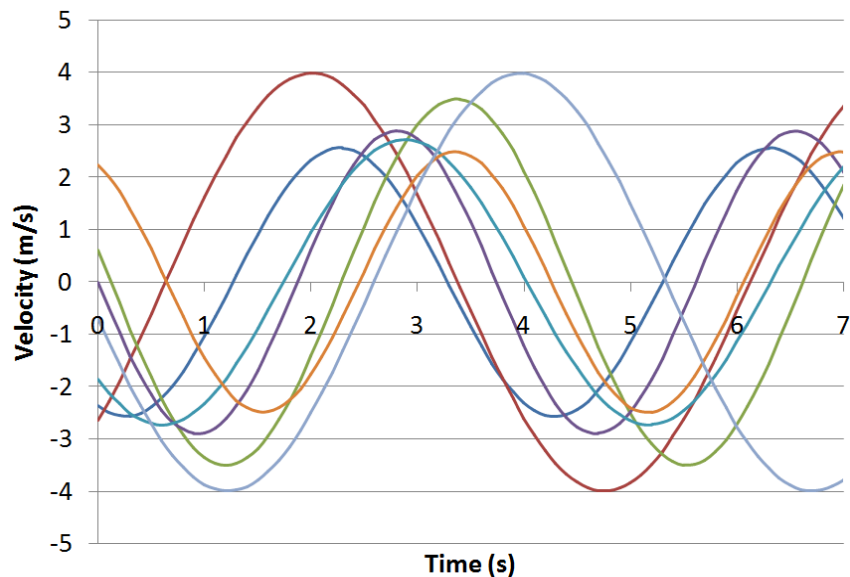


Figure 5.3 Random breathing distribution provided at the nose of passengers.

Figure 5.4 shows the velocity boundary conditions at the mouth and nose respectively for the infected passenger for the coughing case. Figure 5.5 and 5.6 shows the velocity boundary conditions for the breathing and talking cases respectively. It should be noticed that there was no exhalation from the nose during the coughing period and once the coughing process was over there was no exhalation from the mouth while there was an immediate inhalation from nose. User defined routines (UDFs) were developed to implement these boundary conditions in FLUENT.

Table 5.2 Boundary conditions.

Boundary Surface	Velocity	Temperature (°C)	Humidity ratio	Droplet
Human body	No slip	31	zero diffusive flux	Reflect
Seat	No slip	Adiabatic	zero diffusive flux	Reflect
Top Wall1	No slip	23.8	zero diffusive flux	Reflect
Top Wall2	No slip	26.4	zero diffusive flux	Reflect
Left and Right Side wall	No slip	24.5	zero diffusive flux	Reflect
Base 1 (Side)	No slip	24.4	zero diffusive flux	Reflect
Base 2 (center)	No slip	25.1	zero diffusive flux	Reflect
Aisle	No slip	24.1	zero diffusive flux	Reflect
Inlets	2.88 m/s (x=0,y=-0.3,z=±0.95), TI=10%	19.3	0.003 (20%RH)	Escape
Outlets	Outflow			Escape
Mouth and nose of the infected passenger	-	33 (Hoppe, 1981)	0.007 (50% RH)	Reflect
Mouth of rest of the passenger	-	31	zero diffusive flux	Reflect
Nose of rest of the passenger	No slip (Steady) / Random breath(Unsteady)	31 (Steady)/ 33 (Unsteady)	0.007 (50% RH)	Reflect
Back and front	Periodic			

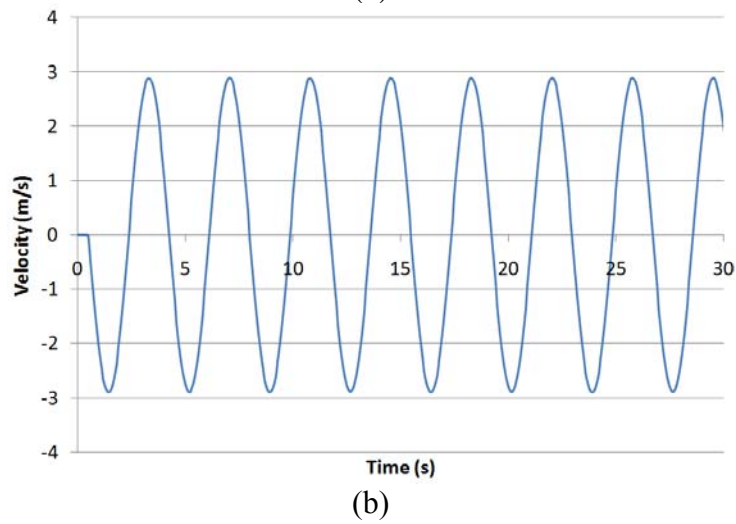
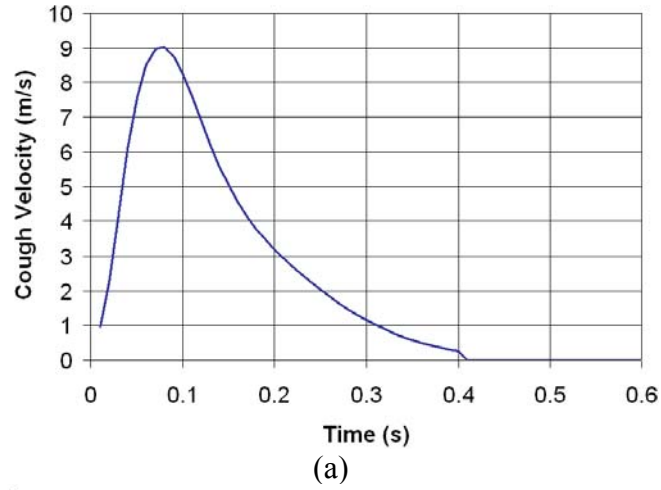


Figure 5.4 Flow boundary condition for the index passenger for the coughing case at the (a) mouth and (b) nose.

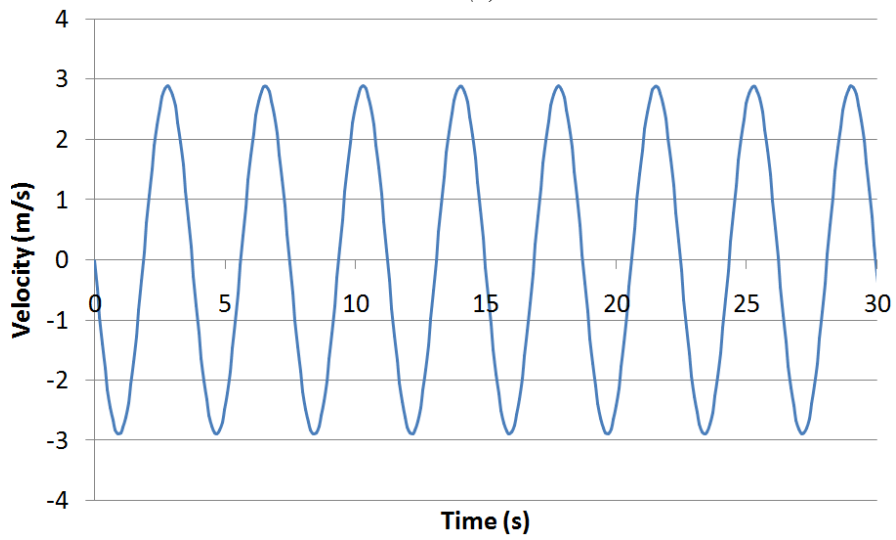


Figure 5.5 Flow boundary condition for the index passenger for the breathing case at the nose.

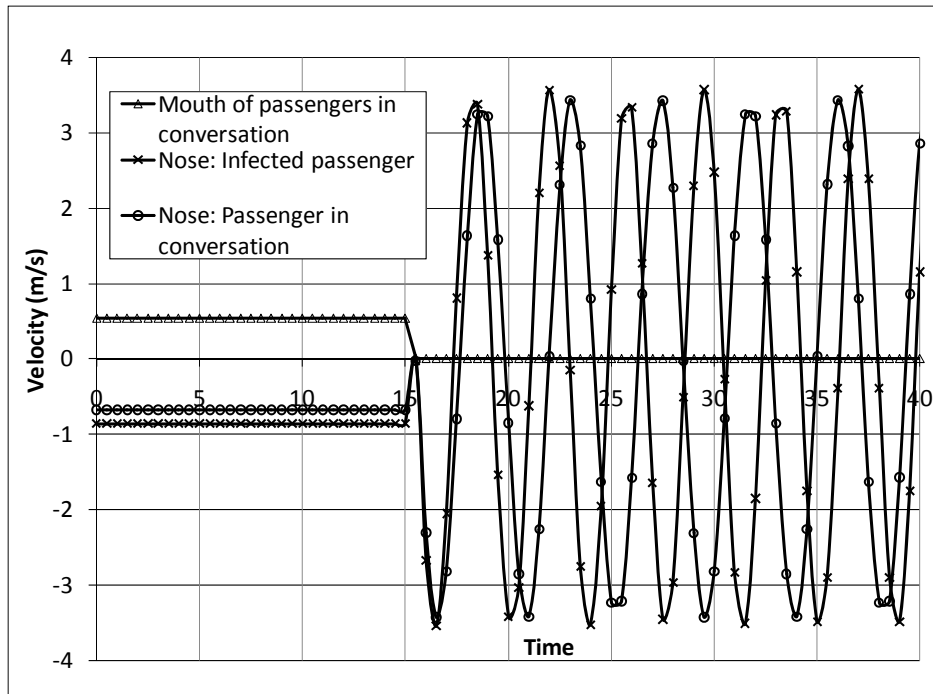


Figure 5.6 Flow boundary condition for the passengers in conversation for the talking case.

The current investigations were performed using mono-dispersed droplets for the coughing, breathing and talking cases. Therefore it was assumed that all the droplets exhaled during a particular exhalation were of one size. A single size droplet and the total amount of droplets exhaled during the exhalation were selected from the literature and used in the simulation. There is a wide range of literature on expiratory droplet size and concentration measurements for coughing, breathing, and talking processes (Duguid, 1946; Fairchild and Stampfer, 1987; Edwards et al., 2004; Yang et al., 2007 and Fabian et al., 2008). There were differences in the finding as these measurements were performed on different subjects using different methods. Yang et al., (2007) found that the average mode size of droplets exhaled during coughing was  $8.35 \mu\text{m}$ , while the droplet concentration was of the order of  $10^3$  per  $\text{cm}^3$ . Therefore droplet size of  $8.5 \mu\text{m}$  and concentration of  $10^6$  per cough (considering the order of volume exhaled during the cough) was used for the current investigation. Fabian et al., (2008) found that the droplets exhaled by the influenza infected subjects were mostly in the range of  $0.3$  to  $0.5 \mu\text{m}$ . The total droplet concentration ranged from 67 to 8500 particles per liter of air (geometric mean of 724). Fairchild and Stampfer, (1987) and Edwards et al., (2004) also indicated that the amount of droplets exhaled during breathing were of the order of  $10^3$  per liter. Thus for the breathing simulated in the current investigation, we obtained 525 droplets exhaled per breath considering  $10^3$  droplets exhaled per liter. A mean droplet size of  $0.4 \mu\text{m}$  and concentration of 525 per breath was thus used for the breathing exhalation simulations. Duguid, (1946) measured the size distribution of droplets exhaled during talking (counting from 1 -100) but did not quantify the droplet concentration (droplets/ $\text{cm}^3$ ). There was no single dominating size for talking (Duguid, 1946); therefore a mean size ( $30 \mu\text{m}$ ) was calculated and used in the current investigations. Fairchild and Stampfer found that the droplet concentration exhaled during talking was of the order of

$10^3$  droplets per liter. Therefore droplet size of 30  $\mu\text{m}$  and concentration of  $10^3$  droplets per liter, which implies 2250 droplets exhaled during the 15 seconds of talking, was used for the CFD simulations. Table 5.3 shows the mean droplet diameter and number of droplets used in the study.

*Table 5.3 Droplet size and concentration for various exhalation activities.*

Exhalation	Droplet Diameter ( $\mu\text{m}$ )	Number of droplets
Coughing	8.5	$10^6$ per cough
Breathing	0.4	525 per breath
Talking	30	2250 for 15 sec of talk

Zhang (2007) reviewed the particle deposition studies in indoor environment and have indicated that the particle deposition velocity for the current range of droplet diameter is  $10^{-6}$  to  $10^{-4}$  m/s. The particle loss coefficient for the aircraft cabin for this range comes out to be .01 to 1 ( $\text{h}^{-1}$ ), this is much less than the air exchange rate in the aircraft cabins (25-40 ACH). ACH is defined as the air change per hour. A recent experimental study by Chao et al. (2008) indicated that the particle deposition fraction for this range of droplet diameter was around 10%-20% for 6-12 ACH exchange rates in hospital environment. An experimental study by Sze To et al. (2009) found out about 75% of particles by mass deposits in aircraft cabins. They had around 90% of the particles of size more than 100 microns and they would have higher tendency to deposit. As the particle deposition rate for the droplets of size 0.16 to 12 micron with 25-40 ACH is less than 10%, no deposition on the surfaces was assumed in the current study. Thus, these droplets reflect from the solid surfaces with a low coefficient of restitution (Zhang et al., 2009). This means that droplet will be stationary when it reaches the wall and thus can only be picked by the bulk airflow.

The random walk model (FLUENT) that was used to account for the turbulent dispersion of expiratory droplets is stochastic in nature and thus it is critical to estimate the optimum number of trajectories required to obtain a stable distribution of the expiratory droplets. The total number of droplets in the vicinity of the nose of each passenger under steady state was calculated using 20, 200, 2000, and 20000 trajectories. The calculations were performed 10 times for each case. It was observed that the mean of the total number of droplets was within  $\pm 9\%$  and  $\pm 12.5\%$  of the 97.5% confidence interval for most of the passengers for 20000 and 2000 trajectories respectively. It should be noticed that more the number of trajectories higher will be the computation efforts. Especially in unsteady cases where these many trajectories will be required every time step. As the differences in the uncertainties associated with the total amount of droplets calculated using the 20000 and 2000 trajectories are low, 2000 droplet trajectories were used every time step for the further analysis for the coughing case. Similarly for breathing and talking 320 ( $\pm 20\%$ ) and 2000 ( $\pm 10\%$ ) droplet trajectories were used respectively. A total of 16000, 11840 and 600000 droplet trajectories were used for the coughing, breathing and talking cases respectively.

#### 5.1.4 Grid Independence and Cabin Section End Conditions

This investigation performed a grid sensitivity analysis to obtain an optimum grid for the further analysis. A grid with 5 mm size on mouth, nose and face of the passengers, 20 mm size on the rest of the body of the passenger and seats, and 40 mm elsewhere was created. More than 98.5% of the cells had equi-size skew angle of less than 0.7. The width of the each cell was then decreased to half to obtain the finer grid. The number of tetrahedral elements for the coarse and find grids was 1.5 million and 10 million respectively.

### Grid Sensitivity

The grids generated were solved for airflow and temperature distribution. The velocities and temperatures at various planes and along the center line were compared. Fig. 5.7 shows the planes and the table 5.4 shows the comparison of the area averaged velocity and temperature for the planes.

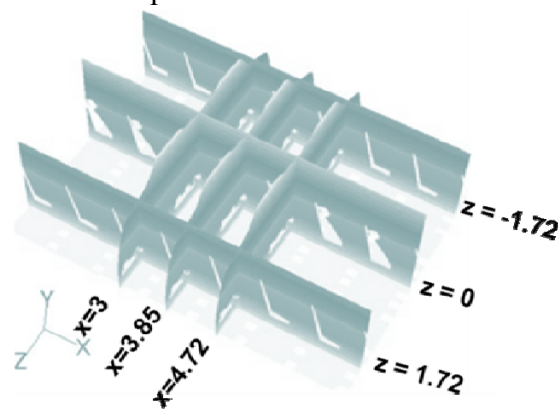


*Figure 5.7 Planes for comparing the averaged velocities and temperatures.*

It can be seen from the table that the difference between the velocities and temperatures is below 10% and 0.6<sup>0</sup>C respectively. The velocities and temperatures were compared along the lines at a lateral plane located at the center of the domain. Figure 5.8 shows the location of the lines and Fig. 5.9 (a), (b) and (c) shows the velocity and temperature variation along the line 1, 2 and three respectively for the two grids.

*Table 5.4 Comparison of area averaged velocity and temperatures for the two grids at planes shown in Fig. 5.7.*

Plane	Velocity (m/s)			Temperature (K)		
	Fine	Coarse	% diff	Fine	Coarse	Difference
x=3	0.26	0.25	-3.09	297.12	296.67	0.45
x=3.85	0.26	0.26	-0.35	297.09	296.60	0.49
x=4.72	0.26	0.26	0.68	297.05	296.57	0.48
z=-1.72	0.28	0.29	4.53	297.15	296.57	0.58
z=0	0.17	0.19	8.46	297.41	296.96	0.45
z=1.72	0.29	0.31	6.41	297.14	296.58	0.56

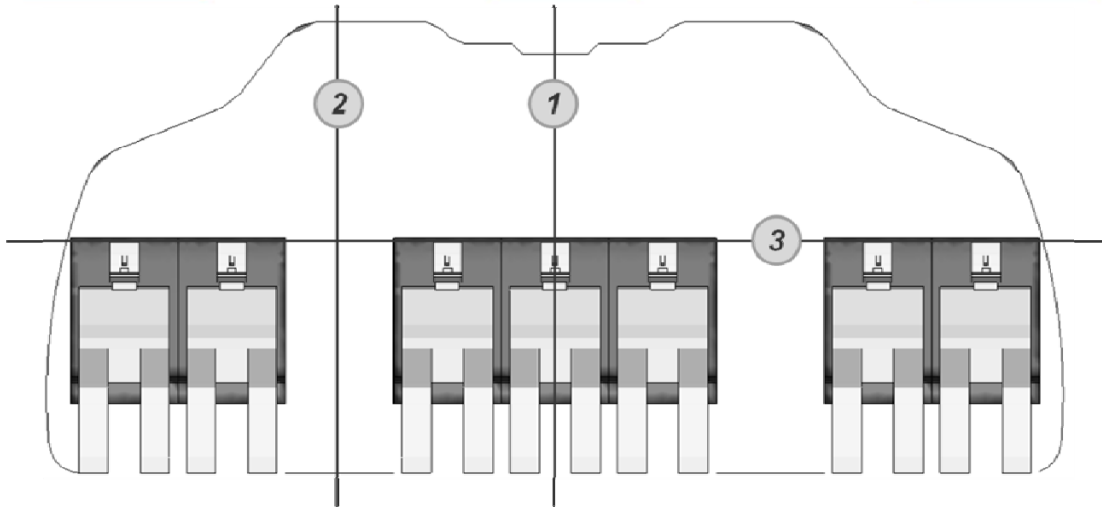


Figure 5.8 Location of the lines located centrally from top to bottom in the domain.

The trend of the velocity and temperature along the lines were similar for both the grids. The differences in the velocity along the lines exist near the walls and are of the order of 0.1 m/s. The finer grid over predicts the temperature by about 0.6<sup>0</sup>C. As the finer grid is about 8 times of the coarser grid in size and the differences in the velocity and temperature are not significant, we decided to do the further analysis on the coarser grid.

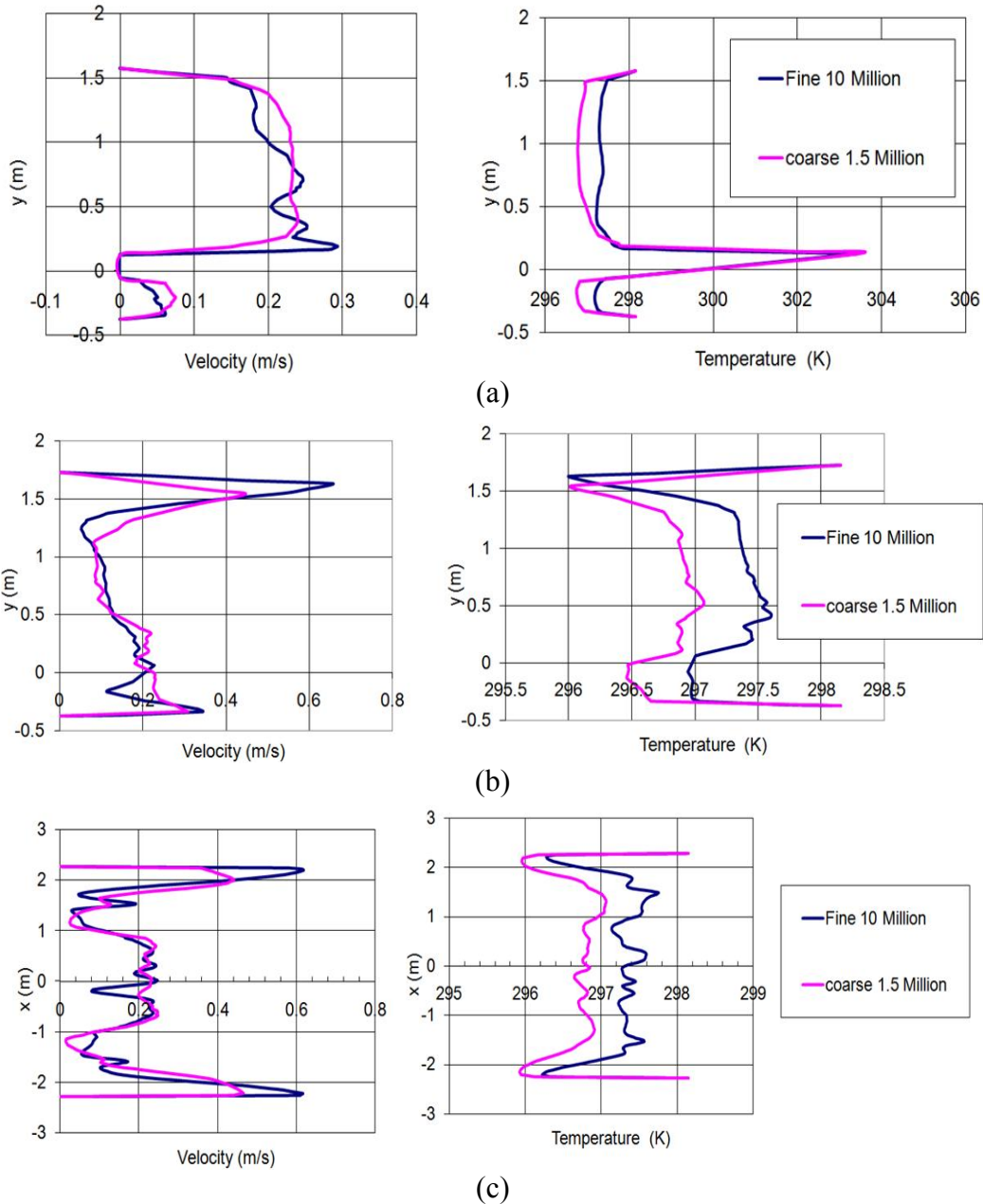


Figure 5.9 Velocity and temperature variation along the lines shown in Fig. 5.8 for the two grids (a) line 1 (b) line 2 (c) line 3.

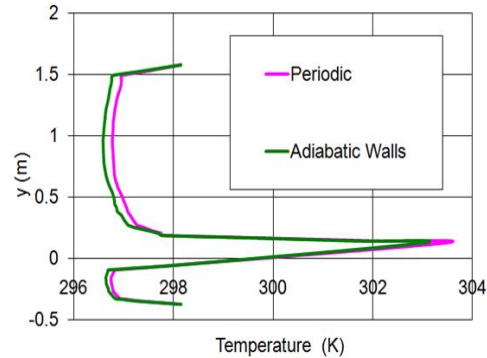
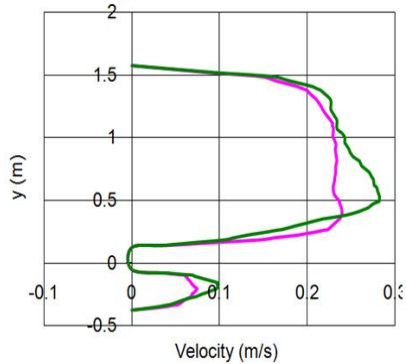
### Cabin Section End Condition

Table 5.5 shows the comparison of the area averaged velocities and temperatures at the planes shown in Fig. 5.7 for the adiabatic and periodic boundary conditions provided at the ends (front and back) of the cabin. It can be seen that the maximum differences in the velocity and temperature is 6% and  $0.25^{\circ}\text{C}$ .

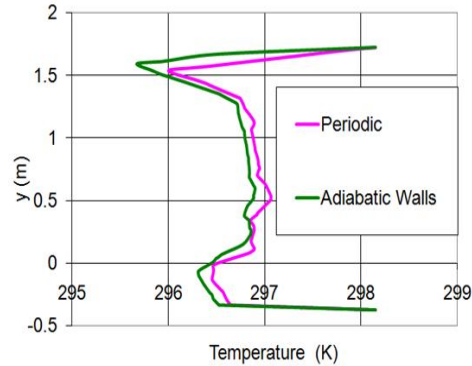
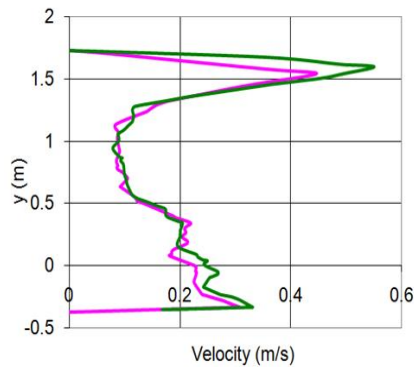
Table 5.5 Comparison of area averaged velocity and temperatures for the two boundary conditions at planes shown in Fig. 5.7.

Plane\	Velocity (m/s)			Temperature (K)		
	Adiabatic	Periodic	% diff	Adiabatic	Periodic	Difference
<b>x=3</b>	0.26	0.25	-2.89	296.51	296.67	-0.16
<b>x=3.85</b>	0.27	0.26	-5.72	296.47	296.60	-0.13
<b>x=4.72</b>	0.26	0.26	1.14	296.46	296.57	-0.11
<b>z=-1.72</b>	0.30	0.29	-2.18	296.45	296.57	-0.12
<b>z=0</b>	0.20	0.19	-3.00	296.71	296.96	-0.25
<b>z=1.72</b>	0.30	0.31	1.90	296.48	296.58	-0.10

Figures 5.10 (a), (b), and (c) show the variation in velocity and temperature along the lines shown in Fig. 5.8. It can be seen that the trend of velocity and temperature variation along all the lines is similar. The maximum difference in the velocity was observed to be 0.06 m/s. The differences in the temperature were observed to be negligible. It was observed that the case with periodic boundary condition needs to be more under-relaxed and thus takes more time to converge to the steady state condition. Thus any of these boundary conditions can be applied at the ends as both show similar trends in airflow and temperature distribution for the cabin.



(a)



(b)

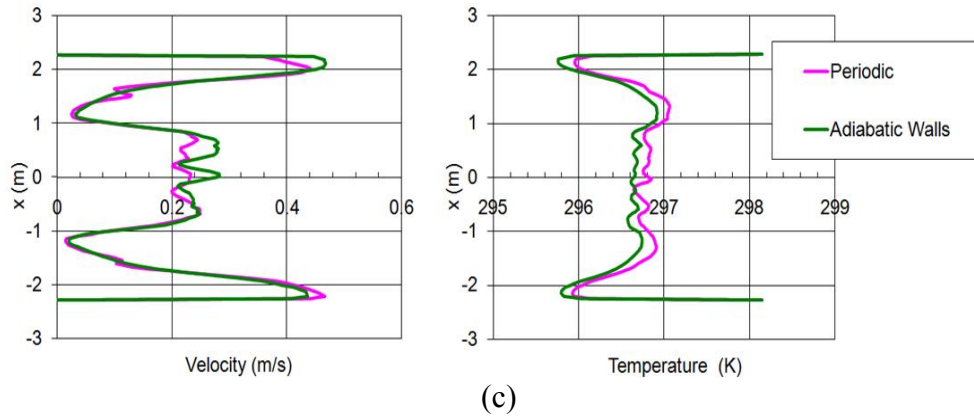
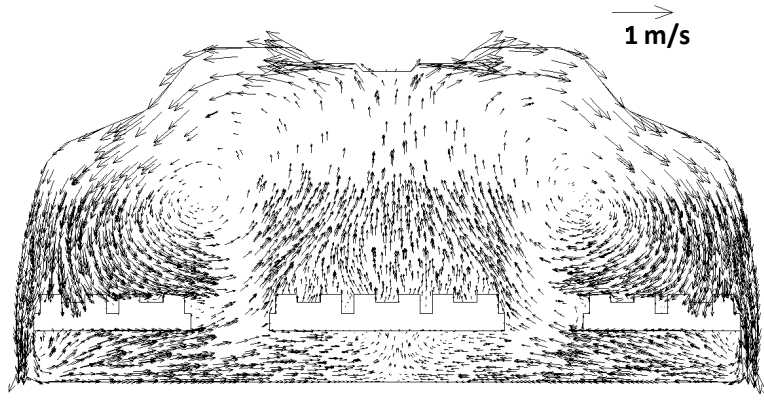


Figure 5.10 Velocity and temperature variation along the line shown in Fig. 5.8 for the two boundary conditions for (a) line 1 (b) line 2 (c) line 3.

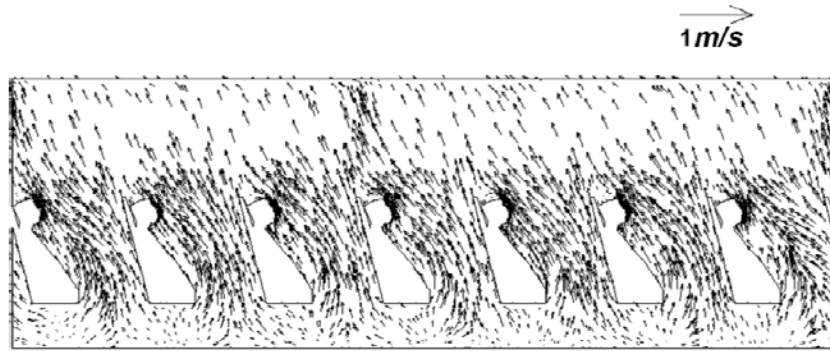
## 5.2 Results

### 5.2.1 Steady-State Airflow in the Cabin

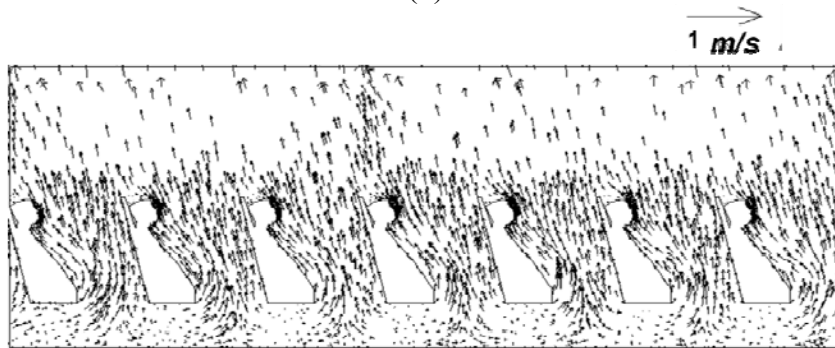
Our studies on the transient transport of droplets exhaled from coughing, breathing, and talking of the index patient in the cabin used the steady state airflow pattern as the initial condition. Figure 5.11 (a) shows the velocity vectors in a cross section located in front of the index patient and Figures 5.11 (b), (c), (d), (e), and (f) in longitudinal sections through the index patient (column D), column C, aisle, column B and the column A respectively. The airflow pattern was similar to those obtained by Zhang and Chen (2007b) and Zhang et al. (2009). The cold air from the supply inlets flowed to the sides along the top wall and a part of it existed through the outlets located at the bottom sides. The other part and the thermal plumes created two large re-circulations in a cross section. The airflow pattern clearly indicates the mixed convection in a cross section. The air velocities at the top, center and window zones (Figure 5.11 (a)) of the cabin ranged from 0.6 to 0.8 m/s, 0.2 to 0.3 m/s, and 0.3 to 0.4 m/s respectively. It should be noticed that the flow was approximately symmetrical about the center line (longitudinal direction) and the airflow current on the top were strong in the lateral direction. The strong airflow near the vicinity of the passengers as shown in Figure 5.11 (b) and 5.11 (c) was due to the thermal plumes around the human bodies. The air velocities around these passengers ranged from 0.2 to 0.3 m/s (Figure 5.11 (b)). The airflow was upwards and towards the back. The airflow in this zone was natural convection dominated While for the plane along the aisle (Figure 5.11(d)) the airflow was upwards and was to the front especially in the lower zone (0.2-0.3 m/s). The airflow around the passengers seated on A and B as shown in Fig. 5.11 (e) and (f) was forced convection dominated. The flow was towards the front along the body. This clearly shows the mixed convection nature of flow in the cabin.



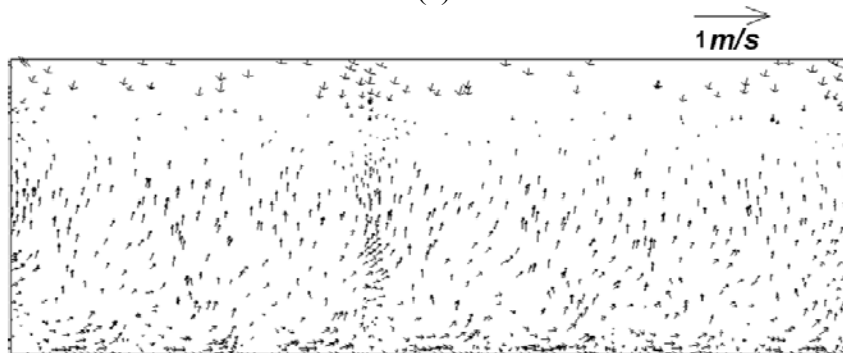
(a)



(b)



(c)



(d)

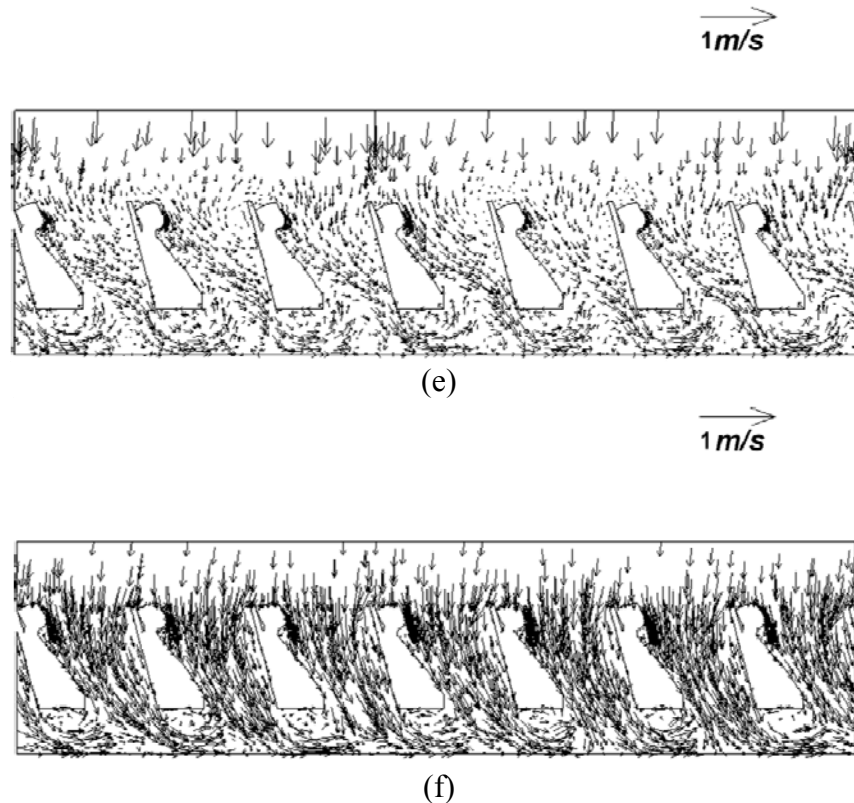


Figure 5.11 Velocity fields in the cabin on (a) cross section through the index patient and longitudinal section through (b) the index patient (Column D) (c) column C (d) the aisle (e) column B (f) column A.

### 5.2.2 Evaporation of Droplets in the Cabin

Figure 5.12 shows the change in diameter due to evaporation for the droplets exhaled through coughing, breathing and talking. All these droplets evaporated to their nuclei in less than 0.3 seconds. The droplets with smaller diameter had higher rate of evaporation and evaporated quickly. The droplets generated from breathing were smallest ( $0.4\ \mu\text{m}$ ) and evaporated in 0.005 s. The droplets produced from talking were the largest ( $30\ \mu\text{m}$ ), so they took 0.3 s to evaporate. The time required for the evaporation of these droplets agrees with the finding by Morawska (2006). It should be noticed that none of these droplets evaporated completely because they contained 10% non-volatile matter. The expiratory droplets from coughing, breathing and talking reduced to 4, 0.19, and 14  $\mu\text{m}$ , respectively, after evaporation completed. The diameter of these droplets was small and thus their deposition on the surfaces was minimal.

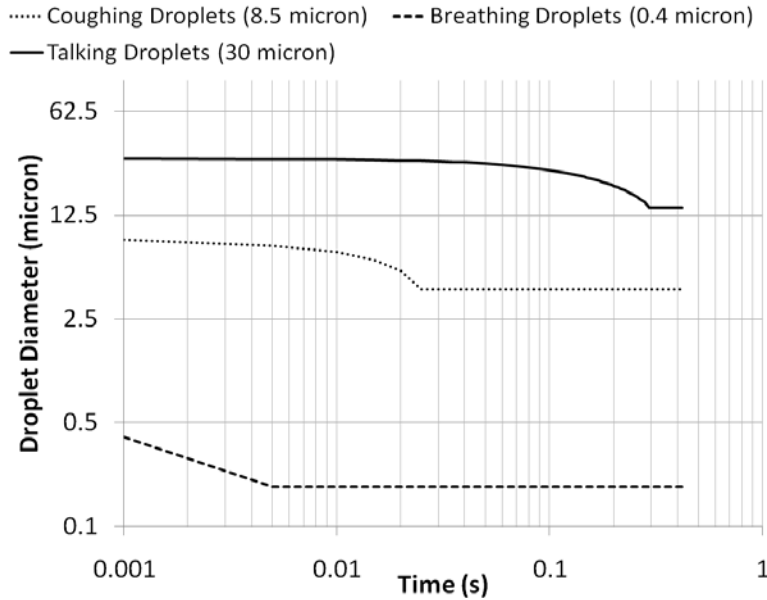


Figure 5.12 Evaporation of droplets from coughing, breathing and talking.

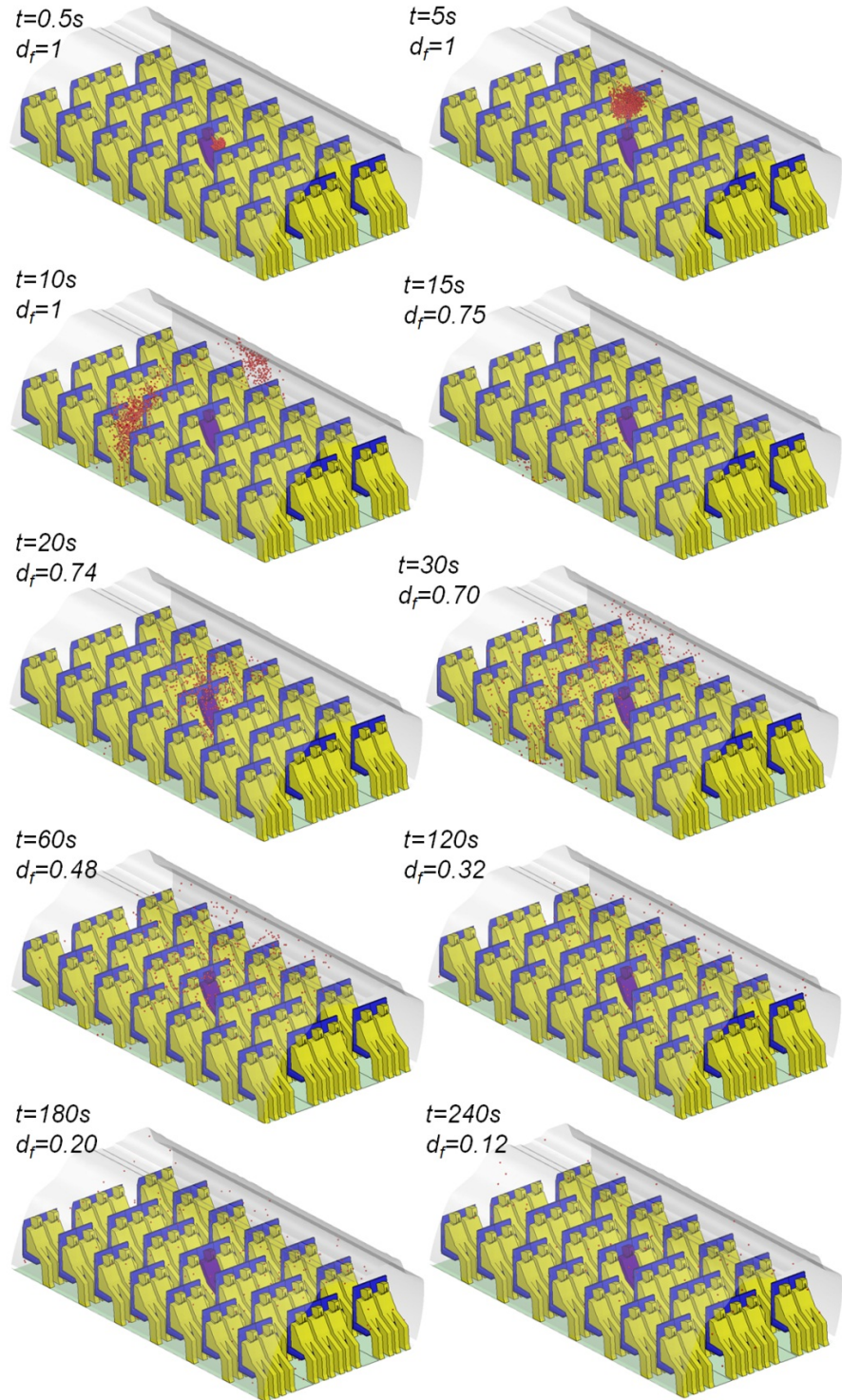
### 5.2.3 Transport of Droplets Exhaled from the Coughing

Figure 5.13 shows temporal distributions of the droplets exhaled due to a single cough of the index patient in a perspective and the side view. The droplets shown are 0.001 times the actual number of droplets ( $1 \times 10^6$ ) contained in a cough. The diameter of the droplets shown in the figure is 1 mm (relative to cabin dimensions), which is two order of magnitude larger than the actual one. This was done to clearly visualize the droplet movement.

The droplets first followed the air jet caused by the cough, which pushed the droplet cloud down forwards. The simulated cough jet was impulsive in nature with peak velocity of 9m/s. The cough jet penetrated to a distance of about 45 cm axially. The air velocities in this zone decayed to around 0.3 m/s after 0.5 seconds. As the background cabin velocities around the index passenger ranged from 0.2 to 0.3 m/s, the cough expired droplets followed the bulk airflow soon after the cough was over. Gupta et al., 2009 also observed a similar jet behavior. Though the bulk airflow and the cough jet velocities in their case were not exactly the same but the cough penetration during the cough period in the domain was found to agree well. Since the jet momentum was weak, the droplets followed the bulk airflow in the cabin. The side view showed that the droplets moved upwards within 5s and went towards the backside of the index patient due to the bulk airflow pattern as shown in Figure 5.11(b). The droplets reached the cabin ceiling and then went to the side walls in 10s due to the jet flow from the environmental control system. The majority of the droplets reached the passengers sitting at the window seats in about 10-12 s. Due to the high droplet concentration and short life of the droplets (pathogens in the droplets may be alive), the passengers seated at these locations (5A, 5G, 4A, and 4G) may have relatively higher risk of infection. The droplets then moved to the lower level of the cabin because of the re-circulation airflow as shown in Figure 5.11(a). When the remaining particles came back the proximity of the index patient, it took around 20s. These droplets then dispersed in the air in the proximity of the index

patient. Figure 5.13(a) also shows the temporal values of the total airborne droplet fraction ( $d_f$ ), defined as the number of airborne droplets in the cabin over the total amount of droplets exhaled. In 20 s, the  $d_f$  become 0.74 (or 74%) that indicates that about 26% of the expiratory droplets exhausted from the outlets. These droplets dispersed to all the seven rows in a minute, but most of the droplets were contained to the row in front, at, and behind of the index patient. Thus the risk of infection for the passengers sitting in these rows can be significantly higher than those sitting in the other rows. The  $d_f$  reduced to 48%, 32%, 20%, and 12% at  $t = 1, 2, 3$  and 4 minutes, respectively. The delay was slow.

It took 4 weeks to run the 4-minute real-time simulation on the 8-parallel-processor computer cluster. The computing time was very long for such a short section of cabin. As the droplet distribution become rather uniform in 4 minutes, a homogenously mixed condition could be used afterwards.



(a)

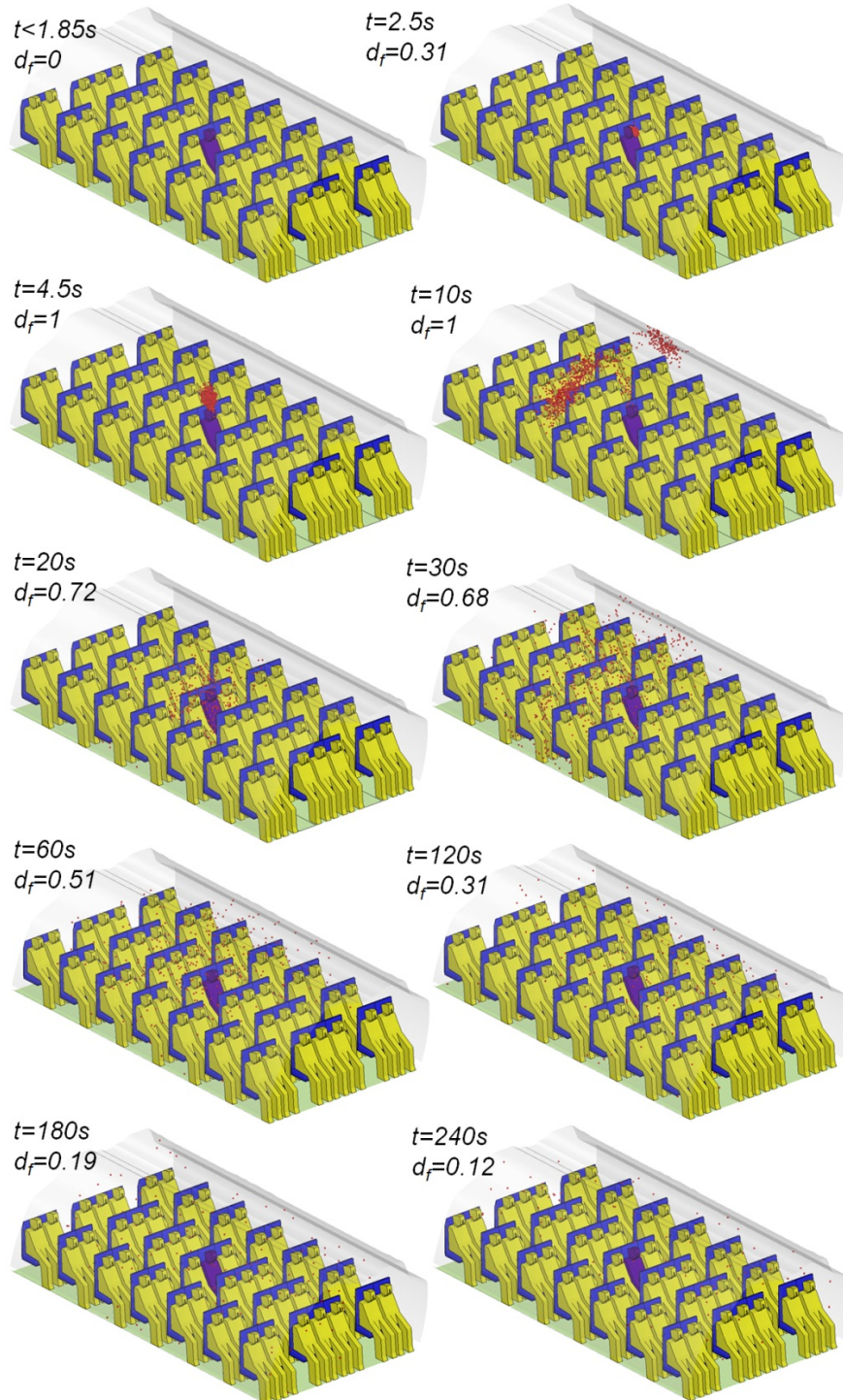


(b)

Figure 5.13 Temporal distributions of droplets due to a single cough from the index patient: (a) a perspective view and (b) the side view.

#### 5.2.4 Transport of Droplets Exhaled from the Breathing

Very similarly, Figure 5.14 shows the temporal distributions of the droplets exhaled through a single breath from the index patient. The number of droplets shown is 1/3 the actual and the diameter of the droplet shown is 1 mm for better visualization. The droplet number from the breath is 3 to 4 magnitude order smaller than that from the cough.



(a)



(b)

Figure 5.14 Temporal distributions of droplets due to a single breath from the index patient: (a) a perspective view and (b) the side view.

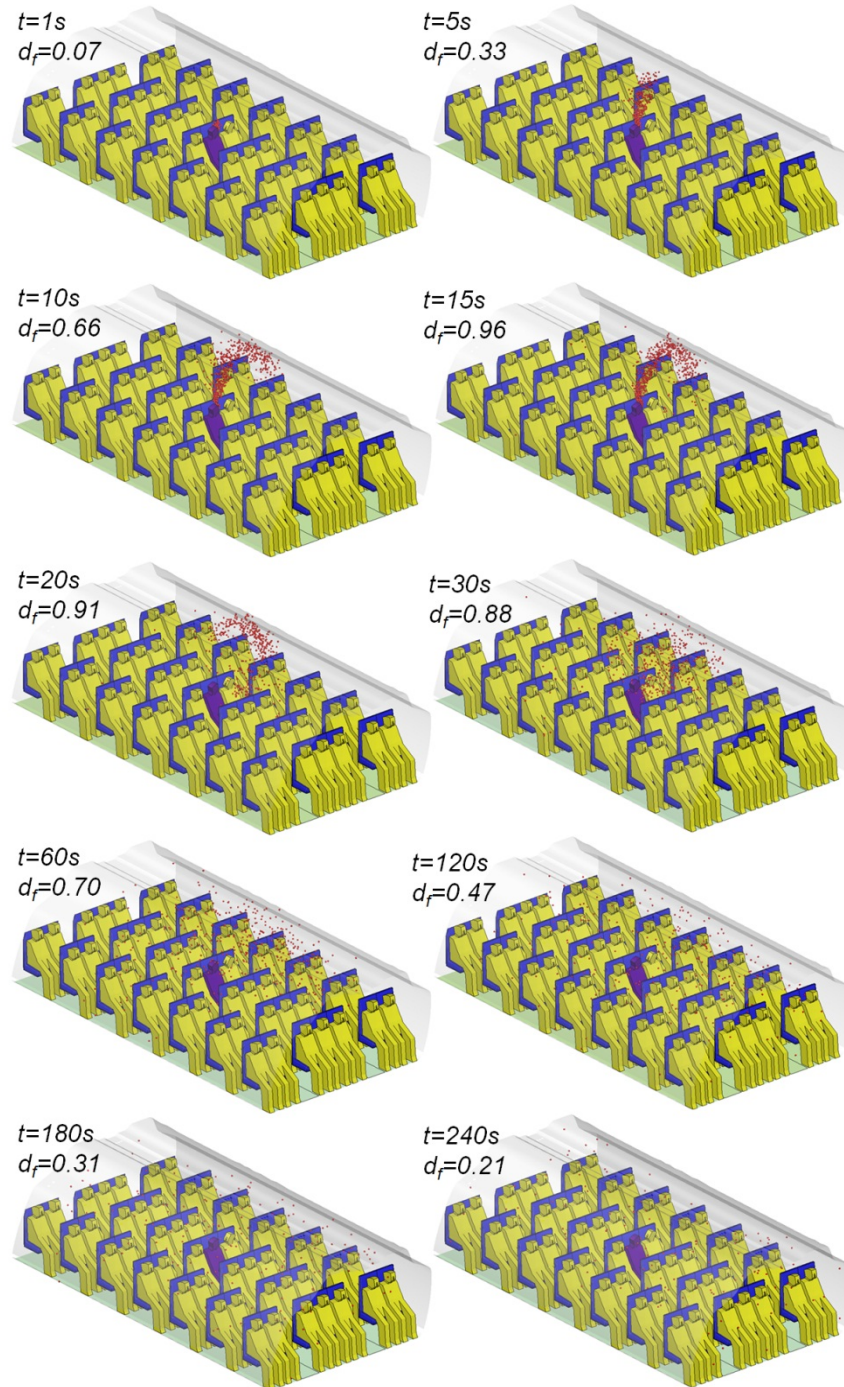
The index patient started to exhale at  $t = 1.85$  s. Since the jet from the breath was much weaker than the cough, the droplets went upwards very quickly due to the bulk airflow pattern. The weak jet did create a slightly different droplet distribution in the first few seconds, but not very evident. In general, the droplet distributions and the  $d_f$  for the breath were similar to those for the cough, but the amount of droplets were much smaller.

### 5.2.5 Transport of Droplets Exhaled from the Talking

This investigation also simulated the droplet distributions in the cabin when the index patient talked with the left passenger (4C) for 15 s. Figure 5.15 (a) and (b) show the temporal distributions of the droplets. Similar to the coughing and breathing cases, the number of droplets shown is increased by 2.5 times compared with the actual for better visualization. The index patient was modeled facing to passenger 4C so the droplets exhaled moved to the left side of the index patient.

It is very interesting to see that all the droplets exhaled initially went to the left side of the cabin that was very different from the coughing and breathing case. This is because the head of the index patient turned to the left and the symmetrical bulk airflow

brought the droplets to the left side of the cabin. Although some droplets could go to the right side of the cabin at the second recirculation due to diffusion, the amount of the droplets was significantly less than that to the left cabin. Please also note that the talk lasted for 15 s so the droplets were generated continuously during this period. This different source character had some effects on the  $d_f$  in initial time. The droplet distribution was uniform in 4 minutes.



(a)



(b)

Figure 5.15 Temporal distributions of droplets due to a 15 s talk from the index patient: (a) a perspective view and (b) the side view.

### 5.3 Discussion

The overall flow pattern predicted by the CFD methods was in agreement with the previous literature. The expiratory droplet dispersion was in accordance with the exhaled jet and bulk airflow in the cabin. Zhang et al., (2007a) studied the contaminant (scalar) transport in a twin aisle cabin under a steady release. They used CFD methods and validated it against experiments. The contaminant trajectories predicted by them agrees qualitatively with the current investigations. A controlled experimental study is still required for a quantitative validation on the droplet evaporation and dispersion predictions. The validation can aid researchers identify the limitations of the CFD methods used in the current investigations and improve the prediction on the transient transport of expiratory droplets. The index passenger location influences the expiratory droplet transport as the airflow in different at different locations.

Moreover, the present study was focused on single exhalation event but the reality is a continuous process with the combination of multiple exhalation events. It is not practical to use the CFD simulations for such a simulation because it would take months of computing time to simulate a one hour flight for an entire cabin. It is required to

develop methods to extend the information for realistic flight durations. It is also required to develop methods to quantify the exposure risk to the fellow passengers.

#### 5.4 Conclusions

This investigation studied the transport of the expiratory droplets from an index patient seated at the center of a seven-row, twin-aisle, fully occupied aircraft cabin by using a commercial CFD program (FLUENT 2005). The exhalation events studied were a single cough, a single breath, and talk for 15 s by using the models developed by us as discussed in chapter 3 and 4. The simulations were performed for four minutes of real time starting from a steady-state airflow and temperature distribution. The study led to the following conclusions:

The droplets exhaled from the cough of the index patient followed mainly the bulk airflow. The droplet concentration in the vicinity of the passengers reduced over time due to the removal from the outlets and dispersion of the droplets. The total airborne droplet fraction reduced to 48%, 32%, 20%, and 12% after the droplets entered the cabin air for 1, 2, 3 and 4 minutes, respectively. Most of the droplets were transported within one row of the index patient in the first 30 s and then could be transported to the entire seven-row cabin with a uniform droplet distribution in 4 minutes.

The droplets exhaled from the breath of the index patient behaved similarly as those from the cough, but the number was much smaller. The expiratory droplets generated during the talking of the index patient were contained on the left side of the cabin since the patient turned the head to the left.

## 6. INHALATION OF DROPLETS IN AN AIRCRAFT CABIN

In the last chapter we developed the CFD methods to predict the spatial and temporal distribution of droplets exhaled from a single cough, single breath and 15s of talking of the index passenger. The simulations were performed for four minutes of flight time and took four weeks of computational time on an 8-parallel-processor computer cluster. A commercial air flight could last between one to 20 hours from gate to gate. Therefore, it is not practical and feasible to perform the CFD simulation for realistic flight durations for multiple exhalations from the index passenger.

This chapter presents the methods developed to predict the spatial and temporal distribution of expiratory droplets and quantifies the amount of inhaled droplets by each passenger in an airliner cabin for realistic flight durations for multiple exhalations from the index passenger. This chapter first presents the method to extend the data obtained from the four minutes of the CFD simulations (discussed in the last chapter) to realistic flight durations. The method to obtain the information on droplet concentrations for a multiple exhalation scenario from the single exhalation cases is then discussed. The method to quantify the amount of droplets inhaled by the passengers then presented. The cases studied to investigate the effect of type of exhalations are then presented.

### 6.1 Research Methods

#### 6.1.1 Extension of Droplet Concentration for Real Flight Durations

As observed in the last chapter that the droplet distributions could be highly non-uniform in an airliner cabin. To assess the exposure risk of fellow passengers caused by the droplets exhaled by an index patient, it is important to know the actual number of droplets inhaled by each passenger. It is required to know the time variation in the droplet concentration around the nose of the passengers to calculate the droplets inhaled by them. As passengers may move their heads around, a zone of  $0.0283 \text{ m}^3$  ( $1 \text{ ft}^3$ ) around the nose of each passenger, as shown in Fig. 6.1, was constructed and a time variation in the droplet concentration in these zones was obtained from the CFD simulations. A user defined routine (UDF) was developed to calculate the droplet concentration in these zones and was integrated with the CFD simulations.

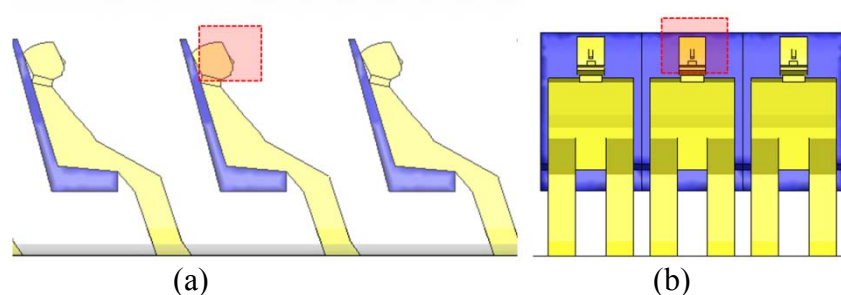


Figure 6.1 The zone of  $0.305 \text{ m} \times 0.305 \text{ m} \times 0.305 \text{ m}$  around the nose region of a passenger for determining the average droplet concentration.

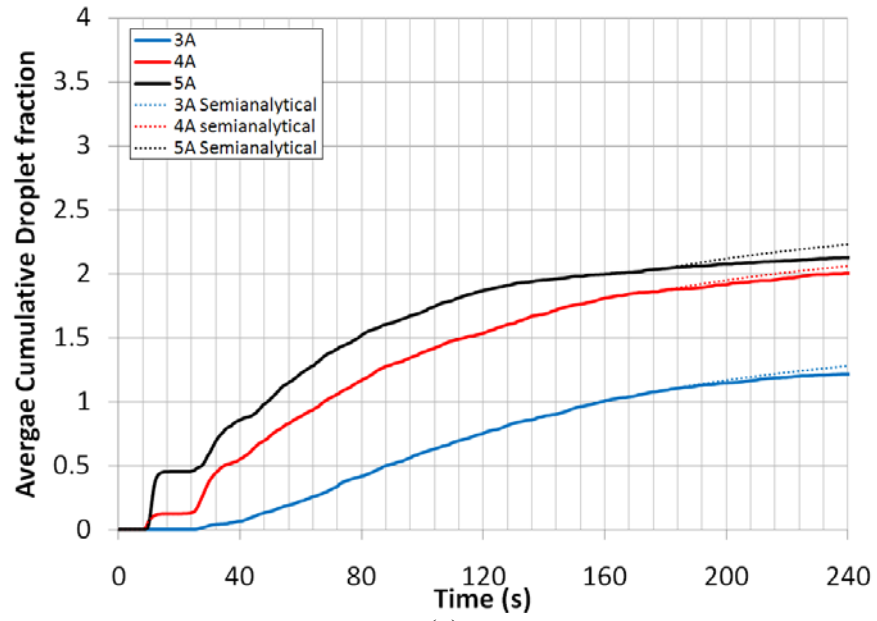
This study defined  $\beta$  (droplet fraction-s/m<sup>3</sup>) as the average number of expiratory droplets in the vicinity of a passenger relative to the total number of droplets exhaled by the index passenger). The  $\beta$  was summed over time in this investigation as:

$$\beta(t) = \sum_{t=0}^t \frac{N_i(t)}{vN_t} \Delta t \quad (6.1)$$

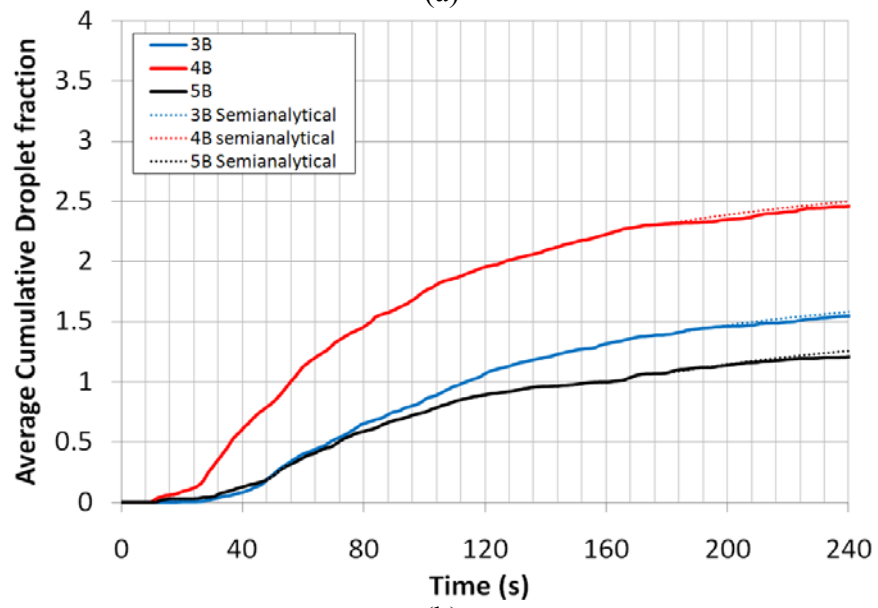
where  $v$  is the zone volume around the passenger,  $N_i$  is of droplets in the zone around the  $i^{\text{th}}$  passenger at time  $t$ , and  $N_t$  is the total number of droplets exhaled for the exhalation of the index patient.

Figure 5.1 (a) shows the cabin configuration and nomenclature for the passengers. The analysis for the configuration with index passenger seated at the seat 4D is presented as an example. As observed in the CFD simulations that the expiratory droplet cloud from the coughing of the index passenger 4D moved in the cabin with the bulk flow. The local droplet concentrations in the zones where the droplet cloud reached first were as high as the cloud was dense for the initial period. It was observed that the droplets eventually dispersed to all seven rows, but the droplet concentrations in the row furthest from the index passenger were relatively low. Therefore, the droplet concentration for the passengers seated only in the 3<sup>rd</sup>, 4<sup>th</sup> (index passenger), and 5<sup>th</sup> rows is discussed here.

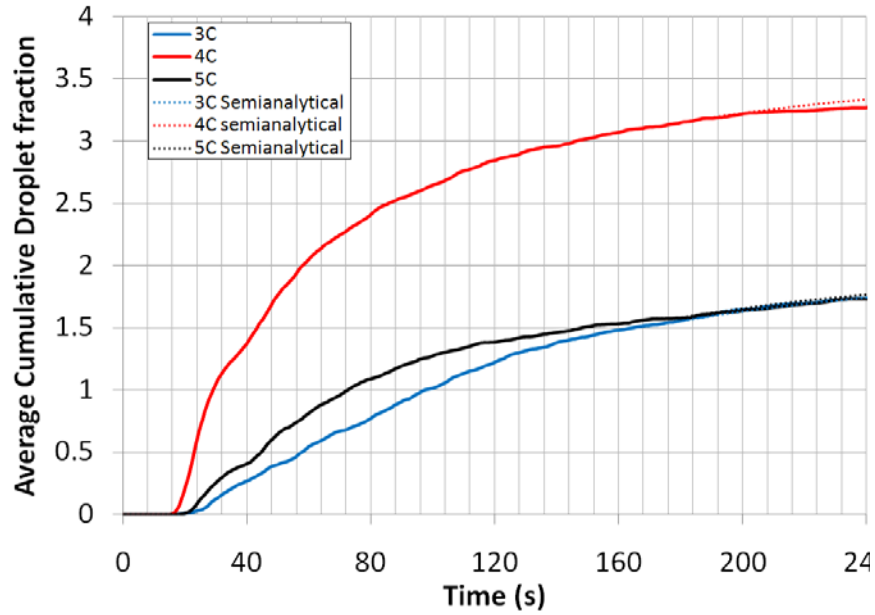
Figure 6.2 shows the average cumulative droplet fraction ( $\beta$ ) for the passengers seated in A (window), B (aisle), C (aisle), and D (center of the row) seats, respectively, for the expiratory droplets from a single cough by index passenger 4D. As shown in Fig. 6.2, the droplets from passenger 4D reached passengers 5A, 5B, 4A, and 4B in about 10s. Therefore, there were sudden increments in  $\beta$  for these passengers at around 10s. The rate of increment was higher for 5A and 4A as the droplets first passed through these zones. The droplet cloud then reached the passenger seated in 4C and dispersed in the 3<sup>rd</sup>, 4<sup>th</sup> and 5<sup>th</sup> rows. The rate of increment in  $\beta$  for the passengers seated in these rows was higher during the initial period (<1 min).



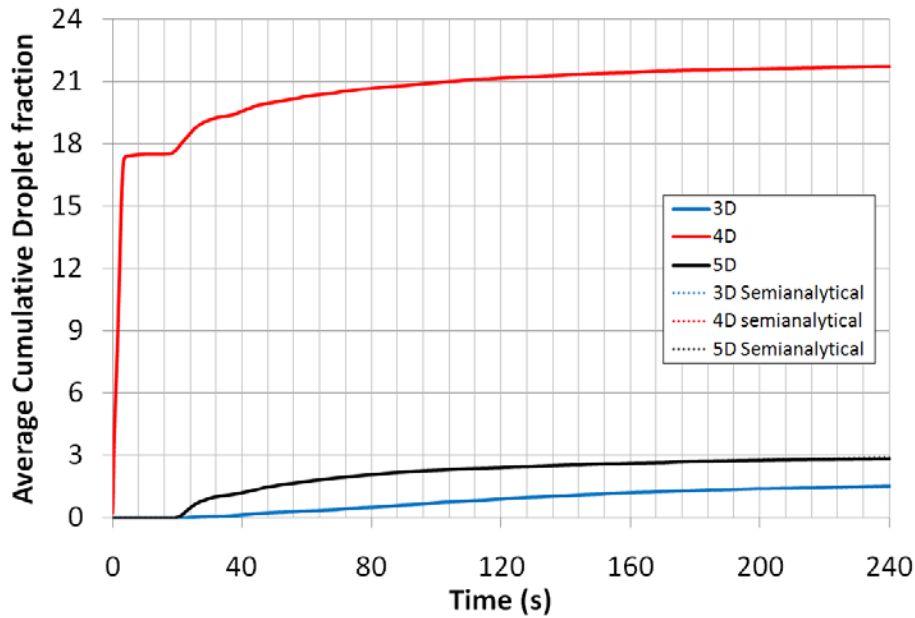
(a)



(b)



(c)



(d)

Figure 6.2 Average cumulative droplet fraction ( $\beta$ ) over time for passengers due to a cough from the index passenger for (a) Column A (b) Column B (c) Column C (d) Column D.

The CFD studies indicated that the droplets dispersed in the cabin in about 1 minute, but they did not perfectly mix in the cabin. In fact, Nazaroff et al. (1998) and Wan and Chao (2007) indicated that a perfectly mixed condition is merely an assumption and cannot be achieved. The variation in  $\beta$  clearly confirms that perfectly mixed conditions cannot be assumed for the initial (<1 min) period due to its sharp changes.

However, the  $\beta$  increments after 3 minutes were steady and similar for the passengers. This indicates a state close to a perfectly mixed state. If perfectly mixed

conditions could be assumed after 3 minutes (180s), the average droplet fraction concentration can be written as:

$$c(t) = \frac{n_i(180)\exp(-Q(t-180)/V)}{V} \quad (6.2)$$

where,  $n_i(180)$  is the total droplet fraction at 180 s, i.e., the total number of droplets in the cabin at 180s divided by the total number of droplets exhaled,  $Q$  is the total supply flow rate to the cabin, and  $V$  is the volume of the cabin.

Therefore, a semi-analytical approach can be adopted to obtain the average droplet fraction concentration ( $c(t)$ ) in the vicinity of the passengers. The CFD simulation can be used to obtain the  $c(t)$  for the first 3 minutes after the droplet release and equation (6.2) to obtain  $c(t)$  beyond 3 minutes. It should be noted that the average droplet fraction concentration given by equation (6.2) is also the rate of increment in the average cumulative droplet fraction ( $\beta$ ). Figure 6.2 compares  $\beta(t)$  calculated using the semi-analytical approach with the CFD simulations for  $t > 3$  minutes. The differences were smaller than 10% and the perfectly mixed method is considered validated for  $t > 3$  minutes. Therefore, one can use the CFD method to obtain the droplet concentrations around the passengers for the initial period of 3 minutes and equation (6.2) for beyond 3 minutes.

Although not presented here in detail, one can expect that the  $\beta$  for the droplets from the breathing and talking of passenger 4D could be different from those of coughing, but the method developed above can be used for breathing and talking.

### 6.1.2 Droplets Inhaled by the Passengers due to Multiple Exhalations from the Index Passenger

An index passenger normally exhales droplets through multiple events, such as combined breathing, coughing, and talking. To carry out CFD simulations for such combined events can be very time consuming. Thus, it is important to further develop the above semi-analytical method for the multiple exhalations from the index passenger.

This investigation started from using continued breathing as an example. An unsteady CFD simulation was carried out for a case with 10 consecutive exhalations from the normal breathing of index passenger 4D. The turbulent flow and the breathing of the passengers made the local airflow in the cabin unsteady. However, the droplets from all the exhalations followed similar trajectories, even though the airflow in the cabin was unsteady. This indicates that the bulk flow in most of the domain was almost steady. Therefore, the information on the droplet concentration obtained using the CFD simulations for a single breath exhalation from the index passenger can be superimposed multiple times to obtain the droplet concentration in the cabin for the multiple exhalations of the index passenger using the following equation:

$$C_i(t) = \sum C_{b,i}(t-t_j) \quad (6.3)$$

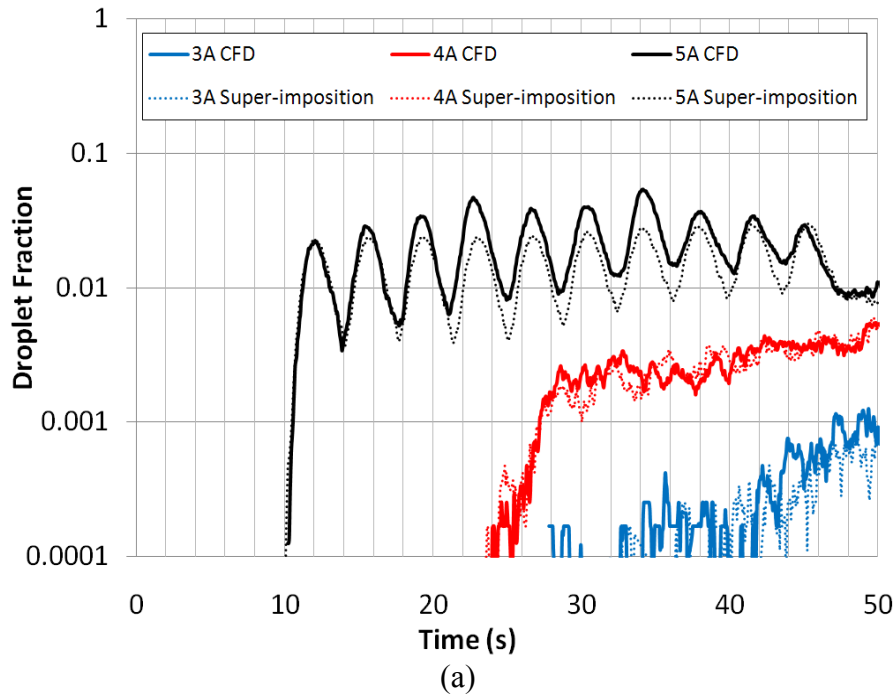
where,  $C_i(t)$  is the average droplet concentration in the breathing zone of the  $i^{\text{th}}$  passenger at time  $t$  and  $C_{b,i}(t-t_j)$  is the average droplet concentration in the zone at time  $t-t_j$  due to the breathing started at  $t_j$ .

If the principle can be extended for coughing and talking, the droplet concentration in a breathing zone can be obtained by summing up that from all the exhalations taking place until current time with a time shift:

$$C_i(t) = \sum C_{c,i}(t-t_i) + C_{b,i}(t-t_j) + C_{ta,i}(t-t_k) \quad (6.4)$$

where,  $C_{c,i}(t-t_i)$  is the average droplet concentration in the breathing zone at time  $t-t_i$  due to the coughing starting at  $t_i$ , and  $C_{ta,i}(t-t_k)$  is the average droplet concentration in the zone at time  $t-t_k$  due to the talking starting at  $t_k$ . The  $C_{c,i}$ ,  $C_{b,i}$ , and  $C_{ta,i}$  can be obtained from the CFD simulations for the droplets exhaled from a single cough, breathing, and talking, respectively.

To validate the model developed, Figure 6.3 compares the droplet fraction in the breathing zones with 10 consecutive exhalations from the index passenger predicted by CFD with the droplet fraction calculated by the super-imposition method. The variation trend of the droplet fraction was similar in the two methods but with differences in the absolute values. The differences could be attributed to the inherent flow transience and the transient breathing. The high frequency variations were very difficult to capture by the simplified super-imposition method. Figure 6.4 further compares the  $\beta$  predicted by the two methods. Again, the two methods yielded very similar results. Thus, this investigation considers the super-imposition method to be validated.



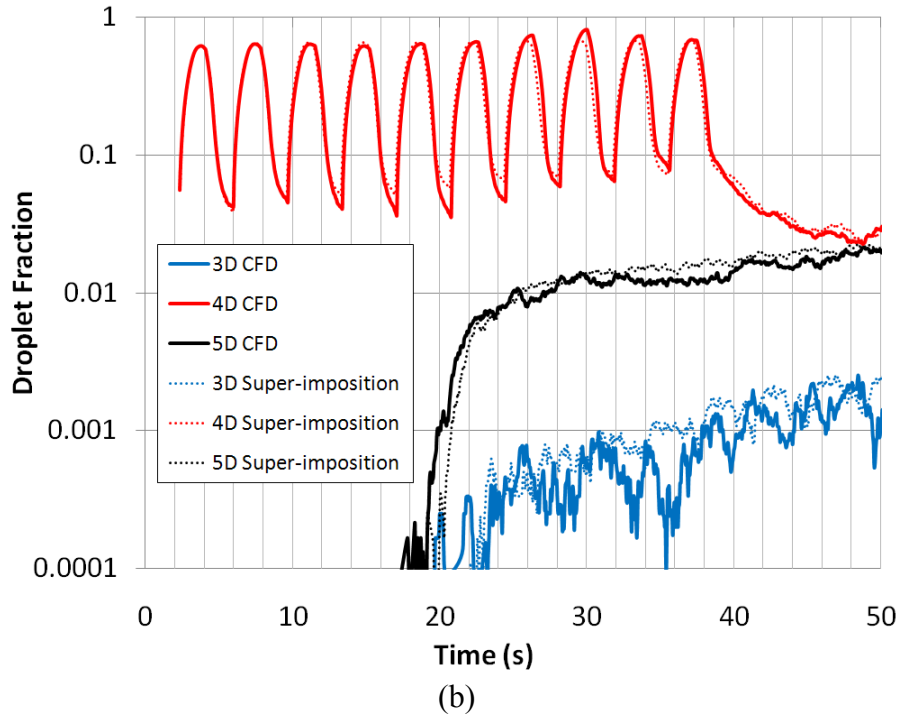


Figure 6.3 A comparison between the droplet fraction predicted by the CFD model and the super-imposition method for passengers seated in (a) 3A, 4A, and 5A seats and (b) 3D, 4D, and 5D seats.

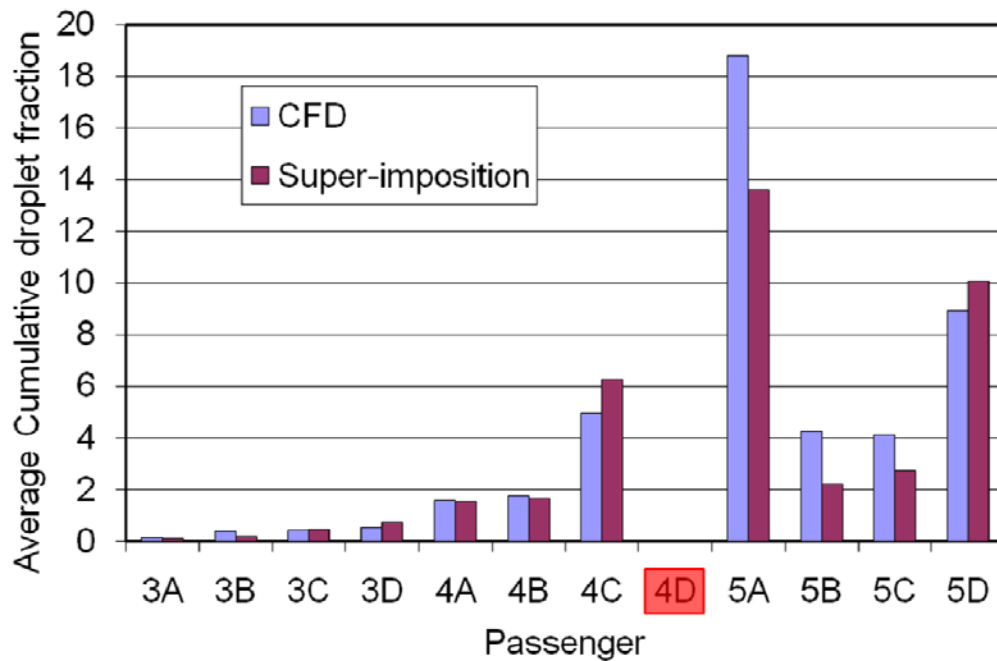


Figure 6.4 A comparison of the  $\beta$  predicted by the CFD and super-imposition methods for passengers sitting in the 4th, 5th, and 6th rows.

The total amount of droplets inhaled by each passenger can be calculated by integrating the breathing profile of each passenger with the droplet concentration in the breathing zone:

$$r_i(t) = \sum q_i(t)C_i(t)\Delta t \quad (6.5)$$

where  $q_i$  is the rate of inhalation (volume/time) of the  $i^{\text{th}}$  passenger and is zero during exhalation, and  $C_i$  is the average droplet concentration (number of droplets/volume) in the zone around the  $i^{\text{th}}$  passenger. Our breathing measurements have developed methods to obtain  $q_i$  based on the physiological details of the passengers.

Figure 6.5 shows a representative variation of the cumulative droplets inhaled by a passenger, the droplet concentration in the breathing zone, and the breathing flow rate. The droplets inhaled by the passenger were zero initially as the droplet concentration in the breathing zone was zero.

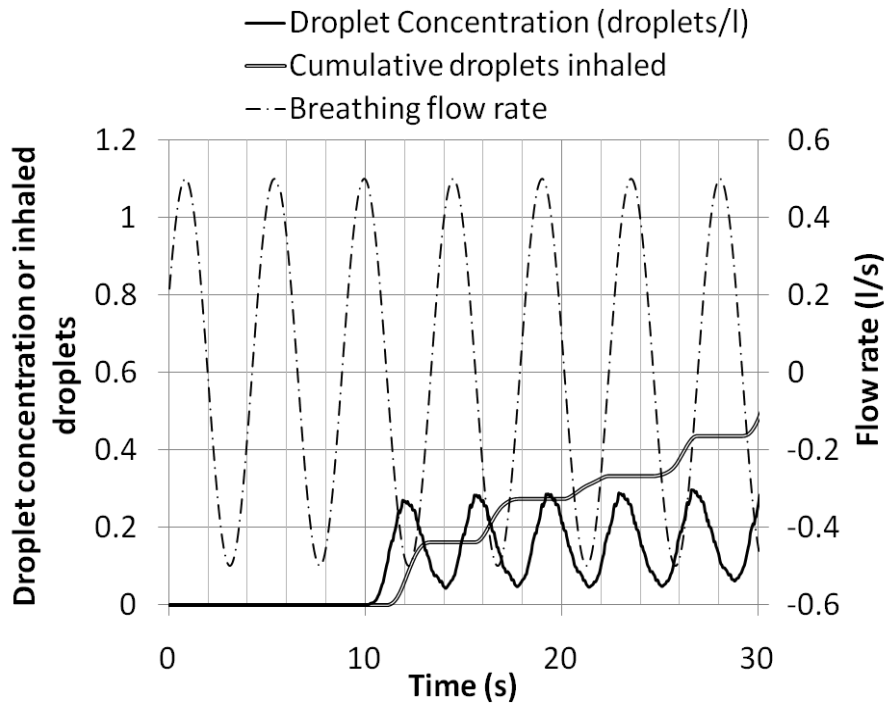


Figure 6.5 A representative variation in droplet fraction and the cumulative droplets inhaled.

### 6.1.3 Case Setup

With the method to extend the CFD data of 3 minutes to the whole flight and the method of super-imposition to calculate the droplet concentration in the breathing zones, this investigation has studied the droplets inhaled by different passengers in the cabin shown in Fig. 5.1 (a) during a 4-hour flight. MATLAB codes were developed to calculate the amount of inhaled droplets using the method of super-imposition. Since the index passenger can exhale droplets through coughing, breathing, talking, or any combination of these exhalations, three hypothetical cases were analyzed and are as follows:

- 1) Breathing only: This case assumed that the index passenger exhaled 525 droplets for every breathing exhalation, as calculated by Gupta et al., (2010b) using the measurements performed by Fabian et al., (2008) and Edwards et al., (2004) on the amount of droplets exhaled during breathing.
- 2) Coughing and breathing: The studies by Hsu et al. (1994) and Loudon and Brown (1967) indicated that the cough frequency can vary from 12 to 35 and 3 to 48 coughs per hour, respectively. By using an average from these studies, this case assumed 100 coughing exhalations for the 4 hour flight. Since the index passenger would also breathe normally, the 100 coughing exhalations were randomly sandwiched between the breathing. It was further assumed that the index passenger exhaled  $10^6$  droplets for each cough, as calculated by Gupta et al., (2010b) using the studies conducted by Yang et al., (2007).
- 3) Talking and breathing: This case assumed that the index passenger would talk for 30 minutes during the flight. The talking exhalations were also coupled with the breathing exhalations. It was assumed that the index passenger released 150 droplets every second through the talking, as calculated by (Gupta et al., 2010b) using the studies of Fairchild and Stampfer, (1987).

## 6.2 Results

Figure 6.6 presents the total amount of droplets inhaled by the fellow passengers due to the exhalations from index passenger 4D for the three cases by using the research method developed and validated in the previous sections. The results are for passengers seated on the 3<sup>rd</sup>, 4<sup>th</sup>, and 5<sup>th</sup> rows. The number of droplets inhaled by the index passenger is not shown as it is not meaningful. The inhaled droplets varied with location and type of exhalation from the index passenger.

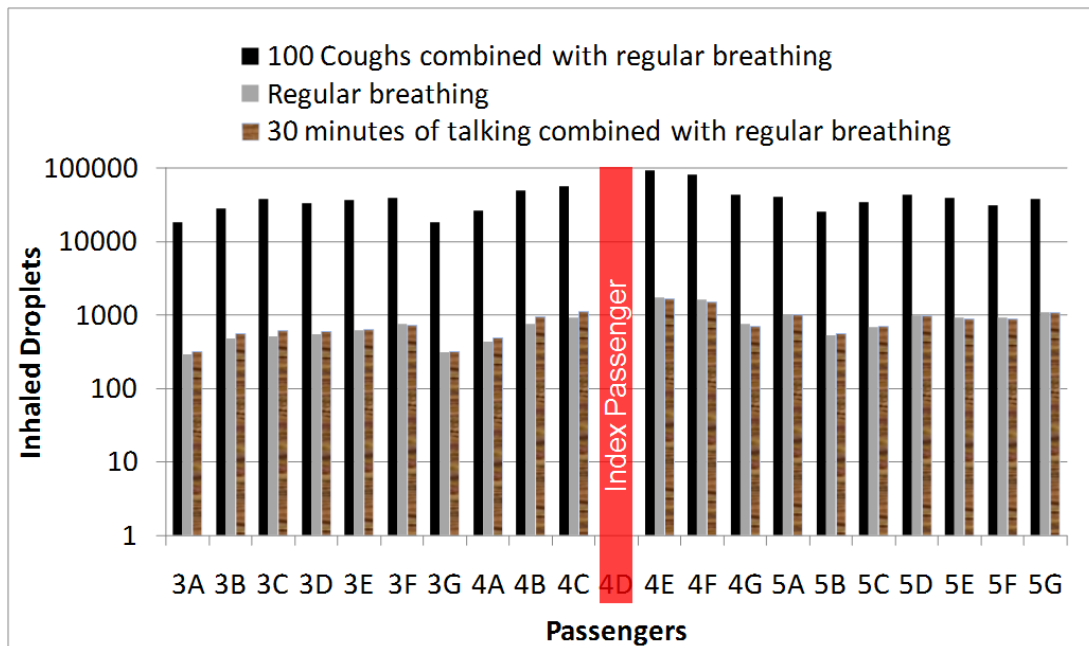


*Figure 6.6 The droplets inhaled by the passengers seated in the 3rd, 4th and 5th rows for regular breathing, 100 coughs combined with regular breathing, and 30 minutes of talking along with regular breathing by the index passenger.*

The droplets inhaled by these passengers, generated by the exhalations from the regular breathing of the index passenger, varied from 300 to 2000 depending on the movement of the droplets. The droplets first went to passenger 5A and 5G but stayed there only for a short period of time due to the high air velocity in that zone. These droplets then went to passengers in 4C, 4D, 4E, 5C, 5D and 5E; thus, the number of droplets inhaled by these passengers was high. The droplet cloud reached the 3<sup>rd</sup> row after some time, then the droplet concentration decreased, so the number of droplets inhaled by passengers seated in this row was relatively low.

When the coughing was combined with regular breathing, the droplets inhaled by the fellow passengers varied from 18000 to 90000. This was because a cough contains  $10^6$  droplets, while a breath contains only 525. Clearly, the exhalation from a cough carries more risk to fellow passengers than the breathing. The droplets inhaled by passengers in 5A, 5G and 5D were relatively fewer than those inhaled by the passengers in row 4. This is because the high velocity of the cough jet pushed the droplets to the front of the index passengers, so fewer droplets moved to the back row (5<sup>th</sup> row) (as discussed in the last chapter).

For the case in which talking was combined with regular breathing, the droplets inhaled by the fellow passengers varied from 300 to 1700. The talking exhaled droplets inhaled by the passenger in 4C were relatively more than those inhaled by the other passengers because the passenger was in conversation with the index passenger. The droplets inhaled by the passengers and the distribution pattern were similar to the case that had only breathing. This implies that the rate of release of droplets from talking was similar to rate of release from breathing. As the combined effect of breathing and talking is shown, the order of effective amount of droplets inhaled is a cumulative of both the processes.

It was observed that the number of droplets inhaled was linear with time. This means that the droplets inhaled in an 8-hour flight would be twice as many, and in a 2-hour flight, half those of the 4-hour flight.

### 6.3 Discussion

The investigation calculated the droplets inhaled by the passengers seated in the row and the neighboring rows of the index passenger for three common scenarios. The droplets inhaled by the fellow passengers were of the order of  $10^3$  due to the breathing and talking in the 4-hour flight and  $10^5$  due to the coughing. It should be noted that not all these droplets contained active infectious agents. The study provided only an estimate of the relative risk of infection to the passengers.

The information on the viability and the amount of the infectious agents should be added to this model to predict the spatial distribution of infection risk in the cabin. The model accounts for the time and spatial variation of parameters such as the breathing flow rate and the droplet concentration. The model can be easily coupled with the viability and amount of infectious agents.

## 6.4 Conclusions

The methods to predict the transport of droplets exhaled from combinations of breathing, talking, and coughing of an index passenger in an aircraft cabin for the whole flight duration were developed. Since the droplets got well mixed in the cabin air 3 minutes after they were released, the method used combined CFD and mixed condition models for the prediction. It was found that the droplet distribution from single exhalations can be superimposed to obtain the droplet distribution for multiple exhalation scenarios. The droplets inhaled by a passenger can consequently be determined for the whole flight duration.

The number of droplets inhaled by the fellow passengers due to the droplets exhaled from regular breathing, 100 coughs sandwiched with regular breathing, and 30 minutes of talking combined with regular breathing from the index passenger in a 4-hour flight were calculated. The coughs generated the most droplets and may impose a very high risk on the fellow passengers if the droplets contained active infectious agents. The risks due to the breathing and talking were almost two orders of magnitude smaller than the risk due to coughing.

## 7. EVALUATION OF AIRBORNE RISK OF INFECTION IN AN AIRCRAFT CABIN

In the previous chapter a method to predict the amount of droplets inhaled by the passengers for realistic flight durations was presented. As not all of these droplets may contain the infectious agents, the number of droplets inhaled may not represent the risk of infection. This chapter first presents a method to quantify the risk of infection based on the amount of infectious agents inhaled by the passengers in the aircraft. Using this method the reduction in the risk to the passengers was also calculated for a scenario with the passengers wearing masks.

### 7.1 Risk Assessment Models

The risk of infection can be quantified using either the deterministic or the probabilistic (stochastic) models. Haas et al., (1999) discussed these models in details. Recently Sze To and Chao, (2010) have reviewed these models. For both the models it is required to calculate the dose inhaled by the susceptible occupants. The dose could be represented as the tissue culture infectious dose (TCID<sub>50</sub>), colony forming unit (cfu), influenza virus RNA particle or quanta (Wells, 1955). To calculate the dose inhaled by the occupants, the information on the dose exhaled by the infectious person during various exhalations such as coughing, sneezing, breathing or talking is required. There are a few studies that quantified the dose exhaled for some of the airborne infectious diseases. Alford et al., (1966) quantified the dose exhaled by the influenza patients in terms of TCID<sub>50</sub>. Yeager et al., (1967) measured the amount of colony forming units in patients with tuberculosis. Recently Fabian et al., (2009) and Milton et al., (2010) conducted controlled experiments and quantified the amount of influenza virus RNA particles exhaled from the breath and cough of influenza infected people. The dose exhaled during various epidemics was also calculated in terms of quanta (Qian et al., 2009 and Rudnick and Milton, 2003). Quanta is a term defined by Wells, 1955 that indicates that if a person inhales one quanta the probability of him getting infected is 1-1/e. Using the information on the amount of dose exhaled and the dose inhaled can be calculated using the equation given by:

$$d_i(t) = \sum f \alpha(t-t_0) p_i(t) C_i(t) \Delta t \quad (7.1)$$

where,  $d_i(t)$  is the dose inhaled by the  $i^{\text{th}}$  passenger till time  $t$ ,  $f$  is the amount of infectious agents contained in a droplet,  $\alpha$  is the viability of the infectious agent, i.e. the fraction of total infectious agents that are active at time  $t$ . This is generally defined with reference to the time, the infectious agents are exhaled.  $t_0$  is the time when the infectious agents are exhaled, therefore it is a function of  $t-t_0$ .  $p_i$  is the rate of inhalation (volume/time) for the  $i^{\text{th}}$  passenger and is zero during exhalation. (Gupta et al., 2009) and  $C_i$  is the concentration of droplets in the vicinity of the  $i^{\text{th}}$  passenger.

For the deterministic models a person will get infected only if he inhales more than or equal to his tolerance dose (Haas et al., 1999). This tolerance dose can vary based

on the type of infectious agent and the immunity of the susceptible person. But to our knowledge there is no study that quantifies the tolerance dose in terms of TCID<sub>50</sub>, cfu or influenza virus RNA particles. Therefore even though the dose inhaled can be quantified the risk can't be quantified. The inhaled dose can give indication on the relative risk of infection.

On the other hand the probabilistic models are based on probability distribution such as Poisson's or Beta-Poisson's distribution. The probabilistic models do not tell if a person will get infected or not, but will estimate the probability of a person to get infected. Some of the most popular probabilistic models are dose-response model (Haas, 1983) and Wells-Riley model (Riley et al., 1978). Recently Sze To and Chao, (2010) have reviewed the pros and cons of these models. Equation (7.2) shows the mathematical form of the probability of risk given by Wells-Riley equation and is given by:

$$P = \frac{D}{S} = 1 - \exp\left(-\frac{Iqp}{Q}t\right) = 1 - \exp(-N_s) . \quad (7.2)$$

The dose response model can be mathematically written as:

$$P = \frac{D}{S} = 1 - \exp(-rN) \quad (7.3)$$

where, P is the probability of infection, D is the number of developed (secondary) infection cases, S is the number of susceptible cases, I is the primary infected cases, q is the quanta release rate, p is the pulmonary ventilation rate, Q is the ventilation rate, r is the contact rate (or capacity to cause infection) and N is the inhalation dose. N<sub>s</sub> represents the infectious inhalation dose under perfectly mixed steady state scenario. The value of r depends on the human response to the airborne infection. Some of the studies on mice for tubercle found that the best fitted r value is one (Wells, 1955). Recently Jones et al., (2009) suggested a value of 0.0218 based on infection in monkeys. Therefore the accuracy of probability of risk will depend on the value of r. Similarly the calculation of risk using the Wells-Riley approach requires information on quanta. The information on quanta for various epidemics was calculated (Riley et al., 1978; Rudnick and Milton, 2003 and Qian et al., 2009) using the Wells-Riley equation (Riley et al., 1978) . The quanta values were back calculated by substituting the number of susceptible and infected people, ventilation rate and pulmonary rate, and the time of exposure. Therefore the quanta calculations were not direct. As the method on predicting the quanta exhaled is not direct, people have debated on its accuracy (Sze To and Chao, 2010). Even though the method is not direct but as the information (quanta) is the infectious dose, we have used the Wells-Riley equation to quantify the risk of infection in an aircraft cabin.

To summarize, we have used the deterministic and probabilistic model (Wells-Riley equation) to quantify the amount of infectious agents inhaled and probability of infection respectively in an aircraft. Finally the reduction in risk was estimated if the passengers wear masks.

## 7.2 Case Description

A fully occupied Boeing 767 flight with index passenger suffering from influenza and seated at the center of the row was studied. The risk of infection for the passengers seated in the row of the index passenger and the neighboring rows was calculated for a four hours of air travel. The CFD studies were performed under the ventilation rate of 33.7 ACH and therefore we assumed the same ventilation rate for the four hours of air travel. The amount of dose inhaled (influenza virus RNA particle or the quanta) by each passenger was first calculated based on the amount of dose exhaled by the index passenger as discussed in the next section. Similar calculations on the dose inhaled were performed assuming that the protection factor provided by the masks is 10 (as discussed in detail in literature review section). Finally the risk of infection was calculated.

### 7.3 Amount and Viability of Dose

#### 7.3.1 Deterministic Models

The dose for the deterministic models was defined in terms of the influenza virus RNA particles. Fabian et al., (2009) and Milton et al., (2010) measured the rate of exhalation of influenza virus RNA particles from the cough and breathe of influenza infected patients. It was observed that an influenza infected subject can exhale 0.01 to 2 influenza virus RNA particles per minute (geometric mean 0.1) through breathing. The amount of such influenza virus RNA particles for a cough combined with one minute of breathing ranged from 0.1 to 20000 per minute (geometric mean 3.1) and 0.1 to 100000 per minute (geometric mean 5) for coarse and fine particles respectively. Therefore a cough alone can contain 8 (geometric mean) influenza virus RNA particles. Harper, (1961) found that the viability of the influenza virus does not change significantly in four hours and thus it was assumed to be 1 ( $\alpha=1$ ). Hsu et al., (1994) and Loudon and Brown, (1967) indicated that the cough frequency can vary from 12 to 35 and 3 to 48 per hour respectively. Thus average of 25 cough exhalations an hour was considered. No breathing exhalations were considered as the amount of infectious agents exhaled from cough was higher than breathing. This information along with the breathing profile and droplet concentration as obtained from the method discussed earlier can be used in equation (7.1) to calculate the inhaled amount.

#### 7.3.2 Probabilistic Model: Wells Riley Equation

The dose inhaled for the Wells-Riley model was calculated in terms of quanta. The rate of exhalation of quanta was calculated based on the influenza epidemic case (Moser et al., 1979). A Boeing 737 flight got delayed for 4.5 hours due to engine failure. There were 54 people on board while 29 remained on board throughout the delay. One index passenger was on board and 25 secondary infection cases were observed. Rudnick and Milton, (2003) formulated an unsteady Wells-Riley equation and calculated the quanta release rate for this case under low air exchange rate. The quanta release rate was 79 and 128 per hour for 0.1 and 0.5 ACH respectively. We took an average and considered a quanta release rate of 103 per hour. Assuming if the same infection spread would have taken place under ventilation rate of 33.7 ACH, we found that the quanta release rate would have been 5226 per hour. As the quanta is an active quantity we

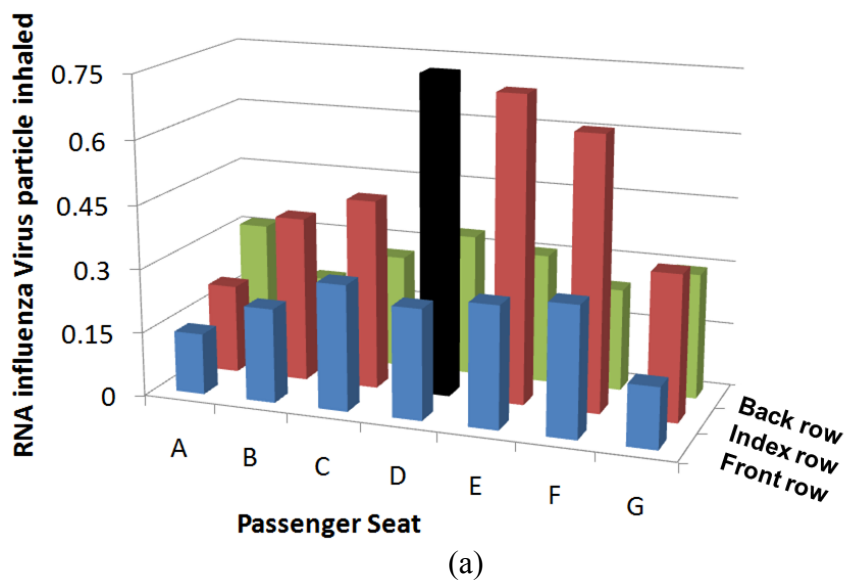
assumed the value of  $\alpha$  to be one. The amount of quanta inhaled was then calculated similarly using equation (7.1) and assuming that all the quanta was exhaled through coughing. The probability of infection was calculated for both the quanta release rate.

## 7.4 Results

This section first presents the results on the risk predicted using the deterministic and probabilistic models. The reduction in risk for a case with everyone except the index passenger is wearing the N-95 masks was then calculated.

### 7.4.1 Risk of Infection from Influenza using the Deterministic and Probabilistic Models

Figure 7.1 shows the risk of infection from influenza for the passengers seated in the row and the neighboring rows of the index passenger, using the deterministic and probabilistic approaches respectively, for a four hours air travel. The risk evaluated using the deterministic approach is represented as inhaled influenza virus RNA particles, as shown in Figure 7.1 (a). The index passenger was located at seat D. It should be noticed that the dose inhaled by the passengers seated in the vicinity of the index passenger were high. The dose inhaled by passenger 5A was high even though the seat is far from the index passenger. It is because the droplet exhaled moved backwards and then towards the window on the back and index passenger rows. The amount inhaled was in accordance with the droplet movement. It can be seen that the amount of influenza virus RNA particles inhaled for four hours of flight was less than one but it does not mean that the risk was low or high, as the influenza virus RNA particles can be more than one influenza virus. Moreover the tolerance dose for influenza for the passengers is not known. Thus any comment on who all can get infected can't be made. But the relative risk of infection to the passengers can be observed.



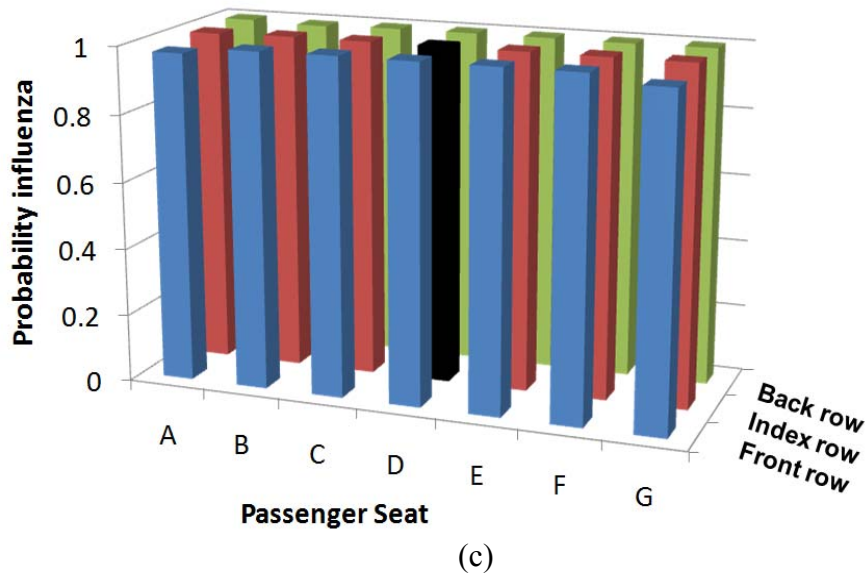
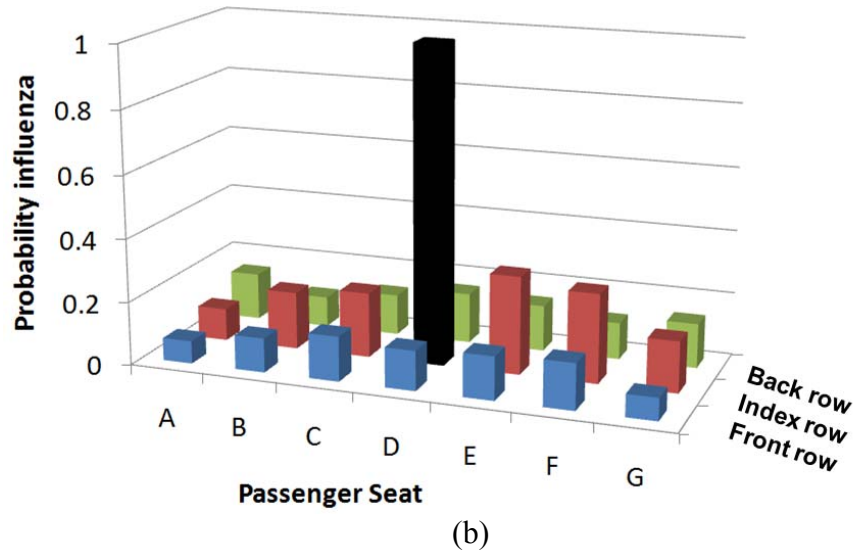


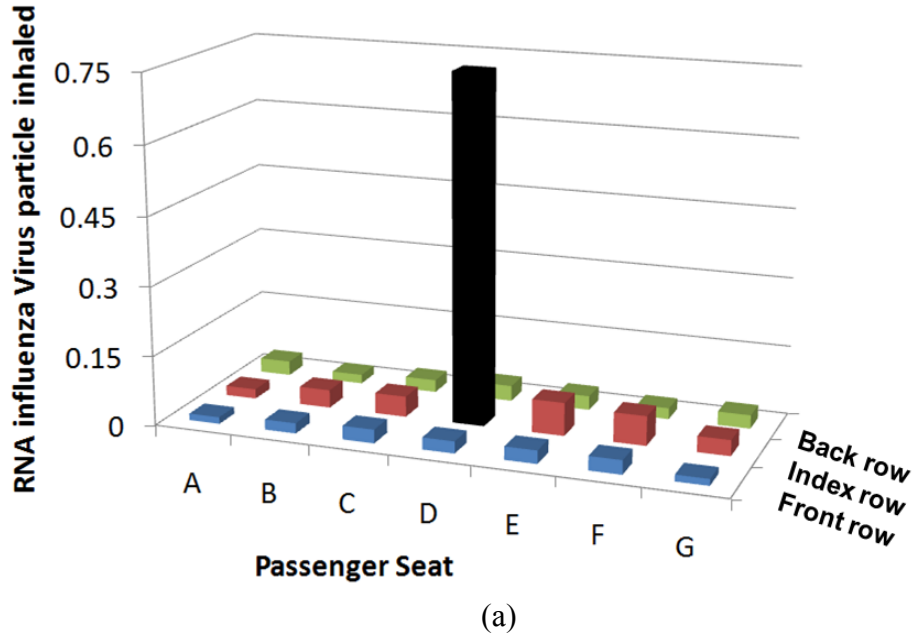
Figure 7.1 Risk of infection from influenza for the passengers in a 4 hours flight (a) Deterministic approach: inhaled influenza virus RNA particles (b) Probabilistic approach: probability of getting infected with influenza for the release rate of 103 quanta per hour (c) release rate of 5226 quanta per hour.

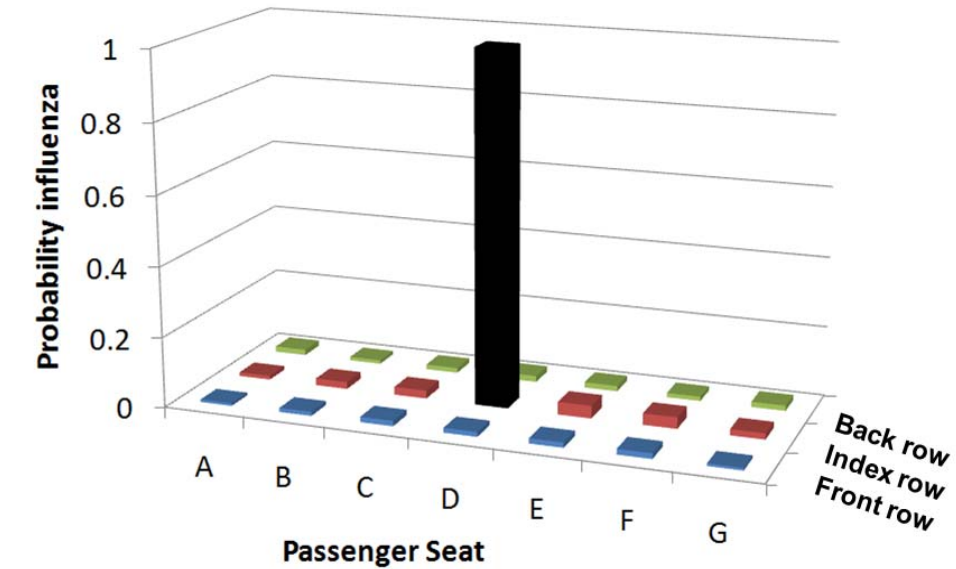
On the other hand, the risk evaluated using the probabilistic approach is represented as the probability of getting infected from influenza (Probability influenza) from an index passenger. Figure 7.1 (b) and (c) show the Probability influenza for the release rate of 103 quanta per hour (low ventilation) and 5226 quanta per hour (33.7 ACH) respectively. The Probability influenza is proportional to the amount of quanta of influenza inhaled. Therefore the Probability influenza was higher for the passengers seated close to the index passenger and 5G and 5A as explained earlier. Higher the probability, more are the chances of getting the infection. Considering the average probability for the passengers, it was found that there is a probability of getting 3 (rounded off) people infected out of 20 for quanta release rate of 103 per hour. This is much lower than the observed case of 25 secondary infection cases out of total 29

passengers (Moser et al., 1979). This is because flight case happened under no or low ventilation, while our calculations were performed assuming a full ventilation of 33.7 ACH. This clearly explains the importance of the ventilation system. Similar calculations on average probability for the quanta release rate of 5226 per hour indicated that there is a probability of all 20 people getting infected with influenza. This is because the quanta release rate of 5226 per hour was back calculated assuming a full ventilated aircraft and 25 secondary infection cases among 29 total passengers.

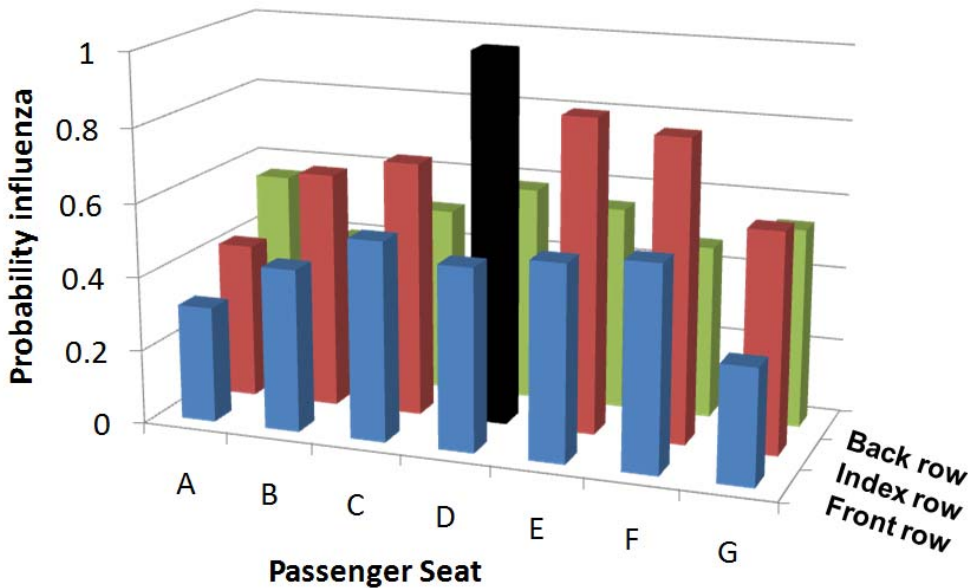
#### 7.4.2 Effect of N-95 Mask

Figure 7.2 shows the risk of infection from influenza for the case with everyone except the index passenger is wearing the mask. As discussed earlier the mask can provide a protection factor of 10, therefore the amount of influenza virus RNA particles would be  $1/10^{\text{th}}$  of inhaled without the masks, as shown in Fig. 7.2 (a). If the index passenger also wears the mask the amount would be even lower.





(b)



(c)

Figure 7.2 Risk of infection from influenza for the passengers in a 4 hours flight for a case with the passengers except the index passenger wearing the masks (a) Deterministic approach: inhaled influenza virus RNA particles (b) Probabilistic approach: probability of getting infected with influenza for the release rate of 103 quanta per hour (c) release rate of 5226 quanta per hour.

Similarly the quanta inhaled with the masks would be 10% of the quanta inhaled without the mask and thus the Probability influenza with the mask would be lower than without mask as shown in Figure 7.2 (b) and (c). Considering the average probability of infection for the passengers wearing mask case, it was found that 0 (rounded off) of 20 and 11 out of 20 passengers may get infected for the quanta release rate of 103 and 5226 per hour respectively. This is lower than the average probability of infection without the

mask case which was 3 out of 20 and 20 out of 20 for the quanta release rate of 103 and 5226 per hour respectively. This clearly indicates the usability of the masks.

## 7.5 Discussion

The model quantified the amount of dose inhaled based on the dose exhaled from the data collected by Fabian et al., (2009) and Milton et al., (2010) and the influenza epidemic case (Moser et al., 1979). As the dose exhaled can vary from index passenger's infectious conditions, the dose inhaled and thus the probability of getting infected by the susceptible passengers would be a direct function of it. Total protection level provided by the N95 respirator mask was considered to be 10% based on the available literature and the values can vary based on the fitting.

## 7.6 Conclusion

A method to predict the spatial and temporal risk of infection in an aircraft based on the deterministic and probabilistic approaches was discussed. Using the methods developed in earlier sections the spatial distribution of dose inhaled by the passengers was calculated. Based on the dose inhaled the risk of infection was quantified for the passengers seated in the row and the neighboring rows of the index passengers with influenza for a four hours of flight.

For the deterministic approach the dose was quantified as the number of influenza virus RNA particles inhaled, but as the tolerance dose for the influenza virus RNA particles is not known nothing can be said on the infection risk to the passengers.

For the probabilistic approach the Wells Riley equation was used to quantify the probability of influenza based on the spatial distribution of quanta inhaled by the passengers. It was found that the probability of influenza can be reduced by using N95 respirator masks.

## 8. INFLUENCE OF MOVING BODY THROUGH EXPERIMENTAL AND CFD INVESTIGATIONS IN A SMALL-SCALE CABIN

In addition to the supply airflow condition from the diffusers, movement of individuals inside enclosed environments such as airliner cabins has been shown to significantly influence contaminant distribution and personal exposure (Brohus et al., 2006; Bjørn and Nielsen, 2002; Bjørn et al., 1997). Passengers seated as far as 7 rows from the infected passenger were affected during the SARS contamination incident on the Air China flight (Olsen et al., 2003), whereas previous investigations, which did not consider the effects of moving crew and passengers, concluded that in-flight transmission of a disease should remain confined to within 2 rows of a contagious passenger (NRC 2002; Kenyon et al., 1996; Jeffrey et al., 1993). The infection of some of the crew members on the Air China flight raises concerns about the mechanisms of transmission, i.e. whether their movement promoted the SARS transmission. This chapter is an attempt to provide an understanding of the influence of moving crew members and passengers on flow and contaminant transport in an airliner cabin.

### 8.1 Research Methodologies

In general, the investigation of the influence of human movements on airborne contaminant transmission in airliner cabins can be done experimentally or through computer simulations, the latter being more practical and cost-efficient. Numerical simulations of movement in a cabin can be handled directly or indirectly. But direct methods are more time-expensive because they involve moving and dynamic grids to simulate body movement. Matsumoto et al. (2004) used a grid deformation approach to generate a computational mesh around a moving body in an empty room. A similar CFD approach was used in studying the airflow due to a walking person and a sliding door in an isolation room (Shih et al., 2007). Edge et al. (2005) applied unsteady Reynolds-averaged Navier–Stokes (RANS) simulations in a study of contaminant transport in the wake of a stationary human model. Choi and Edwards (2008) further modeled contaminant transport induced by human walking motion in simplified situations, with a person walking from one room to another and a person walking from a room into a long hallway. They used a human kinematics model to generate a realistic human walking motion.

In contrast, indirect methods model movements in an approximate way such as using a distributed momentum source (Zhai et al., 2002) or a turbulent kinetic energy source (Brohus et al., 2006). Such methods have been used in the study of contaminant transmission in complex computational domains such as orthopedic surgical rooms. Indirect methods are computationally faster, as they require no remeshing, and are therefore preferred over direct methods. Moreover, any real-life body displacement pattern may be modeled using indirect methods rather than direct methods, which might be beyond practical reach, but at the expense of accuracy (Brohus et al., 2006). Both direct and indirect numerical simulations of people's movements have their own advantages and disadvantages, yet no conclusive indication of the reliability of these

CFD modeling techniques in predicting flow and contaminant transport in airliner cabins and other enclosed environments can be drawn. As these CFD models use approximations, their reliability is always questionable unless validated by high quality experimental data (Chen and Srebric, 2002).

The literature on experimental investigations of diverse enclosed environments indicates a significant influence of movement on the airflow and transport of contaminants (Matsumoto and Ohba, 2004; Bjørn and Nielsen, 2002; Bjørn et al., 1997; Mattsson and Sandberg, 1996). But these studies lacked sufficient spatial and temporal resolutions for validation of CFD models. Moreover, the studies recently conducted by Zhang et al. (2005; 2009) and Kühn et al. (2009) emphasized the difficulty of measuring and understanding the complex airflow inside a full-scale cabin mockup, even under steady-state conditions. The large volume of the enclosure and the complications arising from obstructions such as seats and simulated passengers prevented obtaining detailed data. The presence of body movements would make it even more difficult to acquire data with meaningful resolutions. Small-scale water models produce reasonably well-resolved data to permit an understanding of flow and contaminant transport in ventilated buildings, e.g. Lin and Linden (2002), Thatcher et al. (2004), Settles (2006), and Finlayson et al. (2004). As a consequence, the present study uses a simplified small-scale cabin mockup inside a water tank in an effort to generate the high-quality experimental data required to validate the performance of an associated CFD model. However, changes in the physical scale and working fluid further complicate the interpretation of equivalent effects to a full scale (Thatcher et al., 2004).

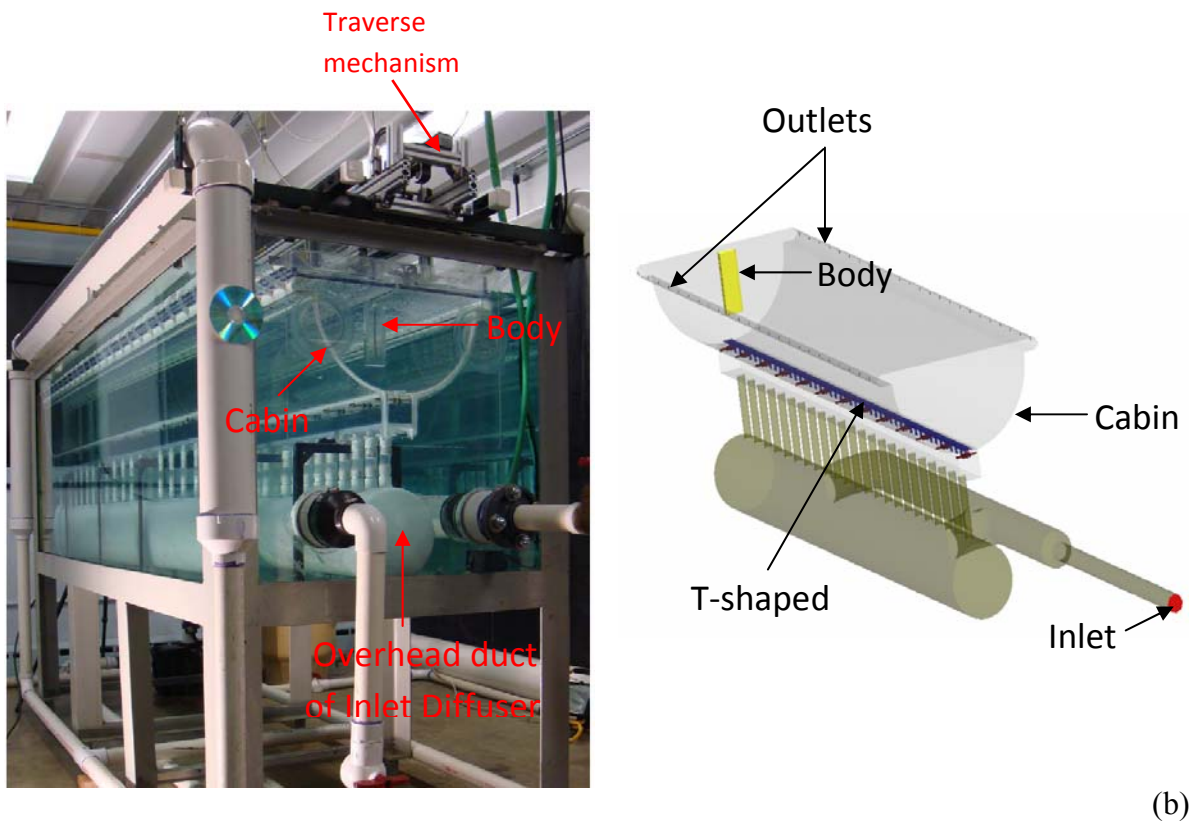
In order to address the influence of body movements on flow and contaminant transport in airliner cabins, the present work is divided into two chapters. This chapter presents the experimental results from the small-scale cabin mockup and discusses the performance of a companion CFD model.

## 8.2 Experimental Method

### 8.2.1 Experimental Setup

Figure 8.1(a) shows the small-scale, water-based experimental test facility consisting of an upside-down cabin mockup. The cabin was made using a transparent semi-circular pipe 45 cm in diameter and 2.44 m in length. The one-tenth scaled mockup, fully submerged in a glass tank, is equivalent to a cabin with 28 rows of economy-class seats. Water temperature was monitored during each experiment to maintain isothermal conditions inside the cabin so that the buoyancy effects could be neglected. The interior of the model cabin was free of obstructions to eliminate secondary flow features. To simulate the environmental control system (ECS) of commercial airliner cabins, provisions were made to inject water through an overhead duct of the inlet diffuser assembly (Fig. 8.1(a)). Water was pumped to the overhead pipe from a 550-liter tank. To achieve uniform inflow to the cabin, the water entered a settling chamber through 23 pipe fittings and was then supplied to the cabin through 48 elongated openings cut along the length, where a T-shaped diffuser diverted the fluid laterally to both sides of the cabin cross section. Water was extracted from two outlets located near the side walls of the

cabin at floor level. An automated mechanism placed above the experimental facility traversed the body (0.02 m thick x 0.05 m wide x 0.17 m tall) along the longitudinal direction of the cabin. In order to isolate the effects of the moving body, measurements were done with (ventilation case) and without (baseline case) the environmental control system (ECS), respectively.



(a) Figure 8.1 (a) The small-scale experimental test facility of the cabin mockup, and (b) the CFD model of the test facility.

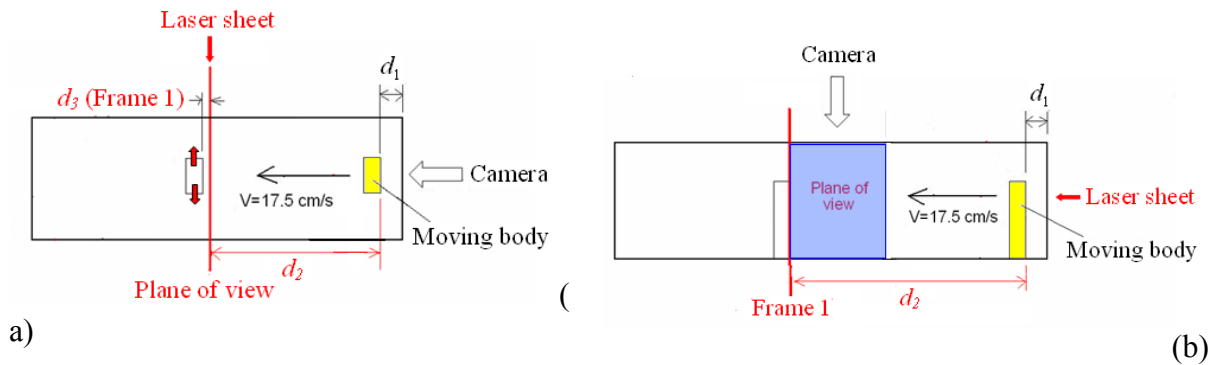
### 8.2.2 Experimental Techniques

Particle Image Velocimetry (PIV) was employed in measuring the velocity distribution inside the water tank, using a dual 50 mJ/pulse NewWave Gemini Nd:YAG laser (Raffel et al., 2007). Table 4-1 presents the configuration of the PIV system. The time interval between two successive laser pulses was typically between 1500 and 2500  $\mu$ s. A digital camera (2,048 $\times$ 2,048 pixels PowerView 4MP) was used to acquire images. The CCD camera and laser were positioned to capture cross-sectional and longitudinal flow images (Fig. 8.2). The flow visualization images were obtained using 14  $\mu$ m diameter silver-coated, hollow-sphere particles with a specific gravity of 1.7. A program was written (Labview) to synchronize the motion of the moving body with the data acquisition system. The body speed was 0.175 m/s at the model scale, which is equivalent to movement through two economy-class rows per second in an actual airliner cabin. The time and velocity scales of the tracer particles under such conditions are shown in Table 4-2. Since the tracer particles have a Stokes number much less than unity, the particles are expected to follow the fluid faithfully (Samimy and Lele, 1991). The physical

resolution of the flow field was  $3.5 \times 3.5$  mm. The experimental uncertainties in the body velocity, the flow rate, and the PIV system were 0.4%, 4%, and 5.2%, respectively (Poussou, 2008).

Table 8.1 Configuration of the PIV system.

Component	Description	Characteristics
Laser	New Wave, Gemini PIV Model #105355	Nd:YAG, 15 Hz, 532 nm 5 ns pulse, 50 mJ/pulse
Camera	TSI Inc., PowerView 4MP Model #630159	12-bit gray levels 2048x2048 pixels Nikon AF Micro-NIKKOR 60mm Nikon 62mm Circular Polarizer II
Synchronizer	TSI Inc., LaserPulse Model #610034	
Computer	Dell T3400, Intel Dual Core	2.4 GHz, 2 Gb RAM
Software	TSI Inc., Insight 3G v8.0.5	
Optics	TSI Inc., cylindrical lenses TSI Inc., spherical lenses	-15, -25, -50 mm 250, 500, 1000 mm
Particles	Laboratory for Experimental Fluid Mechanics at Johns Hopkins University	Silver coating 14 $\mu$ m diameter Specific Gravity = 1.7



Measurement settings		
	Baseline	With Ventilation
Flow rate (L/s)	0	2.5
Cross-sectional view	$d_1 = 16.6$ cm $d_2 = 83.1$ cm $d_3 = 1$ cm	$d_1 = 9.4$ cm $d_2 = 34.2$ cm $d_3 = 1$ cm
Longitudinal view	$d_1 = 16.6$ cm $d_2 = 103$ cm	$d_1 = 9.4$ cm $d_2 = 63.8$ cm

Figure 8.2 The measurement settings for (a) cross-sectional and (b) longitudinal flow visualizations.

Table 4-2. Tracer particle dynamics.

Parameter	Value
Particle response time, $\tau_p$	37.5 $\mu$ s
Flow time scale, $\tau_f$	3.6 ms
Gravitational settling time	3.2 $\mu$ m/s
Centripetal settling time	723 $\mu$ m/s
Particle Stokes number, $St = \tau_p/\tau_f$	0.0104

Planar Laser-Induced Fluorescence (PLIF) was used in visualizing contaminant transport inside the small-scale airliner cabin (Freymuth, 1993). Contaminant was simulated by injecting a dye (uranine,  $C_{20}H_{10}O_5.2Na$ ) into the flow and observing their fluorescence under laser illumination. In the present study, the dye was released from the lateral sides of the moving body (the red arrows in Fig. 8.2 (a)). The configuration details of the PLIF system are shown in Table 4-3. The dye was delivered from an 18-liter container, pressurized to 48 kPa by compressed air which emanated from the moving body at flow rates of 25 mL/s. Upon injection into the flow, the dye was illuminated by a 1-mm-thick laser sheet and recorded by a video camera, as described in Table 4-3. Cylindrical optical lenses were used to form the laser sheet. Continuous movies of the flow were recorded and converted to frame sequences using standard video-editing methods (Adobe Premiere CS3). The frame sequences of the dye transport were used to qualitatively test the CFD model.

Table 8.3 Configuration of the PLIF system.

Component	Description	Characteristics
Dye	ScholAR Chemistry, CAS #518-47-8	Disodium salt, $C_{20}H_{10}O_5.2Na$
Laser 1	New Wave, Gemini PIV, Model #10535	Nd:YAG, 532 nm
Laser 2	Lexel, Model #85	Ar-ion, 514.5 nm
Camera	TSI Inc., PowerView 4MP, Model #630159	12-bit gray levels, 7.25 fps 2048x2048 pixels

### 8.3 CFD Modeling

The CFD model used a second-order upwind scheme and the SIMPLE algorithm. The Re-Normalization Group (RNG)  $k-\epsilon$  was used to model the turbulent flow. Compared to other turbulence models, RNG  $k-\epsilon$  was observed to deliver the best performance in terms of accuracy, computing efficiency, and robustness for modeling indoor environments (Zhang et al., 2007). Note that the above CFD model would predict time-averaged flow field, while the flow visualization images captured using PIV were instantaneous. Hence, the average flow fields computed by CFD were compared with phase-averaged flow fields measured by PIV.

The CFD geometry used for this study is shown in Fig. 8.1(b). Most of the geometrical features of the experimental test facility were accurately modeled, including the pipelines of the simulated environmental control system that supply water to the cabin through the inlet diffusers. The CFD model used a combined dynamic and static mesh scheme. The computational domain was divided into two separate sections: section 1 for the moving body (dynamic mesh, 0.25 million cells) and section 2 for the rest of the cabin (static mesh, 4.4 million cells), as illustrated in Fig. 8.3. Only 5.3 % of the total meshes inside the domain were dynamic, thus reducing the computing time required for remeshing. The maximum mesh size inside the cabin was 5 mm. The dynamic layering meshing scheme was used to keep the grid size in the dynamic zone constant, which reduced the uncertainties due to the size variation of the computational mesh (Brohus et al., 2006). A commercial CFD program, FLUENT (Fluent, 2005), is used for this study. The interactions between the static and dynamic sections were done using interfacing, which can reduce the accuracy of the flow predictions (Tezduyar, 2004). User defined functions were implemented in FLUENT to define and track the movement of the body. The cabin condition was isothermal. Near wall treatment was done using standard wall functions. The speed of the body in the water was 0.175 m/s, which is equivalent to a Re of 9500 based on body width.

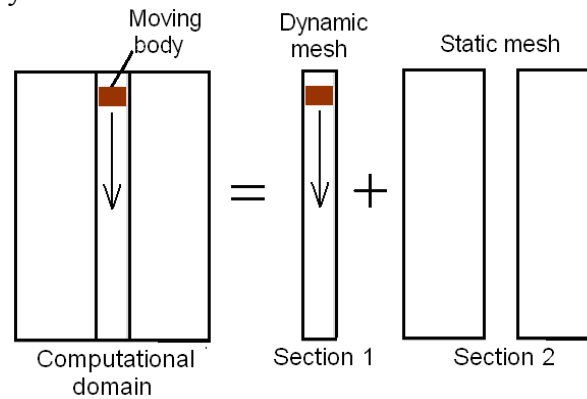


Figure 8.3 Layout of meshing scheme in the cabin section.

Both cases, i.e., with and without ventilation, were computed in a 4-node Linux cluster. Each node had five processors (1.8 GHz AMD 64) and 4GB of memory. The time step used for the computations was 0.01 s.

## 8.4 Results and Discussion

### 8.4.1 Cross-sectional Flow

Figure 8.4 shows instantaneous velocity fields in a cross section at Frame 4 obtained during different runs (runs 1, 50, and 100, respectively), along with the averaged velocity field obtained over 100 runs. The speed of the body in the water was 0.175 m/s. Frame 4 was acquired when the back of the body was at a distance of 8.25 cm from the fixed laser sheet (see Figure 8.2). Figure 8.4 shows strong intermittency in the flow. Vertical symmetry in the wake was observed in the mean velocity field. Averaged velocity field using 25, 50, and 100 measurements is shown in Fig. 8.5. A vertically

symmetric wake is visible after phase-averaging 25 measurements.

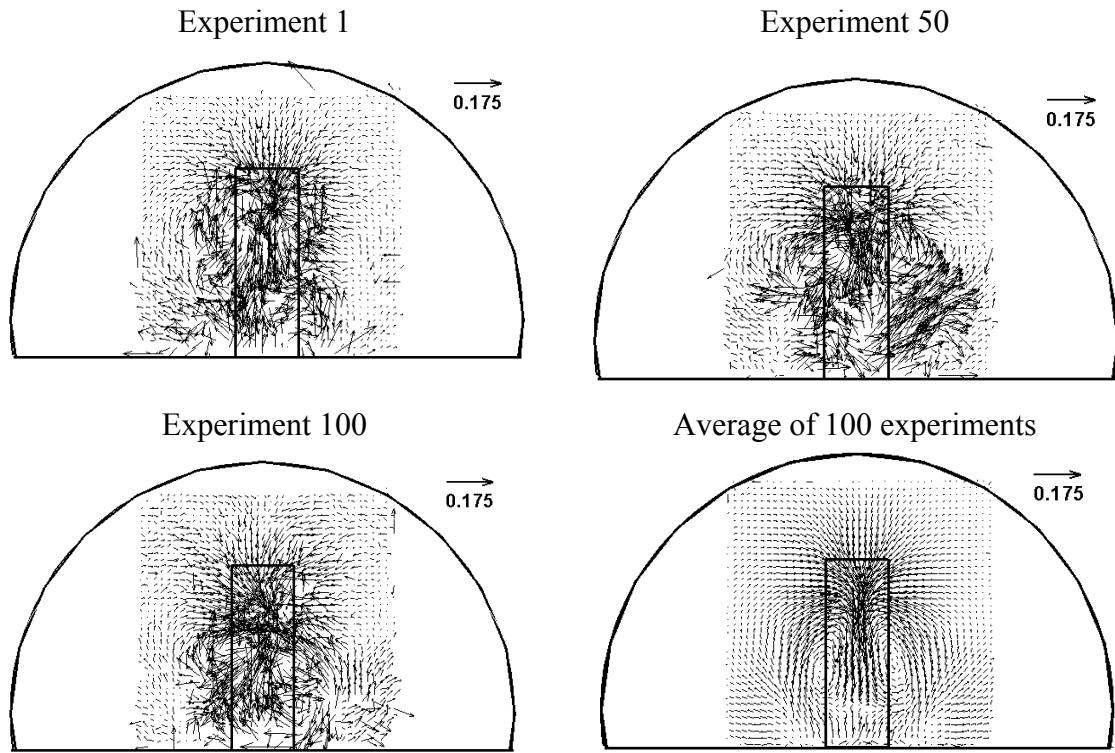
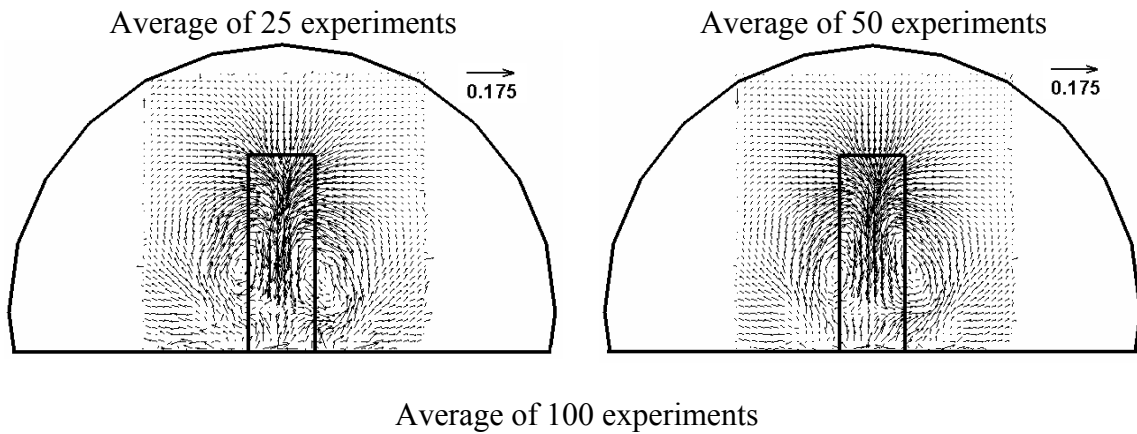


Figure 8.4 Instantaneous and averaged velocity fields at Frame 4 for the baseline case



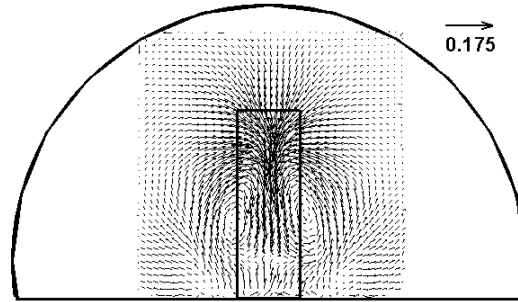
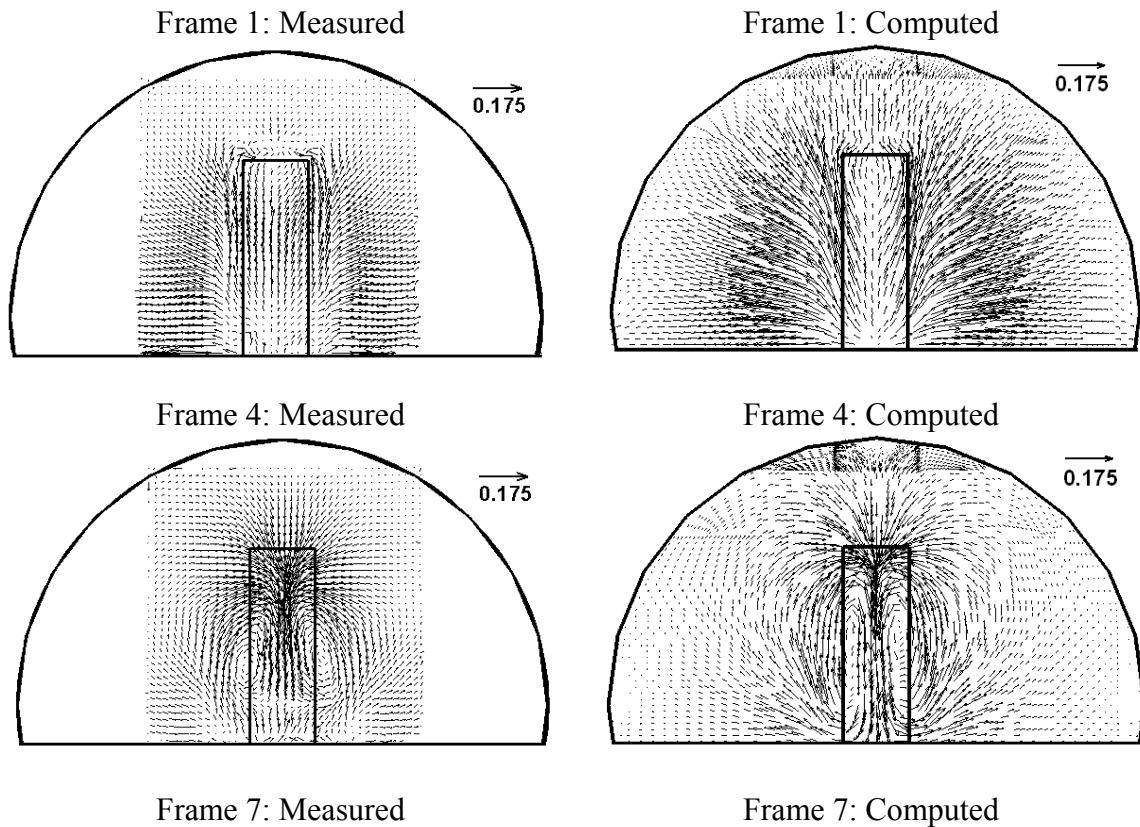


Figure 8.5 The averaged velocity fields at Frame 4 for the baseline case.

Figure 8.6(a) shows the mean flow fields of 100 measurements for baseline flow at Frames 1, 4, and 7, which were acquired when the back of the body moved 1, 8.25, and 15.5 cm past the laser sheet (refer to Fig. 8.2), respectively. A strong downwash in the wake of the moving body is shown in Fig. 8.6, which was produced by the two symmetric eddies around the top corners. Once the two eddies approached the cabin floor, they spread to the sides and dissipated. The disturbance created by the moving body on the stagnant flow field diminished very rapidly after this process.



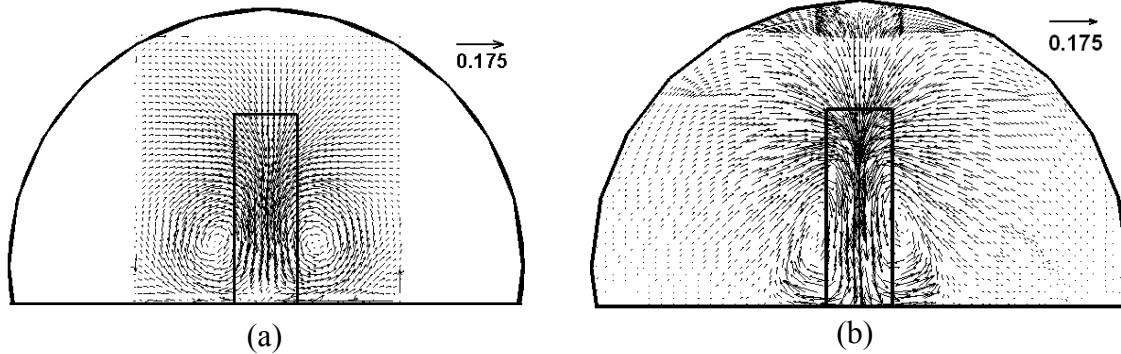
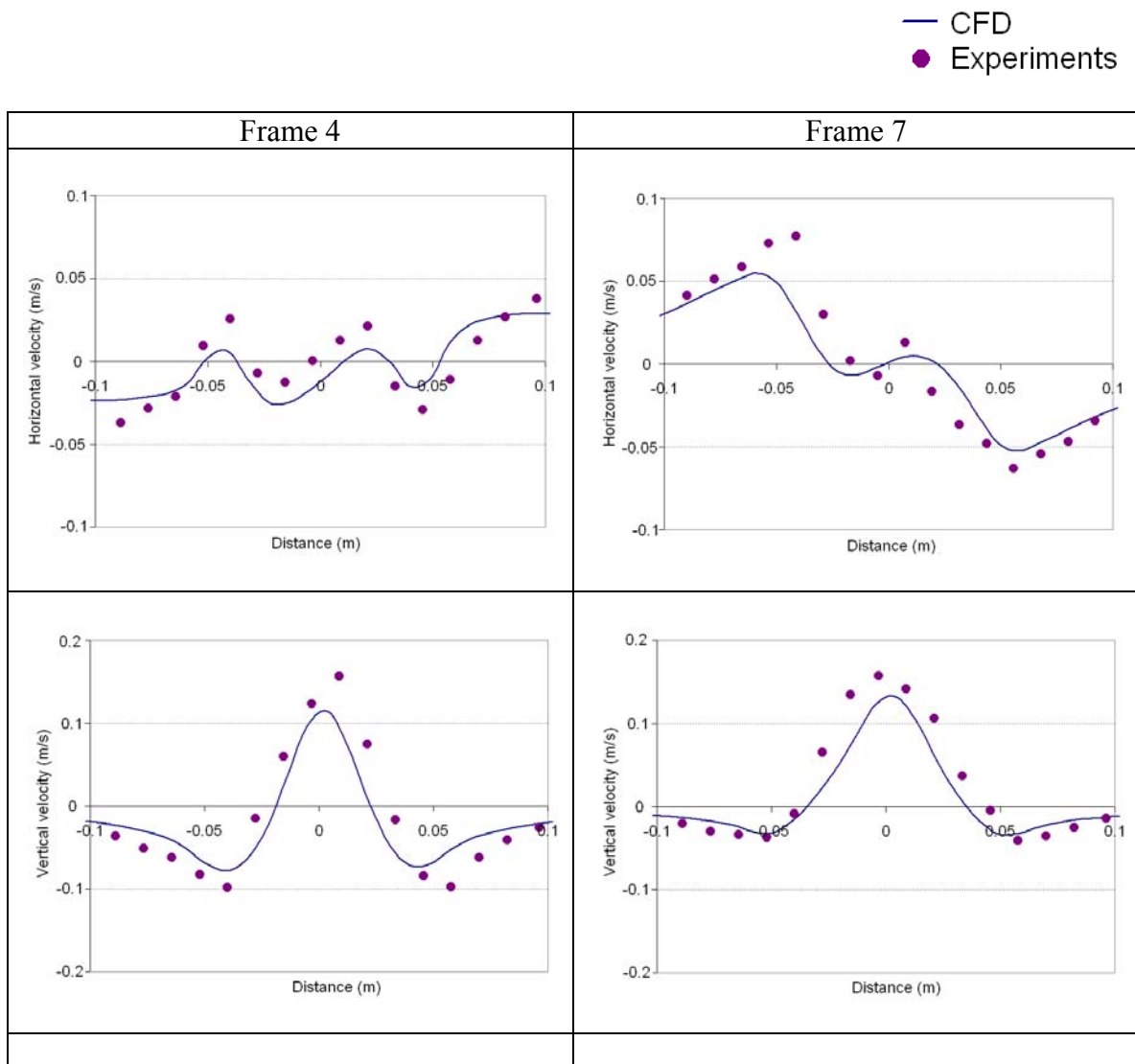
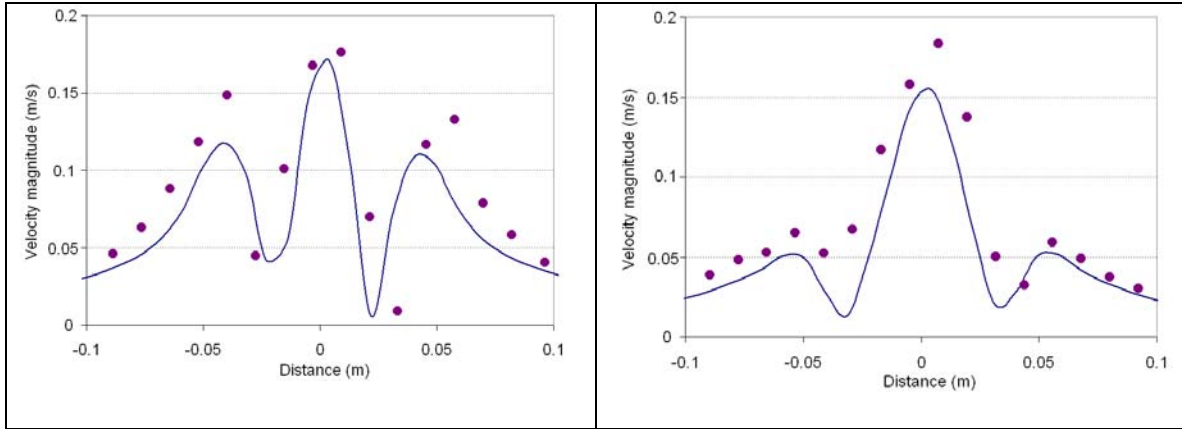


Figure 8.6 The (a) measured and (b) computed mean flow fields at Frames 1, 4, and 7 for the baseline case.





*Figure 8.7 Quantitative estimates of measured and computed velocity magnitudes and its components at Frames 4 and 7 at half the different height of the moving body for the baseline case.*

Figure 8.6(b) shows the corresponding computed flow field for Frames 1, 4, and 7, respectively. Side-by-side comparison using Figs. 8.6 and 8.7 indicated that the CFD model is able to predict the development of the two-eddy system. The predicted flow patterns agree although noticeable differences existed with respect to the vortex aspect ratio. Reduction of mesh size and shifting of the interface boundary between the static and dynamic mesh zones did not alter the CFD predictions. Separated flows behind bluff bodies are typically difficult to model, e.g., the transient RANS simulations by Lubcke (2001). However, the CFD model can reasonably describe the flow physics of the baseline case based on the agreement of the results with the experimental data suggests, which is necessary to study of contaminant transport in airliner cabins.

The cross-sectional flow of the ventilated cabin, when the ECS is operating, is shown in Figs. 8.8 and 8.9 at different instants. As in the baseline case, Fig. 8.7 shows the mean flow fields at  $t=0$ s and at Frames 4 and 7. The injection of water coming into the cabin through the overhead duct of the inlet diffuser assembly (refer to Fig. 8.1(a)) is evident from the CFD results in Fig. 8.8(b). The PIV measurements in Fig. 8.8(a) do not show these incoming jets as the measurement window was focused inside the cabin. The flow field at  $t=0$ s corresponds to the undisturbed flow generated by the ECS before the body started its movement. CFD captured the flow across the cross section much more accurately than in previous attempts (Zhang et al., 2009). This is due to accurate modeling of inlet geometrical features of the experimental setup. The average cross-sectional airflow (at  $t=0$  s) shows a quasi-symmetric vortex structure. The assembly of the experimental setup did not permit perfect symmetry in the flow. The particular section shown in Fig. 8.8 showed the best flow symmetry.

The interacting flow is shown in Frames 4 and 7 in Figs. 8.8 and 8.9. The strong downwash flow behind the moving body is still visible, but the lateral spread of the moving body wake was limited due to the opposing flow from the ECS. The evolution of the downwash was profoundly perturbed by the ventilation. As the body traversed through the measurement plane, the location of the vortex cores at each side of the cabin moved downward in the direction of the side walls. The CFD model was able to capture this transient vortex development. However, discrepancies between the results of the

CFD model and the experiments are evident. This stems from the sensitivity of the overall flow to the computed wake behind the moving body.

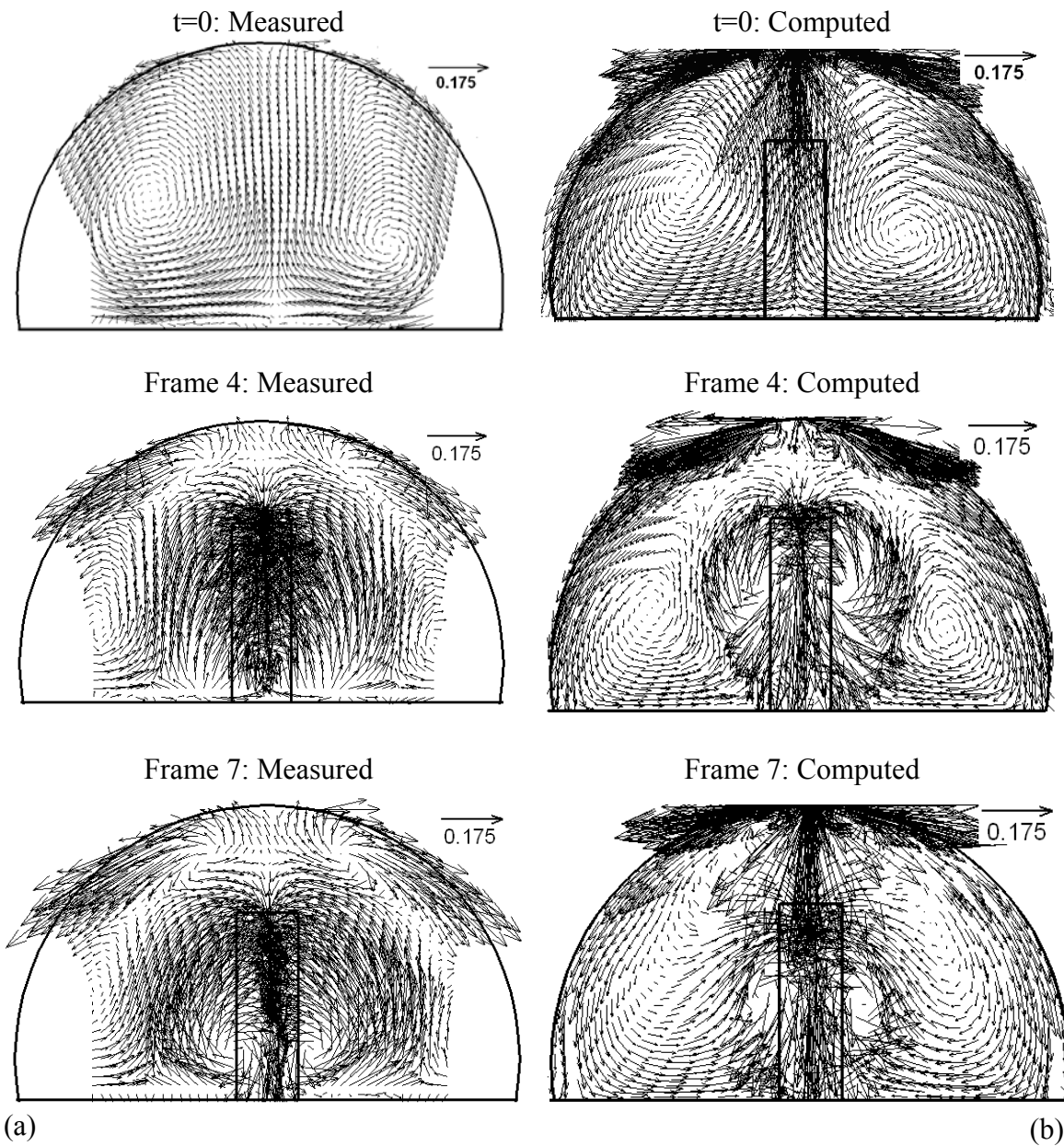


Figure 8.8 The (a) measured and (b) computed mean flow fields at  $t=0s$  and at Frames 4 and 7 for the case with ventilation.

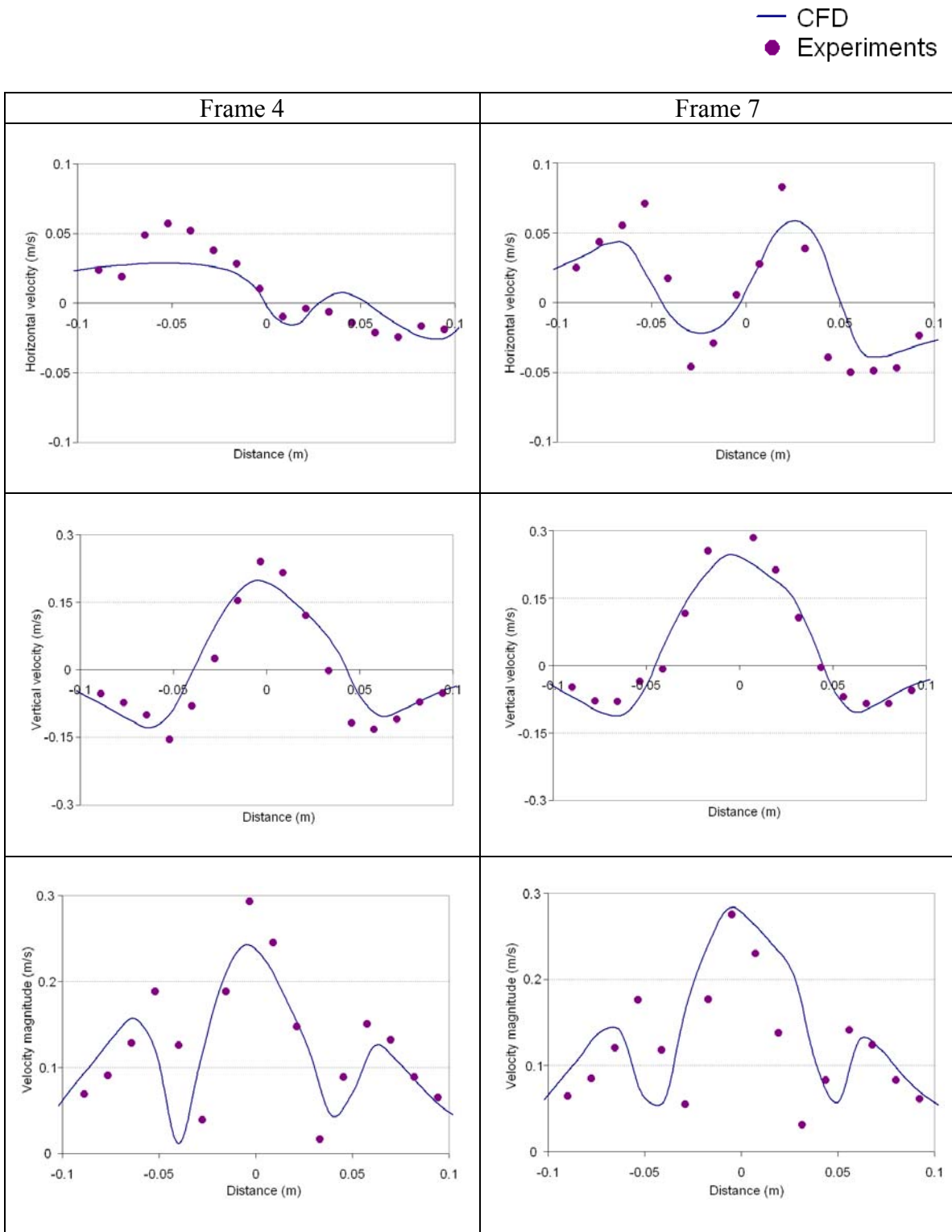
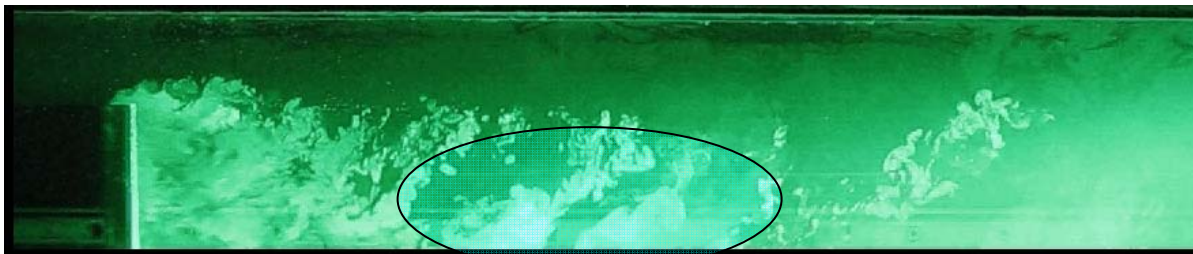


Figure 8.9 Quantitative estimates of measured and computed velocity magnitudes and its

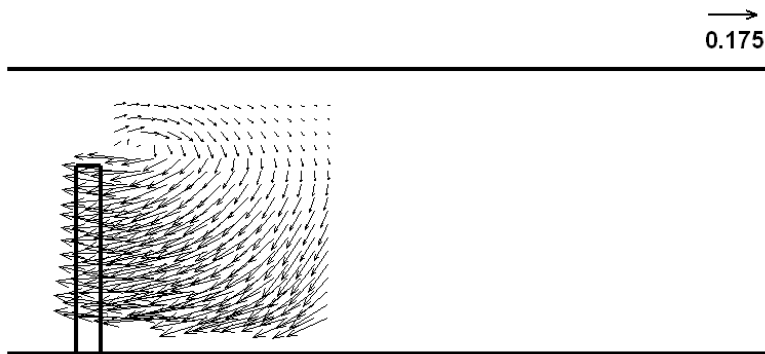
components at Frames 4 and 7 at half the height of the moving body for the case with ventilation.

#### 8.4.2 Longitudinal Flow

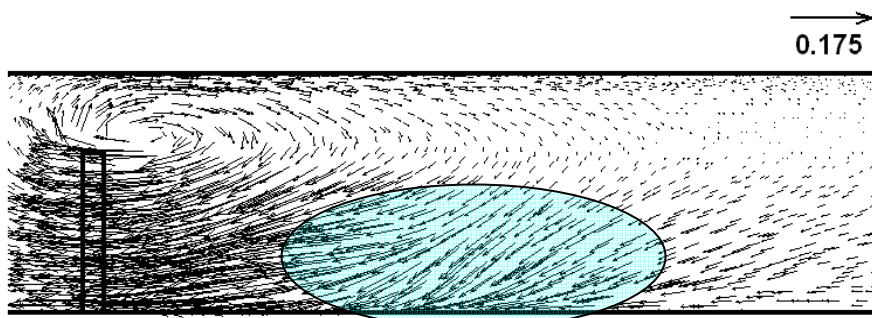
A thorough analysis of the perturbed flow in the wake of the body along the cabin length was conducted for the baseline and ventilation cases. Instantaneous PLIF and PIV measurements were complemented by CFD computations, as shown in Fig. 8.10. Flow recirculation due to flow separation could be observed (Figs. 8.10(b) and (c)). Fig. 8.10(c) shows only a small area of the flow due to the limited image size captured by the PIV. The flow features behind the moving body, approximately inclined at  $45^\circ$  from the vertical as seen in the PLIF measurements, were also captured by CFD (comparing Figs. 8.10(a) and (c)). However, the longitudinal flow computed behind the moving body was stronger than that observed in the PIV measurements, with over prediction of longitudinal momentum transfer. Earlier vertically elongated eddy rings showed lesser momentum transfer in the lateral directions. However CFD captured the fundamental flow features.



(a)



(b)



(c)

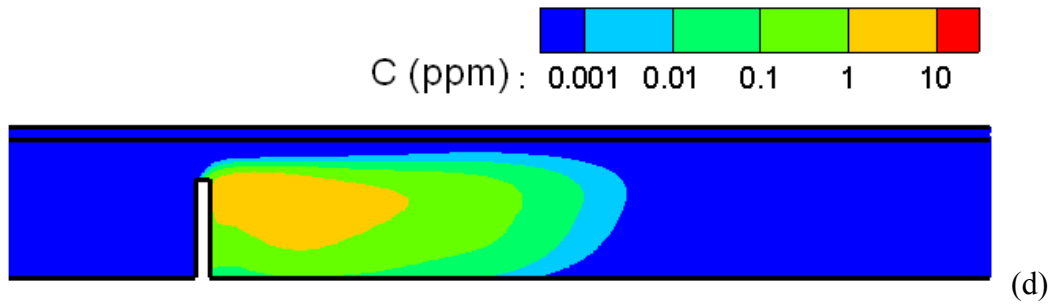
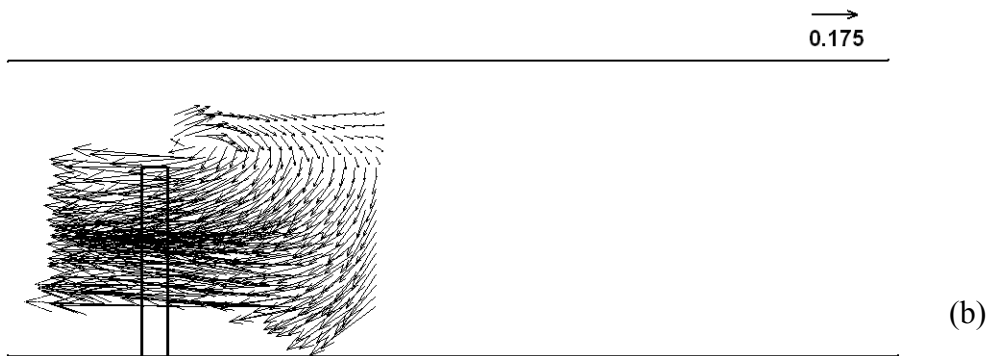
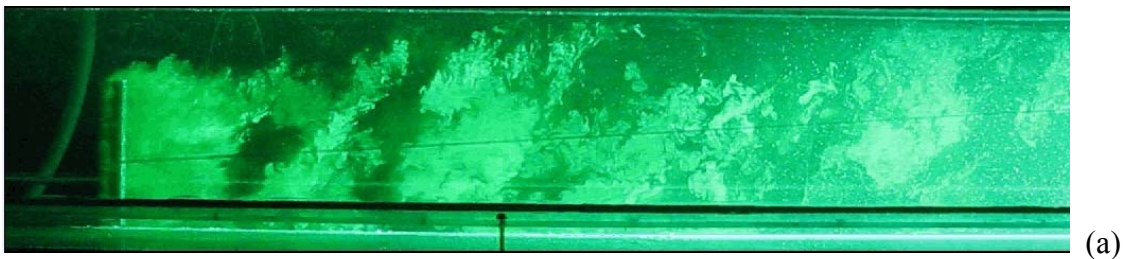


Figure 8.10 (a) Instantaneous flow visualization; (b) mean measured longitudinal flow field; (c) mean computed longitudinal flow field; and (d) the computed dye concentration for the baseline case.

Figure 8.11 shows the measured and computed results of the longitudinal flow with ventilation by the ECS. The injection of water coming into the cabin through the overhead duct of the inlet diffuser assembly (refer to Fig. 8.1(a)) is evident from the CFD results in Fig. 8.11(c). The PIV measurements in Fig. 8.11(b) do not show these incoming jets as the measurement window was focused inside the cabin. The CFD model was able to capture the vortex above the moving body for this case (Figs. 8.11(b) and (c)). The contaminant dye was observed to convect to higher vertical locations (Figs. 8.11 (a) and (d)). The mixing in the wake was modified and a shorter longitudinal recirculation region was observed for the ventilation case versus the baseline case (Figs. 8.10(c) and 11(c)). The flow structures recirculating at  $45^\circ$  behind the body for the baseline case were disrupted due to the interaction of wake behind the moving body and the flow from the ECS.



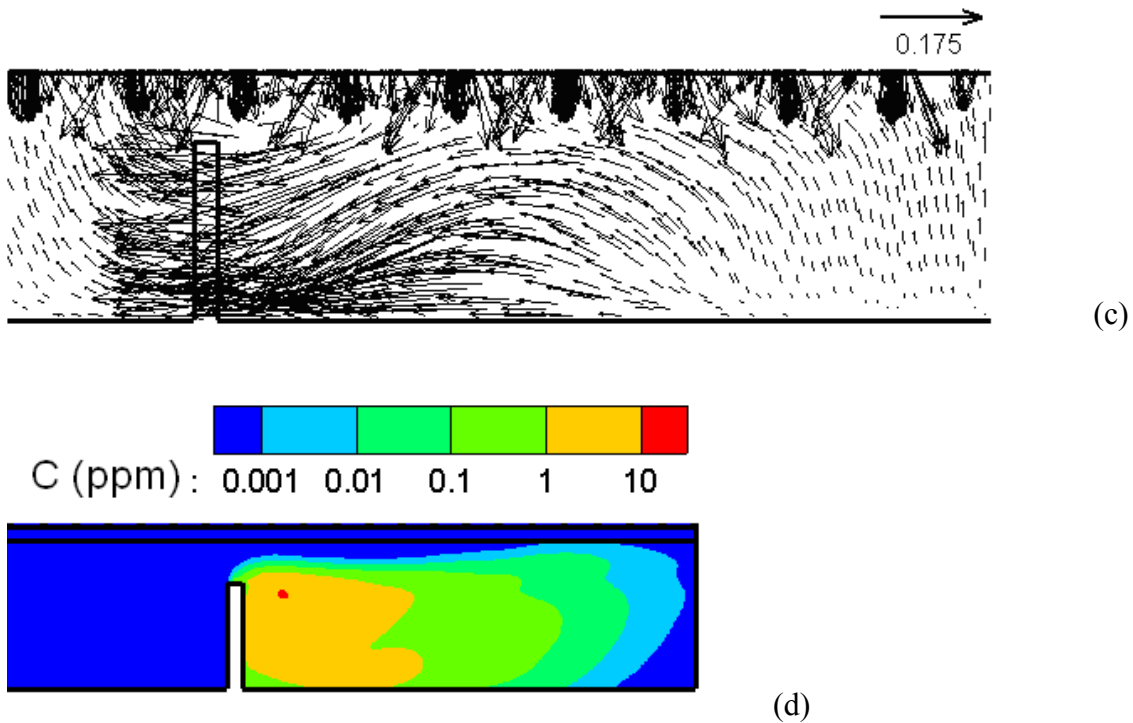
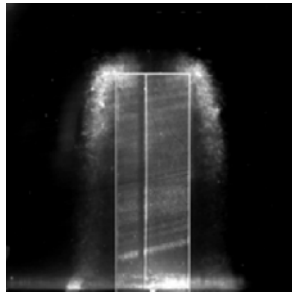


Figure 8.11 (a) Instantaneous flow visualization; (b) mean velocity field; (c) mean computed longitudinal flow field; and (d) the computed dye concentration for the case with ventilation.

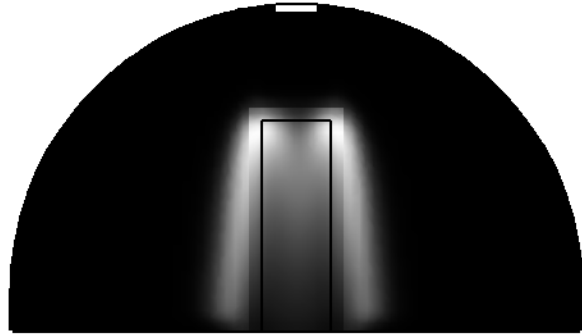
### 8.4.3 Contaminant Transport

Figures 8.12 and 8.13 show a qualitative comparison of contaminant dye transport across the cabin cross section for the baseline and ventilation cases, respectively. Twenty-five instantaneous PLIF images were averaged to obtain the measured mean concentration field. A limited number of realizations were acquired because the water tank had to be cleaned after each dye injection experiment. Twenty-five measurements are typically sufficient to observe vertical symmetry in the wake, as shown in Fig. 8.5. The maximum contaminant concentration occurred behind the top two corners of the moving body in both cases. The CFD model predicted the dye intensity profile and the location of maximum intensity. The intensity of the fluorescent dye across the cross section was lower for the ventilation case due to mixing, thus making a comparison of the measured and computed dye intensities difficult. Overall, the maximum concentration across the cabin cross section was lower for the ventilation case, as one would expect.

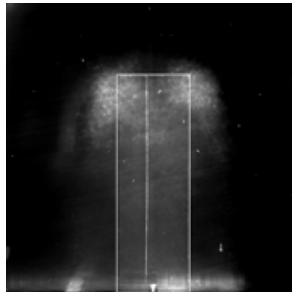
Frame 2: Measured



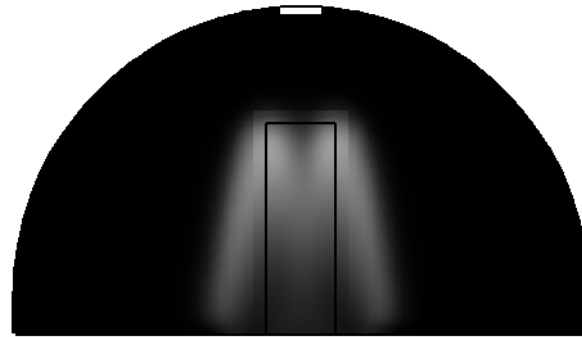
Frame 2: Computed



Frame 4: Measured



Frame 4: Computed



(a)

(b)

Figure 8.12. (a) Measured and (b) computed mean dye concentrations at Frames 2 and 4 for the baseline case.

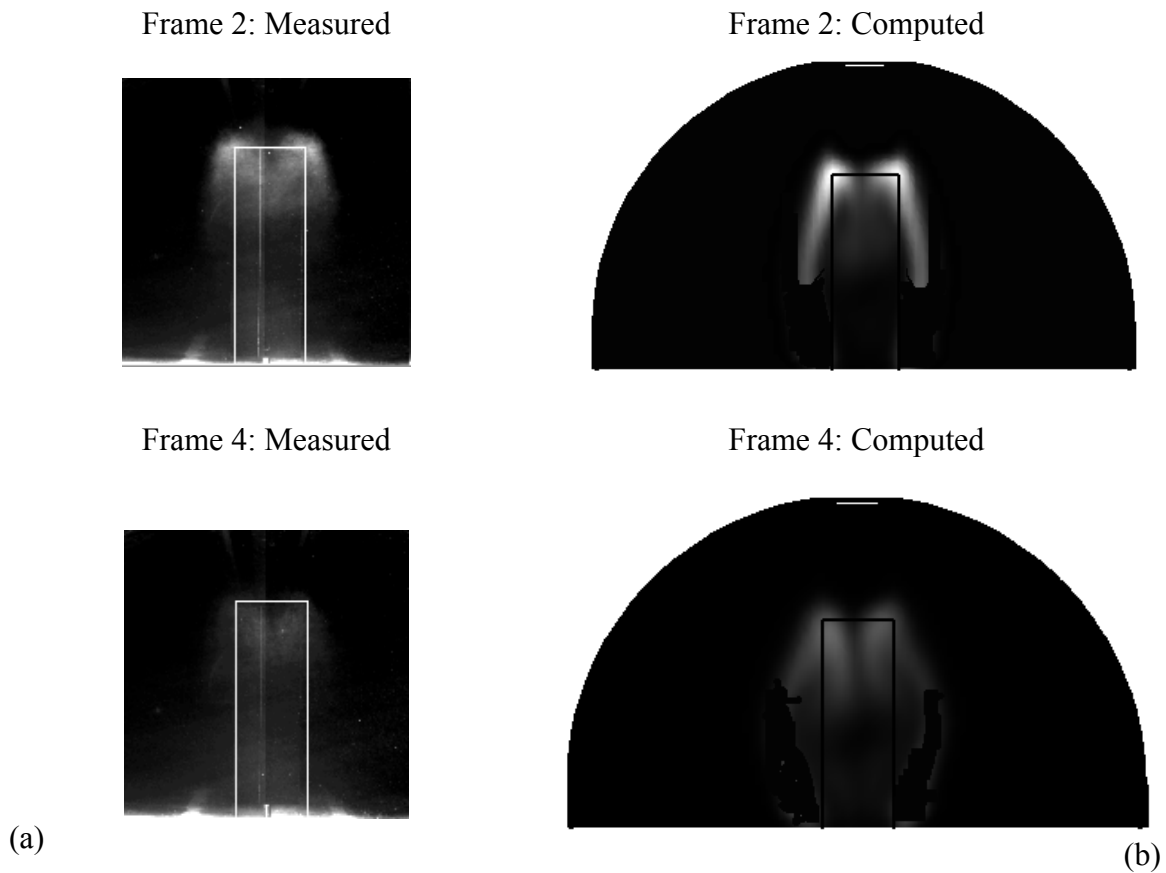


Figure 8.13 (a) Measured and (b) computed mean dye concentrations at Frames 2 and 4 for the ventilation case.

A quantitative comparison between maximum concentrations across the cabin cross section as the body moves through it is shown in Fig. 8.14. The light intensity in the region behind the top edges was compared for both the experimental and the numerical data, as it typically showed maximum levels when compared to the rest of the flow field due to maximum dye concentration. Image processing was done using computational software (MATLAB). At Frame 4, the CFD model predicted that the ventilation would decrease the maximum concentration by 23% relative to the baseline case, compared with 20% as observed during the experiments, although the absolute magnitudes were different. The CFD predictions were within  $\pm 5\%$  of the experimental measurements for the other frames as well. Therefore, CFD captured the comparative strength of the dye concentration between the two cases, despite the complex transient flow phenomena. Moreover, CFD predicted that the maximum dye concentration across the cabin cross section would decay by more than 30% for both cases in less than a second, i.e. from Frame 4 to Frame 10, as the body moved through. Further quantitative comparisons could not be performed due to limitations associated with the experimental technique.

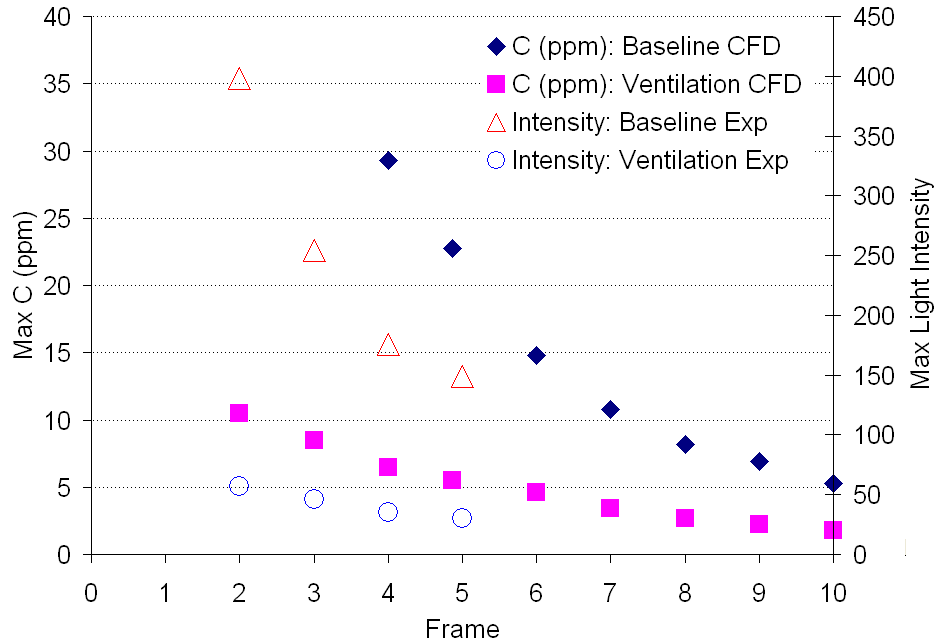
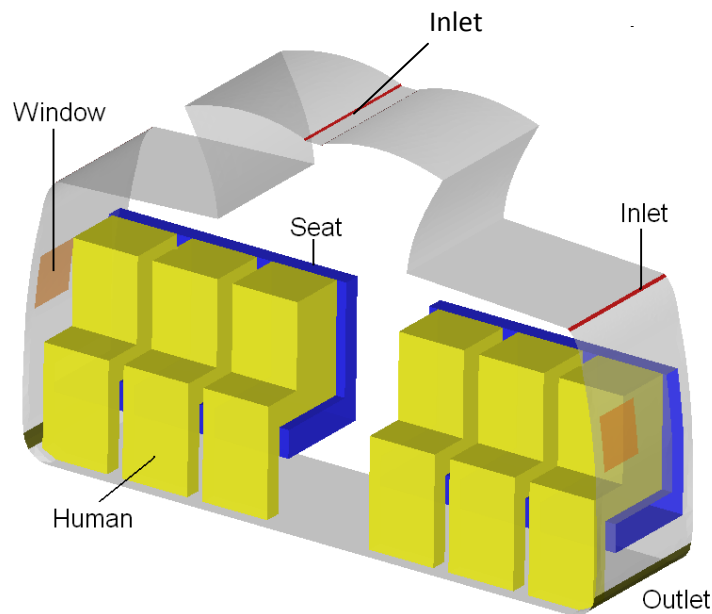


Figure 8.14 Comparison of the decay in maximum concentration (CFD) and dye intensity (PLIF) for the baseline and the ventilation case.

### 8.5 Contaminant Transmission due to Movement in the SARS Infected Cabin

The validated CFD model was used in investigating the influence of movement in the SARS infected Air China Flight 112 from Hong Kong to Beijing (Olsen et al., 2003). Previous studies have reported that the risk of transmission without such movement should remain within 2 rows of the contagious passenger (NRC 2002). But passengers seated as far as 7 rows ahead of the contagious passenger were infected during the SARS contamination incident. This study thus examined whether movement of crew or passengers along the aisle of the cabin could be the reason behind the SARS contaminant transmission.

The study assumed that the air entered the cabin through four linear diffusers as shown in Fig. 8.15: two of the diffusers, placed at the ceiling above the aisle, injected air downwards into the cabin while the other two diffusers at the side walls located below the storage bins injected air inwards towards the aisle. The airflow rate into the cabin was 10 L/s per passenger (Zhang and Chen, 2007) and was distributed equally among the four inlets. Air was exhausted through outlets placed in the side walls close to the floor. A fully occupied 15-row cabin section with a seat pitch of 0.86 m was computed. The thermo-fluid conditions along with the passenger and the seat model were similar to that used by Mazumdar and Chen (2008).



*Figure 8.15 Schematic of one of the rows for the Air China Flight 112 cabin.*

To investigate whether movement can aid transmission of contaminants to 7 rows, this study assumed that a gaseous contaminant was released passively from the infected passenger at a uniform rate of 25 mL/s as is done in the rest of this chapter. The effect of body movement was studied on two contaminant initial distribution patterns: one was for a pulse contaminant released for 30 s and the other had an initial steady-state contaminant distribution simulating a continuous release. A previous comprehensive study done by the authors in a 4-row twin-aisle cabin concluded that the wake behind the moving body traps contaminants and carries them along the cabin (Mazumdar and Chen, 2007). Moreover, as the body stops moving, the contaminants carried by the wake spread to passengers seated near the aisle. This previous experience with a 4-row twin-aisle cabin was used in designing the case for the 15-row single-aisle SARS-infected mockup. It was assumed that once the cabin has the aforementioned initial contaminant distribution pattern, the body starts its movement from the rear end of the cabin at a speed of 1.75 m/s and finally stops 7 rows ahead of the infected passenger without making any intermediate stops. The duration of the movement was 5.2s. The movement was modeled using the combined dynamic and static mesh scheme since the indirect method under predicted the downwash flow behind the moving body. The time step used in the computations was 0.01s.

Figure 8.16 shows the breathing level contaminant distribution inside the cabin for a pulse contaminant released for 30 s. The high concentration zone was localized to 2 rows near the infected passenger at  $t=30$ s. As the body moved along the aisle, the wake carried the contaminant localized in the 2 rows to 7 rows in front. Once the body stopped its movement, the contaminant carried in the wake was distributed to passengers seated near the aisle. A similar phenomenon is seen in Fig. 8.17 with an initial steady-state contaminant distribution for a continuous release. Even though the initial contaminant

concentration inside the cabin was higher, movement increased the contaminant concentration near the passenger seated 7 rows ahead of the infected passenger even for a continuous release. It can be observed that the initial steady-state contaminant distribution for a continuous release was higher behind the infected passenger. The thermal plume of the infected passenger transported the contaminant backward as a passive release scenario was studied. If the contaminant is released via a coughing or a sneezing process, the local distribution of contaminants can vary (Zhang, 2007). Yet the fact that movement can aid transmission of contaminants to 7 rows or more would remain true even for other release scenarios as well.

The contaminant concentration at the breathing level of an aisle passenger seated 7 rows in front of the infected passenger is shown in Fig. 8.18. The movement of a body along the aisle increases the maximum contaminant concentration at the breathing level of the aisle passenger by an order of magnitude for the case of a continuous release with initial steady-state contaminant distribution. For the pulse release case, the maximum concentration is about an order of magnitude lower than that of the continuous release case. Without movement, the contaminant would not have been transmitted to passengers sitting 7 rows ahead for the pulse release case. Moreover, the design of the cabin airflow system in the Air China flight prevented immediate flushing out of the transmitted contaminants to the aisle passenger as is evident from the transient concentration plots in Fig. 8.18. Hence, movement of the crew and passengers along the aisle of the cabin greatly enhanced the risk of contamination from the infected passenger.

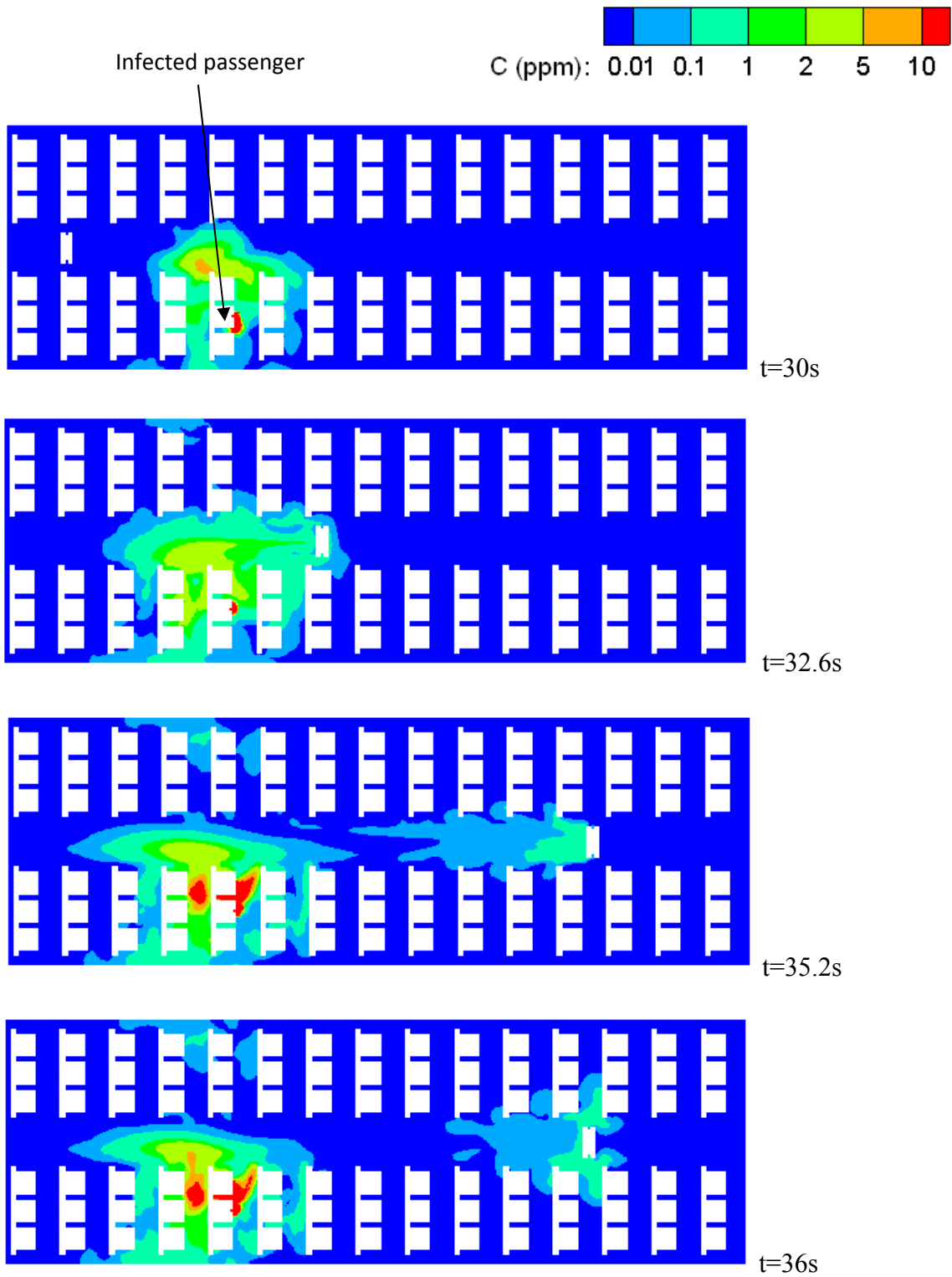


*Figure 8.16 Contaminant transport trends due to movement of a person along the aisle for a pulse release from the infected passenger.*

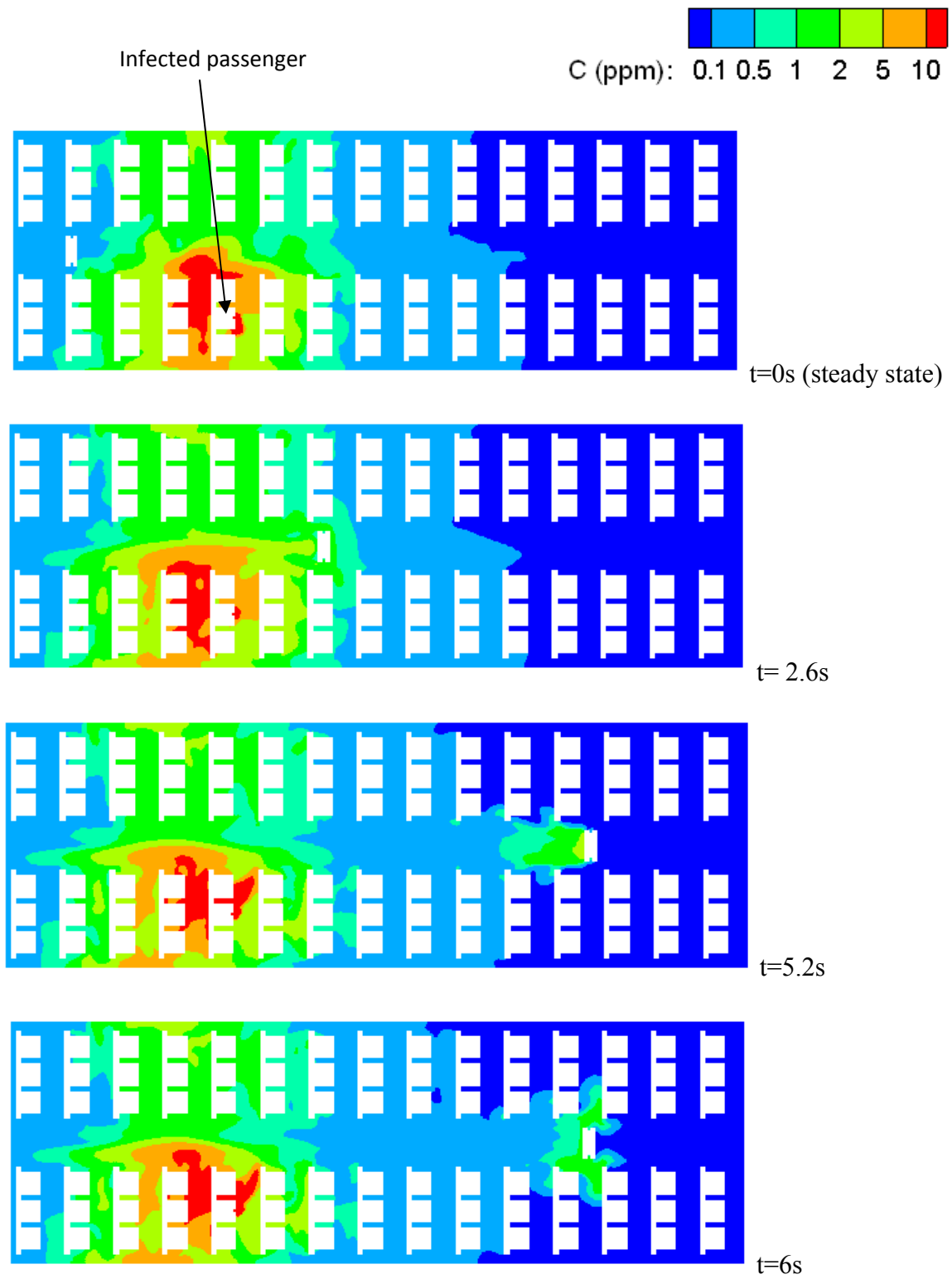


*Figure 8.17 Contaminant transport trends due to movement of a person along the aisle of the cabin with initial steady state contaminant distribution for a continuous release from the infected passenger.*

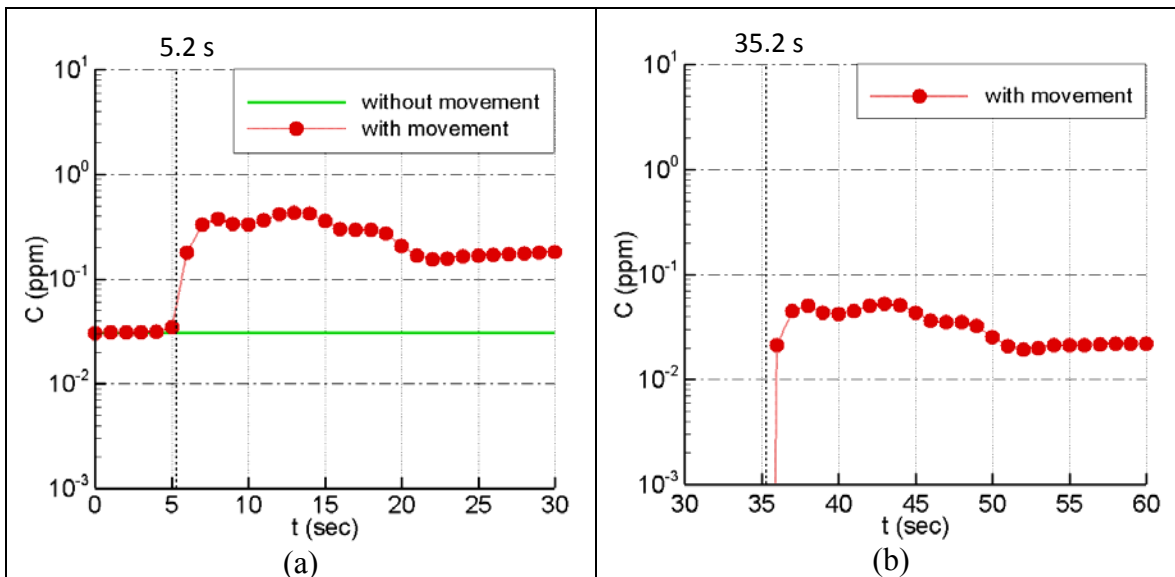


Figure 8.18 Contaminant concentration at a location near the breathing level of the aisle passenger seated 7 rows in front of the infected passenger (a) with an initial steady-state contaminant distribution for a continuous release and (b) with a pulse release.

## 8.6 Conclusions

This chapter used a small-scale, water-filled model to investigate the effect of a moving body on flow and contaminant transport inside an airliner cabin. The small-scale model generated high quality experimental data with good spatial and temporal resolutions for CFD model validation. CFD validation was done for two different conditions: one with the cabin ECS (ventilation case) and the other without (baseline case). PIV was used to measure the flow under these two conditions. The measurements revealed a strong downwash flow along the vertical centerline of the moving body for the baseline case. The evolution of the downwash was profoundly perturbed by the flow from ECS in the ventilation case. A shorter longitudinal recirculation region was also observed for the ventilation case when compared to the baseline case. The CFD model captured these fundamental flow features reasonably well.

The contaminant transport predicted by the CFD model was further validated using PLIF measurements. The contaminant dye was observed to convect to higher vertical locations for the ventilation case. The maximum contaminant concentration was found behind the top two corners of the moving body for both cases. CFD can accurately capture this phenomenon. The CFD model could quantitatively estimate remarkably well the strength of the dye concentration observed across the cabin cross section in the two cases.

Movement of a crew member or passenger along the cabin aisle can carry contaminant from its source to many rows away. The body movement may have caused the transmission of SARS pathogen from the infected passenger to fellow passengers seated as far as seven rows away in Air China Flight 112 in 2003.

## 9. CONCLUSIONS AND FUTURE WORK

This chapter first summarizes the key conclusions from the study and then discusses the future scope of the research.

### 9.1 Conclusions

Airborne infection has always been a major source of morbidity and mortality worldwide. Thus it is important to understand, predict and control the transmission of airborne infection to trim down the deaths. Previous investigations have indicated that the infectious disease transmission in indoor environment, especially in aircraft cabins represents great risk and needs to be studied. It was found that the CFD simulations can accurately predict the disease transmission if are provided with accurate boundary conditions and flow models. The exhaled air is the source of the infectious agents and people can get infected by inhaling the infectious agents, which are generally carried by the expiratory droplets. It was found that there is no comprehensive study that can provide flow boundary conditions to the CFD simulations for the exhalations/inhalations from human beings. Thus, the present study first developed these models.

The flow rate, flow direction of the jet, and the area of opening measurements were conducted on 25 human subjects for coughing, breathing, and talking processes. The cough flow rate was found to be a combination of gamma probability distribution functions. The variables in the functions can be represented by medical parameter i.e. CPFR, PVT, and CEV. These medical parameters were related to the height, weight, and gender of a person. A sequential cough was found to be the combination of two single coughs. The first one behave approximately the same as that of a single cough, while the second one was a scaled down version of the first one. The cough flow direction did not vary very much among the subjects and can be determined by two angles. The mouth opening area was constant during a cough. The mouth opening area varied among the subjects but without a clear correlation with the subject height. Hence this study proposed to use a mean mouth opening area during a cough

The breathing flow rate variation with time was sinusoidal. The amplitude and frequency of the sine function were related to body height, weight, and gender. No significant difference in the breathing flow rate was observed due to either a change of breathing organ or posture. The flow direction of the exhaled jet during breathing can be characterized by two front angles and two side angles for nose breathing and one side-angle for mouth breathing. The breathing flow directions did not change much among the subjects tested. The mouth and nose opening areas were constant during breathing.

The talking flow rate was found to be irregular in nature and, hence, is defined as an average flow rate over time. The flow rate was related to body surface area which can be obtained from the height and weight of a person. As no single event can define talking direction, it is proposed to use the directions of normal mouth breathing. The mouth opening area during talking was found to vary with time and words. A time averaged area, averaged over numbers, is therefore proposed for talking. The mouth opening area varied among subjects, but no clear trend was observed; thus, a mean value is proposed for the mouth opening area during talking.

To summarize, the exhalation/inhalation flow models provided the information on the flow rate, flow direction and the area of nose/mouth opening during coughing, breathing and talking for human beings and can be represented as a set of simple mathematical equations. These equations account for the variation with time and people; and can be easily fed in a CFD simulation to provide thermo-fluidic boundary conditions for the exhalations/inhalations. The set of equations developed can be combined with appropriate infectious agents and droplet distribution information from available literature. Figure 9.1 shows the exhalation/inhalation model layout.

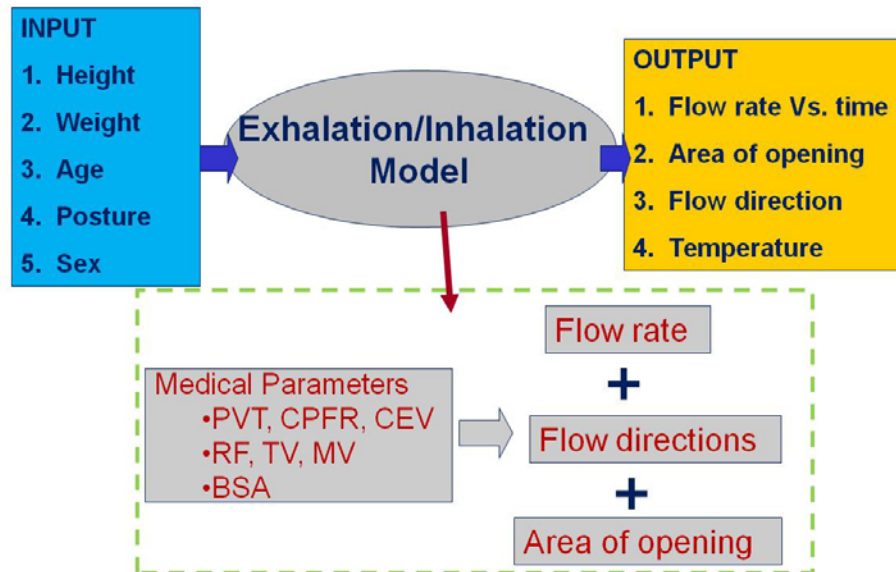


Figure 9.1 Source/Sink Model layout for generating flow boundary conditions for various exhalations/inhalations.

Previous investigations have also indicated that in addition to boundary conditions it is highly essential to select appropriate turbulence and dispersion model along with the suitable control volume (domain). Thus the study further investigated the transport of expiratory droplets that may carry the infectious agents, in aircraft cabin using the CFD methods and addressing the issues in the previous studies.

This investigation studied the transport of the expiratory droplets from an index patient seated at the center of a seven-row, twin-aisle, fully occupied aircraft cabin by using a commercial CFD program (FLUENT 2005). The airflow and temperature distribution was first studied under steady state conditions. A grid sensitivity analysis was carried out and the optimum grid was used for the further analysis. Moreover as the boundary conditions at the ends of the cabin are unknown, two kinds of boundary conditions, adiabatic wall and periodic, were implemented and compared to evaluate the sensitivity of the boundary conditions at the ends on the overall flow. It was found that any of these boundary conditions can be used as the difference found in airflow and temperature distribution was insignificant. The steady state solution was then used as initial condition to study the droplet transport exhaled from a single cough, single breath and 15s of talking. The developed exhalation/inhalation boundary conditions were then fed in the CFD simulation. The RNG k- $\epsilon$  turbulence model was used and the mono-dispersed droplet tracking was performed through Lagrangian scheme. The simulations

were performed for four minutes of real time starting from a steady-state airflow and temperature distribution.

The droplets exhaled from the cough of the index patient followed mainly the bulk airflow. The droplet concentration in the vicinity of the passengers reduced over time due to the removal from the outlets and dispersion of the droplets. The total airborne droplet fraction reduced to 48%, 32%, 20%, and 12% after the droplets entered the cabin air for 1, 2, 3 and 4 minutes, respectively. Most of the droplets were transported within one row of the index patient in the first 30 s and then could be transported to the entire seven-row cabin with a uniform droplet distribution in 4 minutes.

The droplets exhaled from the breath of the index patient behaved similarly as those from the cough, but the number was much smaller. The expiratory droplets generated during the talking of the index patient were contained on the left side of the cabin since the patient turned the head to the left.

In real situations the index passenger can exhale droplets from multiple exhalations over several hours of flight duration. The CFD simulations provided a good insight on the expiratory droplet movement from various exhalations for four minutes of time but took 4 week of computational time on a 8 parallel processor cluster. Therefore performing the CFD simulations for multiple exhalations from the index passenger over several hours of flight is not practical and feasible. Hence, the study further developed methods to predict the transport of droplets exhaled from combinations of breathing, talking, and coughing of an index passenger in an aircraft cabin for the whole flight duration. Since the droplets got well mixed in the cabin air 3 minutes after they were released, the method used combined CFD and mixed condition models for the prediction. It was found that the droplet distribution from single exhalations can be superimposed to obtain the droplet distribution for multiple exhalation scenarios. The droplets inhaled by a passenger can consequently be determined for the whole flight duration.

The number of droplets inhaled by the fellow passengers due to the droplets exhaled from regular breathing, 100 coughs sandwiched with regular breathing, and 30 minutes of talking combined with regular breathing from the index passenger in a 4-hour flight were calculated. The coughs generated the most droplets and may impose a very high risk on the fellow passengers if the droplets contained active infectious agents. The risks due to the breathing and talking were almost two orders of magnitude smaller than the risk due to coughing.

The amount of droplets inhaled may not represent the risk of infection as these droplets may not necessarily contain active infectious agents. Therefore, a method to predict the spatial and temporal risk of infection in an aircraft based on the deterministic and probabilistic approaches was proposed. Using the methods developed to quantify the amount of inhaled droplets, the spatial distribution of dose inhaled by the passengers was calculated. Based on the dose inhaled the risk of infection was quantified for the passengers seated in the row and the neighboring rows of the index passengers suffering from influenza for a four hours of flight. For the deterministic approach the dose was quantified as the number of influenza virus RNA particles inhaled but as the tolerance dose for the influenza virus RNA particles is not known nothing can be said on the infection risk to the passengers. For the probabilistic approach the Wells Riley equation was used to quantify the probability of influenza based on the spatial distribution of

quanta inhaled by the passengers. It was found that the probability of influenza can be reduced by using N95 respirator masks.

In-flight movement of passengers and crew members inside the airliner cabin had changed the airflow and contaminant transmission observed. Experiments performed in an empty one-tenth scale water-based cabin model showed a strong downwash flow along the vertical centerline of the moving body. The flow from the environmental control system of the airliner cabin profoundly perturbed the evolution of the downwash. Maximum contaminant concentration was found behind the two shoulder corners of the moving body. The CFD results indicate that seats and passengers do tend to obstruct the lateral transmission of contaminants and restrict the spread to the aisle of the cabin if a contaminant is released from a moving body. CFD results also predicted that movement can aid transmission of contaminants to 7 rows or more and could be the major reason behind the transmission of SARS contaminants from the infected passenger to fellow passengers seated as far as 7 rows away on the Air China Flight from Hong Kong to Beijing.

## 9.2 Recommendation for Future Studies

The exhalation/inhalation flow measurements in the current study were performed on healthy human subjects. The subjects suffering from infectious disease may have different airflow for these exhalations/inhalations. It is required to conduct these airflow measurements on infected human subjects to characterize the differences. Moreover the current study did not measure the airflow of sneezing as it was difficult to generate a sneeze. Measurements on sneezing should be performed in future as it could be an important source of infectious droplets.

The developed CFD models assumed negligible droplet deposition as the modeled expiratory droplet sizes were small. It is required to quantify the deposition of the expiratory droplets on cabin surfaces as it can help in investigating the infection spread through contact. The current study developed the methods to predict the spatial and temporal distribution of expiratory droplets. The observed airflow agreed qualitatively with other studies and the transport of expiratory droplets was in agreement with the airflow. But it is required to conduct controlled measurements in the cabin to validate the results, as it can aid in improving the CFD models.

The deterministic and probabilistic approaches adopted to quantify the risk can further be developed if the information on the tolerance doze for the infectious diseases is available.

Effectiveness of N-95 mask in reducing the risk of infection was evaluated using the available literature. The available literature quantified the protection level for the occupants wearing the N-95 masks if the ambient air is contaminated, but did not quantify the ambient contamination if an infected occupant wears the mask. It is required to conduct controlled experiments to quantify the filtration of these masks if an infected occupant wears it. If it can effectively reduce the level of contaminants in the ambient air, just the infected passenger needs to wear the mask and it can save cost to the airliners and discomfort for the other occupants.

The effect of jet airflow from personalized supply systems in airliner cabins on contaminant transmission has not been addressed in detail. Personalized airflow on a

contagious passenger may have a major impact on contaminant transmission near the location of release due to the jet momentum. Such a fresh air supply can reduce the risk of transmission to other passengers inside the cabin. Optimization of such personalized systems to reduce risk of transmission can also be addressed in a future study.

This investigation analyzed the influence of movement on contaminant transmission inside airliner cabins using a simplified human model and uniform walking speeds. More realistic human body geometry and walking motions may change the contaminant transmission characteristics due to the change in the structure of the local wake formation behind the moving body. Furthermore, movement patterns of humans have an inherently high level of uncertainty due to the random behavioral nature of people and, hence, a large number of movement scenarios need to be studied to draw general conclusions on the effects of movement on the risk of contaminant transmission.

## 10. REFERENCES

- Aboosaidi, F., Warfield, M. and Choudhury, D. (1991) Computational fluid dynamics applications in airplane cabin ventilation system design. Proceedings of Society of Automotive Engineers, 246, 249-258.
- Afshari, A., Azadi, S., Ebeling, T., Badeau, A., Goldsmith, WT., Weber, KC. and Frazer, DG. (2002) Evaluation of cough using Digital Particle Image velocimetry. Proceedings of Second Joint EMBS-BMES Conference 23-26 October Houston TX IEEE, 975-976.
- Alford, RH., Kasel, JA., Gerone, PJ. and Knight, V. (1966) Human influenza resulting from aerosol inhalation, Proc. Soc. Exp. Biol. Med., 122, 800–804.
- Aliaga, C. and Winqvist, K. (2003) Comment les femmes et les hommes utilisent leurs temps-Résultats de 13 pays européens. Eurostat, KS-NK-03-012-FR-N.
- Altman, PL. and Dittmer, DS. (1971) Respiration & Circulation, Federation of American Societies for Experimental Biology, Bethesda, Maryland.
- Araujo, GAL., Freire, RCS., Silva, JF., Oliveira, A. and Jaguaribe, EF. (2004) Breathing Flow Measurement with constant temperature Hot-Wire Anemometer for forced oscillation technique. Instrumentation and Measurement Technology Conference Como Italy, May, 730-733.
- Axley, J. (2007) Multizone airflow modeling in buildings: History and theory. HVAC&R Research, 13(6), 907-928.
- Badeau, A., Afshari, A., Goldsmith, WT. and Frazer, D. (2002) Preliminary predictions of flow and particulate concentration produced from normal human cough dispersion. Proceedings of Second Joint EMBS-BMES Conference 23-26 October Houston TX IEEE, 246-247.
- Bałazy, A., Toivola, M., Reponen, T., Podgo' rski, A., Zimmer, A. and Grinshpun, SA. (2005) Manikin-based performance evaluation of N95 filtering-facepiece respirators challenged with nanoparticles. Annals of Occupational Hygiene, 1-11.
- Balazy, A., Toivola, M., Adhikari, A., Sivasubramani, SK., Reponen, T. and Grinshpun, SA. (2006) Do N95 respirators provide 95% protection level against airborne viruses, and how adequate are surgical masks? American Journal of Infection Control, 34, 51-7.
- Baldwin, ED., Courmand, A. and Richards, DW. (1948) Pulmonary insufficiency: I. Physiological classification, clinical methods of analysis, standard values in normal subjects. Medicine (Baltimore), 27, 243-278.
- Bjørn, E., Mattsson, M., Sandberg, M. and Nielsen, P.V. (1997) Displacement ventilation - effects of movement and exhalation. Proceedings of Healthy Buildings '96, 5th International Conference on Healthy Buildings, Washington DC, USA, 2: 163 – 168.
- Bjørn, E., and Nielsen, P.V. (2002) Dispersal of exhaled air and personal exposure in displacement ventilated rooms. Indoor Air, 12: 147–164.
- Block, SS. (1991) Peroxygen compounds, In SS Block (ed.), Disinfection, sterilization and preservation. Lea and Febiger, Philadelphia, PA.

- Bongers, T. and O'Driscoll, BR. (2006) Effects of equipment and technique on peak flow measurements. *BMC Pulmonary Medicine*, 6-14.
- Brosseau, LM., McCullough, NV. and Vesley, D. (1997) Mycobacterial aerosol collection efficiency of respirator and surgical mask filters under varying conditions of flow and humidity. *Applied Occupational and Environmental Hygiene*, 12(6), 435-45.
- Brohus, H., Balling, K.D., and Jeppesen, D. (2006) Influence of movements on contaminant transport in an operating room. *Indoor Air*, 16: 356-372.
- Cermak, R., Melikov, A. K., Forejt, L. and Kovar, O. (2006) Performance of personalized ventilation in conjunction with mixing and displacement ventilation. *HVAC&R Research*, 12, 295–311.
- Chao, CYH., Wan, MP. and Sze To, GN. (2008) Transport and removal of expiratory droplets in hospital ward environment. *Aerosol Science Technology*, 42 (5), 377–394.
- Chao, CYH., Wan, MP., Morawska, L., Johnson, GR., Ristovski, ZD., Hargreaves, M., Mengersen, K., Corbett, S., Li, Y., Xie, X. and Katoshevski, D. (2009) Characterization of expiration air jets and droplet size distributions immediately at the mouth opening. *Journal of Aerosol Science*, 40, 122-133.
- Chen, Q. and Xu, W. (1998) A zero-equation turbulence model for indoor airflow simulation. *Energy and Buildings*, 28(2), 137-144.
- Chen, Q., and Srebric, J. (2002) A procedure for verification, validation and reporting of indoor environment CFD analyses. *HVAC&R Research*, 8(2): 201-216.
- Cho, KJ., Reponen, T., McKay, R., Shukla, R., Haruta, H., Sekar, P. and Grinshpun, SA. (2008) Large particle penetration through N95 respirator filters and facepiece leaks with cyclic flow. *Annals of Occupational Hygiene*, 1-9.
- Choi, J.I., and Edwards, J.R. (2008) Large eddy simulation and zonal modeling of human induced contaminant transport. *Indoor Air*, 18: 233–249.
- Code of Federal Regulation Title 42, Part 84. (1994) Respirator Protection, 30382-30383.
- Coffey, CC., Campbell, DL. and Zhuang Z. (1999) Simulated workplace performance of N95 respirators. *Am Ind Hyg Assoc J*, 60, 613–24.
- Cole, EC. and Cook, CE. (1998) Characterization of infectious aerosols in health care facilities: an aid to effective engineering controls and preventive strategies. *American Journal of Infection Control*, 26, 453–464.
- Corbett, EL., Watt, CJ., Walker, N., Maher, D., Williams, BG., Raviglione, MC. and Dye, C. (2003) The growing burden of tuberculosis: global trends and interactions with the HIV epidemic. *Arch Intern Med*, 163, 1009–1021.
- Davidson, L., Nielsen, PV. and Sveningsson, A. (2003) Modification of the v2f model for computing the flow in a 3D wall jet turbulence. *Heat and Mass Transfer*, 4, 577 - 584.
- Douglas, NJ., White, DP., Weil, JV. and Zwillich, CW. (1983) Effect of breathing route on ventilation and ventilatory drive. *Respir. Physiol.*, 51, 209–218
- Duguid, JP. (1946) The size and the duration of air-carriage of respiratory droplets and droplet-nuclei. *Journal of Hygiene*, 54, 471-479.
- Dye, C., Scheele, S., Dolin, P., Pathania, V. and Raviglione, MC. (1999) Global burden of tuberculosis: estimated incidence, prevalence, and mortality by country. *JAMA*, 282,677-68.

- Edge, B.A., Paterson, E.G., and Settles, G.S. (2005) Computational study of the wake and contaminant transport of a walking human. *Journal of Fluids Engineering*, 127(5): 967-977.
- Edgerton, HE. and Barstow, FE. (1959) Multiflash photography. *Photographic Science and Engineering*, 3 (6), 288-291.
- Edwards, LB. and Dragsted I. (1952) BCG-vaccine studies. 4. Further observations on the effect of light on BCG vaccine. *Bull World Health Organ*, 5, 333–336.
- Edwards, DA., Man, JC., Brand, P., Katstra, JP., Sommerei, K., Stone, HA., Nardell, E. and Scheuch, G. (2004) Inhaling to mitigate exhaled bioaerosols. *Proc Natl Acad Sci USA*, 101, 17383-17388.
- Eninger, RM., Honda, T., Reponen, T., KcKay, R. and Grinshpun, SA. (2008) What does respirator certification tell us about filtration of ultrafine particles? *J. Occup. Environ. Hyg.*, 5, 286–295.
- Eshbaugh, J.P., Gardner, P.D. and Richardson, A.W. and Hofacre, K.C. (2009) N95 and P100 respirator filter efficiency under high constant and cyclic flow. *Journal of Occupational and Environmental Hygiene*, 6, 52–61.
- Fabian, P., McDevitt, JJ., DeHaan, WH., Fung, ROP., Cowling, BJ., Chan, KH., Leung, GM. and Milton, DK. (2008) Influenza virus in human exhaled breath: An Observational Study. *PLoS ONE*, July, 1-6.
- Fabian, PM., McDevitt, JJ. and Milton, DK. (2009) Influenza virus in fine particles exhaled during tidal breathing and coughing. In *Proceedings of the American Thoracic Society Conference*, San Diego.
- Fairbanks, G. (1940) *Voice and articulation drillbook* (2nd ed., p. 127). New York: Harper & Row
- Fairchild, CI. and Stampfer, JK. (1987) Particle concentration in exhaled breath. *Am. Ind. Hyg. Assoc. J*, 48. 948-949.
- Fennelly, KP., Martyny, JW., Fulton, KE., Orme, IM., Cave, DM. et al. (2004) Cough generated aerosols of *Mycobacterium tuberculosis*: a new method to study infectiousness. *Am J Respir Crit Care Med*, 169, 604–609.
- Finlayson, E.U., Gadgil, A.J., Thatcher, T.L., and Sextro, R.G. (2004) Pollutant dispersion in a large indoor space. Part 2: Computational fluid dynamics predictions and comparison with a scale model experiment for isothermal flow. *Indoor Air*, 14: 272-283.
- Flatau, PJ., Walko, RL. and Cotton, WR. (1992) Polynomial fits to saturation vapor pressure. *J. Appl. Meteor*, 31, 1507-1513.
- Fluent (2005). *Fluent 6.2 documentation*. Fluent Inc., Lebanon, NH.
- Food and Drug Administration. (2004) *Guidance for industry and FDA staff: surgical masks—premarket notification Submissions*. Washington, DC: US Department of Health and Human Services, Food and Drug Administration, Center for Devices and Radiological Health.
- Freymuth, P. (1993) Flow visualization in fluid mechanics. *Review of Scientific Instruments*, 64:1–18.
- Gehan, EA. and George, SL. (1970) Estimation of human body surface area from height and weight. *Cancer Chemother Rep.*, 54, 225-35.
- Gendreau, MA. and DeJohn, C. (2002) Responding to medical events during commercial airline flights. *New England Journal of Medicine*, 346(14), 1067-1073.

- Germano, M., Piomelli, U., Moin, P. and Cabot, WH. (1991) A dynamic subgrid-scale eddy viscosity model. *Physics of Fluids A*, 3, 1760 - 1765.
- Gibson, MM. and Launder, BE. (1978) Ground effects on pressure fluctuations in the atmospheric boundary layer. *Journal of Fluid Mechanics*, 86, 491-511.
- Goldman, HI. and Becklake, MR., (1959) Respiratory function tests; normal values at median altitudes and the prediction of normal results. *Amer. Rev. Tuberc. Pulm. Dis.*, 79(4), 457-467.
- Grinsphun, SA., Haruta, H., Eninger, RM., Reponen, T., McKay RT. And Lee S. (2009) Performance of an N95 filtering facepiece particulate respirator and a surgical mask during human breathing: two pathways for particle penetration. *Journal of Occupational and Environmental Hygiene*, 6, 593-603.
- Gupta, JK., Lin, CH., and Chen, Q. (2009) Flow dynamics and characterization of a cough. *Indoor Air*, 19 (6), 517-525.
- Gupta, JK., Lin, CH., and Chen, Q. (2010a) Characterizing exhaled airflow from breathing and talking. *Indoor Air*, 30 (1), 31-39.
- Gupta, JK., Lin, CH. and Chen, Q. (2010b) Transport of expiratory droplets in an aircraft cabin, *Indoor Air*, doi:10.1111/j.1600-0668.2010.00676.x
- Haas, CN. (1983) Estimation of risk due to low doses of microorganisms: a comparison of alternative methodologies. *Am. J. Epidemiol.*, 118, 573–582.
- Haas, CN., Rose, JB. and Gerba, CP. (1999) *Quantitative Microbial Risk Assessment*. New York, John Wiley & Sons, Inc.
- Handbook of Physiology*, 1986, Volume 3 Part I, American Physiology Society, Bethesda, Maryland.
- Harper, GJ. (1961) Airborne micro-organisms: survival tests with four viruses, *J. Hygiene*, 59, 479-486.
- Hersen, G., Moularat, S., Robine, E., Gehin, E., Corbet, S., Vabret, A. and Freymuth F. (2008) Impact of health on particle size of exhaled respiratory aerosols: Case-control study. *Clean*, 36(7), 572-577.
- Hoppe, P. (1981) Temperature of expired air under varying climatic conditions. *International Journal of Biometeor*, 25(2), 127-132.
- Houk, VN., Baker, JH., Sorensen, K., et al. (1968) The epidemiology of tuberculosis infection in a closed environment. *Archives of Environmental Health*, 16, 26–50.
- Hsu, JY., Stone, RA., Logan-Sinclair, RB., Worsdell, M., Busst, CM. and Chung, KF. (1994) Coughing frequency in patients with persistent cough: Assessment using a 24 hour ambulatory recorder, *Eur Respir J*, 7, 1246-1253.
- Jeffrey, W.M., Cynthia, H., Michael, T.O., and Kristine, L.M. (1993) Exposure to *Mycobacterium tuberculosis* during air travel. *Lancet*, 342: 112-113.
- Jennison, MW. (1942) Atomizing of mouth and nose secretions into the air as revealed by high speed photography. *Aerobiology*, 17, 106-128.
- Jones, RM., Masago, Y., Bartrand, T., Nicas, M. and Rose JB. (2009) Characterizing the risk of infection from *mycobacterium tuberculosis* in commercial passenger aircraft using quantitative microbial risk assessment. *Risk Analysis*, 29(3), 355 – 365.
- Kera, T. and Maruyama, H. (2005) The effect of posture on respiratory activity of the abdominal muscles. *J Physiol Anthropol Appl Human Sci.*, 24(4), 259-65.

- Kenyon, TA., Valway, SE., Ihle, WW., Onorato, IM. and Castro, KG. (1996) Transmission of multidrug resistant mycobacterium tuberculosis during a long airplane flight. *New England Journal of Medicine*, 334, 933-938.
- Kenyon, TA., Copeland, JE., Moeti, T., et al. (2000) Transmission of *Mycobacterium tuberculosis* among employees in a US Government office, Gaborone, Botswana. *Int J Tuberc Lung Dis*, 4, 962-967.
- Klepeis, NE., Nelson, WC., Ott, WR., Robinson, JP., Tsang, AM., Switzer, P., Behar, JV., Hern, SC. and Engelmann, WH. (2001) The national human activity pattern survey (NHAPS): A resource for assessing exposure to environmental pollutants. *Journal of Exposure Analysis and Environmental Epidemiology*, 11 (3), 231-252.
- Klepeis, NE. and Nazaroff, WW. (2002) Characterizing size-specific ETS particle emissions, *Proceedings: Indoor Air*, 162-167
- Ko, G., Thompson, KM. and Nardell, EA. (2004) Estimation of tuberculosis risk on a commercial airliner. *Risk Analysis*, 24, 379-88.
- Ksiazek, TG., Erdman, D., Goldsmith, CS., Zaki, SR., Peret, T., Emery, S. et al. (2003). A novel evolution, genome and proteome of SARS-coronavirus 1001 coronavirus associated with severe acute respirator syndrome. *New England Journal of Medicine*, 348, 1953-1966.
- Kühn, M., Bosbach, J., and Wagner, C. (2009) Experimental parametric study of forced and mixed convection in a passenger aircraft cabin mock-up. *Building and Environment*, 44(5): 961-970.
- Lamb, JM., Murty, GE., Slater, RM. and Aitkenhead, AR. (1993) Postoperative laryngeal function assessed by tussometry. *British Journal of Anesthesia*, 70, 478-479.
- Lauder, BE. and Spalding, DB. (1974) The numerical computation of turbulent flows. *Computer Methods in Applied Mechanics and Energy*, 3, 269 - 289.
- Laurell, G. and Ronge, H. (1955) Ultraviolet air disinfection in a children's hospital, a technical and biological study. *Acta Paediatr*, 44, 407-425.
- Lee, S., Grinshpun, S. and Reponen T. (2008) Respiratory performance offered by N95 respirators and surgical masks: Human subject evaluation with NaCl aerosol representing bacterial and viral particle size range. *American Occupational Hygiene*, 52, 177-85.
- Leiner, GC., Abramowitz, S., Small, MJ. and Stenby, VB. (1966) Cough peak flow rate. *The American Journal of the Medical Sciences*, 251 (2), 211-214.
- Lilly, DK. (1992) A proposed modification of the Germano subgrid-scale closure model. *Physics of Fluids*, 4, 633 - 635.
- Lin, Y.J.P., and Linden, P.F. (2002) Buoyancy-driven ventilation between two chambers. *Journal of Fluid Mechanics*, 463: 293-312.
- Lin, CH., Horstman, RH., Ahlers, MF., Sedgwick, LM., Dunn, KH., Topmiller, JL., Bennett, JS. and Wirogo, S. (2005a) Numerical simulation of airflow and airborne pathogen transport in aircraft cabins - Part 1: Numerical simulation of the flow field. *ASHRAE Transactions*, 111(1), 755-763.
- Lin, CH., Horstman, RH., Ahlers, MF., Sedgwick, LM., Dunn, KH., Topmiller, JL., Bennett, JS. and Wirogo, S. (2005b) Numerical simulation of airflow and airborne pathogen transport in aircraft cabins - Part 2: Numerical simulation airborne pathogen transport. *ASHRAE Transactions*, 111(1), 764-768.

- Loomans, M. and Lemaire, T. (2002) Particle concentration calculations using CFD - a comparison. Proceedings of Indoor Air 2002, Edinburgh, Scotland, 153 - 156.
- Loudon, R.G. and Brown, L.C. (1967) Cough frequency in patients with respiratory disease. *Am Rev Respir Dis.*, 96, 1137-1143.
- Lubcke, H., Schmidt, S., Rung, T., and Thiele, F. (2001) Comparison of LES and RANS in bluff-body flows. *Journal of Wind Engineering and Industrial Aerodynamics*, 89:1471–1485.
- Mahajan, RP., Singh, P., Murty, GE. and Aitkenhead, AR. (1994) Relationship between expired lung volume, peak flow rate and peak velocity time during a cough manoeuvre. *British Journal of Anaesthesia*, 72 (3), 298-301.
- Mandell, G., Bennett, J. and Dolin, R. (1995) Principles and practices of infectious diseases. Fourth edition. Churchill Livingstone.
- Mangili, A. and Gendreau, MA. (2005) Transmission of infectious disease during commercial air travel. *Lancet*, 365, 989-996.
- Matsumoto, H., and Ohba, Y. (2004) The influence of a moving object on air distribution in displacement ventilated rooms. *Journal of Asian Architecture and Building Engineering*, 75: 71-75.
- Matsumoto, H., Hai, N.L., and Ohba, Y. (2004) CFD simulation of air distribution in displacement ventilated room with a moving object. In: Proceedings of Roomvent 2004, 9th International Conference on Air Distribution in Rooms, Coimbra, Portugal, 5-8 September.
- Mattsson, M., and Sandberg, M. (1996) Velocity field created by moving objects in rooms. Proceedings of 5th International Conference on Air Distribution in Rooms, Roomvent, Yokohama, Japan, 2: 547–554.
- Mazumdar, S. and Chen, Q. (2007) Impact of moving bodies on airflow and contaminant transport inside aircraft cabins. Proceedings of the 10th International Conference on Air Distribution in Rooms, Roomvent 2007, Helsinki, Finland: 165.
- Mazumdar, S., and Chen, Q. (2008) Influence of cabin conditions on placement and response of contaminant detection sensors in a commercial aircraft. *Journal of Environmental Monitoring*, 10: 71-81.
- Mazumdar, S., Priyadarshana, P.A., Keshavarz, A., Chen, Q., and Jones, B.W. (2008) Flow characteristics from air supply diffusers and their effect on airflow and contaminant transport inside an aircraft cabin. The 11th International Conference on Indoor Air Quality and Climate (Indoor Air 2008), Copenhagen, Denmark.
- McClellan RL. (1961) The effect of ultraviolet radiation upon the transmission of epidemic influenza in long-term hospital patients. *American Rev Respiratory Disease*, 83, 36–38.
- Megri, AC. and Haghghat, F. (2007) Zonal modeling for simulating indoor environment of buildings: review, recent developments, and applications. *HVAC&R Research*, 13(6), 887-905.
- Melikov, AK. (2004) Personalized ventilation. *Indoor Air* 14 (Suppl. 7), 157–167.
- Menter, FR. (1994) Two-equation eddy-viscosity turbulence models for engineering applications. *AIAA Journal*, 32, 1598 - 1605.
- Milton, DK., Fabian, PM., Angel, M., Perez, DR. and McDevitt, JJ. (2010) Influenza virus aerosols in human exhaled breath: particle size, culturability, and effect of

- surgical masks. In Proceedings of the American Thoracic Society Conference, New Orleans.
- Morawska, L. (2006) Droplet fate in indoor environments, or can we prevent the spread of infection? *Indoor Air*, 16, 335-347.
- Morawska, L., Johnson, GR., Ristovski, Z., Hargreaves, M., Mengersen, K., Chao, CYH., Li, Y. and Katoshevski, D. (2009) Size distribution and sites of origins of droplets expelled from the human respiratory tract during expiratory activities. *Journal of Aerosol Sciences*, 40, 256-269.
- Moser, MR., Bender, TR., Margolis, HS., Noble, GR., Kendal, AP. and Ritter, DG. (1979) An outbreak of influenza aboard a commercial airliner. *American Journal of Epidemiology*, 110, 1-6.
- Murakami, S., Kato, S., Nagano, S. and Tanaka, S., (1992) Diffusion characteristics of airborne particles with gravitational settling in a convection-dominant indoor flow field. *ASHRAE Transactions*, 98 (1), 82 – 97.
- Nazaroff, WW., Nicas, M. and Miller, SL. (1998) Framework for evaluating measures to control nosocomial tuberculosis transmission, *Indoor Air*, 8, 205-218.
- Nevalainen, A., Willeke, K., Liebhaber, F., Pastuszka J., Burge, H. and Henningson, E. (1993) Bioaerosol sampling. In: Willeke, K. and Baron, P.A.J. (eds) *Aerosol measurement: principles, techniques and applications*, New York, Van Nostrand-Reinhold.
- Norton, T. and Sun, D-W. (2006) Computational fluid dynamics (CFD) – an effective and efficient design and analysis tool for the food industry: A review. *Trends in Food Science and Technology*, 17, 600-620.
- NRC (National Research Council). (2002) *The airliner cabin environment and the health of passengers and crew*. Washington, DC: National Academy Press.
- Oberg, T. and Brosseau, L.M. (2008) Surgical mask filter and fit performance. *American Journal of Infection Control*, 36, 276-82.
- Olsen, S.J., Chang, H.L., Cheung, T.Y., Tang, A.F., Fisk, T.L., Ooi, S.P., Kuo, H.W., Jiang, D.D., Chen, K.T., Lando, J., Hsu, K.H., Chen, T.J., and Dowell, S.F. (2003) Transmission of the severe acute respiratory syndrome on aircraft. *New England Journal of Medicine*, 349(25): 2416-22.
- Papineni, RS. and Rosenthal, FS. (1997) The size distribution of droplets in the exhaled breath of healthy human subjects. *Journal of Aerosol Medicines*, 10, 105-116.
- Patankar, SV. (1980) *Numerical Heat Transfer and Fluid Flow*. Hemisphere, Washington, DC.
- Potter, JL., Matthews, LW., Lemm, J. and Spector, S. (1963) Human pulmonary secretions in health and disease. *Annals of the New York Academy of Sciences*, 106, 692-697.
- Poussou, S.B. (2008) Experimental investigation of airborne contaminant transport by a human wake moving in a ventilated aircraft cabin. Ph.D. Thesis, Purdue University.
- Qian Y, Willeke K, Grinshpun SA, Donnelly J. and Coffey, CC. (1998) Performance of N95 respirators: Filtration efficiency for airborne microbial and inert particles. *American Industrial Hygiene Association Journal*, 59, 128-32.
- Raber, E. and McGuire, R. (2002) Oxidative decontamination of chemical and biological warfare agents using L Gel. *Journal of Hazardous Materials*, 93B, 339-352.

- Raffel, M., Willert, C.E., Wereley, S.T., and Kompenhans, J. (2007) Particle image velocimetry, a practical guide. Springer-Verlag, Berlin and Heidelberg, New York.
- Ranz, WE. and Marshall, WR., Jr. (1952) Evaporation from drops, Part I. Chem. Eng. Prog., 48(3), 141-146.
- Riley, EC., Murphy, G. and Riley, RL. (1978). Airborne spread of measles in a suburban elementary school. American Journal of Epidemiology, 107, 421–432.
- Robinson, S. (1938) Experimental studies of physical fitness in relation to age. European Journal of Applied Physiology, 10, 251-323.
- Rudnick, S.N. and Milton, DK. (2003). Risk of indoor airborne infection transmission estimated from carbon dioxide concentration. Indoor Air, 13, 237–245.
- Samimy, M., and Lele, S. K. (1991) Motion of particles with inertia in a compressible free shear layer. Physics of Fluids, A3(8):1915–1923.
- Sancho, J., Servera, E. and Diaz, J. (2004) Comparison of peak cough flows measured by pneumotachograph and a portable peak flow meter. American Journal of Physical Medicine and Rehabilitation, 83(8), 608-612.
- Seaver, EJ., Dalston, RM., Leeper, HA. and Adams, LE. (1991) A study of nasometric values for normal nasal resonance. Journal of Speech, Language and Hearing Research, ASHA, 34, 715-721.
- Settles, G.S. (2006) Fluid mechanics and homeland security. Annual Review of Fluid Mechanics, 38:87–110.
- Settles, GS., Hackett, EB., Miller, JD. and Weinstein, LM. (1995) Full-scale schlieren flow visualization. Flow Visualization VII, ed. J. P. Crowder, Begell House, New York, Sept., 2-13.
- Shih, Y.C., Chiu, C.C., and Wang, O. (2007) Dynamic airflow simulation within an isolation room. Building and Environment, 42(9): 3194-3209.
- Shur, M., Spalart, PR., Strelets, M. and Travin, A. (1999) Detached-eddy simulation of an airfoil at high angle of attack. The 4th International Symposium on Engineering Turbulence Modeling and Experiments, Corsica, France.
- Singh, A., Hosni, M. and Horstman, R. (2002) Numerical simulation of airflow in an aircraft cabin section. ASHRAE Transactions, 108(1), 1005-1013.
- Singh, P., Mahajan, RP., Murty, GE. and Aithkenhead, AR. (1995) Relationship of peak flow rate and peak velocity time during voluntary coughing. British Journal of Anaesthesia, 74 (6), 714-716.
- Sze To, GN., Wan, MP., Chao, CYH., Fang, L. and Melikov, A. (2009). Experimental study of dispersion and deposition of expiratory aerosols in aircraft cabins and impact on infectious disease transmission, Aerosol Science Technology, 43 (5), 466-485.
- Sze To, GN. and Chao, CYH. (2010) Review and comparison between the Wells–Riley and dose-response approaches to risk assessment of infectious respiratory diseases. Indoor Air, 20, 2-16.
- Tezduyar, T.E. (2004) Finite element methods for fluid dynamics with moving boundaries and interfaces. In: Stein, E., de Borst, R., Hughes, T.J.R. (eds) Encyclopedia of Computational Mechanics, Vol. 3: Fluids, West Sussex, England, John Wiley, 545–577, ISBN 0-470-84699-2.

- Thatcher, T.L., Wilson, D.J., Wood, E.E., Craig, M.J., and Sextro, R.G. (2004) Pollutant dispersion in a large indoor space: Part 1—Scaled experiments using a water-filled model with occupants and furniture. *Indoor Air*, 14(4):258-71.
- VanSciver M, Miller S, Hertzberg J. Particle image velocimetry of human cough. Mechanical Engineering Department University of Colorado, Boulder CO.
- Viboud, C., Boelle, PY. and Pakdaman K, et al. (2004) Influenza epidemics in the United States, France, and Australia, 1972–1997. *Emerging Infectious Diseases*, 10, 32–39.
- Walkinshaw, DS. (2010) Germs, flying and the truth. *ASHRAE Journal* April, (52) , 70-73.
- Wan, MP., Sze To, GN., Chao, CYH., Fang, L. and Melikov, A. (2009) Modeling the fate of expiratory aerosols and the associated infection risk in an aircraft cabin environment. *Aerosol Science and Technology*, 43(4), 322-343.
- Wan, MP. and Chao, CYH. (2007) Transport characteristics of expiratory droplets and droplet nuclei in indoor environments with different ventilation air flow patterns. *Journal Biomechanical Engineering Transaction ASME*, 129, 341–353.
- Weiss, MM. (MD), Weiss, PD. (MD), Weiss, DE. (MD) and Weiss, JB. (MD) (2007) Disrupting the transmission of influenza A: Face masks and ultraviolet light as control measures. *American Journal of Public Health*, Supplement 1, 97, No. S1.
- Wells, WF., Wells, MW. and Mudd, S. (1939) Infection of air: Bacteriologic and epidemiologic factors. *American Journal of Public Health*, 29, 863-880.
- Wells, WF. (1955) *Airborne Contagion and Air Hygiene*. Cambridge University Press, Cambridge MA, 117–122.
- WHO 2002. *Bulletin of the World Health Organization*; 80 (3): 261.
- WHO 2004. “WHO guidelines for the global surveillance of severe acute respiratory syndrome (SARS)” Department of Communicable Disease Surveillance and Response, World Health Organization.
- Willeke, K. and Qian, Y. (1998) Tuberculosis control through respirator wear: performance of National Institute for Occupational Safety and Health regulated respirators. *American Journal of Infection Control*, 26, 139–142.
- World Bank 2005.  
<http://web.worldbank.org/WBSITE/EXTERNAL/NEWS/0,,contentMDK:20715408~pagePK:64257043~piPK:437376~theSitePK:4607,00.html>
- World Health Organization. (1998) Tuberculosis and air travel: guidelines for prevention and control. *WHO Doc*, WHO/TB98, 256, 1–45.
- World Health Organization. (1999) Guidelines for the prevention of tuberculosis in health care facilities in resource-limited settings. *WHO Doc*, WHO/CDC/TB/99, 269, 1–51.
- World Health Organization (2009). Pandemic (H1N1) 2009 - update 76". *Global Alert and Response (GAR)*, 11-27.  
[http://www.who.int/csr/don/2009\\_11\\_27a/en/index.html](http://www.who.int/csr/don/2009_11_27a/en/index.html). Retrieved 2009-12-11.
- Yakhot, V. and Orszag, SA. (1986) Renormalization group analysis of turbulence. *Journal of Scientific Computing*, 1, 3-51.
- Yan, W., Zhang, Y., Sun, Y. and Li, D. (2009) Experimental and CFD study of unsteady airborne pollutant transport within an aircraft cabin mock-up. *Building and Environment*, 44(1), 34-35.

- Yang, S., Lee, GWM., Chen CM., WU, CC. and Yu, KP. (2007) The size and concentration of droplets generated by coughing in human subjects. *Journal of Aerosol Medicine*, 20(4), 484-494.
- Yeager, H., Lacy, L., Smith, LR. and LeMaistre, CA. (1967) Quantitative studies of mycobacterial populations in sputum and saliva. *American Review of Respiratory Disease*, 95, 908-1004.
- Zhai, Z., Chen, Q., and Scanlon, P.W. (2002) Design of ventilation system for an indoor auto racing complex. *ASHRAE Transactions*, 108(1), 989-998.
- Zhai, Z., Zhang, Z., Zhang, W., and Chen, Q. (2007) Evaluation of various turbulence models in predicting airflow and turbulence in enclosed environments by CFD: Part-1: summary of prevalent turbulence models. *HVAC&R Research*, 13(6): 853-870.
- Zhang, Z. (2007) Modeling of Airflow and Contaminant Transport in Enclosed Environments. Ph.D. Thesis, Purdue University.
- Zhang, T. (2007a) Detection and mitigation of contaminant transport in commercial aircraft cabins. Ph.D. Thesis. Purdue University.
- Zhang, Z. and Chen, Q. (2006) Experimental measurements and numerical simulations of particle transport and distribution in ventilated rooms. *Atmospheric Environment*, 40(18), 3396-3408.
- Zhang, T., and Chen, Q. (2007) Novel air distribution systems for commercial aircraft cabins. *Building and Environment*, 42(4): 1675-1684.
- Zhang, T. and Chen, Q. (2007b) Identification of contaminant sources in enclosed spaces by a single sensor, *Indoor Air*, 17(6), 439-449
- Zhang, Z. and Chen, Q. (2007c) Comparison of the Eulerian and Lagrangian methods for predicting particle transport in enclosed spaces. *Atmospheric Environment*, 41(25), 5236-5248.
- Zhang, Z., Zhang, W., Zhai, Z. and Chen, Q. (2007) Evaluation of various turbulence models in predicting airflow and turbulence in enclosed environments by CFD: Part-2: Comparison with experimental data from literature. *HVAC&R Research*, 13(6): 871-886.
- Zhang, T., Chen, Q. and Lin, CH. (2007a) Optimal sensor placement for airborne contaminant detection in an aircraft cabin. *HVAC&R Research*, 13(5), 683-696
- Zhang, Z., Chen, X., Mazumdar, S., Zhang, T. and Chen, Q. (2009) Experimental and numerical investigation of airflow and contaminant transport in an airliner cabin mockup. *Building and Environment*, 44(1), 85-94.
- Zhang, Z. and Chen, Q. (2009) Prediction of particle deposition onto indoor surfaces by CFD with a modified Lagrangian method. *Atmospheric Environment*, 43(2), 319-328.
- Zhao, B., Zhang, Z. and Li, X. (2005) Numerical study of transport of droplets or particles generated by respiratory system indoors. *Building and Environment*, 40 (8), 1032-1039.
- Zhao, J. and Yang, X. (2003) Photocatalytic oxidation for indoor air purification: a literature review. *Building and Environment*, 38, 645-654.
- Zhu, S., Kato, S. and Yang, JH. (2006a) Investigation into airborne transport characteristics of air-flow due to coughing in a stagnant room environment. *ASHRAE Transaction*, 112, 123-133.

- Zhu, S., Kato, S. and Yang, JH. (2006b) Study on transport characteristics of saliva droplets produced by coughing in a calm indoor environment. *Building and Environment*, 41, 1691-1702.
- Zuo, W. and Chen, Q. (2009). Real time or faster-than-real-time simulation of airflow in buildings. *Indoor Air*, 19(1), 33-44

## **Part 2:**

# **Measurement of Particle Deposition Behavior in an Aircraft Cabin**

Prepared by  
Byron W. Jones, P.E., Ph.D.  
Institute for Environmental Research  
Kansas State University  
Manhattan, Kansas

February 22, 2012

## 11. INTRODUCTION

As stated in the original work statement for the project, the purpose of this portion of the study is to use the KSU B-767 cabin mockup to experimentally measure particle deposition on aircraft surfaces to supplement the modeling studies. The B-767 mockup is shown in Figure 11.1 and contains 11 rows of seats in a 2-3-2 configuration. It has a fully functioning air supply system using B-767 supply diffusers and associated ducting to faithfully represent air distribution in the actual aircraft cabin. The cabin is supplied with HEPA filtered, temperature controlled air. A simple thermal manikin is placed in each seat to provide a representative thermal load for the cabin. A picture of the interior of the cabin is provided in Figure 11.1.



*Figure 11.1 Eleven-row mockup of the interior of a Boeing 767 cabin.*

The original plan was to use a liquid aerosol generator with recovery of chemical tracers from test areas to measure particle deposition rates. However, a number of methods of measuring particle deposition were considered. In the end, it was decided to use microscopic photographic methods for measuring deposition. There were two key reasons for this approach. First, it is a direct measurement. It is possible to see exactly what is being deposited. All other methods resulted in some indirect indication of the number of particles being deposited. Second, this approach allowed us to use the identical particle dispersion method as used in previous work in the Contaminant Transport Project where extensive airborne data were collected (Beneke 2010, Beneke et al, 2011). Having both airborne concentrations and surface deposition data for the same conditions for the same locations will allow us to relate these two data sets to each other.

## 12. EXPERIMENTAL METHODS

In this work, as in the previous project, a talcum powder dust was used for the particulate measurements. A small amount of talcum powder was loaded into a plastic cup. This cup was placed under a copper tube. A puff of air from the tube aerosolized the talcum powder without disrupting the overall airflows in the cabin. A picture of the apparatus is shown in Figure 12.1. Such a cup was placed at each seat in the second row of the cabin and the release was made for all seven seats at the same point in time. This approach allowed us to focus on the longitudinal transport in the cabin. A point source release tends to have a chaotic result due to the chaotic nature of local airflow patterns. Using seven simultaneous sources provides a much stronger signal at distances several rows from the release, which are of most use, without overwhelming measurements near the release.



*Figure 12.1 Dust injection apparatus*

The particle deposition measurements were made using a traversing digital microscope to scan surfaces of interest. The digital microscope, shown in Figure 12.2, is then used to look at a number of surface locations using the traversing mechanism shown in Figure 12.3. The traversing mechanism spanned the three center seats of each row. A clear plastic tape was used as the deposition surface. This tape slides over the microscope platform as the microscope traversed to allow the microscope focus to be maintained. At the resolution necessary to see particles of a few microns in diameter, the depth of field is very small and, thus, the test surface must be held at precisely the correct depth. A traverse was made prior to and after particle release and the number of new

particles showing up on the image were counted manually at each test location. This process is very tedious and the data reported here took several months to collect.

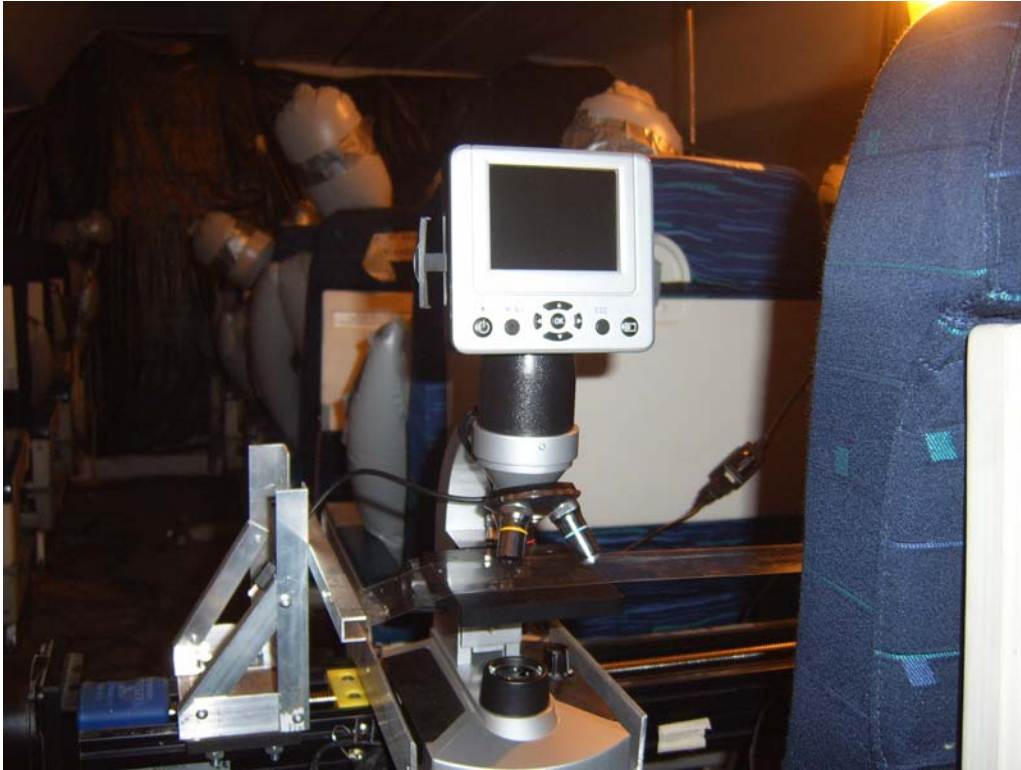


*Figure 12.2 Digital microscope used to inspect surface.*



*Figure 12.3 Microscope traversing system.*

However, by using manual counting, we were able to ensure quality results and caught some measurement problems that would have resulted in substantial, likely

uncorrected, errors if automated methods had been used. Figures 12.4 and 12.5 show camera images before and after particle release.

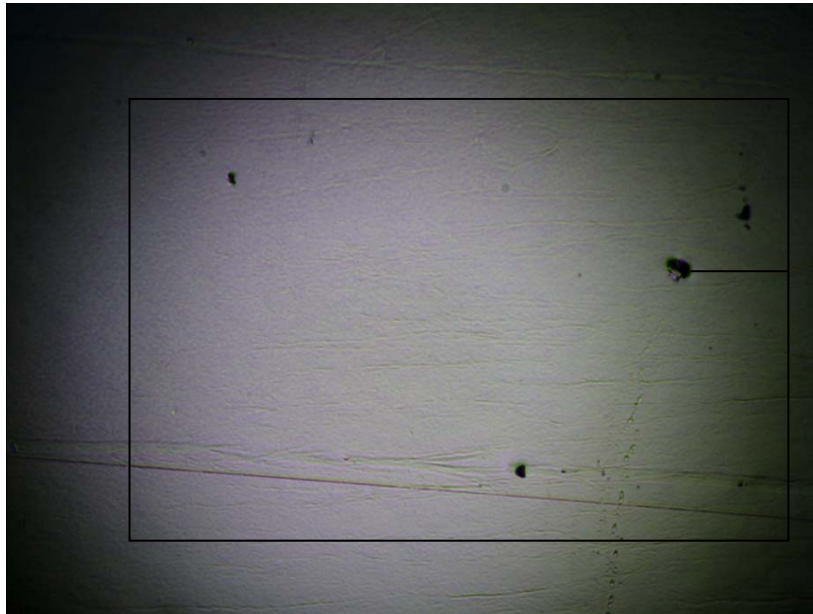


*Figure 12.4 Image before dust release.*

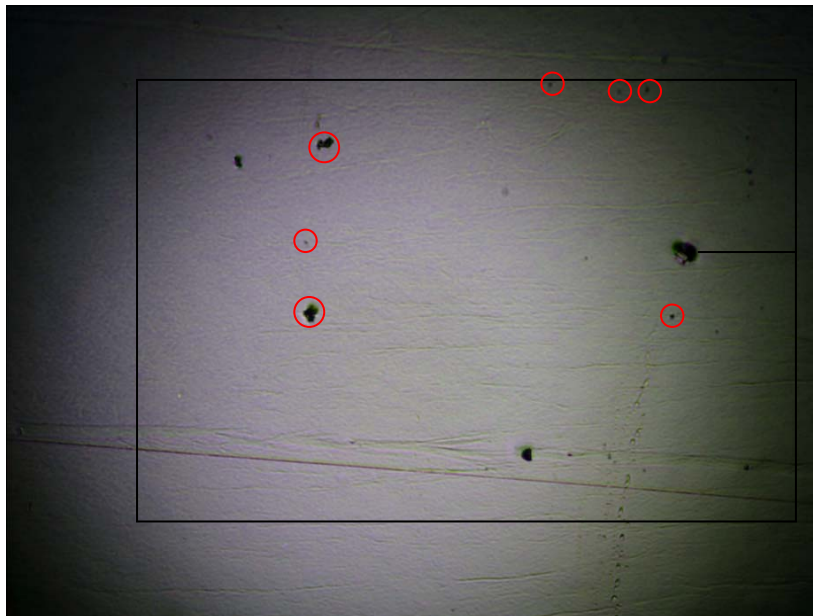


*Figure 12.5 Image after dust release (red circles denote new particles on the surface).*

Figure 12.6 shows the cabin layout and nomenclature for the data reporting. The release was in the second row of seats. This row is referred to as “row 0” and data are reported in terms of the number of rows from the release point. That is, “row 1” is the third seat row of the cabin but is one seat row from the release. Seats are numbered 1-3 with 1 being the left-most of the three center seats, 2 being center seat, and 3 being the right-most seat of the three center seats.



Figure 12.6 Cabin layout and nomenclature for experiments.

### 13. RESULTS

The data reported here were collected in the armrest area of the seat, as can be seen by the location of the clear tape in Figure 12.3. Five locations were measured for each seat and the experiments were all conducted at least twice. Thus, there are at least 10 measurements for each seat for the reported data. Figure 13.1 summarizes the data for these locations. At this point, data are just reported in terms of counts as they will ultimately be related to the airborne concentrations. Each bar shown is the average number of counts for the five locations for that seat. For reference, the count area is 0.7 mm<sup>2</sup>. Figures 13.2-13.4 present the same data but include standard deviation information. As can be seen, the standard deviation is large but that is typical of transport phenomena for aircraft cabins. The flows are quite chaotic and the transport from a given release point to any location in the cabin can depend significantly on the instant the release happens to occur.

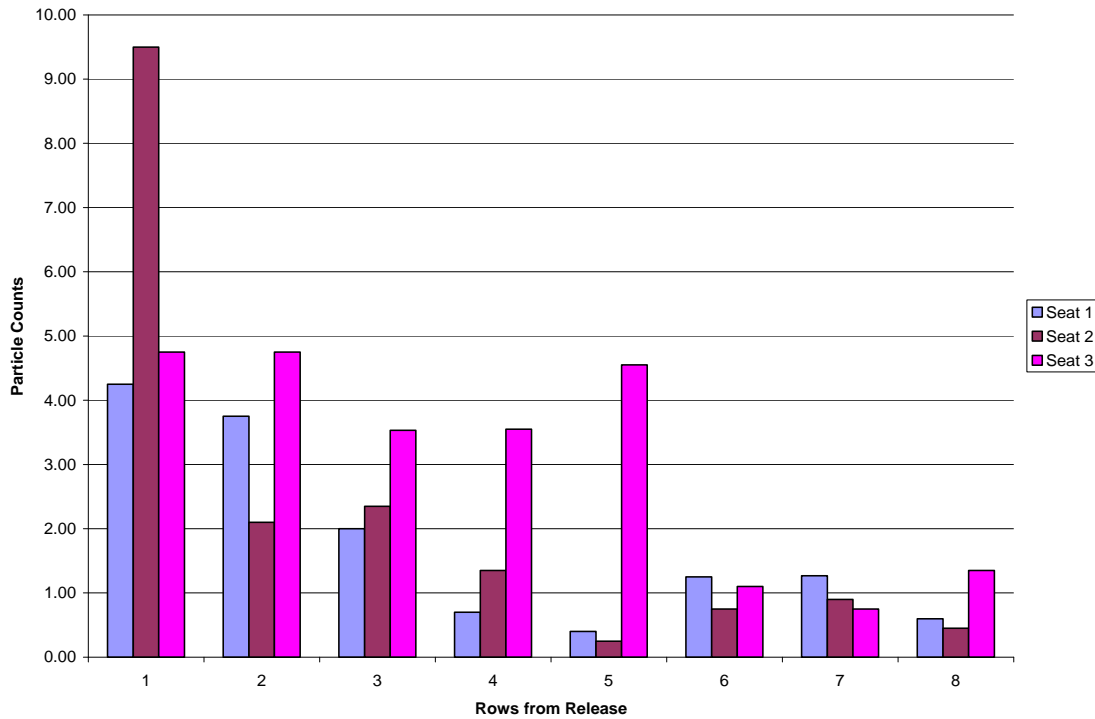


Figure 13.1 Summary of the particle deposition data collected.

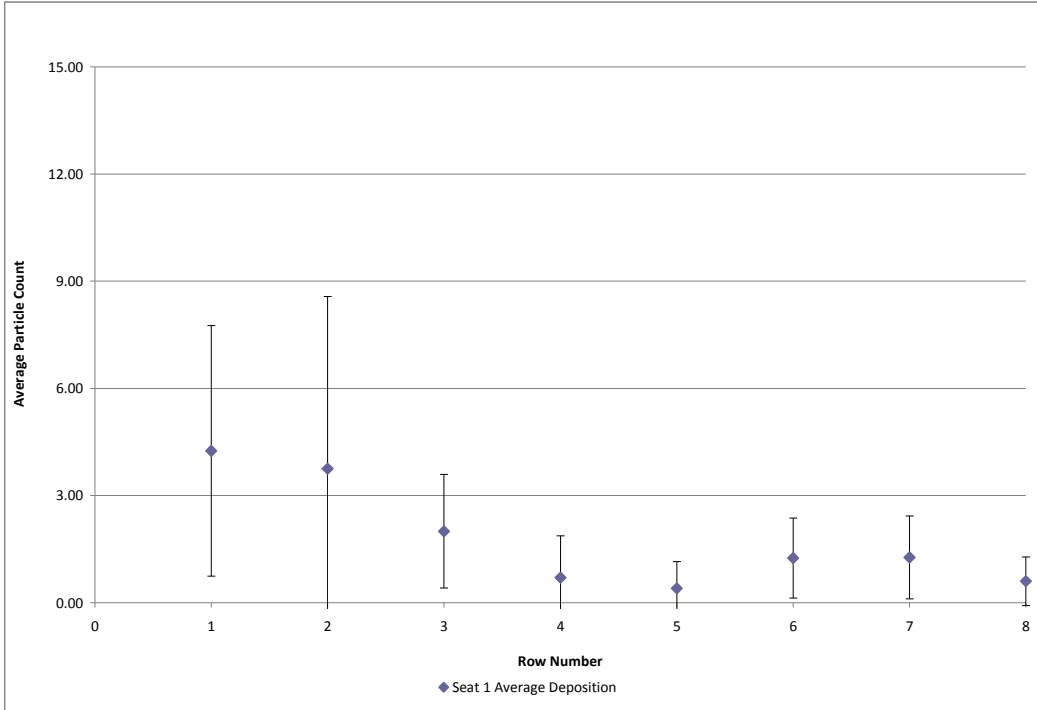


Figure 13.2 Deposition data for seat 1.

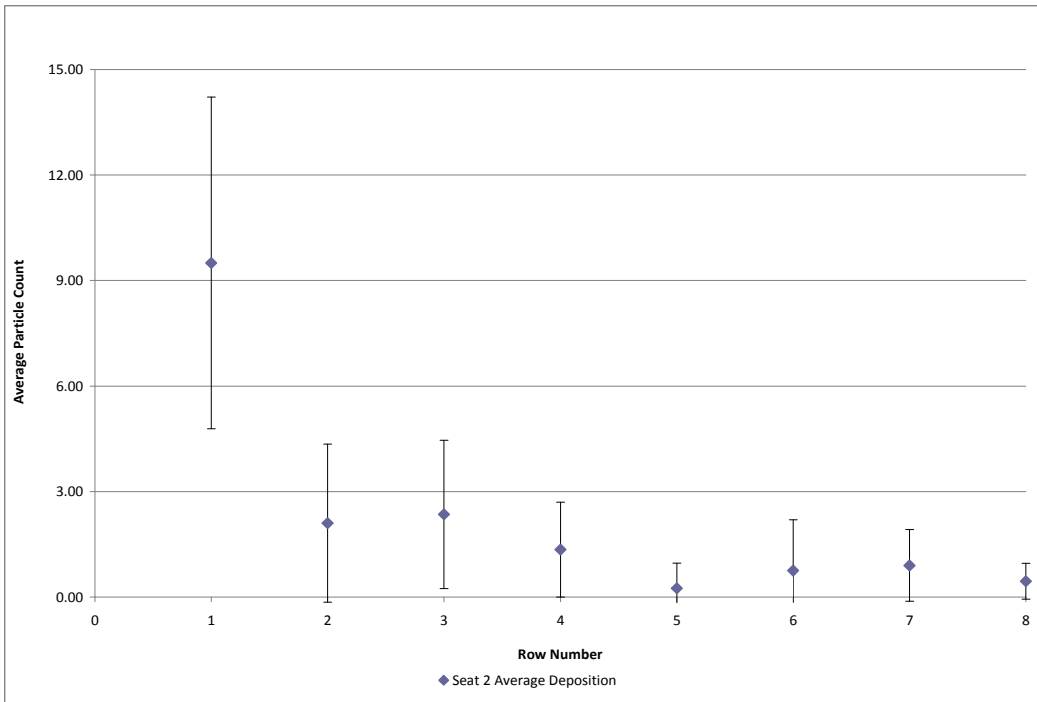
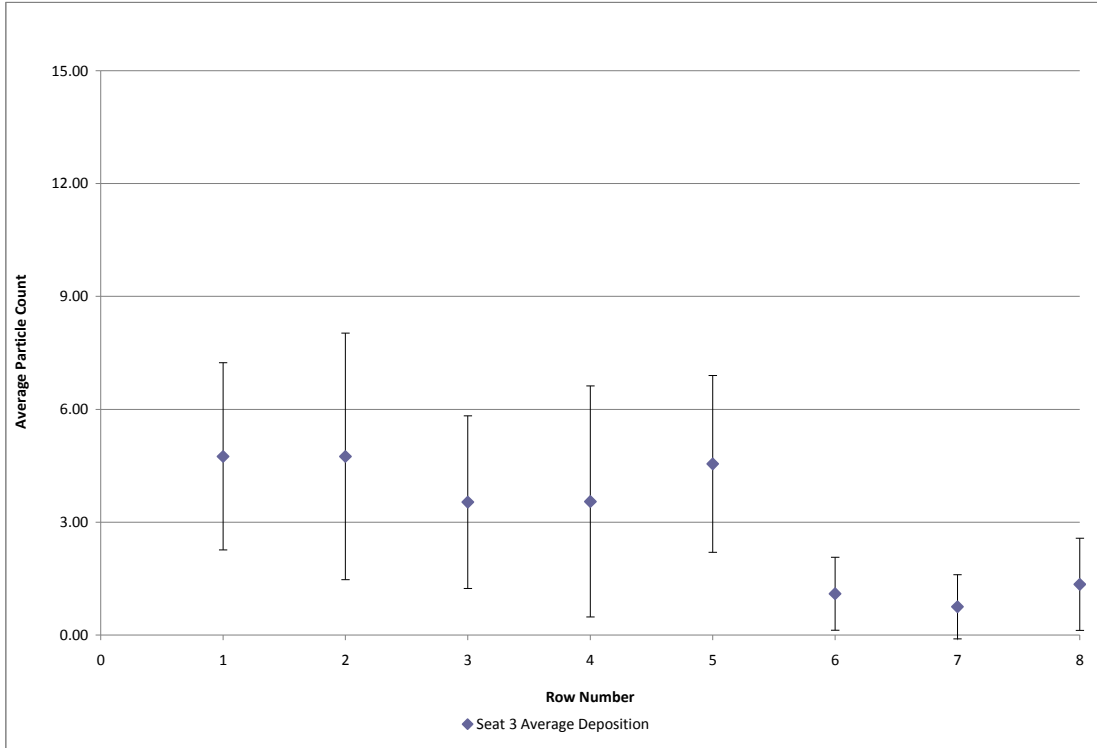


Figure 13.3 Deposition data for seat 2.



*Figure 13.4 Deposition data for seat 3.*

## 14. CONCLUSIONS AND NEXT STEPS

At this point in time, there are no specific conclusions to draw from the data. The deposition rates drop off with distance from the release in a pattern that is similar to what was seen with the airborne concentration measurements, a result that is not particularly surprising but is reassuring. Also, there is a tendency for the deposition rates to be higher on the right side of the cabin than on the left, even though the particles are dispersed uniformly across the width of the cabin. This result, again, is consistent with the airborne measurements and also the nature of the secondary flow patterns seen in the cabin. Currently a similar data set is being collected for vertical surfaces. Since this set is not complete, it is not reported here. Once the vertical data set is complete, we will compare the deposition data to the airborne concentration data to determine deposition rates as a function of airborne concentration.

## 15. REFERENCES

- J. M. Beneke, B. W. Jones and M.H. Hosni, "Fine Particle Dispersion in a Commercial Aircraft Cabin," HVAC&R Research, Volume 17, Issue 1, February 2011.
- J.M. Beneke,. 2010. Small Diameter Particle Dispersion in a Commercial Aircraft Cabin. MS Thesis. Manhattan, KS: Kansas State University.

## **Part 3:**

# **Role of Relative Humidity in the Inactivation of Influenza Viruses on Steel Surfaces and Microbial Surface Sampling in the Air Cabin**

Prepared by  
James J. McDevitt, Ph.D., CIH and John D. Spengler, Ph.D.  
Division of Exposure, Epidemiology and Risk  
Department of Environmental Health  
Harvard School of Public Health  
Cambridge, Massachusetts

February 10, 2012

## 16. INTRODUCTION

The transmission of bacterial and viral pathogens from inanimate surfaces to susceptible persons is a concern with regard to infectious disease transmission. For infection to occur, the pathogenic organisms must be present and survive on the environmental surface until such a time that the pathogen is transferred to a susceptible host at the appropriate route of entry. Bacteria and viruses have been shown to survive on surfaces for hours to months (Kramer, Schwebke et al. 2006; Boone and Gerba 2007). A summary of selected clinically relevant bacteria and virus duration of persistence is shown in Table 16.1.

Table 16.1 Bacteria and Virus Duration of Persistence.

*Adapted from Kramer et. al. BMC Infectious Diseases 2006: 6:130(Kramer, Schwebke et al. 2006).*

<b>Bacterium Type</b>	<b>Duration of Persistence</b>	<b>Virus Type</b>	<b>Duration of Persistence</b>
Acinetobacter spp.	3 days to 5 months	Adenovirus	7 days – 3 mos
<i>Bordetella pertussis</i>	3 – 5 days	Coronavirus	3 hours
<i>Campylobacter jejuni</i>	up to 6 days	SARS associated virus	72 – 96 hours
<i>Clostridium difficile</i> (spores)	5 months	Echovirus	7 days
<i>Corynebacterium diphtheriae</i>	7 days – 6 mos	Influenza virus	1 – 2 days
<i>Mycobacterium tuberculosis</i>	1 day – 4 mos	Norovirus	8 hours – 7 days
<i>Pseudomonas aeruginosa</i>	6 hours – 16 mos	Respiratory syncytial virus	up to 6 hours
<i>Salmonella typhi</i>	6 hours – 4 weeks	Rhinovirus	2 hours – 7 days
<i>Staphylococcus aureus</i> , including MRSA	7 days – 7 mos	Rotavirus	6 – 60 days

The longer pathogens survive once deposited on inanimate surfaces, called fomites, the higher the probability they will be transmitted to susceptible individuals. This is especially true in the air cabin environment which is a unique environment for disease transmission. The air cabin has a high occupation density with high through-put of passengers. While seated for hours at a time, “sick” individuals have ample opportunity to contaminate their surrounding area (i.e. arm rests, tray tables, lavatories, etc). Once surfaces in the air cabin are contaminated, susceptible persons in the immediate area may come into contact with the contaminated surfaces. Contamination may result from coughing out large particles which deposit on these surfaces or by touching surfaces with contaminated hands. Since many pathogens may survive for hours or days, when new susceptible individuals board the plane they are at risk of coming into contact with these surfaces. Likely exposure to the susceptible individual will be via the

hands which then can transfer the pathogens to mucous membranes of the eyes, nose, and mouth.

Environments such as daycare centers and hospitals have been characterized with respect to the presence of bacteria and viruses on contact surfaces and provide a starting point for assessing the risk of infection and interventions for transmission(Boone and Gerba 2005; Kramer, Schwebke et al. 2006; Boone and Gerba 2007). The air cabin environment has been characterized, to some degree, for bioaerosol exposures(Moser, Bender et al. 1979; McKernan, Burge et al. 2007; McKernan, Hein et al. 2008; McKernan, Wallingford et al. 2008; Gerba 2009). However, surface pathogen characterization has not been done in the in the air cabin environment. Pathogens such as influenza virus, norovirus, methacilin resistant staphylococcus (MRSA), measles, rubella, hemorrhagic fevers, mycobacterium tuberculosis(TB) are of concern in the air cabin environment and are under study by the Transportation Reseach Board Airport Cooperative Research Program (ACRP) under project ACRP 02-20A(TRB 2011). With the exception of TB, all of these organisms may be spread from surface contamination. Intuitively, tray tables, arm rests, and other high touch areas are likely contaminated during flights when sick people fly. Furthermore, the air cabin is typically not cleaned (with the exception of lavatories and galleys), between flight segments. However, whether these organisms are commonly found in the aircraft environment is unknown.

The goal of this investigation was to develop a better understanding of surface contamination in the air cabin through laboratory investigation and a pilot field study. The laboratory investigation focused on evaluating survival of influenza virus on surfaces and developing a field, microbial, surface sampling protocol for use in the air cabin environment. While the pilot field study focused on developing a rational method for evaluating microbial contamination on air cabin surfaces.

## 17. BACKGROUND

### 17.1 Relative Humidity and Influenza Surface Survival

Due to the threat of highly lethal bird flu and the recent pandemic associated with seasonal flu, much attention has been focused influenza virus transmission. There is much debate about whether influenza virus is transmitted directly through large droplet, by fine aerosols, or by contact with fomites (Tellier 2006; Brankston, Gitterman et al. 2007). Based on the available data, transmission via fomites cannot be ruled out as a route of exposure and should not be disregarded in an exposure control plan. Although there is no specific data on influenza on air cabin surfaces, influenza nucleic acid has been found on surfaces in daycare centers and hospitals (Boone and Gerba 2005; Bright, Boone et al. 2010). Furthermore, influenza has been found to survive on various surfaces for considerable time on non-porous surfaces such as stainless steel (Rudnick, McDevitt et al. 2009). In these studies survival times were quite variable and ranged from several hours to 2 days. (Bean, Moore et al. 1982; Thomas, Vogel et al. 2008; Greaterox, Digard et al. 2011).

A significant amount of past research has shown that influenza aerosol survival is dependant upon relative humidity with influenza survival favored at low RH (Myatt, Kaufman et al. 2010). Whereas, influenza surface survival research is limited. Buckland et al, evaluated how relative humidity effects influenza survival at only two RH extremes and evaluations by Bean et al. and Greaterox et al. did not vary relative humidity at all (Buckland and Tyrrell 1962; Bean, Moore et al. 1982; Greaterox, Digard et al. 2011). McDevitt et al. measured the effects of RH on influenza surface survival, but experiments were done at temperatures well above those found in the air cabin (>55°C) (McDevitt, Rudnick et al. 2010). Based on the existing research the air cabin may provide an optimum environment for influenza surface survival, which in turn, could increase the probability for disease transmission.

### 17.2 Surface Sampling Protocol Development

The goal of surface sampling in the air cabin was to detect the presence of bacteria and viruses on non-porous surfaces. Bacteria would be analyzed by culture methods to detect and quantify bacteria. Using culture methods, samples are suspended in liquid and inoculated onto agar petri dishes. The agar provides nutrients that allow the bacteria to grow when incubated. The bacterial growth results in the formation of distinct colonies which can be grouped based on morphology and counted. Each colony with a unique morphology can then be identified using standard microbiology techniques. Culture analysis of bacteria provides a means of detecting a large variety of bacterial types in a single sample and in a cost effective manner. Virus analysis is more challenging since viruses require animal cells to infect and replicate. Different viruses require specific, and different, types of cells in which to grow. Thus, it is practically

impossible to grow samples containing unknown viruses. For this reason PCR is used to amplify and detect sequences of nucleic acid which are unique to individual viruses. PCR is also limited since the sequence for each type of virus must be screened. For this reason, methods have been developed to test groups of viruses, called panels, in a single sample. Such a test, the Respiratory MultiCode Assay (RMA)(Lee, Grindle et al. 2007), has been developed for respiratory viruses and was used in this study. The respiratory viruses detected by the RMA are the following: Human Rhinoviruses (HRV), Enteroviruses, Coronaviruses (CoV), Respiratory Syncytial Virus (RSV), Metapneumovirus (MPV), Parainfluenza viruses (PIV), Influenza (InfV), Adenoviruses (AdV), and Bocavirus.

Enteric viruses, those found in the intestinal tract, are also of interest for disease transmission. We considered that respiratory viruses shed by coughing, sneezing, or hand transfer would be more likely to be present on surfaces in the air cabin, than enteric viruses spread by fecal oral or water routes. Thus, for the pilot study we limited our investigation to respiratory viruses.

Surface sampling is commonly done in a dry fashion in which the surface is vacuumed and particulate matter is collected onto a filter. The material on the filter is then subsequently removed and analyzed accordingly. This method is useful for collecting biological materials that are associated with dust which settles or collects on surfaces. However, in the air cabin environment, due in part to high amounts of traffic and air movement, dust does not accumulate on common touch surfaces such as tray tables, arm rests, etc. Furthermore, respiratory secretions or deposits associated with contaminated hands would not be of a dusty nature, but rather “sticky”. Swab sampling methods, such as those, commonly used in hospital and food service evaluations are more suited to surface sampling for pathogens in the air cabin. Generally, swab sampling consists of wetting the swab, moving the swab over the sample surface, extracting the swab, and analyzing the extract. However, specific details are lacking for the best type of swab, method of extraction, etc. Thus, methods require characterization to ensure efficient collection and recovery of organisms from surfaces. To that end, laboratory testing using surrogate organisms to optimize methods and maximize collection and recovery of organisms from surfaces are needed. In our laboratory *Bacillus subtilis* was used as a surrogate for spore forming bacteria and *Serratia Marcescens* for vegetative bacteria. Protocol optimization was focused on bacteria since molecular methods, which detect nucleic acid rather than rely on growing organisms, will be used for virus analysis.

### 17.3 Field Study

Our initial sampling concept was to develop a biological, surface sampling kit for use on aircraft. The original plan was to distribute the sampling kits to volunteers who would be taking a future flight. The volunteer would collect samples during their flight and return the samples to the laboratory for analysis. This strategy would benefit from sampling a large variety of aircraft and numerous air carriers. However, preliminary discussions of regarding this strategy highlighted significant limitations questioning whether this style of sample collection would be feasible or scientifically rigorous.

Relying on volunteers to collect field samples using only printed instructions and no actual training could easily compromise quality of the samples collected. Surface

sampling requires using a swab to remove the pathogens from the surface. Variables such as swab wetting, swab pressure, area of sample would not be controlled from one individual to another and potentially increase variability. Secondly, the potential for cross contamination between samples or contamination of the samples by the person sampling would be much higher with unskilled persons. Post sampling handling would also vary between individuals based on flight times, number of segments, and time to get the samples shipped to the laboratory. Another limitation was that samples would have to be returned to a central lab, processed for analysis and then sent to the analyzing laboratory. Furthermore, samples would also need to be stored for group analysis (for cost effective analysis) and would result in varying storage time between samples. There were also non-scientific concerns associated with the initial protocol. An informal survey of colleagues showed that most were concerned about transporting sampling kits through airport security and issues about the perception of the sampling from other passengers or flight crew. The prospect of coordinating sampling for each individual with FAA, TSA, and individual airlines posed serious concerns.

Instead, our sampling strategy focused on partnering with an airline which serves Logan airport. Logan airport is convenient to our processing laboratory at HSPH and allows for immediate sample processing and shipment to the analytical laboratory in a single batch within 24 hours. Aircraft surfaces were sampled from numerous aircraft at the completion of the flight day and prior to being serviced for the following flight day. This method provided access to multiple types of aircraft servicing routes from across the country. Since sampling was done at the end of the day it provided a composite of the days' contamination by passengers. Also, this strategy allowed samples to be collected in several different areas within the air cabin and subsequent comparison. A limitation of this design is that sampling was restricted to single airline. To overcome this limitation, the number or partner airlines and airports could be expanded in future studies.

## 18. METHODS

### 18.1 Test Organisms

#### 18.1.1 Influenza Virus

Suspensions of influenza viruses (A/PR/8/34 H1N1), were purchased from Advanced Biotechnologies Inc. (Columbia, MD), thawed, divided into single-use, working stock portions, and stored at -80°C until needed.

A fluorescent focus reduction assay, which labels nucleoproteins expressed by infected MDCK cells with fluorescent antibodies, was used to enumerate the number of infective viruses and has been described previously (Hartshorn, White et al. 2007; Rudnick, McDevitt et al. 2009). Briefly, triplicate wells on a 96-well plate containing monolayers of Madin Darby Canine Kidney (MDCK) cells (ATTC # CCL-34) were infected with 50- $\mu$ l rinsate from each sample and allowed to incubate for approximately 8 hours. Then infected cells containing influenza A nucleoproteins were labeled with influenza A virus nucleoprotein antibody (Abcam, Cambridge, MA) and subsequently labeled with rhodamine-labeled goat anti-mouse IgG (Jackson ImmunoResearch Laboratories, West Grove PA). The number of cells having a resulting fluorescent foci, which are referred to as fluorescent focus units (FFU), were then counted at 200x total power using an Olympus CKX-41 inverted fluorescent microscope (Olympus, Center Valley, PA). Each well was scanned in a standard pattern with 10 fields chosen at random for counting (about 30% of the well). For samples with less than 2 FFU per viewing field, the entire well was counted. We summed the counts for the 9 wells associated with each test. The number of FFUs per sample was then computed based on dilution factors and the fraction of the well counted.

#### 18.1.2 Bacteria

##### Serratia marcescens

*S. marcescens* was obtained from the American Type Culture Collection (ATCC 8195) and stored at -70°C. Cells used in the experiments were prepared by inoculating a 100  $\mu$ l of *S. Marcescens* (approximately  $1 \times 10^7$  cfu/ml) into 100 ml of nutrient broth (Difco Laboratories) and culturing the mixture at 25°C for 24 h with 200 rpm of agitation on a shaker table. The cell suspension was transferred to 50 ml centrifuge tubes and pelleted at 250xg. The supernatant was removed and the pellet re-suspended in PBS. This procedure was repeated 3 times with the pellet being suspended in a final volume of 50 ml of PBS. One ml portions of the cell suspension were stored at 70°C for later use. Representative portions were thawed and titered to determine the cell concentration.

All sample extracts containing *S. Marcescens* were plated in duplicate with 100  $\mu$ l volumes on 100 mm petri dishes containing nutrient agar (BD, Franklin, NJ). Cultures were left at room temperature to grow and were counted after incubating for 24 hours.

## Bacillus atrophaeus

Spores of *Bacillus atrophaeus* (ATCC 9372) were provided by the Baker Company (Sanford, Maine). Spores were prepared using the protocols contained in NSF/ANSI 49, Biosafety Cabinetry: Design, Construction, Performance, and Field Certification. Concentrated stocks were thawed, diluted 10-fold in cell culture grade water, portioned into 1 ml volumes, frozen, and stored at -70 until use. Representative portions were thawed and tittered to determine the cell concentration.

All sample extracts containing *B. atrophaeus* were plated in duplicate with 100 ul volumes on 100 mm petri dishes containing tryptic soy agar (BD, Franklin, NJ). Cultures were left at room temperature to grow and were counted after incubating for 24 hours.

## 18.2 Relative Humidity and Influenza Surface Survival

### 18.2.1 RH Control Chamber

Stainless-steel coupons measuring 7.6 x 2.5 x 0.4 cm were used as test surfaces. Prior to use the coupons were cleaned with soap and water, rinsed with 70% ethanol, allowed to dry, and then autoclaved. Fifty microliters of virus suspension was pipetted onto a clearly marked section of each coupon. Coupons were placed into drying chamber maintained at 50% RH for 30 minutes until dry. After drying the coupons were transferred to a RH and temperature controlled test chamber. The test chamber consisted of an insulated box with interior volume of dimensions of 0.12m<sup>3</sup>. A mix of dry air and water saturated air were pumped into the chamber to yield the desired relative humidity. Room air was saturated by pumping the air through 2 liters of water via a fritted bubbler. Dry air was produced by pumping room air through 3 Drierite laboratory gas drying units (Xenia, OH) which were connected in series. The total air flow through the chamber was approximately 6 lpm. Test coupons were loaded onto a thin tray which was able to be slid into and out of the chambers through narrow slot. This feature allowed for loading and unloading of test coupons from the chamber over the course of the experiments (up to 120 hrs) without impacting the RH level being maintained in the chamber. The RH and temperatures within the chambers were continuously monitored with Omega RH32 temperature and RH meters (Stamford, CT).

### 18.2.2 RH Survival Tests

In preparation for an experiment, influenza working stocks were thawed and separated into single use 55 ul portions and then refrozen at -80C. At the start of an experiment, three of portions were thawed and 50ul of virus from each portion was applied onto separate coupons. Triplicate coupons were used for each test condition. The coupons were put into the drying chamber for 30 minutes and subsequently transferred to the RH control chamber. After a predetermined time, another three, single use portions were thawed, placed onto the coupons, dried, and transferred to the RH control chamber. This procedure was repeated multiple times and at the end of the experiment all of the

coupons were rinsed and analyzed at the same time. Exposure times were generally for 120, 48, 24, 12, and 0 hours of exposure. RH levels were set at 25, 50, or 75%. All RH conditions were tested in triplicate, separate experimental runs. Zero hours of exposure corresponded to coupons which were seeded, dried in the drying chamber, and then immediately rinsed without being placed into the RH control chamber.

### 18.2.3 Data Analysis

The log reduction,  $n$ , for each exposure time interval was calculated according to the equation:

$$n = -\log_{10} (C_{ti} / C_{t0}) \quad (18.1)$$

where  $n$  is the  $\log_{10}$  reduction of virus, concentration  $C_{ti}$  is the concentration of viruses after  $i$  hours of exposure,  $C_{t0}$  is the concentration of viruses at time=0. Where  $n=3$  would correspond to 3  $\log_{10}$  reductions or 99.9 percent inactivation of the virus. Linear regression through the origin was used to estimate the decay constant for each level of humidity. The log-reduction was our outcome variable, and the dose level was our response. The estimated coefficient of the regression line then was our estimate of the decay constant. All statistical analysis was performed using Excel (Redman, CA).

## 18.3 Surface Sampling Protocol Development

### 18.3.1 Swab Selection

A complete evaluation of commercially available swabs was not within the scope of this research. For example one of the major swab manufacturers had over 30 types of swabs available, another manufacture had over 10 varieties of single type of swab. Instead, swabs samples were solicited from various suppliers to provide a variety of tip materials and sizes that would be suited for environmental studies. These swabs were then evaluated qualitatively for performance based on factors such as: swab size, swab durability, swab shaft flexibility, liquid holding capacity, hydrophobicity, liquid holding capacity (Table 18.1). These qualitative tests consisted of wetting the swab with buffer, moving them across a non-porous surface, and squeezing the liquid out of the swab. Those swabs which met the qualitative requirements were then subjected to replicate surface recovery experiments using *B. Subtilis* and *S. Marcescens*.

*Table 18.1. Swab selection criteria.*

Swab Factor	Explanation
Size	<ul style="list-style-type: none"> <li>– Large size swabs will require large amounts of liquid for extraction and result in sample dilution</li> <li>– Swabs which are too small require tedious swabbing of the surface</li> </ul>
Durability	<ul style="list-style-type: none"> <li>– Swab must not degrade during swabbing operations or during vortexing</li> </ul>
Flexibility	<ul style="list-style-type: none"> <li>– The swab shaft must be stiff enough to exert “adequate” pressure on the surface while swabbing</li> </ul>
Hydrophobicity	<ul style="list-style-type: none"> <li>– Swab must be wettable</li> </ul>
Liquid holding capacity	<ul style="list-style-type: none"> <li>– The swab must be able to hold enough liquid to wet the surface during swabbing without excessive rewetting of the swab</li> <li>– The swab must not retain excessive amounts of liquid during recovery</li> </ul>

### 18.3.2 Swab Surface Testing

The general swab testing protocol consisted of suspending 50ul portion of bacteria suspended in PBS/0.1% BSA onto stainless steel coupons. The coupons were dried in the drying chamber at 50%RH for approximately 30 minutes. The test swab was wetted with 100ul of PBS and moved across the horizontal surface with a zigzag pattern vertically and horizontally (Fig. 18.1). The swab tip was then broken off into a 1.5ml microcentrifuge tube containing 1ml of PBS. The microcentrifuge tube was vortexed on maximum for 30 seconds. The tip was then “dewatered” by pressing and rolling against the tube wall. Serial dilutions were made of the extract, plated, and incubated as described previously.

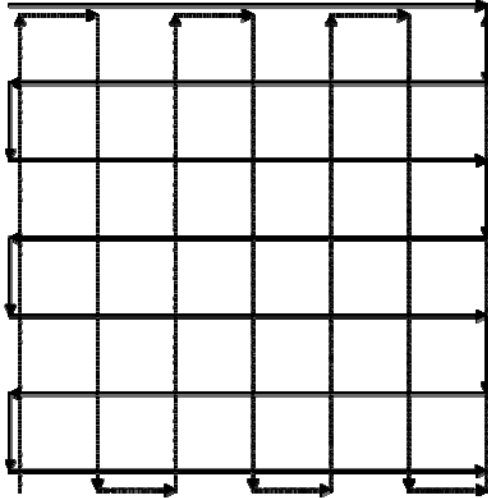


*Fig 18.1 Swab sampling diagram*

### 18.3.3 Surface Testing Data Analysis

Swab performance was compared in a relative manner. Results were normalized, as a percentage, against a reference swab:

$$\text{Recovery \%} = C_T / C_R \quad (18.2)$$

where  $C_T$  is the concentration of bacteria recovered from the test swab and  $C_R$  is the concentration of bacteria recovered from the reference swab. By convention, the reference swab was defined as the cotton swab in any series of given tests.

## 18.4 Field Study

### 18.4.1 Field Study Sampling Plan

Our intent was to perform a preliminary characterization of bacteria and viruses present on “high touch” surfaces within the air cabin. Surface sampling was performed in the air cabin of 5 aircraft. Individual sample kits were used for each sample. Each kit contained a nitrile surgical glove, a sterile swab, and 1.5 ml microcentrifuge tube containing 1.0ml of PBS. All materials for each kit were contained in sealed Chex-All Sterilization Pouches (Propper Manufacturing Laboratory Consumables).

Each sample consisted of swabbing surfaces with a moistened swab over a predetermined surface. The swab was pre-moistened with PBS buffer contained in the 1.5ml microcentrifuge tube. The swab was moved along the sampling surface in an up and down pattern vertically and horizontally (Fig. 18.1). The swab was re-moistened as needed using the PBS buffer in the 1.5 ml tube. At the completion of sampling the swab tip was placed into the 1.5ml microcentrifuge tube and the swab handle snapped off. The microcentrifuge tube was then closed. Three seating areas were sampled in the front,

middle, and rear of the aircraft while randomly alternating sides. For each seating area the following was sampled: tray table top, tray table bottom, arm rests. In addition, the rear lavatory in each aircraft was sampled. The lavatory surfaces sampled were the sink handles, counter, and trash receptacle cover.

#### 18.4.2 Field Study Sample Processing

All samples consisted of the swab tip contained in a 1.5 ml centrifuge tube with approximately 0.75ml of PBS. All sample processing took place in a class II-A biological safety cabinet (BSC) while wearing gloves. Gloves were replaced frequently in any case of contact with the tube contents. All tubes were kept on ice while processing. Each 1.5 ml centrifuge tube was vortexed at max setting for 15 seconds. The tube was opened and forceps were used to grab the end of the swab and press against the side of the tube to remove liquid absorbed onto the swab. PBS was added to the 1ml line on the microcentrifuge tube using a P-1000 Pipetteman equipped with a new 1 ml filter tip. The tube was vortexed for 5 seconds and 500 ul was removed and put into a new 1.5 ml microcentrifuge tube. Half of the tubes were packed on “blue ice” and sent via overnight courier for bacterial analysis by EMSL Analytical, Inc. Cinnaminson, NJ. The remaining samples were stored at -70 awaiting RMA analysis. The RMA samples were subsequently thawed and split into two 250ul portions. One set of samples was packed on dry ice and sent via overnight courier for RMA analysis to the laboratory of Dr. James Gern at the University of Wisconsin, Madison, WI. The set was archived at -70°C.

## 19. RESULTS

### 19.1 Relative Humidity and Influenza Surface Survival

Figure 19.1 shows the average number of log reductions of influenza viruses measured for the four exposure times (120, 48, 24, 12 hrs) and three RH levels (25%, 50%, and 75%). Generally, surface inactivation of influenza virus increased with increasing exposure time and RH. The number of viruses detected after 120 hours was typically very low (<10 per coupon) and at times none were detected. Thus, only data for 0, 12, 24, and 48 hours was included in our analysis. A greater than 2.5 log reduction of influenza virus on surfaces was achieved after 48 hrs at 75% RH compared to less than 1.5 log reduction at either 25 or 50%RH in the same time period. After 24 hours of exposure, greater than 1.5 log reduction of influenza virus on surfaces was achieved at 75% RH compared to less than 1.5 log reduction at either 25 or 50%RH in the same time period. The number of  $\log_{10}$  reductions versus exposure time was approximated with linear regression. The results are summarized in Table 19.1. Accordingly, the decay rates of influenza were estimated at 0.025, 0.027, and 0.062  $\log_{10}$  reductions per hour at 25, 50, and 75% RH, respectively. This would correspond to half-lives of 12.2, 10.9, and 4.8 hours at 25, 50, and 75%, respectively. There was no statistical difference between influenza inactivation at 25 and 50% RH, while influenza inactivation at 75% RH was statistically different from 25 and 50% RH conditions.

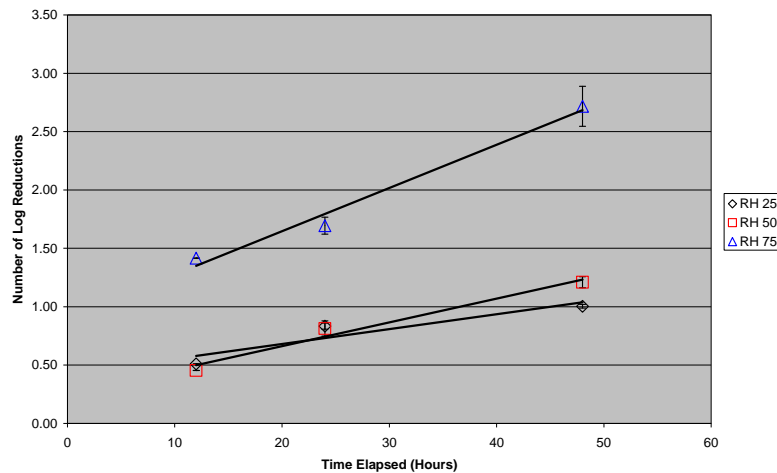


Figure 19.1 Log reduction of influenza A virus at 25, 50, and 75% relative humidity.

Table 19.1 Decay constant and half-life for influenza virus survival on stainless steel surfaces at varying relative humidities.

RH Level %	Decay Constant (Log <sub>10</sub> Reductions/hr) (95% CI)	R <sup>2</sup>	Half-Life (hrs)
25	0.025 (0.020-0.030)	0.93	12.2
50	.027 (.023-0.031)	0.97	10.8
75	0.062 (.051-.074)	0.95	4.8

The median concentration of viruses measured on the control coupons (time=0) after drying was  $3.9 \times 10^5$  FFU per slide and ranged from  $2.9 \times 10^5$  to  $3.6 \times 10^6$  FFU/slide. Previous research has shown using these procedures have shown an average loss of 63% of viruses during the drying process (McDevitt, Rudnick et al. 2010). These drying losses were assumed to be the same for the control and test coupons during this investigation.

## 19.2 Surface Sampling Protocol Development

Ten different swabs were evaluated from 4 different suppliers. The original selection was primarily based on availability and swab tip composition. Based on the results of the qualitative testing 4 of the 10 original swabs were selected for recovery, comparison testing: cotton, polyester, rayon, and foam. A summary of the testing results are shown in Figs. 19.2 and 19.3. Four replicate tests were carried out for *B. atrophaeus* and 3 replicate tests for *S. Marcescens*. The results changed remarkably between tests and organisms. As can be seen in Fig. 19.1, there is no clear trend in recovery between swabs among the replicate experiments for *B. atrophaeus*. When viewed as an average the performance from best to worst was: polyester, rayon, foam, and cotton. However, based on the large amount of variability there were no statistical differences in swab performance. Conversely, the data is more consistent for tests with *S. marcescens* as shown in Fig. 19.3. The cotton swab had the best performance, followed by the polyester swab. Despite the small number of samples, there was a significant difference between cotton when compared to rayon or foam and between polyester and rayon swabs (Paired, One-tail, T-test, 90% Confidence Level). Field tests, in which the surfaces of office desks were swabbed and cultured, showed polyester recovering 6-times more environmental bacteria as cotton swabs.

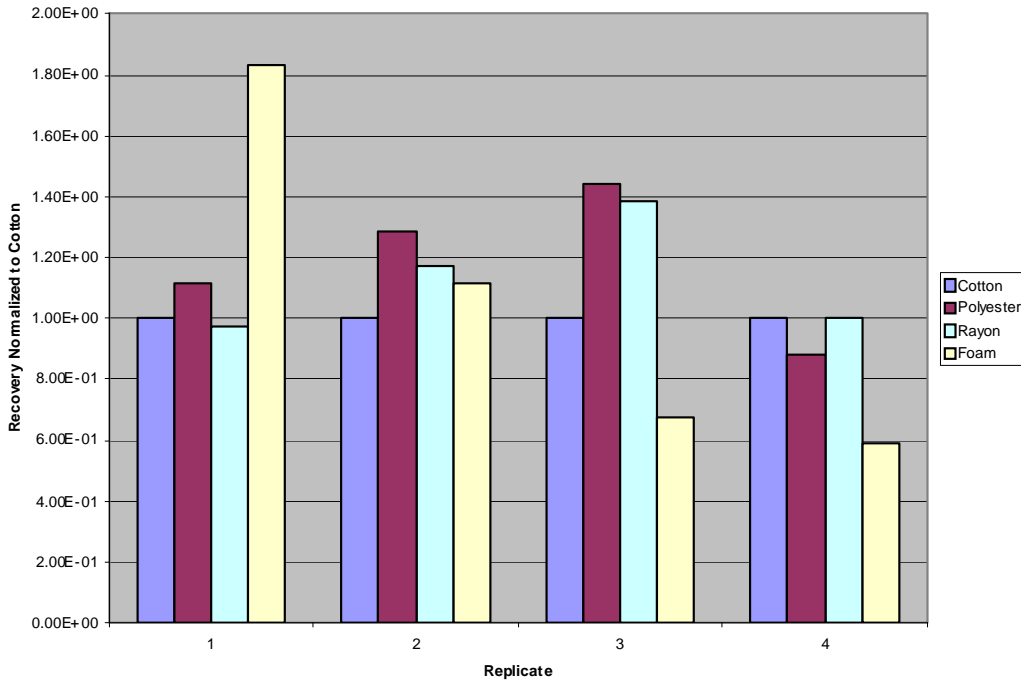


Figure 19.2 Summary of swab testing with *Bacillus atrophaeus*.

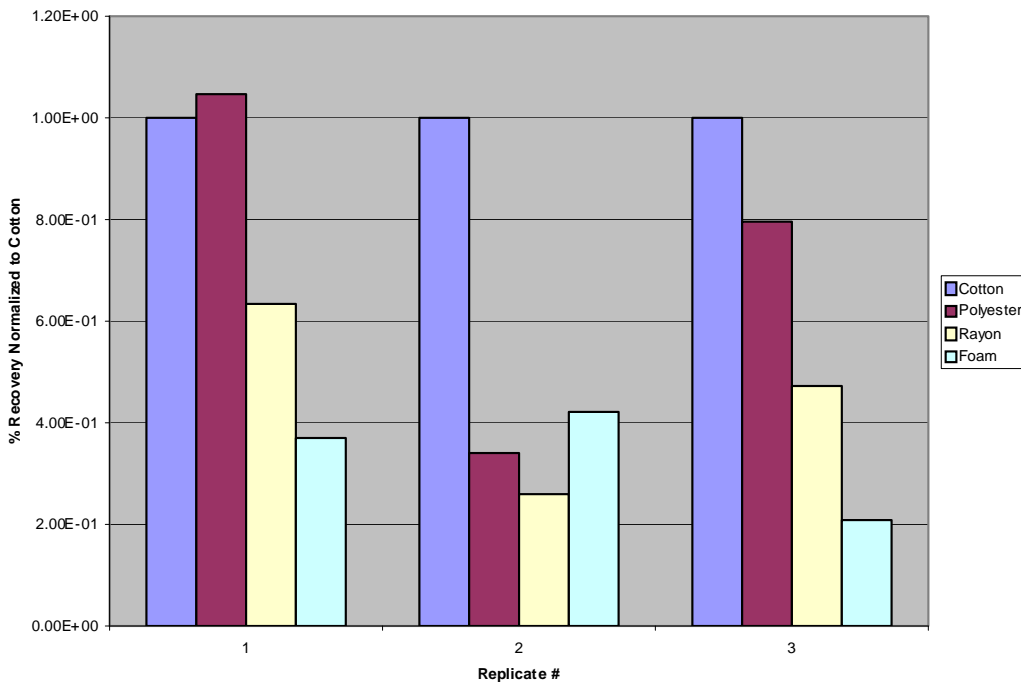


Figure 19.3 Summary of swab testing with *Serratia Marcescens*.

### 19.3 Field Study

Surface sampling was conducted at Logan Airport during the evening when aircraft were finished flying for the day. The aircraft were basically left “as is” after the last passengers left and were sampled prior to end of day cleaning. Five different aircraft were sampled (Table 19.2) which represent 3 “long haul” aircraft and 2 regional jets. The results of surface sampling are shown in Table 19.3 for bacterial and respiratory viruses.

*Table 19.2 Description of aircraft sampled*

Tail Number	Aircraft	Total Passengers
672	Boeing 757-200	180
3725	Boeing 737-800	160
N316	Airbus 320SR	148
753	Embraer CRJ700-EV	65
641	Embraer 170	69

Table 19.4 provides a composite summary of all aircraft. A total of 24 different bacteria were identified from the 50 surface samples collected. Of these 50 samples, 74% were positive for bacterial growth and an average of 1.5 species were identified in each sample. The most frequently identified species of bacteria was *Staphylococcus epidermidis*, followed by *Micrococcus luteus*, and *Staphylococcus (not aureus)*. Each of the remaining bacteria listed in Table 19.4 were not predominant and were identified in less than 3 of the 50 samples collected. The median number of colonies on each surface was 46 colonies/100cm<sup>2</sup> with a range of 0-7450 colonies.

Table 19.5 provides a summary of surface sampling stratified by tail number. There were no obvious trends noted. Perhaps the two regional jets had generally lower types and numbers of bacteria than the long haul aircraft. However, limited sample size precludes statistical analysis. Table 19.6 provides a summary of surface sampling stratified by the sampling location (arm rest, tray table, or lavatory). A review of Table 19.7 suggests that tray tables had fewer varieties and number of bacteria than the arm rests and the lavatory. The tray table bottom (exposed when in the upright position) had few varieties and number of bacteria than the tray table top (exposed when in the down position). The lavatory was the only location to have all positive samples. There was a higher average number of species identified in the lavatory (3.8) versus other areas (1.8, 1.5, and 0.6). The mean and median number of colonies/100cm<sup>2</sup> was higher in the laboratory compared to the other areas samples.

Only Bocaviruses tested positive of the 9 respiratory viruses in the RMA screening. Bocaviruses were detected on two aircraft. One sample was positive for the lavatory sample, while the other sample was positive for a single tray bottom. We do note that there were numerous positive samples for influenza A virus. However, these results were not considered valid since a field blank was also positive for influenza A virus.

Table 19.3 The results of surface sampling for bacterial and respiratory viruses.

Tail #	Location	Item	# Species	Total Colonies	Bacillus cereus	Bacillus circulans	Bacillus pumilus	Bacillus sp.	Corynebacterium coylea	Corynebacterium sp.	Flavobacterium aquatile	Kocuria rhizophila	Lactococcus lactus	Micrococcus luteus	Moraxella sp.	Paenibacillus	Paenibacillus alvei	Psuedomonas aeruginosa	Rothia dentocariosa	Staphylococcus auricularis	Staphylococcus epidermidis	Staphylococcus haemolyticus	Staphylococcus hominus	Staphylococcus sp. (not aureus)	Staphylococcus pasteurii	Staphylococcus saprophyticus	Staphylococcus warneri	Streptococcus oralis	Bocavirus
641	13D	Arm Rest	2	130																104							26		
641	13D	Tray Bottom	0	0																									X
641	13D	Tray Top	0	0																									
641	15A	Arm Rest	1	78																78									
641	15A	Tray Bottom	1	23											23														
641	15A	Tray Top	1	23									23																
641	6D	Arm Rest	1	26																26									
641	6D	Tray Bottom	0	0																									
641	6D	Tray Top	1	23								23																	
641	Lav	Lav	4	1258			37						74							555		592							
672	43E	Arm Rest	1	7540								7540																	
672	43E	Tray Bottom	1	46			46																						
672	43E	Tray Top	2	345									276							69									
672	B22	Arm Rest	2	130																				26		104			
672	B22	Tray Bottom	2	46									23							23									
672	B22	Tray Top	1	92																			92						
672	F28	Arm Rest	1	26					26																				
672	F28	Tray Bottom	1	69																69									
672	F28	Tray Top	3	161															69	69			23						
672	Lav	Lav	5	1776								37	740				296		148	555									
753	13C	Arm Rest	2	52	26											26													
753	13C	Tray Bottom	1	23			23																						
753	13C	Tray Top	2	69			23																46						
753	15A	Arm Rest	4	104	26	26							26									26							
753	15A	Tray Bottom	0	0																									
753	15A	Tray Top	1	23												23													
753	6C	Arm Rest	0	0																									
753	6C	Tray Bottom	0	0																									
753	6C	Tray Top	1	23									23																
753	Lav	Lav	2	148															74		74								
3725	31D	Arm Rest	1	26									26																
3725	31D	Tray Bottom	2	69									46										23						
3725	31D	Tray Top	2	575	46																	529							
3725	B12	Arm Rest	5	2210		26		156												208		416				1404			
3725	B12	Tray Bottom	0	0																									
3725	B12	Tray Top	3	598									69							345		184							
3725	E19	Arm Rest	3	78								26	26							26									
3725	E19	Tray Bottom	0	0																									
3725	E19	Tray Top	4	138															23	23		46						46	
3725	Lav	Lav	3	1406							444									333		629							
N316	12E	Arm Rest	1	780																780									
N316	12E	Tray Bottom	0	0																									
N316	12E	Tray Top	0	0																									
N316	24B	Arm Rest	0	0																									
N316	24B	Tray Bottom	0	0																									
N316	24B	Tray Top	1	23															23										
N316	7D	Arm Rest	3	230						23												92				115			
N316	7D	Tray Bottom	1	23									23																
N316	7D	Tray Top	0	0																									
N316	Lav	Lav	5	555						148								37				74	37	259					X
N316	Blank	Blank	0	0																									
672	Blank	Blank	0	0																									
Lab	Blank	Blank	0	0																									
Lab	Blank	Blank	0	0																									

There were no other positive results for any blanks for other viruses or bacteria. Laboratory contamination is suspected since high titers of influenza A virus was commonly used in the laboratory in which the sample kits were prepared and were the field samples were processed on two separate occasions. No other respiratory viruses are used in the processing laboratory. The sequence of positive of influenza samples does not suggest cross contamination in the field. Furthermore, flu activity was at low to minimal levels during the time of the study. As such, few people would be expected to be infected with influenza while on the aircraft. Considering these factors, the positive results for influenza A were suspect and not considered valid.

*Table 19.4. Composite summary of all air cabin samples*

	Total
Number of Species Identified	24
% Positive Samples (n=56)	74
% Negative Samples (n=50)	26
Average Number of Species/Sample	1.5
1 <sup>st</sup> Most Frequently Identified Species	<i>Staphylococcus epidermidis</i>
2 <sup>nd</sup> Most Frequently Identified Species	<i>Micrococcus luteus</i>
2 <sup>nd</sup> Most Frequently Identified Species	<i>Staphylococcus (not aureus)</i>
Average # Colonies/100cm <sup>2</sup>	379
Median # Colonies/100cm <sup>2</sup>	46
Range of Colonies/100 cm <sup>2</sup>	0-7450

Table 19.5 Summary of air cabin surface sampling results stratified by tail number

	Tail Number				
	641	672	753	3725	N316
Number of Species Identified	7	12	7	13	9
% Positive Samples (n=10)	70	100	70	80	50
% Negative Samples (n=10)	30	0	30	20	50
Average Number of Species	1.1	1.9	1.3	2.3	1.1
1 <sup>st</sup> Most Frequently Identified Species	<i>Staphylococcus epidermidis</i>	<i>Staphylococcus epidermidis</i>	<i>Staphylococcus sp. (not aureus)</i>	<i>Staphylococcus epidermidis</i>	<i>Staphylococcus hominus</i>
2 <sup>nd</sup> Most Frequently Identified Species	<i>Micrococcus luteus</i>	<i>Micrococcus luteus</i>	*	<i>Staphylococcus sp. (not aureus)</i>	<i>Cornybacterium sp.</i>
Average # Colonies/100cm <sup>2</sup>	156	1023	44	510	161
Median # Colonies/100cm <sup>2</sup>	23	111	23	108	12
Range of Colonies/100 cm <sup>2</sup>	0-1258	0-7450	0-148	0-2210	0-780

Table 19.6. Summary of air cabin surface sampling stratified by surface type

	Surface Type				Arm Rest	Lavatory
	Tray Top	Table	Tray Bottom	Table		
Number of Species Identified	11		5		12	12
% Positive Samples (n=10)	80		47		87	100
% Negative Samples (n=10)	20		53		13	0
Average Number of Species	1.5		0.6		1.8	3.8
1 <sup>st</sup> Most Frequently Identified Species	<i>Staphylococcus sp. aureus</i>	(not)	<i>Micrococcus luteus</i>		<i>Staphylococcus epidermidis</i>	<i>Staphylococcus epidermidis</i>
2 <sup>nd</sup> Most Frequently Identified Species	<i>Staphylococcus epidermidis</i>		<i>Staphylococcus epidermidis</i>		<i>Micrococcus luteus</i>	<i>Staphylococcus sp. (not aureus)</i>
Average # Colonies/100cm <sup>2</sup>	140		20		761	1028
Median # Colonies/100cm <sup>2</sup>	23		0		78	1258
Range of Colonies/100 cm <sup>2</sup>	0-598		0-96		0-7450	148-1776

## 20. DISCUSSION

### 20.1 Relative Humidity and Influenza Surface Survival

The results of our investigation systematically show that RH survival on surfaces is a function of relative humidity. There was a trend of increasing influenza inactivation with increasing relative humidity. However, the inactivation rates for influenza virus were statistically higher at 75% compared to 25 and 50% RH. We have previously reported that influenza inactivation at elevated temperatures (55-65°C) was a function of RH, temperature and exposure time (McDevitt, Rudnick et al. 2010). In these experiments inactivation rates increased with temperature and RH.

Buckland and Tyrrel also deposited influenza virus on slides and reported a 1.7-log reduction after 2.5 h at room temperature at 20% RH and up to a 3.5-log reduction when RH was increased to 84%. These trends of increasing inactivation with increasing RH, determined from a single exposure time and widely varying RHs, are consistent with our findings. However, much more pronounced log reductions were reported by Buckland and Tyrrell over shorter time periods compared to the current investigation. Bean et al. investigated influenza survival for up to 72 hours on stainless steel surfaces at 35-40% relative humidity (Bean, Moore et al. 1982). Log reductions based on the published figure were approximately 1.0, 1.5, and 2.2. These reductions were higher than our values for 25 and 50% RH, but somewhat lower than our data at 75% RH. Interestingly, Bean et al. reported in their study that log reductions of influenza B on stainless steel were higher than Influenza A. This difference was attributed to the type of virus. However, they note that the RH levels when testing influenza B were higher than those when testing influenza A. Perhaps this difference may have been due to RH. Similarly, Greatorex et al. evaluated influenza inactivation on stainless steel surfaces. Experiments were completed at 23-24% RH and they reported log reductions of 1.5 and 2.2 after 4 and 9 hrs, respectively. These reductions are similar in magnitude to those found in the current study, but occur much more quickly.

Knowing the log reduction of virus yields is important information for decontamination, but determination of the decay rate or half life is more useful for risk assessment purposes. In our experiments, influenza virus survived on stainless steel surfaces for hours to days. However, the survival time in our experiments, and of other investigators, is a function of the very high initial inoculums seeded onto the surfaces. Since the decay appears to be a first order function, the more viruses that are deposited on a surface the longer that infective viruses will be detected. Researchers often use extremely high influenza virus inoculums to allow measurement of large reductions of viruses and the associated lengthy survival times are likely not reflective of inoculums deposited on surfaces by persons infected with influenza virus.

It is potentially more useful to look at the data as a rate function in terms of half-lives to determine how quickly initial inoculums deposited on a surface will decrease. Our data show half-lives of greater than 10 hrs when humidity is 50% or lower. If we assume the RH is 50% or less (a reasonable assumption for the air cabin considering the low moisture content of air when flying at altitude), only half of the dried, infective influenza virus initially deposited on a surface would become inactivated during the

length of most regional flights. Our data showed inactivation rates for influenza virus decreased by more than two-fold when relative humidity was maintained at 75% versus either 25 or 50%. Thus, increasing relative humidity could facilitate virus inactivation.

Maintaining elevated RH in the air cabin environment during flight, or in most ground operations, would be impractical. Perhaps a control strategy incorporating elevated relative humidity in the air cabin during evenings, when aircraft are not in use, warrant further investigation. However, such a strategy should be well thought out considering potential problems with molds associated with elevated RH.

Although estimated half-lives for influenza virus inactivation on surfaces have been computed, more information is needed for sound risk assessment. For example, little is known about the amount of virus shed to the environment by infected persons. Thus, we have no estimate of the concentration of influenza virus actual on surfaces. Furthermore, information is also limited on influenza inactivation during the drying process or the efficiency of virus transfer from the surface. Although we note 63% reductions during drying in a controlled laboratory environment, reductions may vary when virus is expelled from an actual person infected with influenza. These additional characterizations are needed to before meaningful models of influenza infection risks from contaminated surfaces are developed.

Although there have been differences noted between the current study and previously mentioned studies in magnitude of inactivation or half-live of influenza virus, the associations of increasing RH and increasing influenza surface inactivation is consistent. The difference associated with the magnitude of log reductions or decay rates in the present study compared to other investigations may be a function of experimental methodologies or conditions. There are no widely accepted methods for surface testing and laboratories use varying methods of virus deposition, recovery from surfaces, and culture methods. Influenza virus survival may also depend on the type of influenza virus or how it is cultured(Schaffer, Soergel et al. 1976). Survival differences based on the type of virus have been reported previously for influenza aerosols. However, due to laboratory safety restrictions only one virus was tested as part of this investigation.

## 20.2 Surface Sampling Protocol Development and Field Study

There was no clear trend which indicated a superior swab type for sampling bacteria from surfaces. Both cotton and polyester swabs appeared to outperform foam and rayon swabs. Field tests also showed polyester swabs have increased recovery over cotton. Based on our analysis and concern about degradation of the cotton swab after extended immersion and vortexing, the polyester swab was chosen for the pilot field study. Furthermore, clinical research also suggested superior recoveries from polyester swabs(Esposito, Molteni et al. 2010).

Initially our plan for the pilot study was to recruit persons of opportunity to perform surface sampling while taking planned flights. This method appeared to provide a means of obtaining air cabin samples from a wide variety of aircraft and flight routes. However, this strategy was changed due to study design weaknesses associated with data collection reliability, sample processing, and security/perception issues. Past research experience has shown that placing a trained researcher on actual flight segments is costly and time consuming. Therefore, a new strategy was developed that would allow a trained

technician to collect samples from a variety of aircraft, which had flown a variety of routes, in a single evening. The strategy consisted of partnering with a local airline to allow access to aircraft on the ramp at the airport after completion of the days flying, but before janitorial crew serviced the aircraft. Using this strategy two technicians were able to collect 50 samples from 5 aircraft within a 3 hour time period. Samples could be processed locally and avoid multiple days of sample shipping. The single sampling kits provided were small in size and easily transported on the ramp from aircraft to aircraft.

Due to the pilot scale of the study, data analysis was limited to descriptive statistics. Increasing sample size in future studies would certainly be feasible by extending the sampling campaign over several nights. Despite the limited sample size, multiple trends were suggested by the data. Far and above, *Staphylococcus epidermidis* and *Micrococcus luteus* were the most commonly identified bacteria. This is not unexpected considering that these bacteria are part of the normal, human skin flora and are continually sloughed off from the skin. The presence of these bacteria does not indicate an increased risk of infection, but does show the method was capable of consistently recovering bacteria from the environment. Potentially pathogenic species of skin flora, such as *Staphylococcus aureus* or methicilin resistant *Staphylococcus aureus* (MRSA) were not found. The data trends appeared logical. The variety and number of bacteria was generally lower on tray table tops than tray table bottoms and is consistent with tray table bottoms being contacted less frequently than tray table tops. Likewise, high touch surfaces such as arm rests had a generally higher variety and number of bacteria than the tray tables. Not surprising, the lavatories had the greatest variety and numbers of bacteria. In addition, the lavatories were the only location where clinically relevant bacteria, *Pseudomonas auriginosa* (and potentially *Moraxella sp.*, depending upon the specific species), was found.

There are no standards or limits available to compare the surface levels of bacteria found during the study. The risk of infection associated with the absolute number of bacteria present on the surfaces is difficult to determine. Many factors play a role in determining whether a susceptible person becomes infected such as: surface to hand transfer rate, hand to entry point (mouth, eyes, nose, etc.) transfer rate, health of the individual, or pathogenicity of the organism. Thus, it is not possible to determine if a *number* of bacteria is “low or high” or “acceptable or unacceptable”. Rather, these data are useful in a relative manner and can be used to evaluate cleaning methods, cleaning frequency, cleaning materials, other decontamination methods, or risk compared to other modes of transportation. However, the presence of highly pathogenic bacteria, in and of itself, may trigger concern regardless of the amount present. For example the fact that *Pseudomonas auriginosa* was found in 2 out of 5 lavatories tested may be justification for concern and increased lavatory cleaning.

Bocavirus was the only type of respiratory virus detected. These positive virus samples were found on a tray table bottom in one aircraft and in the lavatory of another. Bocavirus is found in respiratory samples of patients with respiratory complaints, is associated with mild disease, and its etiology not fully understood. The relevance of bocavirus is somewhat limited, but its detection demonstrates the potential usefulness of the RMA assay. However, it is difficult to determine if a lack of positive detections of respiratory viruses was due to a lack of these viruses in the environment, rapid degradation of respiratory viruses in the environment, low virus recovery, or issues

associated with the RMA. The RMA relies on using polymerase chain reaction, based molecular methods for amplifying and detecting nucleic acid associated with viruses. These techniques can be highly sensitive and specific, but are also sensitive to inhibitory substances which are commonly found in environmental samples. Further laboratory research is needed to evaluate the usefulness of the RMA for environmental surface sampling.

The introduction of influenza A virus into many of the samples was likely the result of laboratory contamination at the HSPH Environmental Microbiology Lab (EML). Very high titers ( $10^9$ /ml) of influenza A virus, such as those used in surface survival experiments, are handled in the EML. Sample kits were assembled and samples were processed for bacterial and viral analysis at the EML. Procedures were used in the lab to prevent cross contamination such as: working in a Class IIA BSC, using barrier pipet tips, and changing gloves frequently. However, the RMA assay is highly sensitive and can detect down to a few copies of nucleic acid. In the future, all sample kits and sample processing will be performed in laboratories which do not handle influenza or other respiratory viruses.

## 21. CONCLUSIONS

The results of our investigation show that RH survival on stainless steel surfaces is impacted by relative humidity. There was a trend of increasing influenza inactivation with increasing relative humidity. However, the inactivation rates for influenza virus were statistically higher at 75% compared to 25 and 50% RH. The low RH in the air cabin may be conducive to influenza survival and increase infection risk. Surface recovery of bacteria from surfaces varied and was inconsistent among a variety of swab types. The sampling kit used in the pilot field study recovered a wide variety of bacteria, but only a single type of virus. The strategy of sampling aircraft at the end of the flight day, and prior to cleaning, provided an efficient means of evaluating microbial surface contamination of a variety of aircraft.

## 22. REFERENCES

- Bean, B., B. M. Moore, et al. (1982). "Survival of influenza viruses on environmental surfaces." J Infect Dis **146**(1): 47-51.
- Boone, S. A. and C. P. Gerba (2005). "The occurrence of influenza A virus on household and day care center fomites." J Infect **51**(2): 103-9.
- Boone, S. A. and C. P. Gerba (2007). "Significance of fomites in the spread of respiratory and enteric viral disease." Appl Environ Microbiol **73**(6): 1687-96.
- Brankston, G., L. Gitterman, et al. (2007). Transmission of influenza A in human beings. Lancet Infect Dis. United States. **7**: 257-65.
- Bright, K. R., S. A. Boone, et al. (2010). "Occurrence of bacteria and viruses on elementary classroom surfaces and the potential role of classroom hygiene in the spread of infectious diseases." J Sch Nurs **26**(1): 33-41.
- Buckland, F. E. and D. A. Tyrrell (1962). "Loss of infectivity on drying various viruses." Nature **195**: 1063-4.
- Esposito, S., C. G. Molteni, et al. (2010). "Comparison of nasopharyngeal nylon flocked swabs with universal transport medium and rayon-bud swabs with a sponge reservoir of viral transport medium in the diagnosis of paediatric influenza." J Med Microbiol **59**(Pt 1): 96-9.
- Gerba, C. P. (2009). Research on Fomite Transmission in Airports and on Aircraft. Research on the Transmission of Disease in Airports and on Aircraft: A Symposium presented by the Transportation Research Board of the National Academies, Washington, DC.
- Greatorex, J. S., P. Digard, et al. (2011). "Survival of influenza A(H1N1) on materials found in households: implications for infection control." PLoS One **6**(11): e27932.
- Hartshorn, K. L., M. R. White, et al. (2007). "Reduced influenza viral neutralizing activity of natural human trimers of surfactant protein D." Respir Res **8**: 9.
- Kramer, A., I. Schwebke, et al. (2006). "How long do nosocomial pathogens persist on inanimate surfaces? A systematic review." BMC Infect Dis **6**: 130.
- Lee, W. M., K. Grindle, et al. (2007). "High-throughput, sensitive, and accurate multiplex PCR-microsphere flow cytometry system for large-scale comprehensive detection of respiratory viruses." J Clin Microbiol **45**(8): 2626-34.
- McDevitt, J., S. Rudnick, et al. (2010). Role of absolute humidity in the inactivation of influenza viruses on stainless steel surfaces at elevated temperatures. Appl Environ Microbiol. United States. **76**: 3943-7.
- McKernan, L. T., H. Burge, et al. (2007). "Evaluating fungal populations by genera/species on wide body commercial passenger aircraft and in airport terminals." Ann Occup Hyg **51**(3): 281-91.
- McKernan, L. T., M. J. Hein, et al. (2008). "Assessing total fungal concentrations on commercial passenger aircraft using mixed-effects modeling." J Occup Environ Hyg **5**(1): 48-58.
- McKernan, L. T., K. M. Wallingford, et al. (2008). "Monitoring microbial populations on wide-body commercial passenger aircraft." Ann Occup Hyg **52**(2): 139-49.
- Moser, M. R., T. R. Bender, et al. (1979). "An outbreak of influenza aboard a commercial airliner." Am J Epidemiol **110**(1): 1-6.
- Myatt, T. A., M. H. Kaufman, et al. (2010). "Modeling the airborne survival of influenza virus in a residential setting: the impacts of home humidification." Environ Health **9**: 55.

- Rudnick, S. N., J. J. McDevitt, et al. (2009). "Inactivating influenza viruses on surfaces using hydrogen peroxide or triethylene glycol at low vapor concentrations." Am J Infect Control **37**(10): 813-9.
- Schaffer, F. L., M. E. Soergel, et al. (1976). "Survival of airborne influenza virus: effects of propagating host, relative humidity, and composition of spray fluids." Arch Virol **51**(4): 263-73.
- Tellier, R. (2006). "Review of aerosol transmission of influenza A virus." Emerg Infect Dis **12**(11): 1657-62.
- Thomas, Y., G. Vogel, et al. (2008). "Survival of influenza virus on banknotes." Appl Environ Microbiol **74**(10): 3002-7.
- TRB (2011). Evaluating and Mitigating the Risk of Disease Transmission at Airports and on Aircraft, National Academies Transportation Research Board. **2012**.